Università
Ca'Foscari
Venezia

Corso di Dottorato di ricerca

in Environmental Science

ciclo 31°

Tesi di Ricerca

Human and environmental exposure to Copper-based engineered nanomaterials (Cu-ENMs): transformation and toxicological effects

SSD: CHIM/12

Coordinatore del Dottorato
ch. prof. Bruno Pavoni

Supervisore
ch. prof. Antonio Marcomini

Dottorando
Alessandro Bonetto
Matricola 810420

Human and environmental exposure to Copper-based engineered nanomaterials (Cu-ENMs): transformation and toxicological effects

I) Index

II) List of publication

De Jong W.H., De Rijk E., Bonetto A., Wohlleben W., Stone V., Brunelli A., Badetti E., Marcomini A., Gosensn I., Cassee F., "Toxicity of copper oxide and basic copper carbonate nanoparticles after short-term oral exposure in rats" *Nanotoxicology*, (*2018*)
DOI: 10.1080/17435390.2018.1530390

Volpato G.A., Bonetto A., Marcomini A., Mialane P., Bonchio M., Natali M., Sartorel A. "Proton coupled electron transfer from Co_3O_4 nanoparticles to photogenerated $Ru(bpy)_3^{3+}$: Base catalysis and buffer effect", *Sustainable Energy Fuels*, 2, 1951-1956, (*2018*)
DOI 10.1039/C8SE00275D

Ortelli S., Costa A.L., Blosi M., Brunelli A., Badetti E., Bonetto A., Hristozov D., Marcomini A., "Colloidal characterization of CuO nanoparticles in biological and environmental media", *Environmental Science Nano*, 4, 1264-1272, (*2017*)
DOI: 10.1039/C6EN00601A

Manuscript under preparation:

Bonetto A., Badetti E., Ambrosi E., De Jong W.H., Marcomini A. "Detection of CuO and $Cu_2CO_3(OH)_2$ nanoparticles in rats after short-term oral exposure"

III) Acronyms List

AFW	Artificial Fresh Water
AMW	Artificial Marine Water
ASC	Sodium Ascorbate
BEC	Background Equivalent Concentration
BET	Brunauer–Emmett–Teller
BM	Ball Milling
BMD	Bench Mark Dose
CE	Capillary Electrophoresis
CIP	Consumer Product Inventory
CIT	Sodium Citrate
CSA	Centrifugal Separation Analysis
Cu-ENMs	Copper based Engineered Nanomaterials
CuO-MP	Micro Particle CuO
d_{DLS}	Hydrodynamic Diameters
DLS	Dynamic Light Scattering
DL_s	Size Limit of Detection
DLVO	Derjaguin – Landau – Verwey – Overbeek
DMEM	Dulbecco's Modified Eagle Medium
DNOM	Dissolved Natural Organic Matter
EDL	Electrical Double Layer
EDX	Energy Dispersive X-ray
EHS	Environmental Health & Safety
ELS	Electron energy-Loss Spectroscopy
ENMs	Engineered Nanomaterials
EPA	Environmental Protection Agency
EUSES	European Union System for the Evaluation of Substances
EXAFS	Extended X-ray Absorption Fine Structure
FA	Fulvic Acid
FBS	Fetal Bovine Serum
FE-SEM	Field Emission-Scanning Electron Microscopy
FeSSIF	Fed-State Simulated Intestinal Fluid
FFF	Field-Flow Fractionation
GE	Gel Electrophoresis
GI-tract	Gastro-Intestinal Tract
GPC	Gel Permeation Chromatography
HA	Humic Acid
HC	Hydrodynamic Chromatography
ICP-EOS	Inductively Coupled Plasma Emission Optical Spectroscopy
ICP-MS	Inductively Coupled Plasma Mass Spectrometry
IS	Ionic Strength

KED	Kinetic Energy Discrimination
LOD	Limit Of Detection
LOQ	Limit Of Quantification
MALS	Multiple Angle Light Scattering
MEM	Minimum Essential Media
NanoFASE	Nanomaterial FAte and Speciation in the Environment
NOAEL	No-Observed-Adverse-Effect-Level
NPs	Nanoparticles
NSC	Nanosafety Cluster
NTA	Nanoparticle Tracking Analysis
PBS	Phosphate Buffered Saline
PCC	Particle Collision Coulometry
PEI	Polyethylenimine
PVP	Polyvinylpyrrolidone
RCF	Relative Centrifugal Force
REACH	Registration, Evaluation, Authorization of Chemical
RIVM	National Institute for Public Health and the Environment
ROS	Reactive Oxygen Species
SbD	Safety by Design
SD	Standard Deviation
SEC	Size Exclusion Chromatography
SEM	Scanning Electron Microscopy
sp-ICP-MS	Single particle-Inductively Coupled Plasma Mass Spectrometry
SRM	Standard Reference Material
SR-NOM	Suwannee River Natural Organic Matter
STEM	Scanning Transmission Electron Microscopy
STIS	Short-Term Inhalation Study
STOS	Short Term Oral Exposure
SUN	SUstainable Nanotechnology
TE	Transport Efficiency
TEM	Transmission Electron Microscopy
UCF	Ultra-Centrifugal Filter
UV-Vis	Ultraviolet-Visible spectroscopy
vdW	van der Waals
VIP	Voltammetry of Immobilized Particles
W_D	Sum of attractive and repulsive forces
WWTP	Waste Water Treatment Plants
XANES	X-ray Absorption Near Edge Structure
XAS	X-Ray Absorption Spectroscopy

IV) Acknowledgment

“We must find time to stop and thank the people who make a difference in our lives.”

John F. Kennedy
(1961-1963)

V) Abstract

The peculiar properties of engineered nanomaterials (ENMs), i.e. high surface-to-volume ratio and quantum effect, provide great opportunity for technical development of novel or improved products, but the potential risk associated with exposure to these materials is still largely unknown and thus requires further research work.

Unlike bulk chemicals, where the main environmental fate processes are controlled by the partition coefficient, nanoparticles are dynamic entities that undergo a wide range of transformations depending on the chemical composition and on the properties of the media in which they are dispersed (e.g. pH, ionic strength, organic matter and suspended particulate matter). As a consequence, the study of nanoparticle behaviour in the environment and the interactions with organisms necessitates a new approach, which included a suitable choice and adjustment of the available investigation methods. However, due to the difficulties encountered in this relatively recent research field, a number of knowledge gaps still exist about the optimization and appropriate application of these methods.

In this context, copper-based nanoparticles (Cu-ENMs) have recently attracted considerable attention for wood preservation, in paints formulation and in antibacterial products, because of the recognized efficiency in killing a wide range of microorganisms. However, widespread production and use of Cu-ENMs can induce uncontrolled release along their life cycle, raising concerns about potential exposure to NPs for human health and environment.

This Ph.D. thesis focused on the characterization of CuO and $Cu_2CO_3(OH)_2$ nanoparticles, and on the study of their transformations in several media. In detail, the colloidal characterization as well as the distribution and dissolution of Cu-ENMs in both biological and environmental media, have been investigated by using a combination of analytical techniques such as: Dynamic Light Scattering (DLS), Centrifugal Separation Analysis (CSA), Transmission Electron Microscopy (TEM) and single particle Inductively Coupled Plasma-Mass Spectrometry (sp-ICP-MS).

The results obtained from this study are helpful to elucidate the dynamic equilibria between Cu-ENMs and the media investigated, for pristine materials in artificial media, as well as to interpret the toxicological data from in-vivo studies.

Furthermore, an attempt to develop a methodological approach to detect and quantify Cu-ENMs in biological tissues from toxicological tests was undertaken, by combining microscopy and mass spectrometry techniques. However, even though the quantification of ENMs in biological tissues is highly desirable, the instability of Cu-ENMs associated to the instrumental limits makes this task still a challenge.

The overall experimental activity led to the draft of three manuscripts that are discussed in detail in this thesis.

VI) Objectives and Thesis structure

The main objective of this PhD thesis, which is part of both the EU-FP7 project "SUstainable Nanotechnology" (SUN) and the Horizon 2020 project Nanomaterial FAte and Speciation in the Environment (NanoFASE), was to investigate both human and environmental exposure to copper-based engineered nanomaterials (Cu-ENMs) by answering to the following questions:

1. How Cu-ENMs physical-chemical properties and environmental and biological media characteristics can affect Cu-ENMs transformation processes?
2. Are $Cu_2CO_3(OH)_2$ ENMs less toxic than CuO ENMs for mammalians?
3. After short-term oral toxicity, are Cu-ENMs still present in rats tissues? Is it possible to quantify Cu-ENMs residues by conventional analytical techniques?
4. Can a Safe-by-Design approach reduce the toxicity of Cu-ENMs?

The thesis is made up of four chapters, the first of which is an introduction to the topics covered, while the other chapters explore in deep aspects such human and environmental exposure, and advance analytical techniques for analyzing the nanoparticles transformations in real biological media. Specifically:

Chapter 1 describes briefly ENMs, their basic properties and their use in commercial products. After this short introduction, it illustrates in detail the intrinsic properties of inorganic ENMs and the state-of-the-art of the advanced techniques used for their detection and quantification in complex matrices. Then, the chapter focuses on Cu-ENMs, presenting the current knowledge about their transformation and behavior in biological and environmental media, together with the associated toxicological aspects. A brief description of the European projects studying these materials is also included.

Chapter 2 describes the investigation on the behavior of Cu-ENMs in biological and environmental media and is divided in two main sections. The first one presents a study about the dissolution of CuO ENMs in environmental media, performed within the European project NanoFASE, while the second one includes a peer-reviewed paper focused on the colloidal characterization of modified CuO ENMs in biological and environmental media.

Chapter 3 illustrates the research activity carried out to investigate the toxicological effects of different copper-based ENMs in rats and to evaluate their bioaccumulation in rat tissues. It describes the toxicological tests performed within the European project SUN; in particular, it reports the bioaccumulation data related to the in-vivo short-term inhalation study using modified CuO ENMs, and a peer-reviewed containing the data concerning an in-vivo short-term oral study using both CuO and $Cu_2CO_3(OH)_2$ ENMs.

Chapter 4 reports further research aimed at implement the findings about Cu-ENMs bioaccumulation in rat tissues. Specifically, analytical techniques such as sp-ICP-MS and electron microscopy have been employed in an attempt to detect and quantify CuO and $Cu_2CO_3(OH)_2$ still present in liver of rats as nanoform.

My contribution to the papers presented within this thesis is specified in a footnote at the beginning of each section containing the articles.

Chapter 1

Introduction

1.1) Inorganic ENMs in commercial products

1.1.1 Definitions

All natural systems, both aquatic and terrestrial, contain small particles, covering the size range from 1 nanometer to several micrometers. Particles in the range from 1 to 1000 nm are defined as colloids, and they show in solution different properties and behavior compared to dissolved species (<1 nm) and particles with sizes higher than 1000 nm.[1] Within this colloidal fraction, the European commission defined nanomaterials as:

"A natural, incidental or manufactured material containing particles, in an unbound state or as an aggregate or as an agglomerate and where, for 50 % or more of the particles in the number size distribution, one or more external dimensions is in the size range 1 nm - 100 nm. In specific cases and where warranted by concerns for the environment, health, safety or competitiveness the number size distribution threshold of 50 % may be replaced by a threshold between 1 and 50 %. By derogation from the above, fullerenes, graphene flakes and single wall carbon nanotubes with one or more external dimensions below 1 nm should be considered as nanomaterials".

According to this definition, nanoparticles can be further classified into three main categories based on their source: naturals, incidentals and engineered.
Regardless the source, physical and chemical properties of nanoparticles are strongly dependent on the sizes, shapes, compositions, and structures of the nanocrystals. Interesting phenomena such as remarkable increase in surface-to-volume ratio, significant change in surface energy, and quantum confinement effects occur when a bulk material is reduced to nanoscale dimension.[2,3,4] Moreover, particles in the nano-range can move inside a fluid by Brownian motion, without been affected by gravity; on the contrary, large particles exhibit sedimentation.

1.1.2 Formulation of inorganic ENM in commercial use

The rational control of the nanoparticles surface properties leads to the production of new materials that can be added at the everyday-life objects for improving their properties (i.e. resistance, strength, brilliant colors, UV-Vis reflection, ecc). These engineered nanomaterials (ENM) are already presents in consumer products, and their trade has reached remarkable values.
In fact, as it is reported in the literature (2011), the worldwide demand of nanomaterials has reached $2 billion in 2011, $ 3.6 billion in 2013 and it is expected to reach $ 34 billion in 2025 (Freedonia Group Report). In order to classify and track these new materials in the market, several inventories have been made; the most frequently cited is the Consumer Product Inventory (CIP) that reports 1827 commercial products containing ENMs.[5]

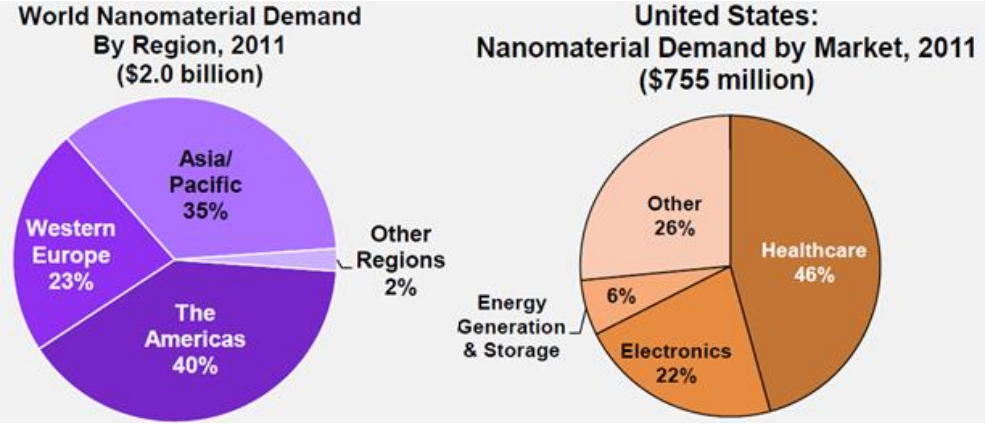

Figure 1 A) Worldwide market distribution of ENMs; B) USA ENMs Market sectors (from Freedonia Group Inc)

United States has the largest market of ENMs, with 773 consumer products available, 290 companies and 40% of the world trade of ENMs (Figure 1A). As it is reported in CIP, the health and fitness products cover more than 40% of listed products while electronics and other application cover each one the 20%. Within the health and fitness products category are grouped ingredients for pharmaceutical purposes (e.g. drug delivery system, therapeutic agents, dental products) but also personal care products (e.g. toothbrushes, hairstyle products, cosmetics, and sunscreen) and clothing (Figure 1B).[5]

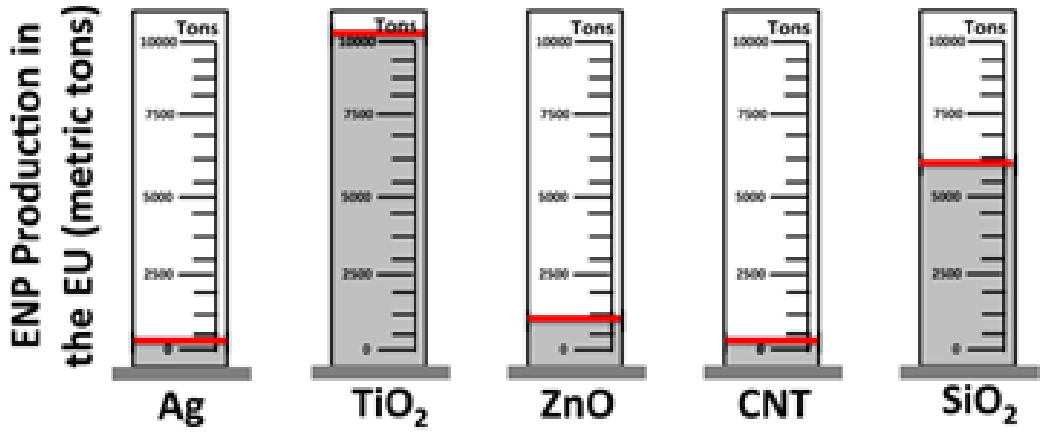

Figure 2 ENMs production (from Mitrano et al 2015) [6]

Mitrano et al. (2015) reported that metal oxides such as silicon dioxide (SiO_2), titanium dioxide (TiO_2), and zinc oxide (ZnO) are the most widely produced nanomaterials on a global scale (on mass basis) Figure 2.[6] Besides them, silver is the most frequent ENMs that can be find in the products listed in CIP (24%). It is also reported that the 31% of the products listed in CIP apply ENMs as antimicrobial protection, while both material-coating and environmental treatments, cover the 15% each one (Figure 3).[5]

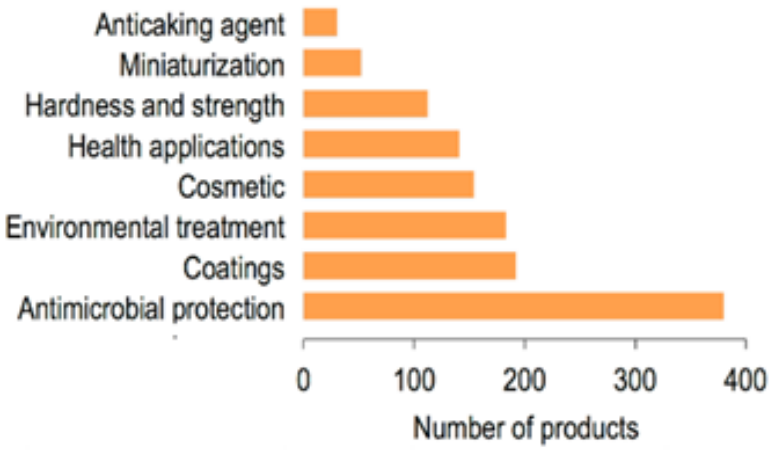

Figure 3 ENM application fields (from Vance et al 2015) [5]

According to CPI, resulted that ENMs are suspended in fluids (e.g. water, oil, lubricant, and lotion) in about 29% of consumer products, while in the 17% they are bound at their surfaces. The most part of these ENMs are composed by metal and metal oxide nanomaterials. In Figure 4, the concentration range (% by weight) of the most common ENMs present in commercial products and their applications are reported.

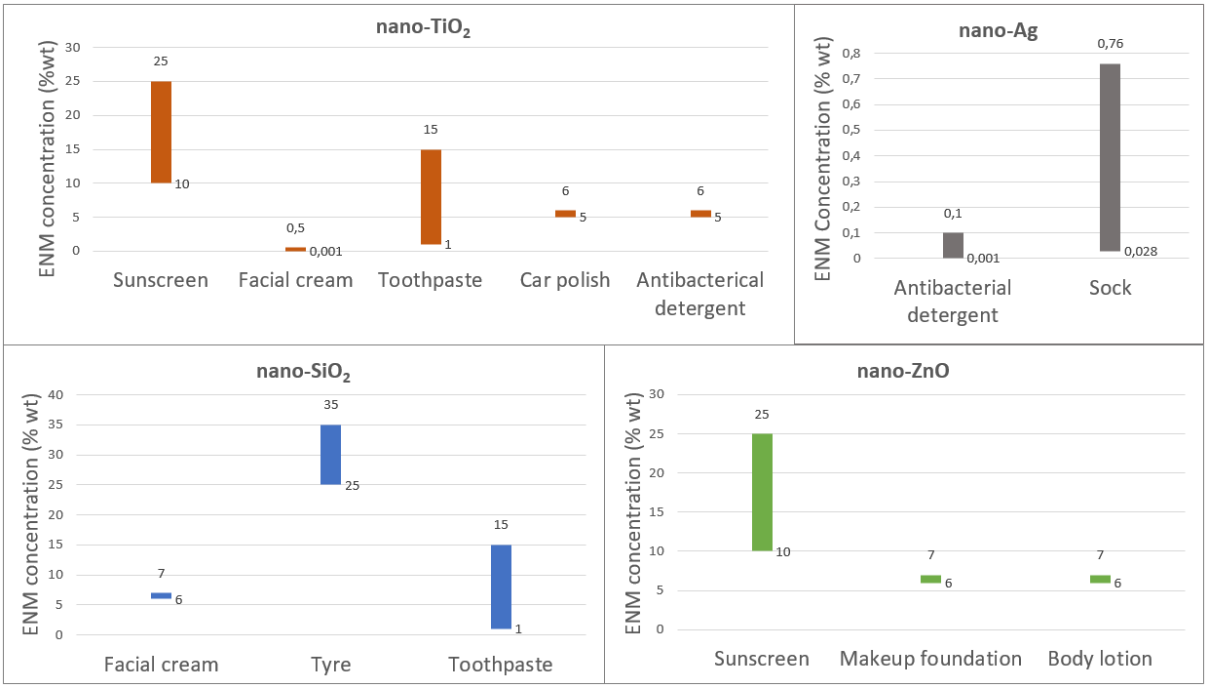

Figure 4 Concentration ranges of nano-scale TiO_2, SiO_2, ZnO, and Ag in different consumer product categories [7]

1.2) Inorganic ENMs properties and analytical techniques

As is widely reported in the literature, compared to bulk materials, due to their large surface-to-volume ratio, nanoparticles exhibit remarkable physical and chemical properties such as high surface reactivity and quantum effect.[8,9] Understanding the interaction between nanoparticles and other entities (i.e. biological molecules, nanoparticles of the same type or completely different), become essential for the assessment of the transport and fate of ENMs and their transformation. Nanoparticles are entities that can move in a liquid by Brownian motion without being affected by the gravity, that instead leads to the sedimentation of any other suspended material with a size higher than 1000 nm. It is clear, that the mechanisms involved for describing their behavior can be considered a hybrid between what happened at the atomic level and at the macroscopic level, thus allowing to use the mathematical tools already present.

1.2.1 DLVO theory

Particle-particle interaction and particle-surface interaction have been described by the Derjaguin – Landau – Verwey – Overbeek (DLVO) theory, but forces such as steric, magnetic, and hydration forces can also play an important role in the aggregation and settling of ENMs.[10]

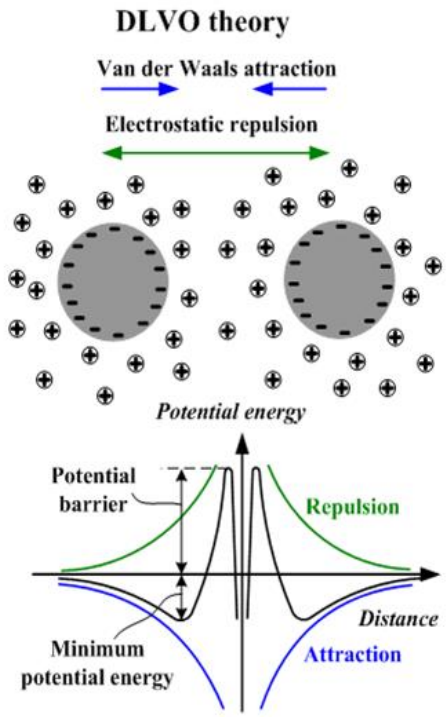

Figure 5 Graphical representation of DLV theory (from Israelachvili et al. 20111)

In DLVO theory, two forces determine the stability of particles: van der Waals attraction (vdW) and electrical double layer repulsion (EDL). The attraction or repulsion between two particles or particle surface (W_D), depends on the sum of these two forces. Petosa et al. (2010) reported a list of detailed equation that can be used for calculating the particle-particle and particle-surface interaction[10] (Figure 5)[11]. The main parameters involved in these equations are radius of the particle, the surface charge, the distance between two particles and other medium/particle constants.[12]

$$W_D = vdW + EDL$$

Equation 1 DLVO theory

An integration to the above equation is given by the addition of the steric force that take into account the adsorption of polymers or surfactants, magnetic dipole moment for magnetic ENMs, and hydration energy that consider the amount of water adsorbed on ligands such as, for example, proteins. In literature there are also described other variations of this equation, but for simple applications, DLVO it is still the most used.

Modelling the behavior of ENMs is fundamental for predicting fate and transport of ENMs in the environment since, as reported before, they can interact with a wide range of substances

that can alter their aggregation state, composition, concentration and size. For this reason, characterization by suitable analytical techniques play a key role in the nanoparticle study and development.

1.2.2 Analytical methods for inorganic ENMs characterization

The growing demand of ENMs in commercial products, has led the scientific community to develop new analytical techniques (or adapt existing ones) to evaluate the behavior of these analytes in increasingly complex matrices. However, while in the past the attention was focused on the characterization of newly developed ENMs, which means characterization of homogenous systems at high concentrations and without the presence of complex matrices, nowadays the analytical challenge involved the detection and the quantification of ENMs at low concentration in complex matrices (i.e. biological or environmental matrices),[13] (Figure 6).

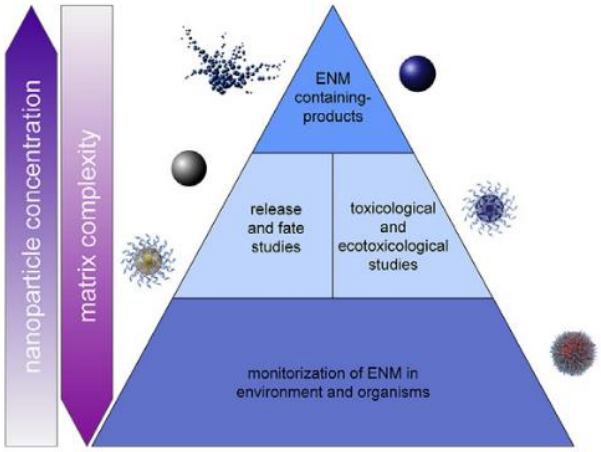

Figure 6 Complexity on ENMs analysis (from Laborda et al 2016) [13]

The information required for the characterization of ENMs, independently from the complexity of the matrices, can be quantitative (e.g. mass concentration, number concentration) or qualitative (e.g. core and coating composition, size, shape, aggregation/agglomeration)(Figure 7). Besides this, if ENMs show additional properties resulting from e.g. dissolution or redox activity, more information must also be provided.

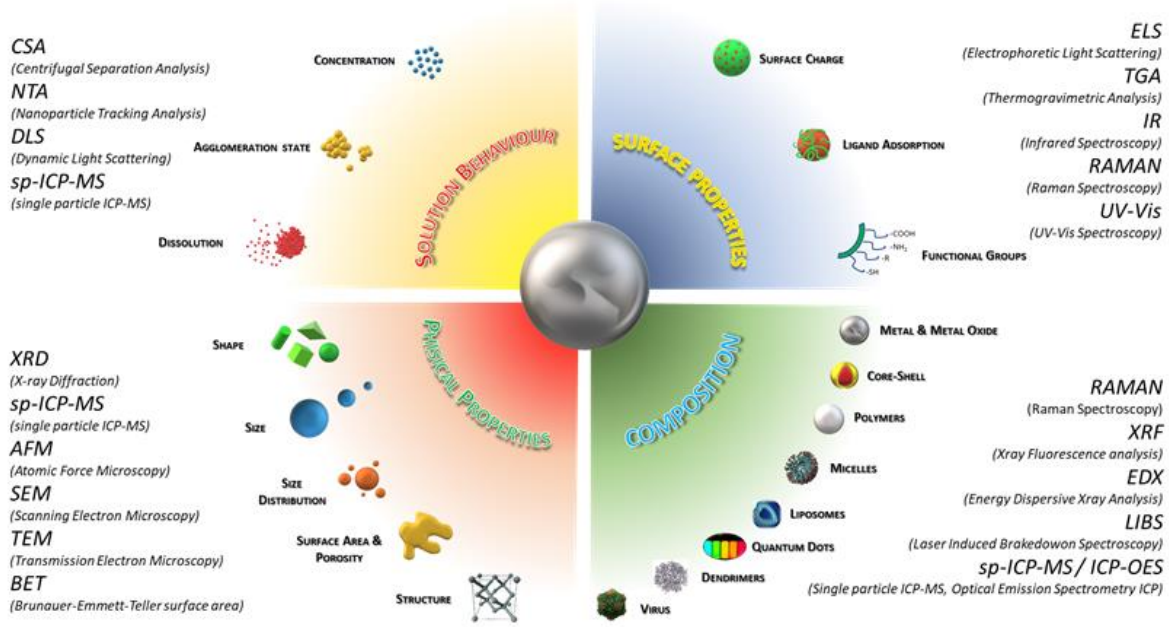

Figure 7 ENMs characterization techniques

1.2.2.1 Sample preparation

In most cases, when real samples containing ENMs must be analyzed, a sample pre-treatment is required prior to the direct analysis, in order to remove the possible interferences from the matrices.

The pre-treatment selection depends mainly on the type of ENMs and matrices to be removed. Acidic digestion of solid samples leads to the total destruction of the matrices and, in most cases, to the ENMs. This strong procedure is usually applied to get quantitative information of the ENMs content in the sample, or for the extraction of insoluble ENMs (e.g. SiO_2) from weak matrices (e.g. biological tissue).[14,15]

For organic matrices, as an alternative to the acidic digestion, a softer alkaline or enzymatic digestion is often employed by using tetramethylammonium hydroxide or proteases respectively. Performing this pretreatment, ENMs can be released intact from the matrices, allowing the direct detection, quantification and size characterization of the particles.[13,16,17]

Centrifugation and dialysis/ultrafiltration are the common approaches to isolate ENMs from an aqueous suspension containing dissolved species. Centrifugation involves the relation between the centrifugal force applied to the particles and other parameter describe in the equation below:

$$D = \sqrt{\frac{18\eta \ln\left({R_f}/{R_i}\right)}{\omega^2 t\left(\rho_p - \rho_f\right)}}$$

Equation 2 Centrifugal settling equation

where D is the minimum diameter of the particle settled, η is the dynamic viscosity of the fluid, R_f and R_i are the final and initial radius of rotation respectively, ρ_p and ρ_f are the density of the particle and fluid, ω is the angular velocity and t is the time required to settle from R_i to R_f.

Equation 2 is a modification of Stokes law, and it is commonly used for both the purification of proteins or particles and the centrifugal separation analysis (CSA). Result clear that knowing particle, fluid and centrifuge parameters it is possible to settle the whole suspended particulate or fractionize it only by acting on time or angular velocity.

On the contrary, ultra-centrifugation and dialysis use a nanoporous membranes made of different materials with a well define cut-offs. Also in this case, this procedure is used for the isolation of nanoparticle from dissolved species, especially in ENMs dissolution study.[18]

1.2.2.2 Analytical techniques

Electron microscopy

The capability to visualize nanoparticles, leads the electron microscopy as one of the powerful techniques for the ENMs analysis; the direct visualization of the particles allows to obtain information on their size, size distribution and shape. In addition, Scanning Electron Microscopy (SEM) and Transmission Electron Microscopy (TEM) can be equipped with Energy

Dispersive X-ray spectroscopy module (EDX) to semi-quantify the elemental composition of ENMs.[19] TEM can also be equipped with Electron energy-Loss Spectroscopy (ELS) in order to obtain information regard crystal structure, chemical composition and elements oxidation state. Electron microscopy can be very useful to gain information regarding size and shape, but it cannot be used for quantification, because to have a statistically significant value, a high number of particles should be sized and counted, making this operation dramatically time-consuming.[13]

For the microscope analysis, sometimes a sample pre-treatment is needed, as in the case of biological tissue imaging[20,21], or to study agglomeration state; in the latter case in fact, the drop deposition of the solution containing ENMs, followed by evaporation, can lead to the formation of aggregates changing the particle size distribution. To avoid this phenomena, the grid's surface where the drop is deposited, can be treated with a substance that via electrostatic interaction fix the particles reducing the "evaporation induced aggregation" effect. Other fixation methods are also reported such as water-soluble resins to embed the particles, or the cryofixation.[2]

Light scattering

Photon correlation spectroscopy, better known as Dynamic Light Scattering (DLS), is maybe the most common technique used to characterize ENMs in liquid suspension. The interaction between light and particle is used to calculate the diffusion coefficient (D) of a particle that is moving in the solution by Brownian motion:

$$d_h = \frac{K_B T}{3\pi\eta D}$$

Equation 3 Stock-Einstein equation

The Stock-Einstein equation (Equation 3) predicts the behavior of a particle having a diffusion coefficient D and a hydrodynamic diameter d_h (where d_h is the diameter of a sphere with the same diffusion coefficient D of the particles investigated), which is moving in a fluid with viscosity η at the temperature *T*. The diffusion coefficient is the variable measured by the correlator by recording the time-dependent fluctuation of the light scattering intensity, caused by the interaction between the particle and the light itself. Unfortunately, the scattering intensity depends by the sixth power of the particle diameter, and if heterogeneous size distribution is present (typical of real samples), smaller particles cannot be distinguished among bigger particles, making the data difficult to interpret.[22,23] However, coupling DLS with a size separation technique can be helpful to overcome the problems related to the polydispersity interference. Another drawback of this technique is the range of applicability in terms of concentration, in fact DLS works at concentrations far above the concentration of ENMs that can be found in the environmental (mg/L instead of ng/L and sub ng/L).

Nanoparticle Tracking Analysis (NTA) is another interesting light scattering technique, which allows to study the size and size distribution of ENMs in solution. NTA employ a video microscopy to record a video of the particles motion that is than processed to obtain the

diffusion coefficient. NTA track and elaborate the motion of individual particles, in this way the analytical data is not affected by the polydispersivity (or aggregation state) of the samples. Moreover, NTA can also be used to quantify the ENMs in terms of particle-number concentration, but, data obtained from particles with sizes below 10 nm might be not reliable.[13]

Atomic spectrometric and spectroscopic techniques

These techniques can be used to quantify the elements present in the ENMs investigated. One of the main techniques used nowadays, is Inductively Coupled Plasma Mass Spectrometry (ICP-MS), due to the lower detection limit (sub ng/L) and reliability of the analytical data. It is worth pointing out that the data obtained are not specific for the particles, and information such as size, size distribution, or the physical state (ionic or particle) cannot be achieved. However, this technique can find significant application in bioaccumulation and biodistribution studies,[24,25] with the possibility to extend its field of use by coupling it with an apparatus for the size separation.

Single particle ICP-MS

Single particle ICP-MS (sp-ICP-MS) is a specific analytical method based on the time-resolved analysis of the sample followed by the deconvolution of the resulted "intensity vs time" plot (Figure 8); providing information such as composition and density of ENMs, it is possible to obtain the number base particle concentration and calculate the size and size distribution.[26]

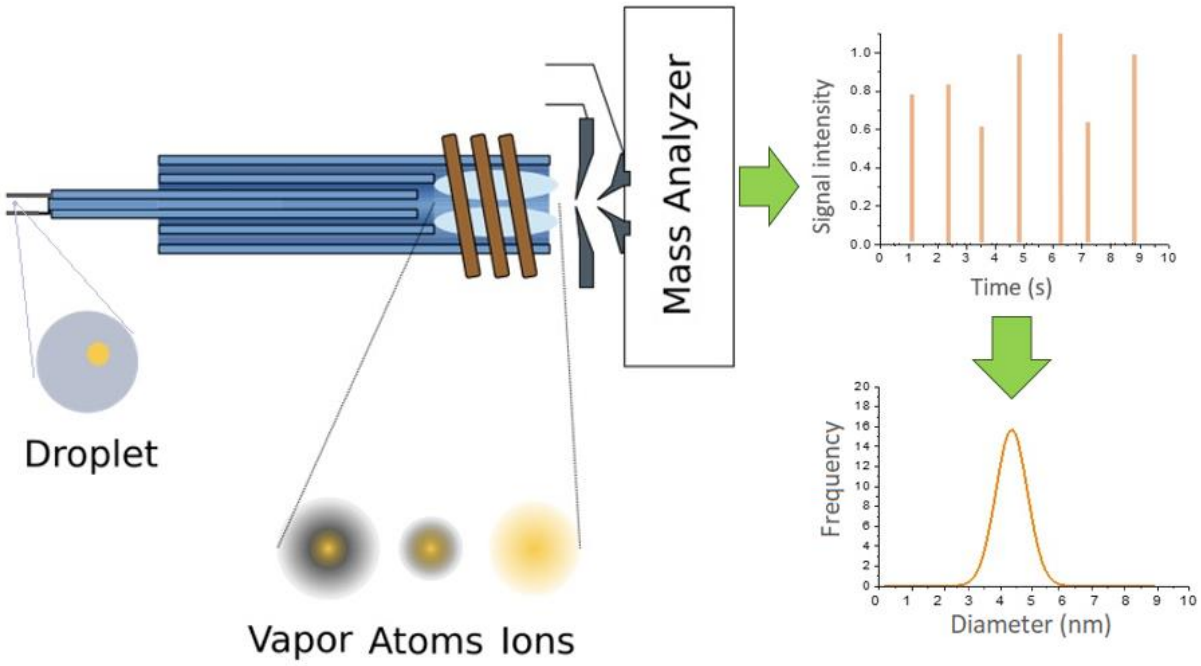

Figure 8 sp-ICP-MS working

This mode of analysis can estimate the number of particles at very low concentration (10^8 part/L) whereas the size detection limits can be respectively 2 nm for mono-elemental and 100 nm for oxides. Size detection limit mainly depends on parameters such as the density, the

relative abundance of the isotope chosen, the mass fraction, the ionization efficiency and the presence of isobaric interference. The detection limits of different elements evaluated by sp-ICP-MS is reported in Figure 9.[27]

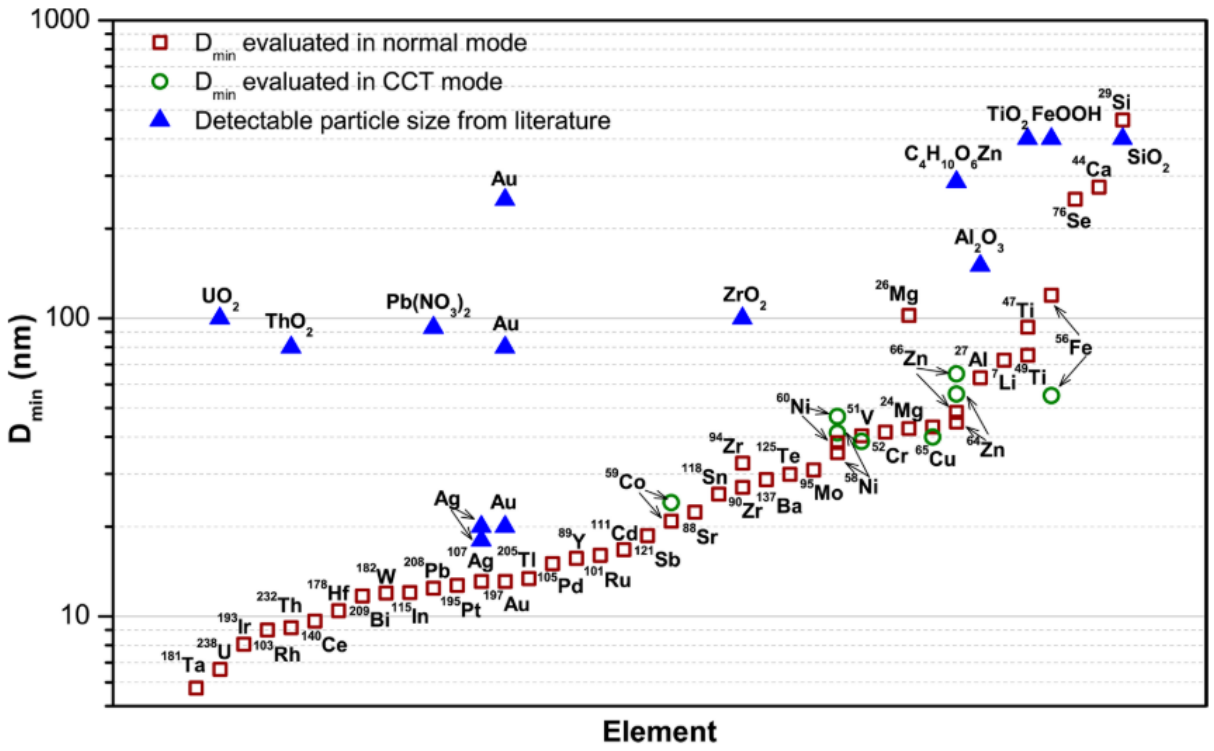

Figure 9 Evaluated DL_S of spICP-MS for 40 elements and reported detectable sizes of some nanoparticles from previous literature. All the evaluated DL_S measurements are performed by assuming single element nanoparticles (from Lee et al. 2014)

The equation below is the mathematical relationship for the conversion of the raw data into size and size distribution:

$$d = \sqrt[3]{\frac{6\eta I_{NP}}{K f_a \rho \pi}}$$

Equation 4 Relationship between Intensity and diameter for sp-ICP-MS analysis

where d is the diameter of an equivalent sphere (nm), I_{NP} is the intensity in count per second (cps) at the detector for each nanoparticle, η is the transport efficiency (TE) in %, K is the slope of the calibration ionic curves of the element analyzed (cps/µg), f_a is the mass fraction of the element in the particle and ρ is the density of the particle.[27]

sp-ICP-MS provides the equivalent spherical diameters calculated on the ENMs parameters described above; if the particle has a sphere-like shape, the diameter obtained by sp-ICP-MS coincide in good agreement with the diameter provided by TEM or SEM. Anyway, by modifying the Equation 4 it is possible to convert the equivalent spherical diameters to particles with other shapes. Recently, Kalomista et al. (2017) reported an additional elaboration of the raw data for the estimation of both the dimensions of gold nanorods.[28]

From equation 4 it is clear that the cubic relation between the diameter and the other parameters strongly affects the size limit of detection (DL_s) and requires huge instrumental development in order to reach the same DL_s of electron microscopy (<1 nm).
This promising technique leads to analyze complex matrices because its ability to detect and quantify ENMs in samples at low concentration, a simply diluting can drastically reduce the matrices interference effects.
Moreover, by sp-ICP-MS it is also possible to analyze biological samples after a pre-treatment of the sample which can be performed via alkaline or enzymatic digestions.[16] Examples are reported in the literature concerning food matrices spiked with ENMs and tissues of organisms exposed to nanoparticles. [29–32]
From the environmental point of view, sp-ICP-MS has been applied to study the behavior and fate of silver ENMs in lake water,[33] washing solutions from commercial detergents,[34] and wastewater from wastewater treatment plants (WWTP).

X-Ray Absorption Spectroscopy (XAS)

Another atomic technique for the characterization of ENMs in complex matrices, is the X-Ray absorption spectroscopy (XAS) that includes XANES and EXAFS; these technologies can provide information about metal/ metalloid species and their quantitative distribution, although not about their nanoparticle parameters, with minor or no sample preparation. In the literature are reported XAS analysis of matrices such as soil, road dust, plant tissue and sludge.[35–37] The use of XAS is limited by the needed of synchrotron radiation facilities, and the relative sensitivity (mg/Kg).

Electroanalytical techniques

Voltammetry of Immobilized Particles (VIP) and Particle Collision Coulometry (PCC) are two electroanalytical techniques specifically developed for the analysis of ENMs. Nowadays these cost-effective and efficient analytical techniques are not full employed, but in the future they might find more applications.[13]

In Table 1 are reported some analytical application of the techniques described above.

Table 1 Application case studies for analytical techniques involved on the detection of ENMs in commercial product, Environmental samples and ecotoxicological/ toxicological tests.(from Laborda et al. 2016)[13]

Technique	Application	Sample	ENM
Electron microscopy TEM/SEM	Consumer products	Disinfectant	Ag, ZnO
		Dietary supplements	Au
		Bread and bisquits	metal NPs
		Coffee creamer	SiO_2
		Sunscreen	TiO_2, ZnO
	Ecotoxicological/Toxicological studies	Plant tissue	Ag, TiO_2
	Environmental samples	Washing water	Ag
		Waste water	SiO_2, Al_2O_3
		Sewage sludge	TiO_2
Atomic spectrometry (only ICP-MS is considered) (*=sp-ICP-MS)	Consumer products	Dietary supplements	Ag*, Au, Pt
		Antibacterial products	Ag
		Healthcare formulation	Ag
		Coffee creamer	SiO_2
		Sunscreen	TiO_2, TiO_2*, ZnO
	Ecotoxicological/Toxicological studies	Gastrointestinal tract Gills	Ag
		Lumbriculus variegatus	Ag
		Biological tissue homogenate	Ag*
		Human epatoma cells	Ag
		Feces (rat)	Ag
		Various organs (rat)	Ag*, Ag, Au
		Daphia Magna	Ag*
		Plant tissue	Au*
	Environmental samples	Washing water	Ag
		Waste water	Ag*, CuO
		Lake water	TiO_2, TiO_2*
Electroanalytical technique	Consumer products	Healthcare formulation	Ag
		Disinfectant	Ag

1.2.2.3 Separation techniques

As reported in the previous section, sometimes samples are so complicated, due to matrices interference or polydispersivity (or both), that a separation prior to analysis is required. Most of the separation techniques can work online with the detectors described above, but also off-line by collecting the fractions and analyzing them in a second time.

Field-Flow Fractionation (FFF)

Field-Flow Fractionation (FFF) is the widely applied separation technique. According to the Stoke-Einstein equation, particles with different diameters, shows different diffusion in liquid media. If heterogeneous nanoparticles distribution are flowing in a laminar flow, and a

perpendicular stimuli is applied (crossflow for asymmetrical FFF, centrifugal force for centrifugal-FFF, thermal gradient for thermal-FFF), the particles can change their spatial location on the flow profile, moving from the faster layer in the middle towards the slower layer near the wall of the channel. As consequence some particle are decelerate and a delay in the exit of the particle populations is observed (Figure 10).

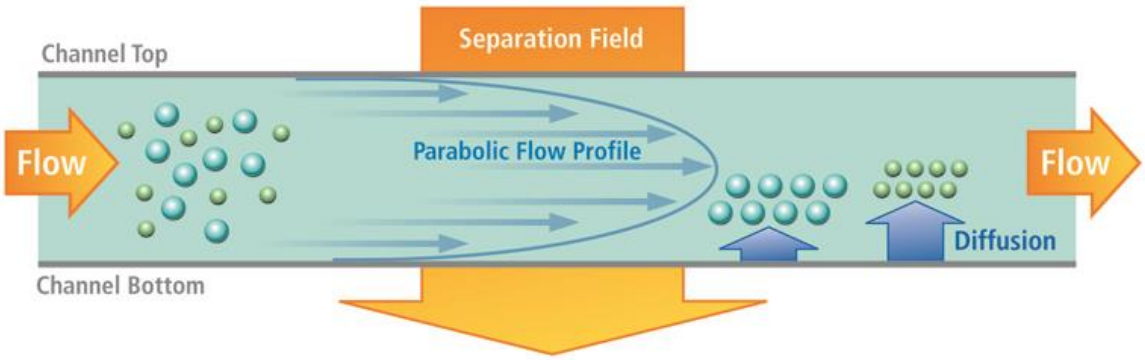

Figure 10 Field-Flow Fractionation working

Although FFF can be used to treat several materials (polymer, biomolecules, ENMs), recoveries below 80% in quantification are reported.[38–41] This limits the application to a qualitative approach. Usually FFF is hyphenated to elemental detectors such ICP-MS/ICP-EOS,[41,42] but can be also coupled to UV-Vis and DLS [43].

Other separation techniques

Among the other separation techniques, the more relevant are Gel Electrophoresis (GE), Capillary Electrophoresis (CE), Hydrodynamic Chromatography (HC), Size Exclusion Chromatography (SEC) and Gel Permeation Chromatography (GPC). As for FFF, the partial adsorption of the ENMs on to the stationary phases limit these techniques to a qualitative application.[13]

Depending on the complexity of the matrices, and the type of information needed, one or more techniques can be used to reach the goal. Usually for inorganic ENMs in complex matrices, the combination of sp-ICP-MS and TEM is reported as a high throughput tool for their detection, quantification and characterization (size, shape, aggregation state).

In Table 2 analytical information and detection/quantification limits (LOD/LOQ) for each techniques are summarize.

Table 2 LOD and LOQ for the techniques used in the ENMs characterizations.(from Laborda et al. 2016)[13]

Technique	Acronym	Size LOD	Concentration LOD	Analytical information
Electron microscopy				
Transmission electron microscopy	TEM	<1 nm		- Size (average and distribution)
				- Shape
				- Elemental composition (+EDS)
				- Chemical structure (+EELS)
				- Crystal structure (+SAED/CBED)
Field-emission scanning electron microscopy FESEM	FESEM	1 nm		- Size (average and distribution)
				- Shape
				- Elemental composition (+EDS)
Environmental scanning electron microscopy	ESEM	30 nm	10^{12}/L	- Size (average and distribution)
				- Shape
Light scattering				
Dynamic Light Scattering	DLS	1 nm	mg/L	- Size (average and distribution)
Nanoparticle tracking analysis	NTA	20 nm	10^{9}/L	- Size (average and distribution)
				- Number concentration
Atomic spectrometry				
Inductively coupled plasma mass spectrometry	ICP-MS	-	ng/L	- Bulk element composition
				- Total mass concentration
Single particle ICP-MS	sp-ICP-MS	2-100 nm	10^{6}/L	- Detection of dissolved element/NP
			ng/L	- Element mass per NP(average and distribution)
				- Size (average and distribution)
				- Number concentration
				- Mass concentration
				- Chemical composition
				- Identification/quantitative distribution of chemical species

Electroanalytical techniques					
	Voltammetry of immobilized particles	VIP	10nm	µg/L	- Element composition
					- Oxidation state
					- Size (average)
					- Mass concentration
	Particle collision coulometry	PCC	5 nm	10^{10}/L	- Detection of NPs
					- Size (average and distribution)
					- Number concentration
					- Mass concentration
Separation techniques					
	Asymmetric field-flow fractionation	AF4-ICP-MS	1-5 nm	1-10 µg/L	- Detection of complexed elements/NP
		AF4-UV-Vis		0,1 mg/L	- Size (average and distribution)
		AF4-DLS		1 mg/L	- Mass concentration
	Capillary electrophoresis	CE-ICP-MS		0,2 µg/L	- Detection of complexed elements/NP
					- Size (average and distribution)
					- Mass concentration
	Hydrodynamic chromatography	HDC-ICP-MS		1 µg/L	- Detection of complexed elements/NP
					- Size (average and distribution)
					- Mass concentration

1.3) Copper based nanomaterials (Cu-ENMs)

Among the transition metal oxides, Copper oxide (CuO) is one of the most studied material because of its interesting electronic properties as p-type semiconductor.[44,45] For this reason, CuO finds several applications in the fields of: materials for the next-generation rechargeable lithium-ion batteries, solar cells and gas sensors,[46] photodetectors,[47] field emissions,[48] supercapacitors,[49] photocatalysis,[50] and magnetic storage media [51]. Recent studies reported that CuO nanocomposites is also active in catalytic oxidation of CO and NO and volatile organic chemicals such as methanol [52,53] and other inorganic pollutants [54,55]. Moreover, CuO ENMs, but in general the copper-based ENMs, showed interesting behavior in application such as self-cleaning coatings (anti-biofouling), surface protection, textiles treatments, water movement, oil–water separation, antibacterial and antifungal treatment. [56,57] Cuprous oxide (Cu_2O) is another important ENMs that shows interesting electronic properties, but differently from CuO is less stable and this limits its practical applications.

The copper-based engineered nanomaterials (Cu-ENMs) annual production was estimated to be 570 tons/year in 2014 but the forecast predict a value of ca 1600 tons/year by 2025. However, in comparison with the global inorganic ENM production, the production of Cu-ENMs is a relatively small fraction.[58]

1.3.1 Synthesis of CuO nanostructures

Nanoscale CuO can be synthetized with several shapes and dimensions by changing the preparation methodology and the related parameters involved; with the opportune productive strategy, it is possible to build-up zero-dimensional nanoparticles, one-dimensional nanotubes, nanowires and nanorods, two-dimensional nanoplates and nanolayers, and several complex three-dimensional structure such nanoflowers, and honeycombs nanostructures. The most common methods include: hydrothermal synthesis, chemical precipitation, electrochemical and thermal oxidation methods. Among these methods, the first two are the most used ones.[51]

Hydrothermal synthetic methods and chemical precipitation methods are often used in the preparation of various metal oxide ENMs with a good control in terms of shape, composition, and reproducibility. In the hydrothermal synthetic method, CuO ENMs are produced in supercritical water condition, with the presence of a copper precursors (i.e. $Cu(NO_3)_2$), a base (i.e.sodium idroxyde, urea) and sometimes surfactants (i.e. cetyltrimethyl ammonium bromide); in this method parameters such as copper precursors type and concentration, pH, growth time and growth temperature, determine the final dimension, shape and size, of the CuO nanoparticles.[51] For example, Chakraborty et al.[59] reported the synthesis of a flower-like CuO nanoparticles by using two different precursors of copper, while Neupane and coworkers[60] have obtained flake-like CuO ENMs by controlling the precipitation temperature; structures such nanorods, nanowires and rectangular shaped nanobat-like are also reported by using this method. Chemical precipitation method is similar to hydrothermal synthesis, but without using supercritic conditions; the benefit of using chemical precipitation, besides

operating in mild condition (temperature around 100°C), is the capability to synthetize complex 2D/3D nanostructures such nanoribbon, nanoring, ellipsoid, flower-like microsphere ecc (Figure 11).[51]

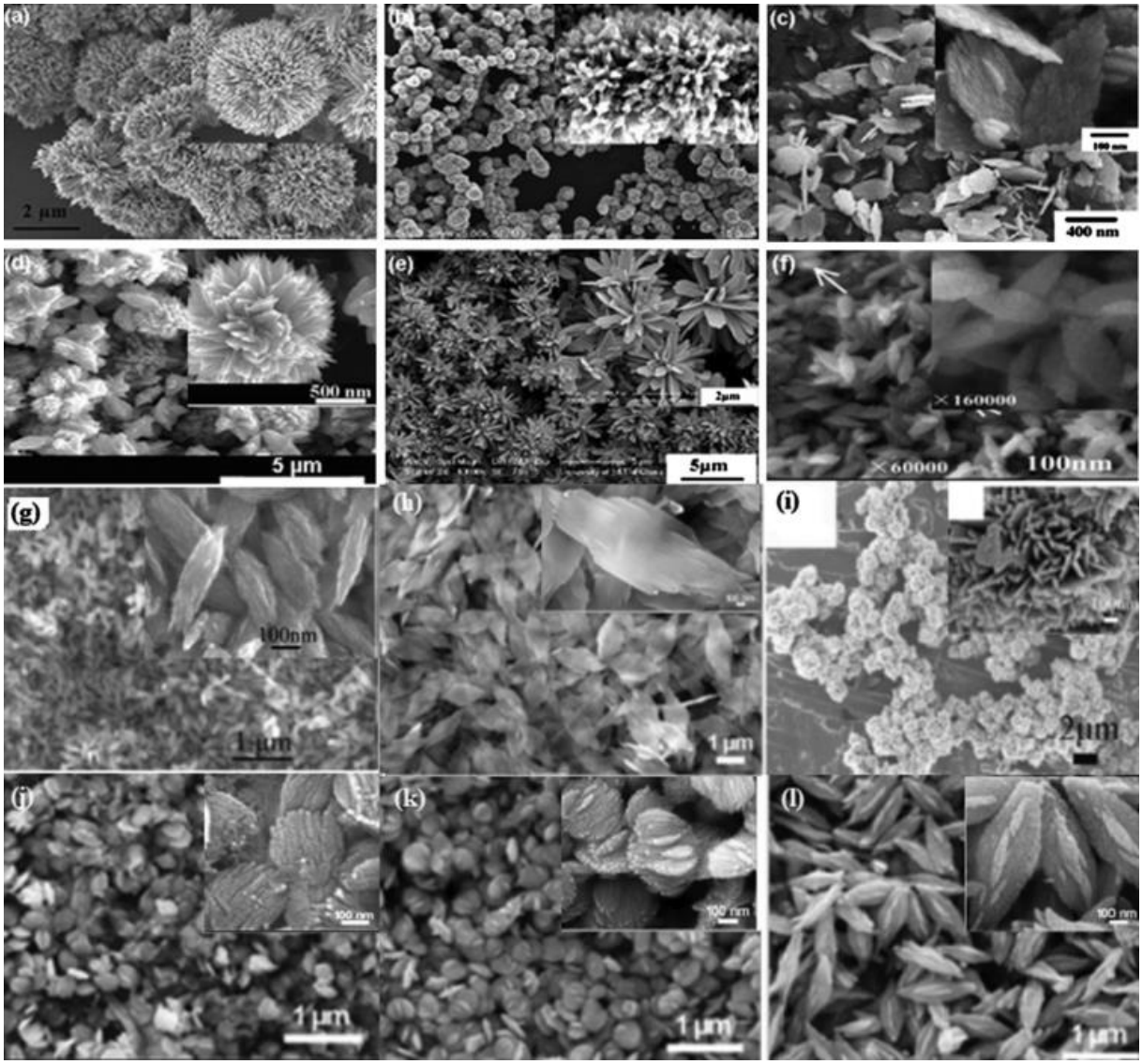

Figure 11 Typical SEM images of CuO synthesis in with different strategies: (a) urchin-like nanostructure, (b) hierarchical nanochains, (c) Nanosheets, (d) flower-like, (e) flower-like assembles, (f) nanoellipsoid, (g) spindle-like, (h) microplates, (i) flower-like microspheres, (j) lenticular-like (k) Pseudo-like, and (l) elliptical-like nanostructure. (from Zhang et al. 2014)[51]

1.3.2 Cu-ENMs for biological applications

The advent of antibiotics in the 1930s has greatly improved the efficacy of the infection treatments, and as consequence the life perspective; unfortunately, the spread of antibiotic resistance forces the scientific community to develop new tools against the pathogenic agents' proliferation.[57] In 2008 EPA officially recognized copper and its alloys as the first effective metallic antimicrobial agent thanks to their ability to kill 99.9% of bacteria within 2 hours. Since now, a lot of studies have been conducted to improve the antibacterial activity of copper, including the development of copper-based nanoparticles. Moreover, recent studies report that Cu-ENMs are active in killing not only bacteria but also fungi and virus, and has been demonstrated that particle size affect their efficacy; indeed, smaller CuO particles

(around 5 nm) can easier penetrate inside the cells than larger particles (around 8 nm), thus showing a better antibacterial activity. [61,62]

The toxicological mechanisms of Cu-ENMs in biological entities (e.g. bacteria, cells, fungi) are still not clear. Espirito Santo et al.(2008-2011)[63,64] showed that the toxic effect towards E. coli is triggered by oxidative damage of membrane phospholipids, resulting in the loss of its integrity; following membrane degradation, copper-released ions can penetrate into the cell and generate Reactive Oxygen Species (ROS), responsible for damage of lipids, proteins, nucleic acids, and sometimes of all the genetic material.[65] Further information on Cu-ENMs biocidal mechanisms is reported in section 5.1 "*Toxicological effects of Cu-ENMs*".
Anyway, the most interesting fact is that all bacteria exposed to copper provide copper-resistance only for a few minutes before death, making Cu-ENMs a suitable material for antimicrobial purposes.

1.4) Transformation and Fate of Cu-ENMs

Significant research has been devoted to characterize the potential environmental and human health impacts engineered nanomaterials incorporated into products extensively used in sectors ranging from healthcare to coatings and paints.[66]

Chemical and physical properties of ENMs depend essentially from the chemical nature of the matter that compose the nanoparticles. The chemical element (and consequently the electronic properties of the element) that build up the ENM, constrains the structure to grow in a well define 2 or 3D structure. Some different crystalline structures can be reach by controlling the energetic pathway during the grown of the nanoparticles. Starting from these principles it is clear that other kind of properties like surface reactivity, solubility, and consequently toxicity are strongly related to the chemical nature of ENM. Moreover, upon entering environmental or biological media, these nanoparticles can change their physical and/or chemical proprieties and partly dissolve.[67] Therefore it is important to consider nanoparticles as dynamic entities that undergo transformations that depend on the pH, ionic strength and composition of the media in which they are dispersed (Figure 12).[68] In particular, the dissolution rate of these NPs in the exposure media can strongly affects the uptake pathway, toxicity mechanisms and the environmental compartment in which NPs may have the highest potential impact.[18]

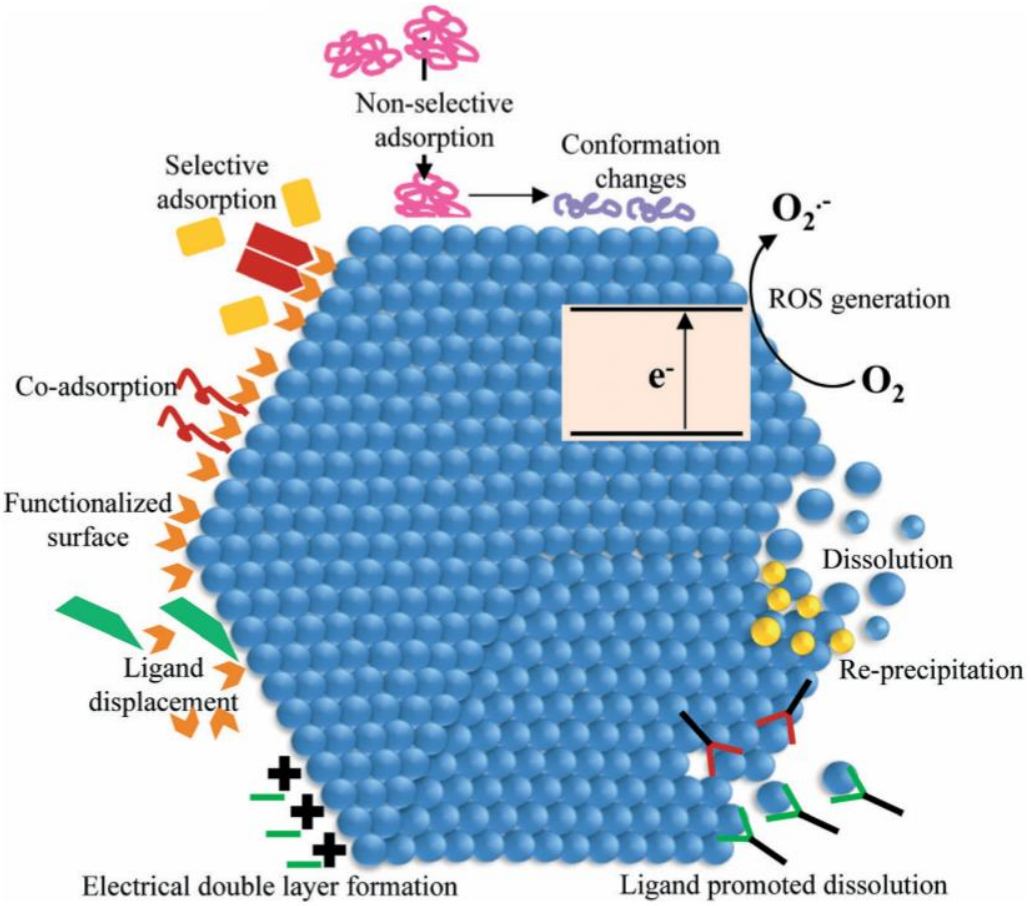

Figure 12 Surface transformation of ENMs in biological and environmental media (from Mudunkotuwa et al. 2015) [68]

1.4.1 Transformation of ENMs in Environmental media: role of pH, organic matter and ionic strength

When performing experiments relevant to natural waters, it can be advantageous to use a medium with an ionic composition as similar as possible to that of the natural water to be studied, but lacking other natural components, such as trace compounds, colloids and organic substances.[69] While seawater has a reasonably constant composition, freshwaters have very different compositions in terms of pH, salts, and organic matter depending on the type of water under examination (i.e. surface water, underground water, wastewater and the geographical source and seasonality). With the aim of standardizing the conditions in the ecotoxicological experiments, protocols for the preparation of Artificial Fresh Water (AFW) and Artificial Marine Water (AMW) have been developed by OECD, as a representative environmental media. These media can be very useful for ecotoxicological purpose, but if water chemistry play a relevant role in the behavior of the system to be investigated, or the experimental design requires to simulate a specific environment, a more specific composition of the medium is needed. Regarding the parameters variability in fresh water, FOREGS database (http://weppi.gtk.fi/publ/foregsatlas/)[70] reports 808 chemical analyses of stream water from across Europe that can be used to summarize the chemical compositions variability of the European streams.

1.4.1.1 pH

From the FOREGS database data (2005), the median pH of the water steams analyzed, shown a median value of 7.7 pH unit (5^{th} percentile= 6.1; 95^{th} percentile= 8.5) by covering in the range between 5 to 8.5 more than 96% of the cases. pH plays the major role in the ENMs transformations because it is responsible of aggregation and dissolution phenomena in water media. According to the DLVO theory, the attraction or repulsion between two particles depends on the surface charge of the particles; by protonating or deprotonating the surface, the electrical double layer can be compressed or expanded causing an increase or decrease in the aggregation phenomena. Berg et al report the relationship between pH and zeta potential of some metal oxide ENMs, and as it was predicted by the DLVO theory, pH far from the isoelectric point decrease the aggregation between the particles (Figure 13).[71]
Moreover, pH is also involved in dissolution processes; in some cases it is able to solubilize ENMs by itself (e.g. CuO and ZnO ENMs), in other cases it works in combination with other reagents (e.g. oxygen with Ag and Cu ENMs).

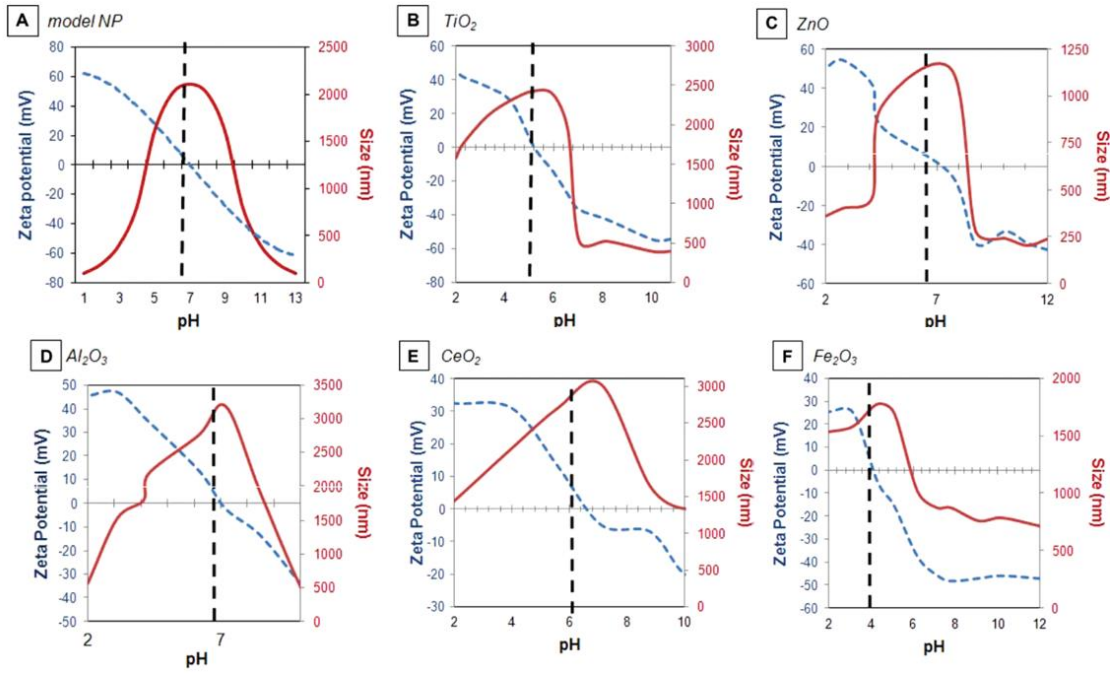

Figure 13 Titration of nanoparticles in ultrapure water (18.2 mW). (A) In a model nanoparticle system, (B) TiO2, (C) ZnO, (D) Al2O3, (E) CeO2, and (F) Fe2O3 from basic (pH > 10) to acidic (pH < 3) conditions. Dashed vertical line represents isoelectric point. (from Berg et al. 2009)[72]

1.4.1.2 Ionic Strength (IS)

Regarding the major ionic contributions, Salminen et al. (2005) reports that the median Ca/Mg ratio of European river waters is 4.48 whit the overall Ca and Mg mean concentrations of 1.36 mmol/L;[70] the amount of Ca and Mg is very fluctuating, reaching value between 0.01 mmol/L and 24.4 mmol/L. Mono and divalent electrolytes can interact with the EDL of the particles by enhancing the aggregation processes.[73,74] According to von der Kammer et al. (2010), divalent cation concentrations exert a dominant influence on the aggregation behavior of nanoparticles since the critical coagulation concentration is proportional to the inverse 6th order of the valency (Schulze-Hardy rule). [75]

1.4.1.3 Dissolved Natural Organic Matter (DNOM)

Dissolved Natural Organic Matter is a natural organic colloid ubiquitous in natural aquatic environments, the main components of which are humic substances (~50%) composed in turn by Humic Acid (HA) and Fulvic Acid (FA).[76] In particular, HA is a heavy (in terms of molecular weight) heterogeneous mixture of organic compounds negatively charged thank to the presence of carboxylic and phenolic groups. In addition, DNOM shows a high seasonal variation related to the activity of the primary production, which is high in spring and low in winter. However, the median value of DNOM for European river waters is 5.39 ppm, ranging between <0.5 ppm and 71.9 ppm.[70] One of the most used reference material for simulate the DNOM in freshwater, is Suwannee River Natural Organic Matter (SR-NOM) from the International Humic Substances Society; SR-NOM is considered as a well-characterized and standardized DNOM.

The surface transformation processes of ENMs influenced by DNOM mainly include adsorption, stabilization/aggregation and dissolution (Figure 14).[67,77] These processes are also influenced by different factors such as ENMs type and water chemistry. Electrostatic attractions play an important role in ENMs–DNOM interaction, especially when pH is higher than pH_{ZPC}. Zhang et al. (2009) for example, described the strong adsorption affinity of some ENMS to DNOM because of the ligand exchange occurring between the carboxyl/hydroxyl groups of DNOM and the hydroxyl groups present on the ENMs surface.[12]

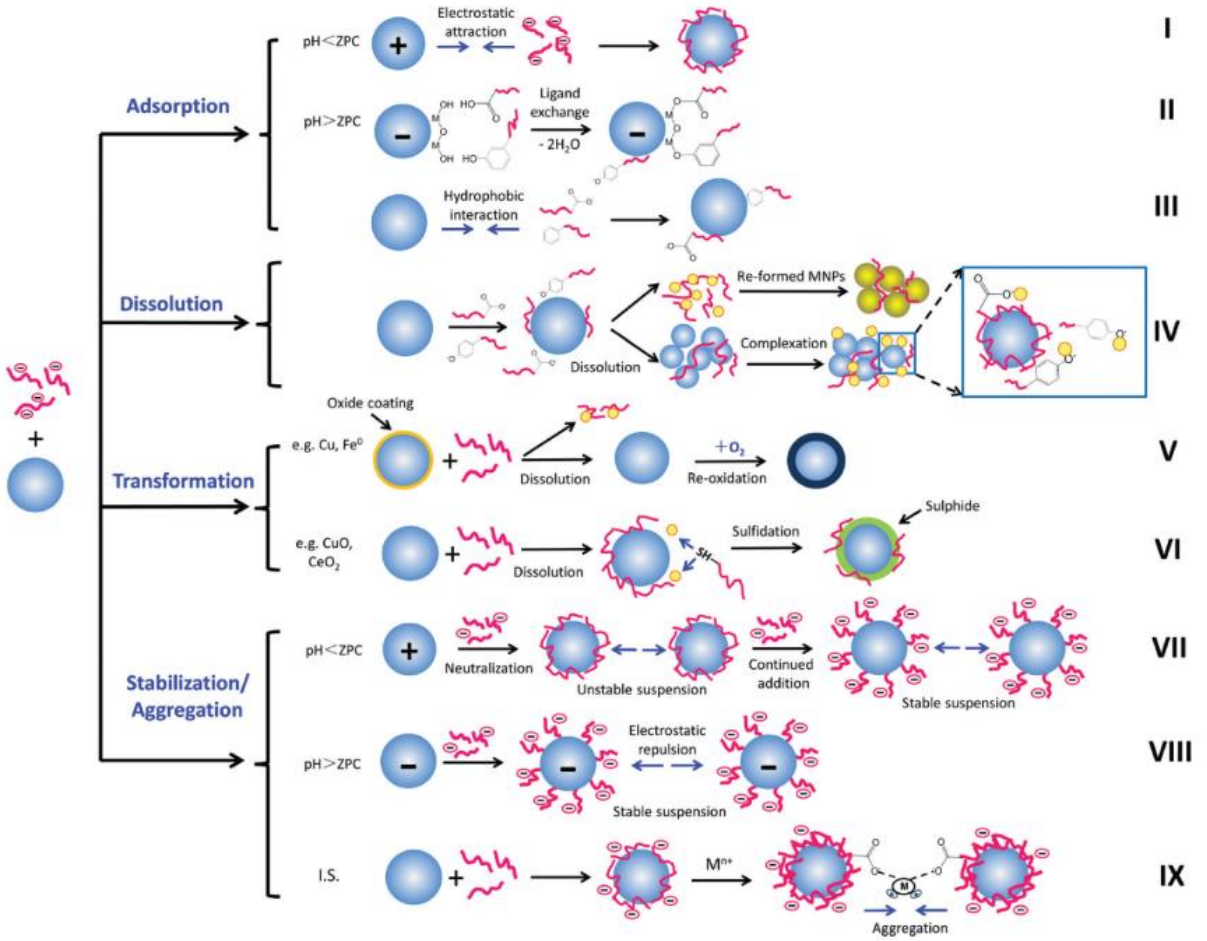

Figure 14 Adsorption (processes I–III), dissolution (process IV), transformation (processes V–VI) and stabilization/aggregation (processes VII–IX) behaviors of MNPs in the presence of NOM. (from Wang et al. 2016) [76]

The importance of DNOM in stabilization of ENMs has also been extensively discussed in literature;[78–80] in particular it is reported that in certain conditions, the DNOM coating around the ENMs (such as ZnO, Ag, SiO_2 and TiO_2) increase both the steric hindrance and the electrostatic repulsions between the particles, leading to a better stabilization.[76] Dissolution can also be promoted by the presence of DNOM; the major contribution is given by the functional groups of DNOM that are able to promote the metal extraction from the surface, but also facilitate the complexation of dissolved metal fractions.[81]

1.4.2 Transformation of ENMs in Biological media: role of biological molecule

Understanding the interaction of ENMs with biological system is the key for a safe application of ENMs in commercial products. While several studies have been conducted to understand

the transformation of nanoparticles in environmental media,[10,67,77] less studies related biological matrices, such as biological media or biological tissue, have been performed. Biological media are surrogate of biological tissues that can be used as simulant for biological fluid in order to testing the transformations of ENMs in vitro, with or without living cell. As well as the chemical properties of tissues and fluids are changing organs by organs, the chemical composition and the related properties of the biological media are changing too, in terms of pH, organic and inorganic ligands (e.g. chlorides, phosphates, carbonates, steroids, amino acids, proteins, lipids...) dissolved. In the literature[82] are present several standard composition of simple biological media that can be prepared to emulate a specific biological context.

1.4.2.1 Protein Corona

Upon entrance of ENMs inside biological environment, a dynamic adsorption/desorption of proteins, lipids, sugars and other complex bio-molecules occurs; this shell of biological molecules is called "protein corona" and its composition depends on both the nature of ENMs and the physical chemical properties of the matrices. The protein corona alters the size and interfacial composition of a nanomaterial, giving it a new biological identity that is what is seen by cells.[83] This new biological identity determines the physiological response of ENMs, including agglomeration, cellular uptake, circulation lifetime, transport, accumulation and toxicity. The proteins adsorption on the surface of ENMs is a thermodynamically driven process called Vroman's effect; this equilibrium is controlled by protein-ENM and protein-protein binding affinities. The proteins that showed high affinity towards the particle surface, form the "hard corona", while proteins that has low binding constant and then can be desorbed or exchanged easily, form the "soft corona"(Figure 15).[83]

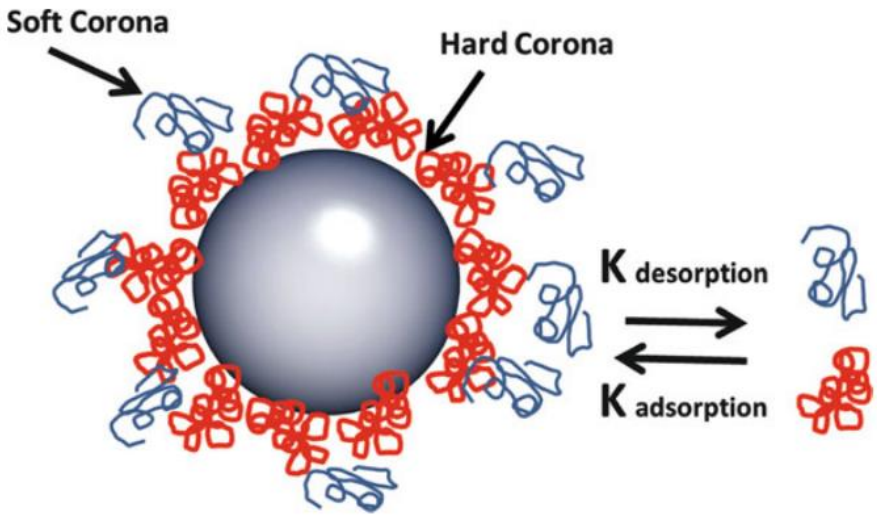

Figure 15 Schematic illustration of soft and hard protein corona. The hard or soft corona is not composed of only a single protein

Aggrwal et al (2009)[84] showed that in the early stage of the corona formation, proteins with high abundance in biological fluids such as albumin, immunoglobulin G, fibrinogen and apoliproproteins are present in the corona of all the studied nanoparticle, while, in the late

stage of the corona's formation (in the time scale of hours-day), a part of these proteins has been replaced by proteins with lower concentration but higher affinity towards ENMs surface. Lundqvist et all [85] studied the protein corona evolution in a simulated process of uptake (transfer from blood plasma to the cytosolic fluid in vitro test), and they showed that hard corona already contained the "proteins fingerprint" of previous environment; this information could be used for reconstructing the pathways of ENMs in living organisms. Unfortunately, Monopoli et al.(2011)[86] reported that protein corona can change significantly between in vitro test (with lower protein concentration) and in vivo tests; this indicates that the in-vitro studies of ENMs are not always able to predict the behavior of ENMs in living biological environments.

As it was introduced above, several parameters are involved in the protein corona formation, but the major contribution in the global binding affinity (of each protein) is given by ENMs surface properties such as hydrophobicity and surface charge. Some studies [84,87] reported that the affinity of proteins to ENMs tends to increase by increasing the surface charge and hydrophobicity of ENMs. It is also described that the presence of polymer coatings in ENMs form a distinct "island" in the particle surface which act as a protein binding site and as a consequence, different polymer functionalization result in major changes in organ/tissue selective bio-distribution and clearance from the body.[83] Moreover, other ENMs properties (i.e. material composition or diameter) have a good relevance in protein corona formation. For example, TiO_2, SiO_2, and ZnO ENMs, besides having a similar surface charge, they bind to different plasma proteins;[88] this evidence can be explained by the different number, spatial distribution and type of active sites present on ENMs surface. Moreover, geometrical properties such as curvature ad particle size can condition the corona formation. Proteins adsorbed to highly curved surfaces has less protein-protein interactions and as result, tend to undergo fewer changes in conformation than those adsorbed to less curved surface. Lynch et al, reported that the amount of bound protein and the thickness of the adsorbed layer increase progressively with nanoparticle size as a consequence of the relative increasing of the available surface area.[89] For this reason, ENMs shape (e.g. spheres, nanorods, plate,..) can also influence the corona composition and their uptake by cells as it was demonstrated by Meng and coworkers (2011)in the case of SiO_2 ENMs.[90]

Proteins corona therefore play a key-role in the biological fate and behavior of ENMs, as in the case of opsonization, where different binding affinity of ENMs surfaces with opsonins ("eat me signal") and with CD47 glycoprotein ("don't eat me signal") leads to different phagocytosis response for macrophages. Therefore, the efficiency and selectivity of this biological labelling allows to ENMs to bypass phagocytic recognition and clearance mechanism or not.[91] In the same way, protein corona can act as "Trojan horse" for ENMs, bypassing the biological defense of the living cell and transporting them in specific target.[91] Furthermore, a change in the hard or soft corona pattern can also change the organ distribution of the ENMs, as it was elucidated by Jansh et al.(2012)[92] in the study of ultrasmall supermagnetic nanoparticles.

As commented above, artificial biological media are simple and suitable systems to reproduce the behavior of ENMs in real biological fluids, but, to assess the fate of these particles, more

complex systems should be taken in account. The presence of complex biomolecules such as enzymes, sugars and proteins, has in fact fundamental implications in fate and transformation of ENMs, without excluding the presence of biological barriers presents in living cells. For this reason, more complex experiments performed by using real biological fluids (e.g. plasma) or tissue are strongly recommended.[86] According to the pharma's drug development reported from the US National Academy Science, "Toxicity Testing in the 21st Century: A vision and strategy", become more useful, convenient in terms of economic costs, and ethic to gain information by applying an advanced tissue culture models (co-culture and 3D spheroid culture) followed by in-vivo models (e.g. chicken embryo model or zebrafish) instead of pharmacokinetics/pharmacodynamics bio-distribution in rodents and big animals.[93] This new approach lead to evaluate mechanisms like adsorption, distribution, metabolism and excretion, toxicokinetics and toxicodynamics, biological target and tissue bio-distribution.

1.4.3 Transformation, Transport and Fate of Cu-ENMs in biological and environmental media

In order to determining the transport, fate, and toxicity of Cu-ENMs in environmental and biological media, stability, in terms of aggregation, sedimentation, and dissolution must be evaluated.

As it is described above, Cu-ENMs (including carbonates, oxide and hydroxides, and the zerovalent metal) are widely used as antimicrobials, fungicides, algaecides, and herbicides, and dissolution to bioavailable ions is a commonly assumed mode of activity. It is reported that oxide or surface oxide are the most likely phase that get in contact with biological and environmental fluid phases, whether copper oxide or copper zero valent. In fact, in comparison to silver, metallic copper ENMs oxidize more readily, first forming a Cu(I) oxide shell around a zerovalent core, and eventually to Cu(II) oxide as a final product.[94,95] Mudunkotuwa et al. (2015) also reported that Cu ENMs could be easily transformed to Cu_2O by citric and oxalic acids by first promoted the dissolution of the oxide coating and then the exposed CuO could react with dissolved O_2 to form Cu_2O.[68]

1.4.3.1 Dissolution

Though Copper(II) oxide is described as insoluble, at the sub-ppm concentration of interest for environmental and nanotoxicology, it is sufficiently soluble to show some toxicological effect.[96–98] Furthermore, dissolution processes can be both assisted by ligands, either thermodynamically by reducing the concentration of the free ion in equilibrium with the solid surface. Wang et al reported that Fetal Bovine Serum (FBS), glutamine and other amino acids promote copper ions release, and form high-affinity complexes with copper.[99] Regarding the role of DNOM in the dissolution of Cu-ENMs, Conway et al. (2015)[66] reported that DNOM may stabilize ENMs, but it can also act as a complexing agent for the dissolved metal fractions as it was already reported by Odzak et al. (2014)[67]. However, dissolution of Cu-ENMs in both environmental and biological media is mainly a proton promoted process, as it is largely reported in literature, although in the case of Cu(0) ENMs dissolution, oxygen is also needed.[66–68,81]

1.4.3.2 Aggregation and sedimentation

Aggregation and consequently sedimentation of Cu-ENMs is influenced by IS, pH and DNOM via electrostatic interaction,[100] following the main assumptions of DLVO theory. Conway and coworkers[66] report that nano-Cu and nano-CuO show an enhanced aggregation at high IS and low DNOM whereas $Cu(OH)_2$ NPs show similar aggregation behaviors in all the waters tested (real and artificial freshwater and marine waters). As consequence, the sedimentation kinetics for nano-Cu, $Cu(OH)_2$, and nano-CuO followed a positive correlation with ionic strength and an inverse correlation with organic content.

However, nano-CuO exhibited an unpredicted stabilizing effect due to the presence of phosphate anions; phosphate is well-known for its ability to covalently bond to metal oxide.[101,102] It is reported that the addition of even low concentrations of PO_4^{3-} to nano-CuO suspensions results in the formation of a negatively charged layer and the polarity's charge of the particles surface switch from positive to negative (Figure 16).

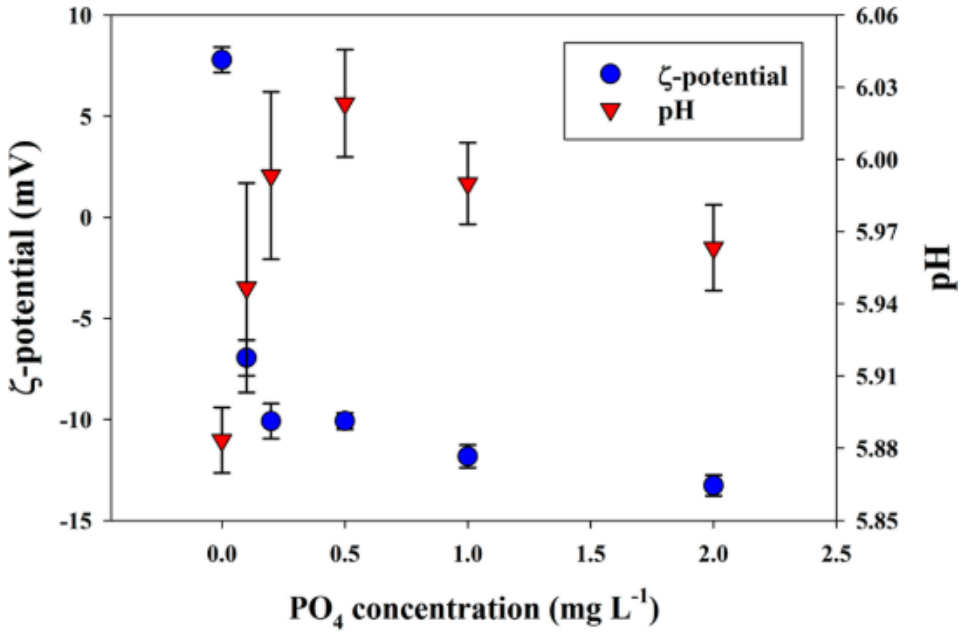

Figure 16 ζ potential and pH of nano-CuO in Nanopure water in the presence of increasing concentrations of $PO4^{3-}$ (from Conway et.al 2015) [66]

This phenomenon leads to an additional stabilization in terms of aggregation, in comparison with other media that show higher IS but different concentrations of PO_4^{3-} (Groundwater <0.02 mg/L PO_4^{3-} vs simulated freshwater 0.64 mg/L PO_4^{3-}).

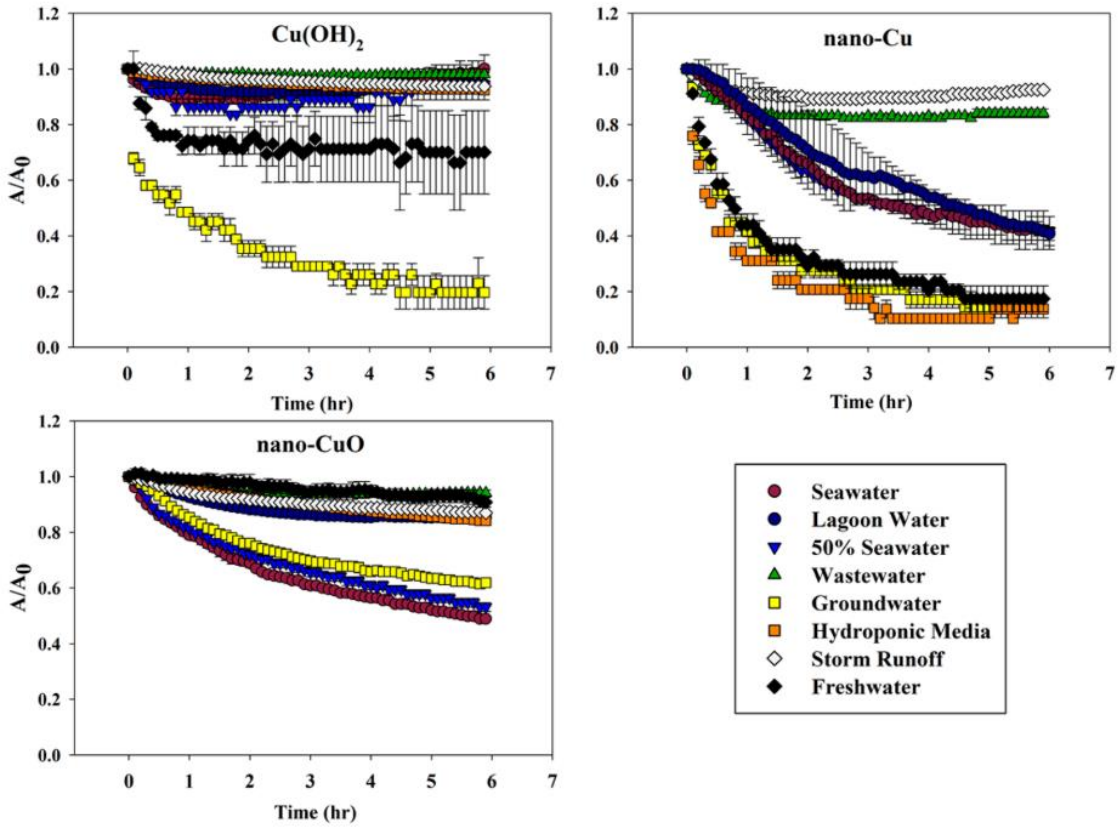

Figure 17 Sedimentation kinetics for $Cu(OH)_2$, nano-Cu(0), and nano-CuO in different artificial water media (from Conway et.al 2015)[66]

On the contrary, this phenomenon does not occur in Cu(0) and $Cu(OH)_2$ nanoparticles since their surfaces are negatively charged throughout a whole range of pH. In addition, independently from the type of Cu-ENMs, the high presence in the media of HCO_3^- and Cl^- can also increase the sedimentation processes (Figure 17), due to the formation of insoluble malachite ($Cu_2CO_3(OH)_2$) and atacamite ($Cu_2Cl(OH)_3$) phase.[66]

1.4.3.3 Sulfidation

According to the literature,[99] sulfidation of several metal base ENMs such as Ag, Zn, Cd has been suggested as a natural detoxification process for metallic nanoparticles. Sulfidation occurs principally in environment that show high sulfide concentration, such as the anaerobic layer in water body or in WWTP effluents. In the same way of the metal cited above, copper shows high affinity for sulfide ligand, and the formation of an insoluble sulfide shell around the Cu-ENMs core, reduce the copper bioavailability by dissolution.[103–105] Although the layer of insoluble CuS reduce the copper bioavailability, the presence of hydrogen peroxide at physiologically relevant concentrations can oxidizes CuS, releasing free copper ions that can partially restore the redox activity.[106]

Anyway, from a recent work emerges that pH, ionic strength, dissolved organic matter, and biomolecular ligands may play an important role in the toxicity of Cu-ENMs, by influencing the total dissolved copper concentration.[107]

1.5) Effects of Cu-ENMs on humans and the environment

1.5.1 Toxicological effects of Cu-ENMs

From the macroscopically point of view, interaction between ENMs and cells can be roughly divided in two cases: ENMs/cell association, and ENMs internalization. Fortunately, none of these nano/biointeractions have been recognized to have pathological consequences for humans, but experimental evidence showed: membrane damage, DNA cleavage, mitochondrial damage, induction of oxidative stress and inflammation processes.[108]

Zhang et al. (2013)[109] attributed cytotoxicity of CuO to the soluble fraction rather than particle surface reactions. On the contrary Studer et al. (2010)[98] proposed a "Trojan horse" type mechanism in which Cu-ENMs penetrated the cell membrane, and dissolved into redox active copper ions that induce oxidative stress, and as consequence the death of the cell. The redox activity in Cu-ENMs systems appears to be associated with the soluble fraction and it is mitigated but not eliminated by ligand binding in solution.[99] Midander et al. (2009)[94] observed size-dependent ion release and toxicity when comparing nano and micrometer-sized copper oxide particles.

The other main biological targets in environment are the plants, but the mechanisms involved in Cu-ENMs uptake by the latter are not clearly understood and still under investigation.[110] Studies have shown that depending on the particle size, ENMs may be uptake through carrier proteins, ion channels, plasmodesmata transport, or as it is reported in the "Trojan-horse" mechanism, the entrance can be facilitated by natural organic matter or root exudates.[111] Some experiments conducted in several plants species (e.g. crop plants, lettuce, wheat, mungbean, kidneybean, maize, cucumber, cilantro, rice, spinach, onion, mustard, tomato, carrot, sweet potato, barley, cotton-chickpea, radish, and zucchini) show negative effects in inhibition of seed germination, growth inhibition, root and shoot growth, oxidative stress and biochemical variations.[112,113]

From the ecotoxicological point of view, mechanisms such as sulfidation of the Cu-ENMs surface or dissolved-ion complexation to form insoluble inorganic salt may reduce the bio-availability of copper in the water column.[66]

1.5.2 Prevention of toxicological effects: Safe-by-design approach

From what has been reported so far, result clear that the surface chemistry is an essential component of rational design of safer ENMs to develop advances material with both low toxicity and new properties.

This approach called ''safe and functional by design'' was firstly applied by integrating the concept of safety and health of the nano-Environmental Health & Safety (EHS) with the ENMs production process, rather than considering EHS as an add-on issue.[114] This preventive approach was then extended to the overall lifecycle of the materials, "from the cradle to the grave", avoiding unexpected effects or unnecessary cost for detoxification and environmental remediation. Although the reduction of toxicity must be the prerogative, the materials properties and functionalities should be conserved, otherwise the purpose of developing new

ENMs fails; therefore, a continuous evaluation of ENMs performances before and after the Safe by Design (SbD) approach must be performed.
SbD is a multidisciplinary approach that combine the analytical data from both chemical-physical characterization and transformation of the ENMs along the whole lifecycle with the toxicological data; the glue that merge these two disciplines is the modelling, that with the help of grouping strategies and predictive models, drives the scientist towards a safest and performing product.[114]

1.5.3 European projects of concern

Research in the field of "nanosafety" remains a centrally important topic in the European vision of the safe implementation of nanotechnologies for the benefit of society. Indeed, the 16 active European "nano-projects" shows an increased emphasis on advanced materials subjected to environmental transformation and ageing, as well as on research with a regulatory focus including Safety-by-design and Life Cycle Assessment approaches.
In order to collectively define strategic agendas for research, regulation and commercialization of nanoproduct, a scientific network called Nanosafety Cluster (NSC, https://www.nanosafetycluster.eu/) was established; this network was also create as a mechanism for ongoing projects to benefit from one another, and for information sharing from recently finished projects. Within this network, several projects has been developed and funded by the European commission, among witch SUstainable Nanotechnology (SUN) and Nanomaterial FAte and Speciation in the Environment (NanoFASE).

Other European projects that consider Cu-ENMs in their case study are:

- GuideNano (2013-2016), whose purpose has been to develop innovative methodologies to evaluate and manage human and environmental health risks of nano-embedded products, considering the whole product life cycle.
- NanoMILE (2013-2017): the aim of the project was to formulate an intelligent and powerful paradigm for the mode(s) of interaction between engineered nanomaterials (ENMs) and organisms or the environment.
- NanoSolution (2013-2017) whose purpose has been to identify and model the relationships between physical-chemical characteristics of ENMs and their biological hazard potentials.

1.5.3.1 SUstainable Nanotechnology (SUN)

SUN project (www.sun-fp7.eu/) is a FP7 project involved 35 research and industrial organizations from 12 European member State (total EU funding 13.5 million €). The main goal of the SUN was to investigate the risks associated to the use and production of real industrial ENMs products, and to find ways to prevent or reduced them along the entire lifecycles (Figure 17). To achieve the goal, has been necessary to develop of reliable methods for characterization of nanoparticles released from various product matrices into complex biological and environmental media. SUN has considered that the available knowledge on the environmental and health risks of ENM, can guide the nanotechnology industry to avoid future

drawback provided that an integrated approach to their risk assessment and management is applied at the entire lifecycle of ENM. SUN has also generated environmental, EHS data and methods and it has integrated them into a decision support system for risk management of ENMs. In Figure 18 the structure of SUN project is reported.

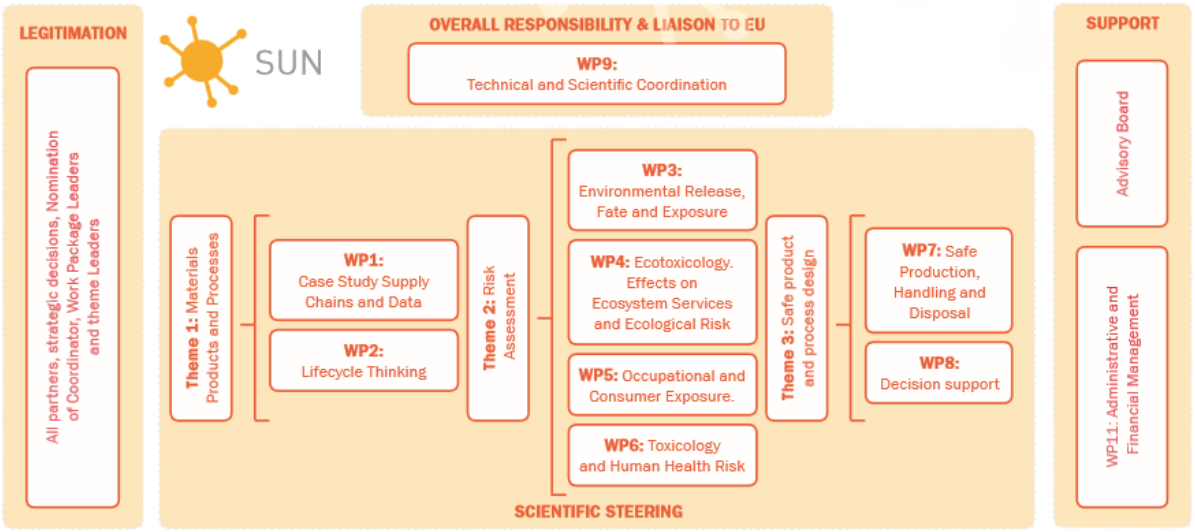

Figure 18 SUN project structure (from www.sun-fp7.eu/)

1.5.3.2 Nanomaterial FAte and Speciation in the Environment (NanoFASE)

NanoFASE project (www.nanofase.eu/) is a Horizon 2020 project involving 35 research and industrial organization form 14 European member (total EU funding: 11.3 €). The main objective of NanoFASE is to build-up an integrated Exposure Assessment Framework models and characterization protocols that are ideally positioned for incorporation into current mainstream chemical assessment tools, policy and regulation (e.g. EUSES & REACH). NanoFASE has considered different release processes, waste-streams and environmental compartments, by idealizing them as a set of “reactors” that are able to transform ENMs from a "as produced" ENMs to an “environmentally transformed materials”. Each “reactor” has a physicochemical or biological environmental characteristic, that simulate the different environmental compartments that the released ENMs will encounter. An array of “reactors” compose the structure of the multimedia fate models (Figure 19). The information gained on both the behavior of ENMs on each reactor, and the way in which ENMs can moves from one reactor to another, allow to group ENMs into Functional Fate Groups according to their “most probable” fate pathways. This approach aim to move from the current mainly mass-based lifecycle approaches, towards dynamic systems that can account for spatial and temporal variability of ENM release, environmental transport and fate.

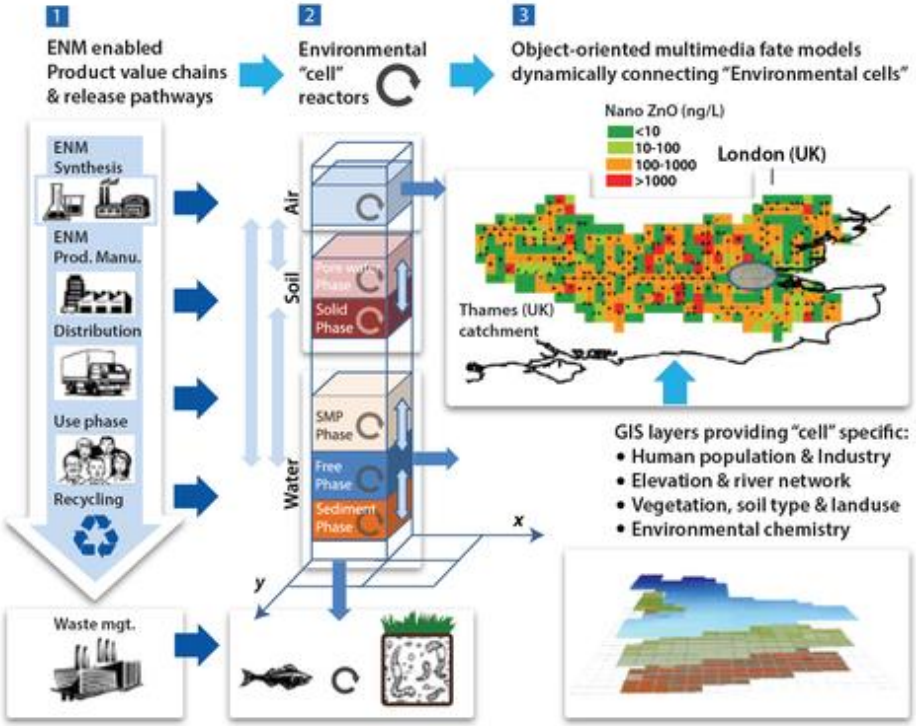

Figure 19 NanoFASE project structure (from www.nanofase.eu)

1.6) References

1. Baalousha, M., Lead, J. R. & Ju-Nam, Y. Natural Colloids and Manufactured Nanoparticles in Aquatic and Terrestrial Systems. *Treatise Water Sci.* **3,** 89–129 (2010).

2. Chen, X. & Mao, S. S. Titanium dioxide nanomaterials: Synthesis, properties, modifications and applications. *Chem. Rev.* **107,** 2891–2959 (2007).

3. Park, J., Joo, J., Soon, G. K., Jang, Y. & Hyeon, T. Synthesis of monodisperse spherical nanocrystals. *Angew. Chemie - Int. Ed.* **46,** 4630–4660 (2007).

4. Zheng, H. *et al.* Nanostructured tungsten oxide - Properties, synthesis, and applications. *Adv. Funct. Mater.* **21,** 2175–2196 (2011).

5. Vance, M. E. *et al.* Nanotechnology in the real world: Redeveloping the nanomaterial consumer products inventory. *Beilstein J. Nanotechnol.* **6,** 1769–1780 (2015).

6. Mitrano, D. M., Motellier, S., Clavaguera, S. & Nowack, B. Review of nanomaterial aging and transformations through the life cycle of nano-enhanced products. *Environ. Int.* **77,** 132–147 (2015).

7. Zhang, Y., Leu, Y., Aitken, R. J. & Riediker, M. Inventory of Engineered Nanoparticle-Containing Consumer Products Available in the Singapore Retail Market and Likelihood of Release into the Aquatic Environment. *Int. J. Environ. Res. Public Health* **12,** 8717–8743 (2015).

8. Wiesner, M. R. *et al.* Decreasing Uncertainties in Assessing Environmental Exposure, Risk, and Ecological Implications of Nanomaterials. *Environ. Sci. Technol.* **43,** 6453–6457 (2009).

9. Dowling, A. P. Development of nanotechnologies. *Mater. Today* **7,** 30–35 (2004).

10. Petosa, A. R., Jaisi, D. P., Quevedo, I. R., Elimelech, M. & Tufenkji, N. Aggregation and deposition of engineered nanomaterials in aquatic environments: Role of physicochemical interactions. *Environ. Sci. Technol.* **44,** 6532–6549 (2010).

11. Israelachvili, J. N. *Intermolecular and Surface Forces: Third Edition*. *Intermolecular and Surface Forces: Third Edition* (2011). doi:10.1016/C2011-0-05119-0

12. Zhang, Y., Chen, Y., Westerhoff, P. & Crittenden, J. Impact of natural organic matter and divalent cations on the stability of aqueous nanoparticles. *Water Res.* **43,** 4249–4257 (2009).

13. Laborda, F. *et al.* Detection, characterization and quantification of inorganic engineered nanomaterials: A review of techniques and methodological approaches for the analysis of complex samples. *Anal. Chim. Acta* **904,** 10–32 (2016).

14. Wagner, S. *et al.* First steps towards a generic sample preparation scheme for inorganic engineered nanoparticles in a complex matrix for detection, characterization, and quantification by asymmetric flow-field flow fractionation coupled to multi-angle light scattering and . *J. Anal. At. Spectrom.* **30,** 1286–1296 (2015).

15. Tadjiki, S., Assemi, S., Deering, C. E., Veranth, J. M. & Miller, J. D. Detection, separation, and quantification of unlabeled silica nanoparticles in biological media using sedimentation field-flow fractionation. *J. Nanoparticle Res.* **11,** 981–988 (2009).

16. Loeschner, K., Brabrand, M. S. J., Sloth, J. J. & Larsen, E. H. Use of alkaline or enzymatic sample pretreatment prior to characterization of gold nanoparticles in animal tissue by single-particle ICPMS Characterisation of Nanomaterials in Biological Samples. *Anal. Bioanal. Chem.* **406,** 3845–3851 (2014).

17. Peters, R. J. B. *et al.* Development and validation of single particle ICP-MS for sizing and

quantitative determination of nano-silver in chicken meat Characterisation of Nanomaterials in Biological Samples. *Anal. Bioanal. Chem.* **406,** 3875–3885 (2014).

18. Misra, S. K., Dybowska, A., Berhanu, D., Luoma, S. N. & Valsami-Jones, E. The complexity of nanoparticle dissolution and its importance in nanotoxicological studies. *Sci. Total Environ.* **438,** 225–232 (2012).

19. Williams, D. B. & Carter, C. B. Transmission electron microscopy - Spectrometry IV. *Book* **4,** (2009).

20. Li, L. *et al.* The potentiation effect makes the difference: Non-toxic concentrations of ZnO nanoparticles enhance Cu nanoparticle toxicity in vitro. *Sci. Total Environ.* **505,** 253–260 (2015).

21. Rückerl, R. *et al.* Ultrafine particles and platelet activation in patients with coronary heart disease--results from a prospective panel study. *Part. Fibre Toxicol.* **4,** 1 (2007).

22. Calzolai, L., Gilliland, D. & Rossi, F. Measuring nanoparticles size distribution in food and consumer products: A review. *Food Addit. Contam. - Part A Chem. Anal. Control. Expo. Risk Assess.* **29,** 1183–1193 (2012).

23. Tiede, K. *et al.* Detection and characterization of engineered nanoparticles in food and the environment. *Food Addit. Contam. Part A* **25,** 795–821 (2008).

24. Krystek, P. *et al.* Method development and inter-laboratory comparison about the determination of titanium from titanium dioxide nanoparticles in tissues by inductively coupled plasma mass spectrometry. *Anal. Bioanal. Chem.* 3853–3861 (2014). doi:10.1007/s00216-013-7580-z

25. Krystek, P. A review on approaches to bio distribution studies about gold and silver engineered nanoparticles by inductively coupled plasma mass spectrometry. *Microchem. J.* **105,** 39–43 (2012).

26. Meermann, B. & Nischwitz, V. ICP-MS for the Analysis at the Nanoscale - A tutorial Review. *J. Anal. At. Spectrom.* (2018). doi:10.1039/C8JA00037A

27. Lee, S. *et al.* Nanoparticle size detection limits by single particle ICP-MS for 40 elements. *Environ. Sci. Technol.* **48,** 10291–10300 (2014).

28. Kálomista, I. *et al.* Dimensional characterization of gold nanorods by combining millisecond and microsecond temporal resolution single particle ICP-MS measurements. *J. Anal. At. Spectrom.* **32,** 2455–2462 (2017).

29. Van Der Zande, M. *et al.* Distribution, elimination, and toxicity of silver nanoparticles and silver ions in rats after 28-day oral exposure. *ACS Nano* **6,** 7427–7442 (2012).

30. Loeschner, K. *et al.* Detection and characterization of silver nanoparticles in chicken meat by asymmetric flow field flow fractionation with detection by conventional or single particle ICP-MS. *Anal. Bioanal. Chem.* **405,** 8185–8195 (2013).

31. Gray, E. P. *et al.* Extraction and Analysis of Silver and Gold Nanoparticles from Biological Tissues Using Single Particle Inductively Coupled Plasma Mass Spectrometry. *Environ. Sci. Technol.* **47,** 14315–14323 (2013).

32. Dan, Y. *et al.* Characterization of Gold Nanoparticle Uptake by Tomato Plants Using Enzymatic Extraction Followed by Single-Particle Inductively Coupled Plasma–Mass Spectrometry Analysis. *Environ. Sci. Technol.* **49,** 3007–3014 (2015).

33. Furtado, L. M. *et al.* The persistence and transformation of silver nanoparticles in littoral lake

mesocosms monitored using various analytical techniques. *Environ. Chem.* **11,** 419–430 (2014).

34. Mitrano, D. M., Arroyo Rojas Dasilva, Y. & Nowack, B. Effect of Variations of Washing Solution Chemistry on Nanomaterial Physicochemical Changes in the Laundry Cycle. *Environ. Sci. Technol.* **49,** 9665–9673 (2015).

35. Valotto, G., Cattaruzza, E. & Bardelli, F. Multi-edge X-ray absorption spectroscopy study of road dust samples from a traffic area of Venice using stoichiometric and environmental references. *Spectrochim. Acta - Part A Mol. Biomol. Spectrosc.* **173,** 971–978 (2017).

36. Ma, R. *et al.* Fate of zinc oxide and silver nanoparticles in a pilot wastewater treatment plant and in processed biosolids. *Environ. Sci. Technol.* **48,** 104–112 (2014).

37. Kaegi, R. *et al.* Behavior of metallic silver nanoparticles in a pilot wastewater treatment plant. *Environ. Sci. Technol.* **45,** 3902–3908 (2011).

38. Loeschner, K. *et al.* In-house validation of a method for determination of silver nanoparticles in chicken meat based on asymmetric flow field-flow fractionation and inductively coupled plasma mass spectrometric detection. *Food Chem.* **181,** 78–84 (2015).

39. Bolea, E. *et al.* Detection and characterization of silver nanoparticles and dissolved species of silver in culture medium and cells by AsFlFFF-UV-Vis-ICPMS: Application to nanotoxicity tests. *Analyst* **139,** 914–922 (2014).

40. Nischwitz, V. & Goenaga-Infante, H. Improved sample preparation and quality control for the characterisation of titanium dioxide nanoparticles in sunscreens using flow field flow fractionation on-line with inductively coupled plasma mass spectrometry. *J. Anal. At. Spectrom.* **27,** 1084–1092 (2012).

41. Contado, C. & Pagnoni, A. TiO2 nano- and micro-particles in commercial foundation creams: Field Flow-Fractionation techniques together with ICP-AES and SQW Voltammetry for their characterization. *Anal. Methods* **2,** 1112–1124 (2010).

42. Meermann, B. Field-flow fractionation coupled to ICP–MS: separation at the nanoscale, previous and recent application trends. *Anal. Bioanal. Chem.* **407,** 2665–2674 (2015).

43. Baalousha, M., Stolpe, B. & Lead, J. R. Flow field-flow fractionation for the analysis and characterization of natural colloids and manufactured nanoparticles in environmental systems: A critical review. *J. Chromatogr. A* **1218,** 4078–4103 (2011).

44. Singh, D. P. & Ali, N. Synthesis of TiO₂ and CuO Nanotubes and Nanowires. *Sci. Adv. Mater.* **2,** 295–335 (2010).

45. Anandan, S. & Yang, S. Emergent methods to synthesize and characterize semiconductor CuO nanoparticles with various morphologies - An overview. *J. Exp. Nanosci.* **2,** 23–56 (2007).

46. Choi, K. J. & Jang, H. W. One-dimensional oxide nanostructures as gas-sensing materials: Review and issues. *Sensors* **10,** 4083–4099 (2010).

47. Wang, S. B. *et al.* A CuO nanowire infrared photodetector. *Sensors Actuators, A Phys.* **171,** 207–211 (2011).

48. Zhu, Y. W. *et al.* Large-scale synthesis and field emission properties of vertically oriented CuO nanowire films. *Nanotechnology* **16,** 88–92 (2005).

49. Zhang, X. *et al.* High-power and high-energy-density flexible pseudocapacitor electrodes made from porous CuO nanobelts and single-walled carbon nanotubes. *ACS Nano* **5,** 2013–2019 (2011).

50. Liu, J. *et al.* Tailoring CuO nanostructures for enhanced photocatalytic property. *J. Colloid Interface Sci.* **384,** 1–9 (2012).

51. Zhang, Q. *et al.* CuO nanostructures: Synthesis, characterization, growth mechanisms, fundamental properties, and applications. *Prog. Mater. Sci.* **60,** 208–337 (2014).

52. Xu, L. *et al.* Novel urchin-like CuO synthesized by a facile reflux method with efficient olefin epoxidation catalytic performance. *Chem. Mater.* **21,** 1253–1259 (2009).

53. Zhou, K. & Li, Y. Catalysis based on nanocrystals with well-defined facets. *Angew. Chemie - Int. Ed.* **51,** 602–613 (2012).

54. Yu, X. Y. *et al.* Novel 3D hierarchical cotton-candy-like CuO: Surfactant-free solvothermal synthesis and application in As(III) removal. *ACS Appl. Mater. Interfaces* **4,** 1954–1962 (2012).

55. Ali, I. New generation adsorbents for water treatment. *Chem. Rev.* **112,** 5073–5091 (2012).

56. Mumm, F., Helvoort, A. T. J. Van & Sikorski, P. Easy Route to Superhydrophobic. *ACS Nano* **3,** 2647–2652 (2009).

57. Vincent, M., Duval, R. E., Hartemann, P. & Engels-Deutsch, M. Contact killing and antimicrobial properties of copper. *J. Appl. Microbiol.* **124,** 1032–1046 (2018).

58. Peng, C. *et al.* Transformation of CuO Nanoparticles in the Aquatic Environment: Influence of pH, Electrolytes and Natural Organic Matter. *Nanomaterials* **7,** 326 (2017).

59. Chakraborty, S., Das, A., Begum, M. R., Dhara, S. & Tyagi, A. K. Vibrational properties of CuO nanoparticles synthesized by hydrothermal technique. *AIP Conf. Proc.* **1349,** 841–842 (2011).

60. Neupane, M. P. *et al.* Temperature driven morphological changes of hydrothermally prepared copper oxide nanoparticles. *Surf. Interface Anal.* **41,** 259–263 (2009).

61. Applerot, G. *et al.* Understanding the antibacterial mechanism of CuO nanoparticles: Revealing the route of induced oxidative stress. *Small* **8,** 3326–3337 (2012).

62. Azam, A., Ahmed, A. S., Oves, M., Khan, M. S. & Memic, A. Size-dependent antimicrobial properties of CuO nanoparticles against Gram-positive and -negative bacterial strains. *Int. J. Nanomedicine* **7,** 3527–3535 (2012).

63. Santo, C. E. *et al.* Bacterial killing by dry metallic copper surfaces. *Appl. Environ. Microbiol.* **77,** 794–802 (2011).

64. Santo, C. E., Taudte, N., Nies, D. H. & Grass, G. Contribution of copper ion resistance to survival of Escherichia coli on metallic copper surfaces. *Appl. Environ. Microbiol.* **74,** 977–986 (2008).

65. Dalecki, A. G., Crawford, C. L. & Wolschendorf, F. *Copper and Antibiotics: Discovery, Modes of Action, and Opportunities for Medicinal Applications*. *Advances in Microbial Physiology* **70,** (Elsevier Ltd., 2017).

66. Conway, J. R., Adeleye, A. S., Gardea-Torresdey, J. & Keller, A. A. Aggregation, dissolution, and transformation of copper nanoparticles in natural waters. *Environ. Sci. Technol.* **49,** 2749–2756 (2015).

67. Odzak, N., Kistler, D., Behra, R. & Sigg, L. Dissolution of metal and metal oxide nanoparticles in aqueous media. *Environ. Pollut.* **191,** 132–138 (2014).

68. Mudunkotuwa, I. A. & Grassian, V. H. Biological and environmental media control oxide nanoparticle surface composition: The roles of biological components (proteins and amino acids), inorganic oxyanions and humic acid. *Environ. Sci. Nano* **2,** 429–439 (2015).

69. Smith, E. J., Davison, W. & Hamilton-Taylor, J. Methods for preparing synthetic freshwaters. *Water Res.* **36,** 1286–1296 (2002).

70. Salminen, R. *et al. FOREGS Geochemical Atlas of Europe. Part 1. Background Information, Methodology, and Maps.* (2005). at <http//gtk/publ/foregsatlas>

71. Berg, J. M., Romoser, A., Banerjee, N., Zebda, R. & Sayes, C. M. The relationship between pH and zeta potential of ∼ 30 nm metal oxide nanoparticle suspensions relevant to in vitro toxicological evaluations. *Nanotoxicology* (2009). doi:10.3109/17435390903276941

72. Berg, J. M. *et al.* The relationship between pH and zeta potential of ∼ 30 nm metal oxide nanoparticle suspensions relevant to in vitro toxicological evaluations. **5390,** (2009).

73. Afrooz, A. R. M. N., Khan, I. A., Hussain, S. M. & Saleh, N. B. Mechanistic heteroaggregation of gold nanoparticles in a wide range of solution chemistry. *Environ. Sci. Technol.* **47,** 1853–1860 (2013).

74. Ottofuelling, S., Von Der Kammer, F. & Hofmann, T. Commercial titanium dioxide nanoparticles in both natural and synthetic water: Comprehensive multidimensional testing and prediction of aggregation behavior. *Environ. Sci. Technol.* **45,** 10045–10052 (2011).

75. Von Der Kammer, F., Ottofuelling, S. & Hofmann, T. Assessment of the physico-chemical behavior of titanium dioxide nanoparticles in aquatic environments using multi-dimensional parameter testing. *Environ. Pollut.* **158,** 3472–3481 (2010).

76. Wang, Z., Zhang, L., Zhao, J. & Xing, B. Environmental processes and toxicity of metallic nanoparticles in aquatic systems as affected by natural organic matter. *Environ. Sci. Nano* **3,** 240–255 (2016).

77. Levard, C., Hotze, E. M., Lowry, G. V. & Brown, G. E. Environmental transformations of silver nanoparticles: Impact on stability and toxicity. *Environ. Sci. Technol.* **46,** 6900–6914 (2012).

78. Philippe, A. & Schaumann, G. E. Interactions of dissolved organic matter with natural and engineered inorganic colloids: A review. *Environ. Sci. Technol.* **48,** 8946–8962 (2014).

79. Gallego-Urrea, J. A., Perez Holmberg, J. & Hassellöv, M. Influence of different types of natural organic matter on titania nanoparticle stability: Effects of counter ion concentration and pH. *Environ. Sci. Nano* **1,** 181–189 (2014).

80. Bharti, B., Meissner, J. & Findenegg, G. H. Aggregation of silica nanoparticles directed by adsorption of lysozyme. *Langmuir* **27,** 9823–9833 (2011).

81. Odzak, N., Kistler, D., Behra, R. & Sigg, L. Dissolution of metal and metal oxide nanoparticles under natural freshwater conditions. *Environ. Chem.* **12,** 138–148 (2015).

82. Pietrzyńska, M. & Voelkel, A. Stability of simulated body fluids such as blood plasma, artificial urine and artificial saliva. *Microchem. J.* **134,** 197–201 (2017).

83. Rahman, M., Laurent, S., Taxil, N., Yahia, L. & Mahmoudi, M. in *Protein-Nanoparticle Interactions* (ed. Springer) 21–44 (2013). doi:10.1007/978-3-642-37555-2_2

84. Aggarwal, P., Hall, J. B., McLeland, C. B., Dobrovolskaia, M. A. & McNeil, S. E. Nanoparticle interaction with plasma proteins as it relates to particle biodistribution, biocompatibility and therapeutic efficacy. *Adv. Drug Deliv. Rev.* **61,** 428–437 (2009).

85. Lundqvist, M. *et al.* The evolution of the protein corona around nanoparticles: A test study. *ACS Nano* **5,** 7503–7509 (2011).

86. Monopoli, M. P. *et al.* Physical-Chemical aspects of protein corona: Relevance to in vitro and

in vivo biological impacts of nanoparticles. *J. Am. Chem. Soc.* **133,** 2525–2534 (2011).

87. Gessner, A., Lieske, A., Paulke, B. R. & Müller, R. H. Influence of surface charge density on protein adsorption on polymeric nanoparticles: Analysis by two-dimensional electrophoresis. *Eur. J. Pharm. Biopharm.* **54,** 165–170 (2002).

88. Deng, Z. J. *et al.* Differential plasma protein binding to metal oxide nanoparticles. *Nanotechnology* **20,** (2009).

89. Lynch, I. & Dawson, K. A. Protein-nanoparticle interactions. *Nano Today* **3,** 40–47 (2008).

90. Meng, H. *et al.* Aspect ratio determines the quantity of mesoporous silica nanoparticle uptake by a small gtpase-dependent macropinocytosis mechanism. *ACS Nano* **5,** 4434–4447 (2011).

91. Meng, H., Leong, W., Leong, K. W., Chen, C. & Zhao, Y. Walking the line: The fate of nanomaterials at biological barriers. *Biomaterials* **174,** 41–53 (2018).

92. Jansch, M., Stumpf, P., Graf, C., Rühl, E. & Müller, R. H. Adsorption kinetics of plasma proteins on ultrasmall superparamagnetic iron oxide (USPIO) nanoparticles. *Int. J. Pharm.* **428,** 125–133 (2012).

93. Nel, A. *et al.* Nanomaterial toxicity testing in the 21st century: Use of a predictive toxicological approach and high-throughput screening. *Acc. Chem. Res.* **46,** 607–621 (2013).

94. Midander, K. *et al.* Surface characteristics, copper release, and toxicity of nano- and micrometer-sized copper and copper(II) oxide particles: A cross-disciplinary study. *Small* **5,** 389–399 (2009).

95. Mudunkotuwa, I. A., Pettibone, J. M. & Grassian, V. H. Environmental implications of nanoparticle aging in the processing and fate of copper-based nanomaterials. *Environ. Sci. Technol.* **46,** 7001–7010 (2012).

96. Zhang, H. *et al.* Use of metal oxide nanoparticle band gap to develop a predictive paradigm for oxidative stress and acute pulmonary inflammation. *ACS Nano* **6,** 4349–4368 (2012).

97. Gunawan, C., Teoh, W. Y., Marquis, C. P. & Amal, R. Cytotoxic origin of copper(II) oxide nanoparticles: Comparative studies with micron-sized particles, leachate, and metal salts. *ACS Nano* **5,** 7214–7225 (2011).

98. Studer, A. M. *et al.* Nanoparticle cytotoxicity depends on intracellular solubility: Comparison of stabilized copper metal and degradable copper oxide nanoparticles. *Toxicol. Lett.* **197,** 169–174 (2010).

99. Wang, Z., Von Dem Bussche, A., Kabadi, P. K., Kane, A. B. & Hurt, R. H. Biological and environmental transformations of copper-based nanomaterials. *ACS Nano* **7,** 8715–8727 (2013).

100. Adeleye, A. S., Keller, A. A., Miller, R. J. & Lenihan, H. S. Persistence of commercial nanoscaled zero-valent iron (nZVI) and by-products. *J. Nanoparticle Res.* **15,** (2013).

101. Boehm, H. P. Acidic and basic properties of hydroxylated metal-oxide surfaces. *Discuss. Faraday Soc.* 264- (1971).

102. Daou, T. J. *et al.* Phosphate adsorption properties of magnetite-based nanoparticles. *Chem. Mater.* **19,** 4494–4505 (2007).

103. Reinsch, B. C. *et al.* Sulfidation of silver nanoparticles decreases Escherichia coli growth inhibition. *Environ. Sci. Technol.* **46,** 6992–7000 (2012).

104. Levard, C. *et al.* Sulfidation processes of PVP-coated silver nanoparticles in aqueous solution:

Impact on dissolution rate. *Environ. Sci. Technol.* **45,** 5260–5266 (2011).

105. Surfaces, N., Liu, J., Sonshine, D. a, Shervani, S. & Hurt, R. H. Controlled Release of Biologically Active. *ACS Nano* **4,** 6903–6913 (2010).

106. Yamamoto, K. & Kawanishi, S. Hydroxyl free radical is not the main active species in site-specific DNA damage induced by copper (II) ion and hydrogen peroxide. *J. Biol. Chem.* **264,** 15435–15440 (1989).

107. Erickson, R. J., Benoit, D. a., Mattson, V. R., Leonard, E. N. & Nelson, H. P. The effects of water chemistry on the toxicity of copper to fathead minnows. *Environ. Toxicol. Chem.* **15,** 181–193 (1996).

108. Meng, H., Xia, T., George, S. & Nel, A. E. A predictive toxicological paradigm for the safety assessment of nanomaterials. *ACS Nano* **3,** 1620–1627 (2009).

109. Zhang, E. *et al.* A new antibacterial titanium-copper sintered alloy: Preparation and antibacterial property. *Mater. Sci. Eng. C* (2013). doi:10.1016/j.msec.2013.06.016

110. Rajput, V. D. *et al.* Effects of Copper Nanoparticles (CuO NPs) on Crop Plants: a Mini Review. *Bionanoscience* **8,** 36–42 (2018).

111. Rico, C. M., Majumdar, S., Duarte-Gardea, M., Peralta-Videa, J. R. & Gardea-Torresdey, J. L. Interaction of nanoparticles with edible plants and their possible implications in the food chain. *J. Agric. Food Chem.* **59,** 3485–3498 (2011).

112. Singh, A., Singh, N. B., Hussain, I., Singh, H. & Yadav, V. Synthesis and characterization of copper oxide nanoparticles and its impact on germination of Vigna radiata (L.) R. Wilczek. *Trop. Plant Res.* **4,** 246–253 (2017).

113. SHAMS, M. *et al.* Nitric Oxide Alleviates Copper Toxicity in Germinating Seed and Seedling Growth of Lactuca sativa L. *Not. Bot. Horti Agrobot. Cluj-Napoca* **46,** 167 (2017).

114. Zhao, F., Meng, H., Yan, L., Wang, B. & Zhao, Y. Nanosurface chemistry and dose govern the bioaccumulation and toxicity of carbon nanotubes, metal nanomaterials and quantum dots in vivo. *Sci. Bull.* **60,** 3–20 (2015).

Chapter 2

Cu-ENMs behavior and transformation in biological and environmental media

2.1) Behavior of nano-CuO in environmental media ([a])

2.1.1 Introduction

As reported in Chapter 1 section 4 "*Transformation and fate of Cu-ENMs*", Cu-ENMs are dynamic systems that are subjected to several processes such as dissolution, aggregation and surface transformation when dispersed in biological or environmental media. For this reason, the European Project NanoFASE has selected CuO ENMs as one of the material case study to model the dissolution behavior of ENMs in freshwater. To ensure good accuracy and a wide range of applicability for NanoFASE model (multi-media fate model), an intensive and detailed dissolution study was needed. For this purpose, a multidimensional parameter matrix representing the parameters variability of European surface and coastal waters has been developed (Chapter 1 section 4.1 *"Transformation of ENMs in Environmental media: role of pH, organic matter and ionic strength"*). This 3D matrix considered different ranges of pH and concentrations of DNOM and divalent electrolytes, as reported in Figure 1.

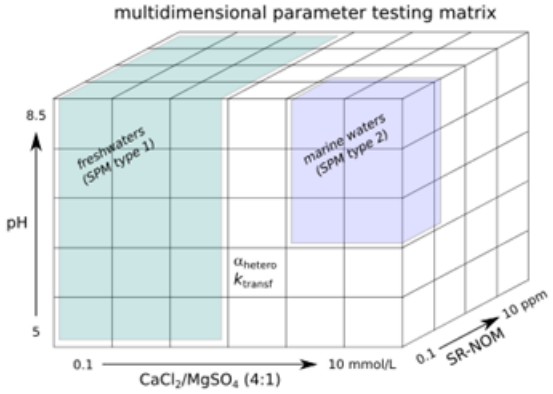

Figure 1 Multidimensional parameter testing matrix developed for simulate the European surface and costal water

The dissolution of bulk materials proceeds through several coupled processes, including transport of solutes between the bulk material and the background solution, the ad- and desorption of solutes at the bulk material's surface, hydration and dehydration of ions and surface migration. All those processes have to occur simultaneously, but some of them may be slower than others. Since the overall dissolution rate depends on the rate of the slowest process, it is important to identify the rate limiting mechanism.[1] The dissolution rate describes the speed of the dissolution of a material. The rate is dependent on various factors (Figure 2) such as temperature, pH, solubility of the material, background solution, ionic strength,

[a] My contribution in this work is related to the development of the sp-ICP-MS method for the dissolution experiment, the data treatment and the rationalization of Cu-ENMs behavior in environmental media

surface area of the specific material and presence of inhibitors (e.g., inorganic complexing ligands).[2]

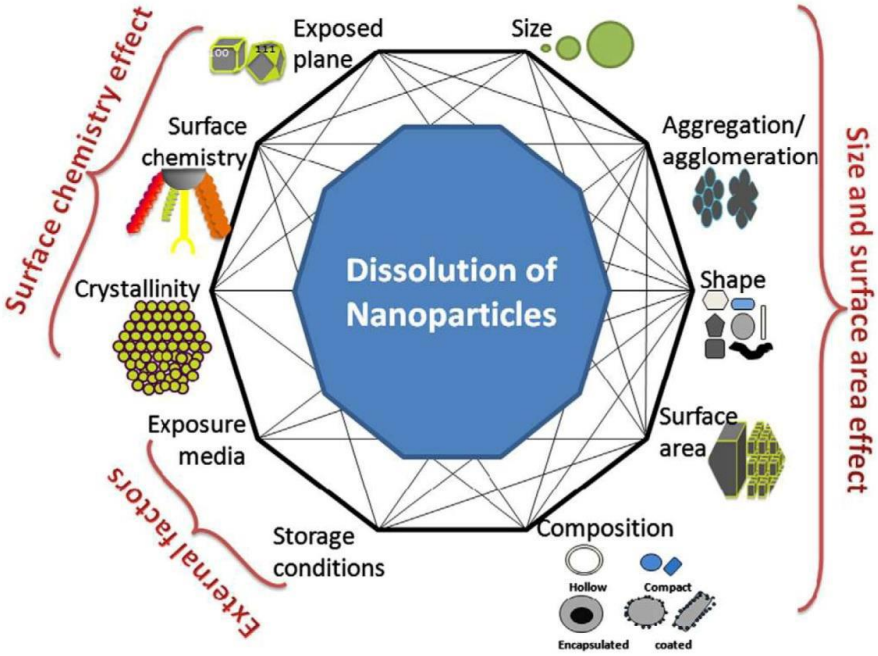

Figure 2 A simplistic representation showing the factors that can affect dissolution of ENMs (from Misra et al. 2012)[2]

Dissolution experiments are usually performed in background electrolyte solutions, which are adjusted with nitric acid (HNO_3) or sodium hydroxide (NaOH) to the desired pH, and the ENMs are introduced to the solution. As it was deeply described in Chapter 1 section 2.2.2 "*Analytical techniques"*, the common techniques used for study the dissolution behavior of Cu-ENMS are electrochemical techniques (i.e. Cyclic Voltammetry), UV-Vis absorption spectroscopy or atomic spectroscopy techniques (i.e. ICP-EOS, ICP-MS) preceded by offline separation procedure (i.e. ultrafiltration, ultracentrifugation) or online separation (i.e. FFF, SEC).[2] In this work, the dissolution mechanism of CuO ENM by using single particle Inductively Coupled Plasma-Mass Spectrometry (sp-ICP-MS) has been studied. sp-ICP-MS allows to distinguish between ionic and nano-form, and provides information on particle number concentration and particle size at environmentally relevant concentrations.[3]

2.1.2 Equipment and Method

According to the testing matrix (Figure 1), the dimensions for the freshwater ranged from 5.0 to 8.5 for the pH, and from 0.1 to 1 mmol/L for the electrolyte's concentration ($CaCl_2$/$MgSO_4$ fixed ratio 4:1). Only 0.1 ppm_{TOC} for the DNOM concentration was considered (Suwannee River natural organic matter). CuO ENMs from Plasmachem was diluted in MQ water by reaching a final concentration of 100mg/L; this suspension was probe sonicated for 10 minutes and then diluted 1:1000 (100 µg/L). According to the matrix shown in Figure 1, different media conditions were investigated by changing parameters such as pH and ionic strength. 100 µL of the diluted CuO suspension (100 µg/L) were added to 10 ml of the selected media, and then analyzed by sp-ICP-MS. All the reagents were purchased from Sigma-Aldrich.

sp-ICP-MS analysis

Sample analysis was performed by using Perkin Elmer ICP-MS Nexion 350D in single particle mode by using Syngistix Nano for the data treatment. Transport Efficiency (TE) was estimated using 50 and 100 nm gold nanoparticle standard;[3] a Dwell time of 100 µs was used and the acquisition time was set to 100 seconds. In order to reach the low DL_S of 15 nm, isotope ^{63}Cu was selected; the amount of Cu^{2+} was quantified using a multi-point curve (blank and 6 points over the concentration range 50 ng/L to 10 µg/L). In the first screening test, samples were analyzed every 18 minutes, while for the initial dissolution rate studies, the samples were analyzed every 3 minutes.

2.1.3 Results

It is known from literature that the dissolution of Cu-based ENMs depends from pH, total organic carbon (DNOM) content and ionic strength.[4]

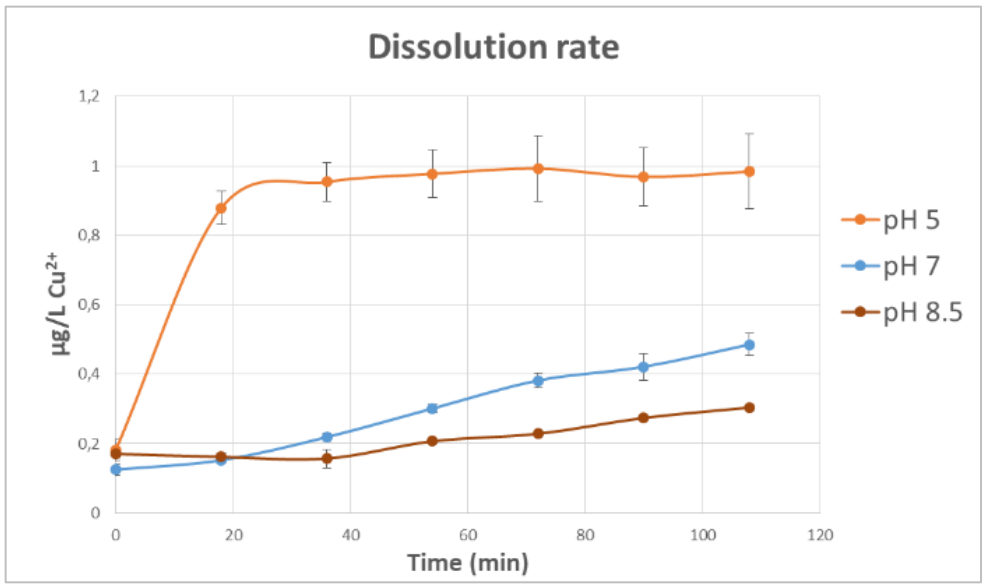

Graph 1 CuO ENMs dissolution kinetics over 110 minutes at pH 5, 7, 8.5

According to the literature,[2,4–6] the screening tests (Graph 1) performed showed that pH play a key role in the dissolution processes, indeed at pH 5 after 18 min the CuO ENMs reach the total dissolution, while at pH 7 and 8.5 the concentration of Cu^{2+} dissolved did not change. In order to estimate the initial dissolution rate, the frequency of sampling has been increased, and the samples were analyzed every 3 minutes for 24 minutes. Results are reported below (Graph 2-4).

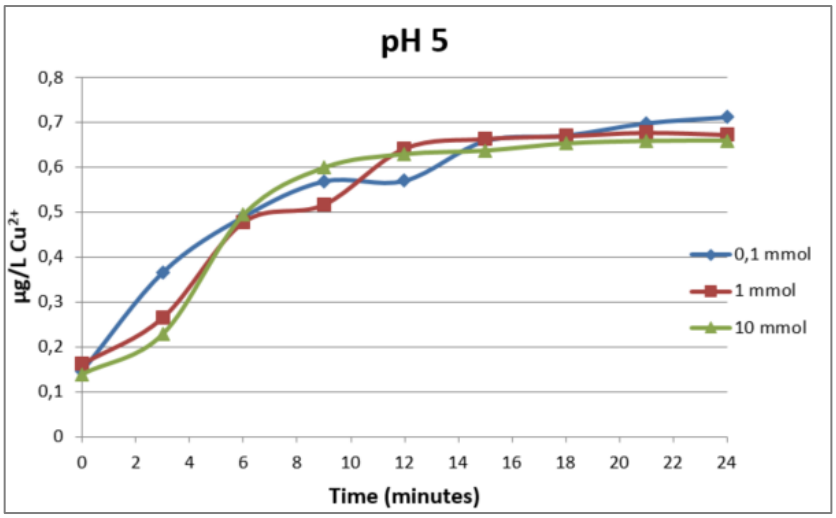

Graph 2 CuO ENMs dissolution kinetics over 18 minutes with 0.1, 1 and 10 mmol of Ca/Mg (4:1) at pH 5 and 0.1 ppm_{TOC}

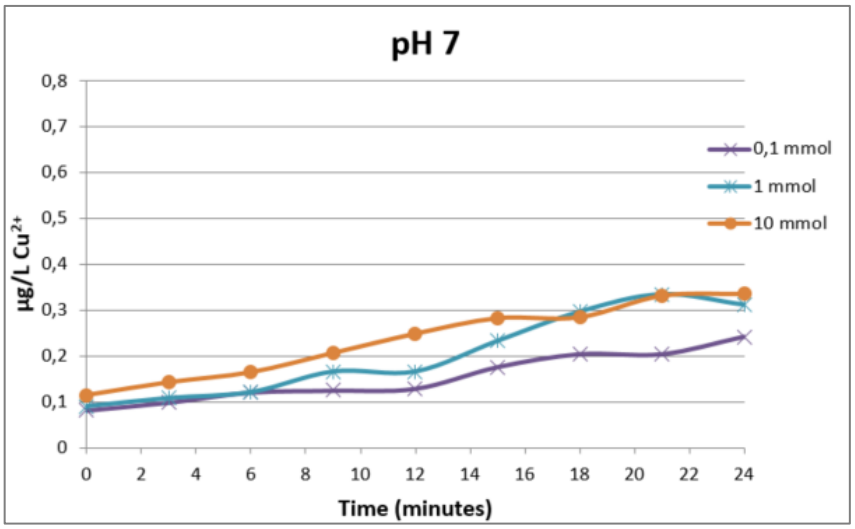

Graph 3 CuO ENMs dissolution kinetics over 18 minutes with 0.1, 1 and 10 mmol of Ca/Mg (4:1) at pH 7 and 0.1 ppm_{TOC}

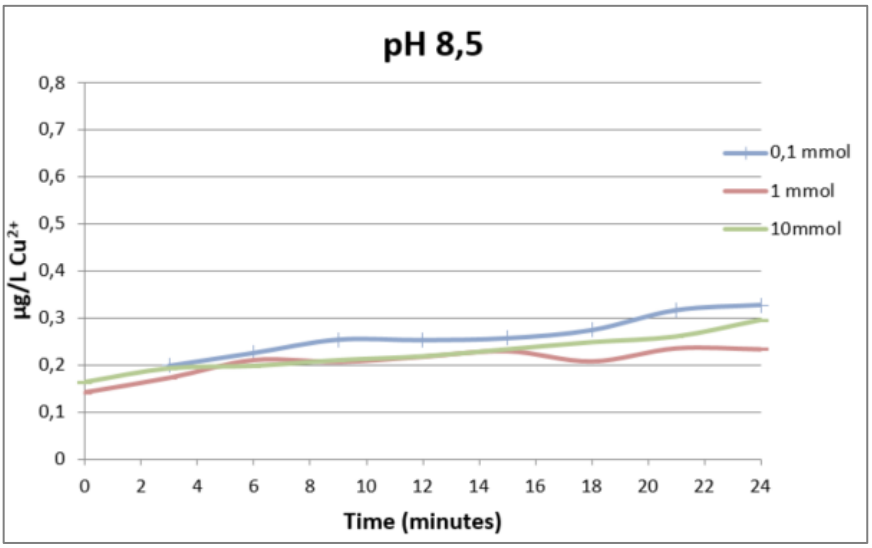

Graph 4 CuO ENMs dissolution kinetics over 18 minutes with 0.1, 1 and 10 mmol of Ca/Mg (4:1) at pH 8.5 and 0.1 ppm_{TOC}

As shown in Graph 3-5, the dissolution rate resulted independent from the ionic strength of the medium, with minimal differences between pH 7 and 8.5. The initial rate of dissolution process was calculated for each of the conditions investigated by performing a linear regression of the curve obtained after 10 minutes of analysis. The results of the kinetics studies are reported in Table 1.

Table 1 : CuO ENMs dissolution rate calculated by linear regression

SR-NOM: 0,1 ppm_{TOC}		pH					
		5		7		8,5	
		µg/(Kg*s)	R^2	µg/(Kg*s)	R^2	µg/(Kg*s)	R^2
Ca^{2+}/Mg^{2+} mmol	0,1	8,31E+05	0,9502	9,03E+04	0,9432	1,14E+05	0,8822
	1	7,65E+05	0,9422	1,44E+05	0,9205	1,39E+05	0,8643
	10	9,85E+05	0,9592	1,78E+05	0,9817	8,56E+04	0,8947

These experimental data are not in total agreement with the hypothesis of Conway et al (2015),[4] according to which the ionic strength of the medium should decrease the dissolution rate of CuO-NPs. A high content of salts in fact, should increase the homoaggregation between the particles, reducing the surface area available for the interface mass process. However, in the propose experimental set, the high dilution (~60000 particles/mL) of the samples decrease the probability of collision between the particles, making the aggregation phenomenon negligible. The high dissolution can also explain the low influence of ionic strength on CuO NPs dissolution rate. In order to investigate the behavior's dependence from the concentration, the amount of ENMs (concentration ppm) was increased, and the samples was analyzed previous opportune dilution.

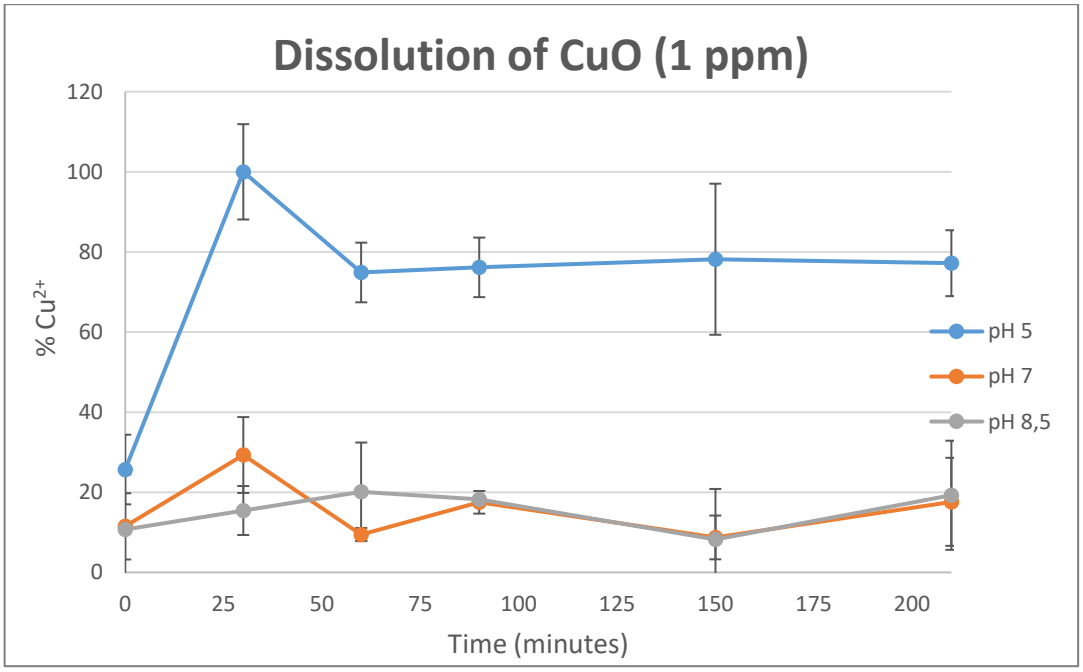

Graph 5 Normalized dissolution of 1 ppm of CuO ENMs kinetics over 210 minutes with at pH 5, 7, 8.5

Data shows (Graph 5) that the dissolved fraction in neutral and basic pH at higher concentration is negligible in compare to the previous dissolution kinetics, where a partial dissolution it's also present. It can be notice that at time 30 min, the dissolution curves of pH 5, shows a decrease in the dissolved Cu^{2+} in solution. This phenomenon was already reported by Vogelsberger and co-workers (2008),[7] by studying the dissolution of several metal oxide nanoparticles; they observed that the solubility shows a maximum at the beginning of the dissolution process, whereas over time, the solubility levels are shown to decrease. This was called "Kinetic size effects" and the main parameters involved are particle size, and surface tension of the solid. It was also reported that if a large amount of nanoparticles were dispersed in water media, significant increase in the dissolved species occurs; the quickly return to the equilibrium concentration levels, may be caused by the formation of new small particles, surface deposition or additionally aggregation and sedimentation of large aggregated particles.[7]

2.1.4 Conclusion

The results obtained so far, showed major contribution of pH in CuO ENMs dissolution phenomenon with respect to ionic strength. Moreover, the study provides not only the data for the NanoFASE models, but also revealed that many phenomena are involved in the transformation of Cu-ENMs (i.e. kinetic size effect). In particular, to assess the transport and fate of Cu-ENMs it must be taken into account the effect of concentration in several transformation and interaction mechanism. Anyway, further investigation should be done.

2.2) Colloidal characterization of CuO nanoparticles in biological and environmental media ([b])

In this section the paper "Colloidal characterization of CuO nanoparticles in biological and environmental media" published on the journal Environmental Science Nano is reported; this work was developed within the European project SUN. CuO ENMs were modified with opportune coatings [polyethylenimine (PEI), sodium ascorbate (ASC), sodium citrate (CIT), and polyvinylpyrrolidone (PVP)] by following a safe by design approach. The effects of these four stabilizers on the CuO NPs' physicochemical properties were investigated in different biological and environmental media by combining dynamic and electrophoretic light scattering (DLS and ELS), centrifugal separation analysis (CSA) and inductively coupled plasma optical emission spectroscopy (ICP-OES). The results showed improved dispersion stability for CuO-CIT, CuO-ASC, and CuO-PEI in both Milli-Q and phosphate buffered saline (PBS) as compared to pristine CuO and CuO-PVP. The increased ionic strength of artificial fresh (AFW) and marine (AMW) waters strongly destabilized all the CuO NP suspensions, except for CuO-PEI dispersed in AFW. The presence of proteins and amino acids in the test media had a strong influence on the colloidal stability of all the dispersions. The characterized materials have been used within the project for toxicological and ecotoxicological purposes, in order to estimate if the coatings can reduce the toxic effects towards humans and environment, but still active in bacteriological applications.

Authors: Ortelli, S. Costa, A.L., Blosi, M., Brunelli, A. Badetti, E., Bonetto, A., Hristozov, D., Marcomini, A.

2.2.1 Introduction

There are already many engineered nanomaterials on the market and their number continues to increase. These materials are optimised for a variety of properties (e.g. size, morphology, purity and surface coating) that enable their formulation in different consumer products (nanodb.dk). This enormous complexity of nanoforms has made the analysis of their environmental health and safety implications impossible without highly demanding case-by-case testing, which poses a huge problem to the regulation of their risks[8–10]. It has been widely accepted by regulators, industries and scientists that grouping and read-across can address this issue as they are useful approaches to reduce the cost and enhance the efficiency of testing for the purposes of risk assessment and safer product design.[11,12] In order to develop such approaches for ENMs it is essential to gain fundamental understanding of which (combinations of) intrinsic and extrinsic structural and physicochemical characteristics of ENMs dispersed in environmental or biological media, or embedded in product matrices, affect their release, uptake, biokinetics and toxicity. This involves the investigation of key

[b] My contribution in this paper is related to the colloidal characterization of Cu-ENMs in both artificial marine and freshwater, and in artificial biological media, by using DLS, CSA and ELS; moreover I was also involved in the drafting of the manuscript and in the data/evidence collection.

interactions at the interface between ENMs and environmental or biological media,[13] which depend on both the ENMs physicochemical properties and the characteristics of the surrounding media.[14,15] Therefore, any testing strategies for the purposes of risk assessment and safer product design should also consider the interactions between ENMs and the other substances present in a medium, regardless of whether they are biological (e.g. proteins and amino acids) or environmental (e.g. natural organic matter or extracellular polymeric substances) compounds. Many studies investigated such interactions[16–19] focusing on *core* intrinsic properties (i.e. chemical composition, size, shape, coating), their *shell* evolution in testing and life-cycle media (i.e. agglomeration/aggregation, charge, corona formation)[20,21] and the resulting *specific reactivity* (i.e. potential generation of reactive oxygen species (ROS) or release of toxic metal ions). Most of these studies concluded that ENMs should be considered as dynamic entities that undergo chemical and physical transformations once embedded in product matrices and exposed to environmental and biological stressors.[22]

This study focuses on the physicochemical characterization of Copper Oxide nanoparticles (CuO NPs), performed in the EU FP7 SUN project, in order to support the interpretation of (eco)toxicological data from *in vivo* and *in vitro* testing. In fact, the exposure route by which these contaminants enter an organism after contact, can strongly depend on ENMs dispersion stability (i.e. NPs that quickly settle from the water column can increase the interaction with benthonic species).[23]

Nanoscale CuO was chosen as case study because it is widely used for its antibacterial properties in wood preservation, paints and textiles.[24–26] The timber preserving applications include outdoor residential decking, gardening, fencing, playground equipment. Specifically, the SUN case study involves CuO-based paint, which, in addition to wood preservation, also provides an aesthetic functionality to the softwood cladding. The pristine CuO NPs were mixed with an acrylic base to produce the paint according to specified composition. The fixation mechanism of this formulation involves reaction of the cupric ion with carboxylic and phenolic groups from cellulose, hemicellulose and lignin. This leads to homogenous distribution of the ions in the wood cells, including penetration through cell wall voids. Once the wood is saturated, the remaining copper precipitates as basic copper carbonate and can be released in the environment through leaching, which leads to exposure of ecosystems and humans.
This may pose health and environmental risks as the CuO is generally a toxic substance.[27,28] In order to prevent those, we modified the surface of the CuO NPs by a “Safety by Design” (SbD) approach.[29–33] The surface modification involved the attachment of four non-hazardous modifying agents representative of different surface charges [negative for sodium citrate and sodium ascorbate, positive for branched polyethylenimine, neutral for polyvinylpyrrolidone]. Key properties (i.e. colloidal stability including surface charge and ions release) of pristine and modified CuO NPs were investigated in MilliQ water, Phosphate Buffered Saline, biological and environmental media. We studied their evolution at increasing levels of complexity of the embedding matrices (from distilled water to biological fluids) to understand how the intrinsic identity of the NPs is affected by the extrinsic characteristics of the media (i.e. pH, ionic strength, presence of biomolecules). The obtained results are highly relevant for

hypothesizing key nano-bio/eco interactions in relation to modes of toxicological action in order to derive criteria and guiding principles for grouping and read-across.

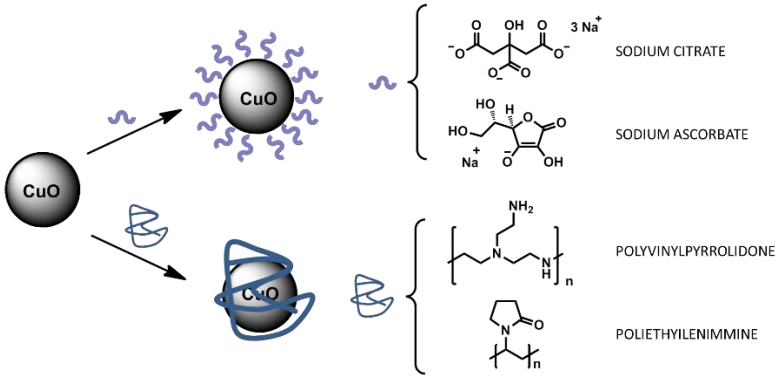

Figure 3 Schematic representation of SbyD strategy applied: introduction of modifying agents (i.e. CIT, ASC, PEI and PVP) by self-assembling

2.2.2 Materials and Methods

2.2.2.1 Materials

Commercial CuO nanopowder (average particles diameter: 12 ± 4 nm) was provided by PlasmaChem GmbH (Germany). Minimum Essential Media (MEM), Dulbecco's Modified Eagle Medium (DMEM – high glucose), Fetal bovine serum and Penicillin/Streptomycin (Pen-Strep) were purchased from Life Technologies Corporation (Carlsbad, USA). Dulbecco's Phosphate Buffered Saline, sodium citrate, sodium ascorbate, polyvinylpyrrolidone (PVP – MW 29000), branched polyethylenimine (PEI – solution 50% in H_2O) and Nitric Acid 70% (redistill 99.99% trace metal basis) were purchased from Sigma-Aldrich. Artificial Fresh Water and Artificial Marine Water were prepared according to standardized protocols.[34,35] All inorganic salts were of analytical grade and purchased from Sigma-Aldrich (St. Louis, MI, USA).

2.2.2.2 Methods

CuO pristine stock suspension at a concentration of 10 g/L of Cu (1 wt%) was prepared dispersing CuO powder in PBS (total phosphate concentration: 0.05 M, pH=7.4). Starting from the stock suspension, modified CuO dispersions were prepared by adding 10 wt% of modifying agents (i.e. CIT, ASC, PEI and PVP) (Figure 1) with respect to the total amount of copper oxide. This amount was estimated by stabilizers titration with electroacoustic technique (Acoustosizer, Colloidal Dynamics, USA) (see *Supporting Information*). An amount of modifying agent equal to 10 wt% guarantees a complete covering on CuO NPs. Both pristine and modified stock suspension were mixed via Ball Milling (BM) process over 95 h with zirconia spheres (3 mm diameter). Five different stock suspensions were obtained after the ball milling process: pristine NPs (CuO-pristine), CuO NPs modified with sodium citrate (CuO-CIT), with sodium ascorbate (CuO-ASC), with polyethylenimine (CuO-PEI) and with polyvinylpyrrolidone (CuO-PVP).

The colloidal characterization was performed on CuO stock suspensions diluted to 100 mg/L in PBS (which was diluted 1:10 to reach the same salt concentration of the biological media tested, ionic strength 16mM), in "complete" DMEM and MEM (consisting in the commercial

biological medium with 10% v/v FBS and 1% v/v Pen-Strep) as well as in AFW and AMW (simulating media usually used for ecotoxicological testing, ionic strength of 2 and 630 mM respectively). The complete compositions of all media are reported in the *Supporting Information*.

2.2.2.3 Characterization

A morphological characterization of pristine CuO NPs was performed by Scanning Transmission Electron Microscopy (STEM) analysis using Field Emission-Scanning Electron Microscopy (FE-SEM) instrument (Carl Zeiss Sigma NTS Gmbh, Oberkochen, DE). One drop of CuO NP suspension diluted in MilliQ water (100 mg/L) was deposited on a film-coated copper grid and then dried at air. Image analysis was performed on more than 50 particles to estimate the particle size distribution. The hydrodynamic diameter (d_{DLS}) was determined by Dynamic Light Scattering measurements, performed with a Zetasizer nano ZSP (model ZEN5600, Malvern Instruments, UK). Zeta potential (ζ-pot_{ELS}) measurements were performed by electrophoretic light scattering technique. Smoluchowski equation was applied to convert the electrophoretic mobility to zeta potential. The pH measurements were carried out on diluted stock suspensions (100 mg/L) after 24h in order to achieve the colloidal stabilization. Sedimentation velocity data of the colloidal dispersions were obtained from Centrifugal Separation Analysis, using the Multi-wavelength Dispersion Analyzer LUMiSizer 651®, based on STEP™ technology (space and time resolved extinction profiles), according to ISO/TR 13097:2013. The separation of different components in dispersion, performed by CSA, was speeded up by applying a Relative Centrifugal Force (RCF), which accelerates the movement of materials compared to gravity up to 2325 times. Sedimentation velocity data were calculated from the transmittance values obtained setting the wavelength of the transmitted light at 470 nm and selecting the transmittance (%) over time at three different positions (115, 120 and 125 mm far from the rotor) of the length of the cuvette. Sedimentation velocity at gravity was extrapolated after proving the linear dependency between RCF and sedimentation velocity at the RCF selected (2325).

Copper ions release was calculated as the ratio between dissolved copper ions and the total copper present in suspension. The quantification of copper ions dissolved in each medium was performed centrifuged 15 mL of each working stock suspension by Ultra-Centrifugal Filter (UCF) unit (Amicon Ultra-15, 10 kDa, Millipore), under centrifugal force of 5000 rpm and spin time of 30 min. The filtered solution (10 mL) was analyzed by inductively coupled plasma optical emission spectrometry using ICP-OES 5100 – vertical dual view apparatus (Agilent Technologies, Santa Clara, CA, USA). Total copper was quantified from each diluted suspension, which was previously treated with 2 mL of ultrapure HNO_3 to ensure a complete digestion. According to the experimental conditions typical of toxicological and ecotoxicological testing, the ions release experiments were performed at 37°C after 24h in biological media and at 25°C in MilliQ, PBS and environmental media. The results from DLS, ELS, LUMiSizer and ICP-OES were reported as an average of three independent measurements.

2.2.3 Results and Discussion

The morphological characterization of pristine CuO NPs by STEM analysis showed the presence of spherical and monodispersed CuO NPs (Figure 4). The magnified image (Figure 4b) highlights the presence of well dispersed NPs with a primary nanoparticle average diameter of about 12 ± 8 nm, according to supplier specification. As expected, some agglomerated NPs have also been detected (Figure 4a and 4c).

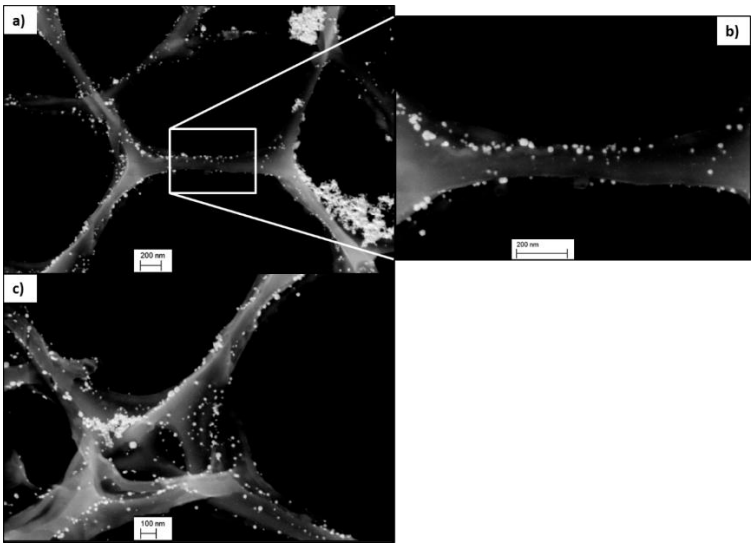

Figure 4 STEM images of pristine CuO NPs in MilliQ water (100 mg/L).

The colloidal stability, which has already been reported in literature, that can strongly affect toxicological outcomes[36–38] was investigated by measuring hydrodynamic size, ζ-pot and sedimentation velocity of both pristine and modified CuO NPs. The influence of the modifying agents on the CuO NPs stability and agglomeration when dispersed in different biological and environmental media was assessed. DLS results, referred to pristine and modified CuO NPs diluted in MilliQ water, PBS, MEM, DMEM, AFW and AMW, are reported in Table 2.

Table 2 Hydrodynamic diameters (nm) of pristine and modified CuO samples dispersed in different media: MilliQ water, PBS, MEM, DMEM, AFW and AMW.

	Hydrodynamic Diameter (nm)					
	MilliQ	PBS	MEM	DMEM	AFW	AMW
CuO-pristine	1093 ± 50	2756 ± 347	47 ± 6	55 ± 16	1663 ± 210	1281 ± 393
CuO-CIT	368 ± 10	271 ± 43	89 ± 5	37 ± 2	1050 ± 16	1062 ± 159
CuO-ASC	122 ± 1.4	1314 ± 525	52 ± 4	73 ± 21	1293 ± 278	1234 ± 25
CuO-PEI	247 ± 14	209 ± 16	46 ± 4	45 ± 14	675 ± 199	1281 ± 168
CuO-PVP	797 ± 84	2765 ± 432	44 ± 2	53 ± 25	1159 ± 256	1661 ± 580

The data collected in MilliQ water confirmed the expected effect of surface modifiers addition. Samples coated by ionic agents (negative CIT and ASC, positive PEI) resulted better dispersed with a significant decreasing of average hydrodynamic diameter in comparison with pristine

sample. On the other hand, neutral PVP did not improve significantly the dispersion of CuO NPs. The long aliphatic chains probably force NPs aggregation by depletion flocculation phenomenon.[39] In comparison with MilliQ water, data collected in PBS showed an increase of the hydrodynamic diameter for CuO-pristine as well as for CuO-ASC and CuO-PVP. This is correlated to aggregation phenomena and justified by the increase of ionic strength due to the salts content in Dulbecco's Phosphate Buffered Saline (PBS) medium. It has already been reported that the salts screen the charge on the NP surface reducing electrostatic repulsion.[40] However, CuO-CIT and CuO-PEI modified samples were not affected by the presence of salts in solution, showing hydrodynamic size values comparable with that measured in MilliQ water. From DLS measurements, CuO-PEI resulted the best dispersed in both MilliQ water and in a higher ionic strength medium (PBS). A possible explanation could be related to the electrosteric action of polyethylenimine.[41] The overall outcomes highlighted that ascorbate and citrate salts improved only the repulsive potential due to the negative charge transferred to particle surface, while PEI provides both electrostatic (due to positive charge) and steric contribution (due to the polymeric structure). All DLS data collected in MEM and DMEM cell culture media showed very similar values. Biological components (amino acids and proteins) of the *milieu* seems to strongly levelled the hydrodynamic size data in spite of the stabilizers used. However, taking into account the samples dispersed in AFW and AMW, an increase of the hydrodynamic diameters was observed for both the pristine and modified NPs. The salts present in environmental media, in particular divalent cations (e.g. Ca(II) and Mg(II)) that can get adsorbed to the nanoparticles surface, induced particles agglomeration. This phenomenon was already observed in AFW, which presents an ionic strength ten time lower than AMW. Agglomeration in AFW seems to be prevented only by PEI, which loses its efficacy in AMW at highest ionic strength.[13]

Table 3 ζ-potential (mV) of pristine and modified CuO samples dispersed in different media: MilliQ water, PBS, DMEM, MEM, AFW and AMW

	ζ-pot (mV)					
	MilliQ (pH=6.5)	PBS (pH=7.4)	MEM (pH=7.9)	DMEM (pH=8.2)	AFW (pH=8.1)	AMW (pH=8.1)
CuO-pristine	-9.1 ± 0.4	-2.3 ± 2.1	-10.1 ± 0.5	-8.2 ± 0.4	-3.5 ± 0.4	+7.6 ± 0.4
CuO-CIT	-18.0 ± 0.3	-3.4 ± 1.2	-10.5 ± 0.2	-9.7 ± 0.6	-3.6 ± 0.4	+4.5 ± 0.7
CuO-ASC	-17.4 ± 0.3	-8.1 ± 0.1	-9.5 ± 0.2	-9.2 ± 0.2	-8.1 ± 0.4	+2.7 ± 0.6
CuO-PEI	+28.3 ± 0.7	+13.8 ± 0.1	-10.5 ± 0.9	-10.1 ± 0.7	+20.9 ± 0.9	+10.1 ± 1.1
CuO-PVP	-8.1 ± 2.3	-0.9 ± 0.7	-10.1 ± 0.4	- 9.4 ± 0.8	+1.6 ± 0.3	+6.5 ± 1.5

ζ-potential represents another important property directly affecting colloidal stability and interaction of NPs with the surrounding medium.[19,42] Basically, the charge is often quantified in terms of ζ-potential which depends on the *milieu* in which the NPs are dispersed and, therefore, it is strongly correlated to the pH.[43] ζ-potentials of biological media were measured at around pH 8 and values of -9.9 ± 0.2 mV and -10.6 ± 0.3 mV were obtained for MEM and

DMEM respectively. The results collected for pristine and the modified samples are listed in Table 3.

Pristine CuO NPs diluted in MilliQ water showed negative ζ-potential, despite to the expected positive value of copper oxide and in general of basic metal oxides when dispersed in water.[44,45] The reversal of CuO pristine surface charge sign is due to the presence of phosphate ions (PO_4^{3-}) used for the sample preparation, which are specifically adsorbed onto CuO NPs surface (Figure 3a). The key role of phosphate adsorption has been already reported in literature.[40,45] The modified samples diluted in MilliQ water showed values coherent with the charge lead by the stabilizers, confirming the preferred interaction of aforementioned modifiers over phosphate ions (Figure 3b). As expected, the addition of neutral PVP coating did not modify the ζ-potential of pristine sample. An increase of ionic strength induced a colloidal destabilization in PBS, as confirmed both by the increased agglomeration rate (Table 2) and by ζ-pot decrease (Table 2). ζ-pot values of CuO-pristine and CuO-PVP are close to zero, indicating the proximity to the isolectric point (pH_{IEP}). The coherence between NP size and ζ-pot results confirmed that DLS coupled with ELS represents an effective tool for the colloidal stability evaluation. As far as complete DMEM and MEM, ζ-pot data are leveled off on the value measured for the biological media without NPs (negative ζ-pot around -10 mV, see Table 3 and Figure 5c). This can be in accordance with the protein-corona theory, in which NPs are probably covered by proteins upon contact with a biological medium.[45,46] As a result, amino acids and proteins seemed to overwhelm the effects of surface-modifying agents driven the colloidal stability.

On the other hand, particles dispersed in AFW showed ζ-pot values similar to PBS while a slightly increase was observed when the stabilization was performed by polymers. According to the media preparation, the ionic strengths of AFW and PBS were comparable. Positive ζ-pot values were detected for all the samples dispersed in AMW (Figure 5d). As already described in the literature, inorganic divalent cations seem to get adsorbed on the NPs surface and to control the electrical double layer formation.[13]

A hypothetic scheme on how the different coatings (i.e. phosphate ions, modifiers, divalent cations, amino acids and proteins) affect the colloidal stability (in terms of aggregation and surface charge) of pristine and CuO-modified NPs is reported in Figure 5.

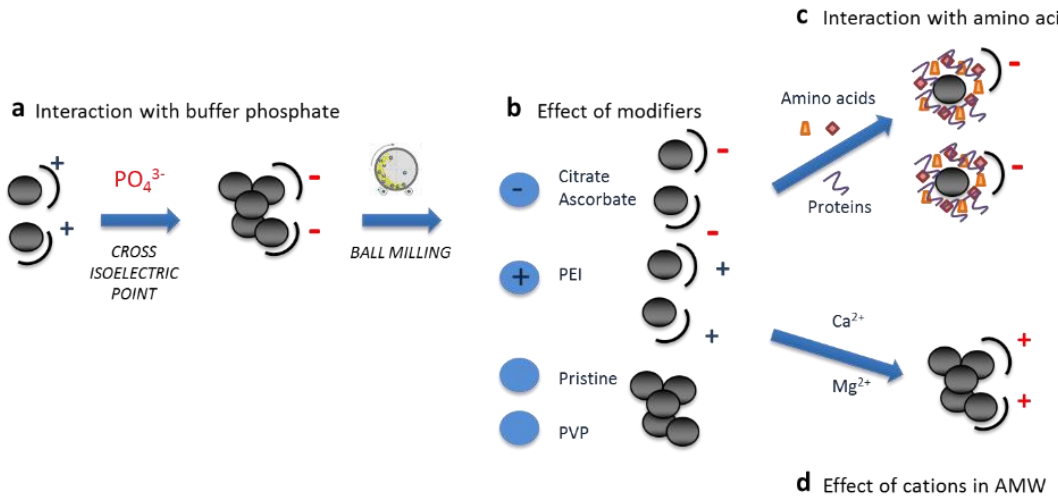

Figure 5 Hypothetic scheme of the interactions between CuO NPs and different coatings.

Colloidal stability was also investigated through CSA by means of LUMiSizer, calculating sedimentation velocity of the CuO NPs previously dispersed at 100 mg/L in MQ, PBS, MEM, DMEM, AFW and AMW.

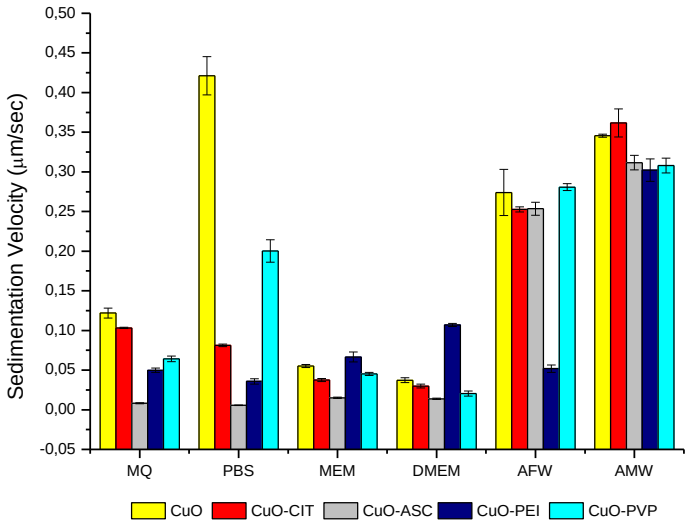

Figure 6 Average sedimentation velocity data for pristine and modified CuO NPs dispersed in MilliQ, PBS, MEM, DMEM, AFW and AMW.

Figure 6 shows the average sedimentation velocity data for pristine and modified CuO NPs dispersed in the six different media selected, highlighting a correlation with the hydrodynamic diameter determined by DLS (Table 2). Sedimentation velocity distributions are reported in Figure 5. In general, it was confirmed that the modifying agents improved the colloidal stability of the dispersions, avoiding or decreasing the formation of CuO aggregates with respect to pristine CuO NPs. In particular, as far as MilliQ and PBS media, the sedimentation velocity distribution decreased for all the modified suspensions compared to pristine CuO NPs. The sedimentation velocity rate in these two aqueous media followed the same rank observed for hydrodynamic diameter data in MilliQ (Table 2), in which pristine and CuO-PVP suspensions

are less stable than CuO-CIT followed by CuO-PEI and CuO-ASC. The correlation between LUMiSizer and DLS data was also noticed for CuO-pristine and CuO-PVP dispersed in PBS, showing both the highest sedimentation velocity values and agglomeration rates. Surprisingly, CuO-ASC dispersion revealed the lowest sedimentation velocity values in PBS but high average hydrodynamic diameter (> 1 µm). Taking into account the two different biological media, the results from LUM and DLS suggest that proteins and amino acids enhance the stability rate of the dispersions, both for pristine as well as for modified CuO. The only exception is represented by slightly higher sedimentation velocity values of CuO-PEI than the other dispersions. However, a more precise analysis of the sedimentation rates can be achieved by considering LUMiSizer numerical data thorough their quartiles, using box plot as a graphical descriptive statistic (Figure 7).

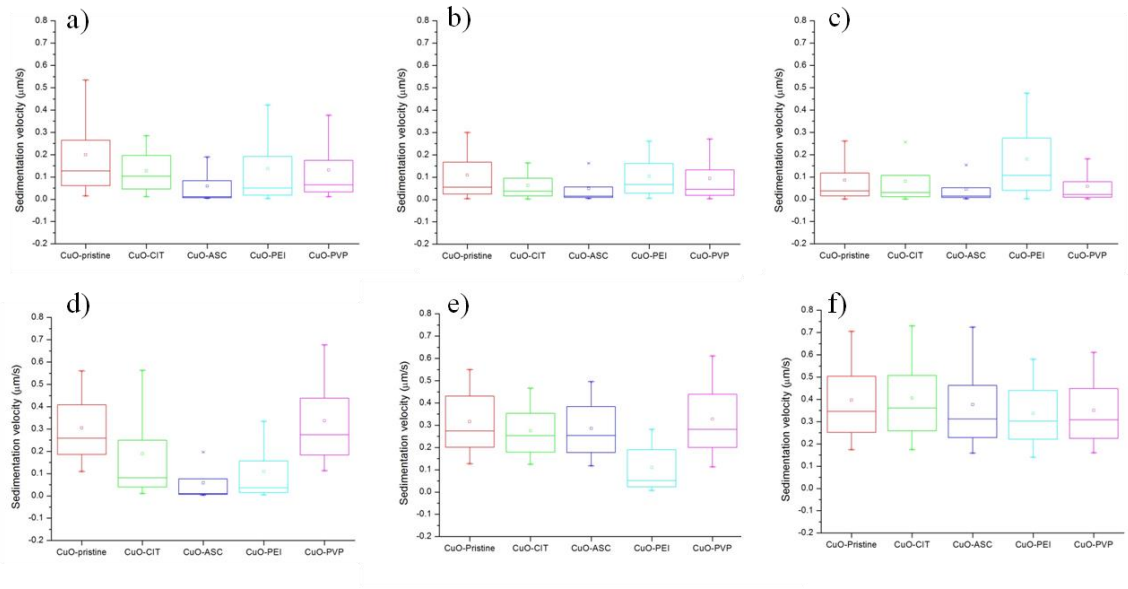

Figure 7 Sedimentation velocity distribution of pristine and modified CuO NPs dispersed in a) MilliQ, b) MEM, c) DMEM, d) PBS e) AFW and f) AMW.

Knowledge on the degree of dispersions (spread), the skewness in the data and the outliers allow to achieve more accurate information on the colloidal stability of the different dispersions with respect to the DLS data previously obtained. For example, CuO-ASC, despite the high hydrodynamic diameter detected by DLS in PBS, shows a very narrow distribution of data (due to the homogeneity of the NPs) and in general the best suspension stability in all the media analyzed. Finally, NPs dispersed in environmental media followed the same rank observed by DLS. An increase of instability was shown for all the samples both in AFW and AMW, except for CuO-PEI which showed a higher stability in AFW, resulting in agreement with hydrodynamic size and ζ-pot values (see Table 2 and 3).

Ions release data, determined by the ionic copper dissolved to total copper ratio through ultra-centrifugation followed by ICP-OES analysis, are presented in Table 4.

Table 4 $Cu_{dissolved}/Cu_{total}$ weight ratio % of pristine and modified CuO samples dispersed in different media after 24 h at 25°C (in MilliQ, PBS and environmental media) and at 37°C (in biological media).

	$Cu_{dissolved}/Cu_{total}$ weight ratio %					
	MilliQ (rsd%)	PBS (rsd%)	MEM (rsd%)	DMEM (rsd%)	AFW (rsd%)	AMW (rsd%)
CuO-pristine	0.2 (1.1)	<0.3 (0.1)	60 (0.7)	67 (0.5)	0.3 (5.5)	0.3 (5.8)
CuO-CIT	2 (0.5)	1.8 (0.4)	55 (0.5)	69 (1.0)	2.1 (0.7)	2.4 (0.6)
CuO-ASC	2 (0.5)	<0.3 (0.1)	48 (0.3)	65 (0.4)	0.7 (0.7)	0.7 (1.1)
CuO-PEI	2.8 (0.6)	2.5 (0.6)	34 (0.4)	67 (0.5)	6.3 (0.9)	7.4 (0.5)
CuO-PVP	0.2 (1.0)	<0.3 (0.1)	43 (0.3)	66 (1.3)	0.1 (2.8)	0.1 (1.6)

As it can be observed by data collected in MEM and DMEM, the dissolution greatly increased in both biological media compared to values in MilliQ, PBS, AFW and AMW media. Taking into account the dissolution experiments for all the dispersions performed in DMEM, $Cu_{dissolved}/Cu_{total}$ ratio reached values between 65 and 69% after 24h. As far as dissolution experiments in MEM, dissolution rate was slightly lower compared with data recorded in DMEM, ranging from 34 to 59% after 24h. One of the reason of the high dissolution rate of CuO NPs in the biological media tested can be ascribed to the chelating effect of amino acids and proteins.[47,48] Taking into account the different composition of the media tested, the general low CuO NPs solubility rate observed in both MilliQ and PBS (dissolution below 3%), as well as in AFW and AMW (dissolution below 8%) further confirmed the primary role of protein components that promote dissolution. Among all the media, CuO NPs dissolution rate reached the highest values in DMEM because contains approximately four times as much of glucose, amino acids and vitamins with respect to MEM.

As far as the media without amino acids and proteins (MilliQ, PBS, AFW and AMW), it was observed that the highest values were found for CuO-CIT and CuO-PEI dispersions. This confirms that the particle dissolution rate depends on the CuO NPs characteristics as well as on the chemical composition of the medium surrounding NPs, unless the features of the medium not prevail over the complete system.[27] Furthermore, in support to this, a size dependent solubility is shown in the samples dispersed in MilliQ and PBS. At low aggregation rate corresponds a high solubility (CuO-CIT and CuO-PEI). Otherwise, the samples resulted more aggregated (CuO-pristine, CuO-PVP and CuO-ASC) showed very low values of $Cu_{dissolved}/Cu_{total}$ weight ratio (%).

2.2.4 Conclusions

Four different non-hazardous modifying agents, sodium citrate (CIT), sodium ascorbate (ASC), polyethylenimine (PEI) and polyvinylpyrrolidone (PVP), were added to CuO NP suspensions for promoting the *in situ* coating of particles within a $S_{by}D$ approach. Comprehensive colloidal characterization was performed to study the evolution of pristine and modified CuO NP properties at increasing complexities of the selected media (from MilliQ water to biological

and environmental fluids). The good agreement among NPs size, ζ-pot, sedimentation velocity and dissolution results confirmed that the light scattering techniques combined with ICP-OES represent an effective tool for the assessment of NPs risk relevant properties, providing useful information for reading-across hazard and exposure potential. The overall results clearly show that the four modifying agents strongly affect CuO NPs dispersion stability only in media with ionic strength < 16 mM and without any biological component (i.e. MilliQ, PBS and AFW). However, media such as MEM and DMEM, rich in amino acids and proteins, and AMW containing high amounts of inorganic salts (especially divalent cations) totally drive the colloidal stability regardless the coating agent involved.

The obtained results contributed to understand the interactions between NPs and media components such as amino acids, proteins, divalent cations and phosphates. We expect that these results will facilitate the interpretation of (eco)toxicological data and will contribute to our knowledge of key nano-bio/eco interactions and modes of action as the basis to establish criteria and guiding principles for grouping and read-across for the purposes of risk assessment and safer product design.

2.3) Open issue

From these studies on Cu-ENMs in both environmental and biological media, it emerges that many variables influence particle transformations, especially in dissolution phenomena. Furthermore, as dissolution is a dynamic transformation also affected by the particle diameter, become difficult to express a dissolution rate in ppm/sec, because as it was described before, small particles dissolve more quickly than larger particles. For this reason, the dissolution rate must be normalized on the surface area or on the diameter. In this context, sp-ICP-MS can be the right technique to solve this problem, because it can provide information on both particle diameters and dissolved ions. In literature is reported the dissolution of Ag ENMs in freshwater (surface water, tap water and artificial freshwater) by using the sp-ICP-MS and it was shown that after 1 week, silver nanoparticles decrease their diameters (Figure 8).[49]

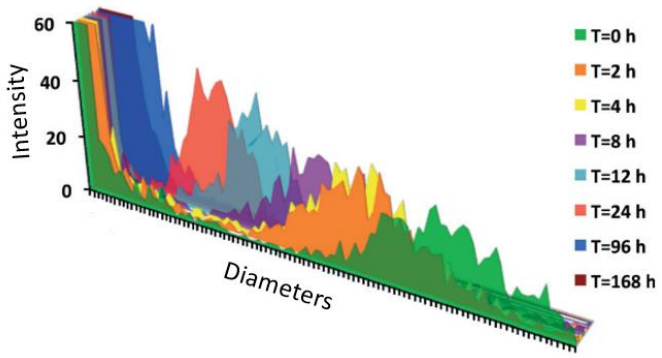

Figure 8 Dissolution of 100 nm Tannic Acid capped Ag ENMs at 50 ng/L over time, as evidenced by the decrease in diameters over time.(from Mitrano 2014)[49]

A size decrease was not observed for CuO ENMs, but rather a decrease in particle number, as is reported in Graph 6.

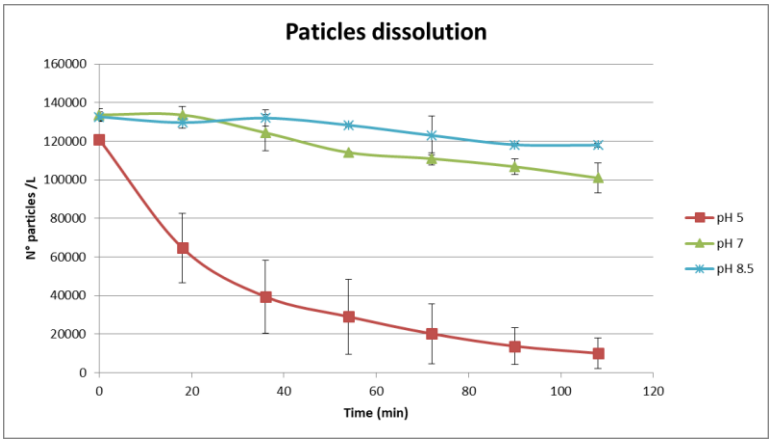

Graph 6 CuO Particle number decrease over 110 minutes at pH 5, 7, 8.5

This phenomenon may be due to the relative proximity of the primary particle diameter to the DL_S, which make it impossible to monitor a rapid decrease in diameter. It could be possible that following bigger nanoparticles, far away from the DL_S, better results can be obtained as reported by Mitrano et al. (2014)[49] for the dissolution of silver.

2.4) References

1. Appelo, C. A. J. & Postma, D. Geochemistry, Groundwater and Pollution, Second Edition. *Can. J. Microbiol.* (2010). doi:10.1201/9781439833544

2. Misra, S. K., Dybowska, A., Berhanu, D., Luoma, S. N. & Valsami-Jones, E. The complexity of nanoparticle dissolution and its importance in nanotoxicological studies. *Sci. Total Environ.* **438,** 225–232 (2012).

3. Pace, H. E. *et al.* Determining transport efficiency for the purpose of counting and sizing nanoparticles via single particle inductively coupled plasma mass spectrometry. *Anal. Chem.* (2011). doi:10.1021/ac201952t

4. Conway, J. R., Adeleye, A. S., Gardea-Torresdey, J. & Keller, A. A. Aggregation, dissolution, and transformation of copper nanoparticles in natural waters. *Environ. Sci. Technol.* **49,** 2749–2756 (2015).

5. Studer, A. M. *et al.* Nanoparticle cytotoxicity depends on intracellular solubility: Comparison of stabilized copper metal and degradable copper oxide nanoparticles. *Toxicol. Lett.* **197,** 169–174 (2010).

6. Odzak, N., Kistler, D., Behra, R. & Sigg, L. Dissolution of metal and metal oxide nanoparticles in aqueous media. *Environ. Pollut.* **191,** 132–138 (2014).

7. Vogelsberger, W., Schmidt, J. & Roelofs, F. Dissolution kinetics of oxidic nanoparticles: The observation of an unusual behaviour. *Colloids Surfaces A Physicochem. Eng. Asp.* **324,** 51–57 (2008).

8. Hristozov, D. *et al.* Frameworks and tools for risk assessment of manufactured nanomaterials. *Environ. Int.* **95,** 36–53 (2016).

9. Hristozov, D. R., Gottardo, S., Critto, A. & Marcomini, A. Risk assessment of engineered nanomaterials: A review of available data and approaches from a regulatory perspective. *Nanotoxicology* (2012). doi:10.3109/17435390.2011.626534

10. Hristozov, D. & Malsch, I. Hazards and Risks of engineered nanoparticles for the environment and human health. *Sustainability* (2009). doi:10.3390/su1041161

11. Oomen, A. G. *et al.* Grouping and read-across approaches for risk assessment of nanomaterials. *Int. J. Environ. Res. Public Health* **12,** 13415–13434 (2015).

12. Stone, V. *et al.* ITS-NANO - Prioritising nanosafety research to develop a stakeholder driven intelligent testing strategy. *Part. Fibre Toxicol.* (2014). doi:10.1186/1743-8977-11-9

13. Mudunkotuwa, I. A. & Grassian, V. H. Environmental Science Nano Biological and environmental media control oxide nanoparticle surface composition : the roles of biological components (proteins and amino acids), inorganic oxyanions and humic acid †. *Environ. Sci. Nano* **2,** 429–439 (2015).

14. Sohaebuddin, S. K., Thevenot, P. T., Baker, D., Eaton, J. W. & Tang, L. Nanomaterial cytotoxicity is composition, size, and cell type dependent. *Part. Fibre Toxicol.* (2010). doi:10.1186/1743-8977-7-22

15. Docter, D. *et al.* The nanoparticle biomolecule corona: lessons learned - challenge

accepted? *Chem. Soc. Rev.* **44,** 6094–6121 (2015).

16. Fadeel, B. & Garcia-Bennett, A. E. Better safe than sorry: Understanding the toxicological properties of inorganic nanoparticles manufactured for biomedical applications. *Advanced Drug Delivery Reviews* (2010). doi:10.1016/j.addr.2009.11.008

17. Lynch, I., Weiss, C. & Valsami-Jones, E. A strategy for grouping of nanomaterials based on key physico-chemical descriptors as a basis for safer-by-design NMs. *Nano Today* (2014). doi:10.1016/j.nantod.2014.05.001

18. Bergamaschi, E. *et al.* Impact and effectiveness of risk mitigation strategies on the insurability of nanomaterial production: Evidences from industrial case studies. *Wiley Interdiscip. Rev. Nanomedicine Nanobiotechnology* (2015). doi:10.1002/wnan.1340

19. Deng, Z. J., Liang, M., Monteiro, M., Toth, I. & Minchin, R. F. Nanoparticle-induced unfolding of fibrinogen promotes Mac-1 receptor activation and inflammation. *Nat. Nanotechnol.* (2011). doi:10.1038/nnano.2010.250

20. Johnston, R. L. & Wilcoxon, J. P. *FRONTIERS OF NANOSCIENCE Series Editor : Richard E . Palmer The Nanoscale Physics Research Laboratory , The School of Physics and Astronomy , The University of Birmingham , UK Vol . 1 Nanostructured Materials edited by Gerhard Wilde Vol . 2 Atomic and Mol*. **1,**

21. Moore, T. L. *et al.* Nanoparticle colloidal stability in cell culture media and impact on cellular interactions. *Chem. Soc. Rev.* (2015). doi:10.1039/C4CS00487F

22. Nowack, B. *et al.* Potential scenarios for nanomaterial release and subsequent alteration in the environment. *Environmental Toxicology and Chemistry* (2012). doi:10.1002/etc.726

23. Meißner, T., Oelschlägel, K. & Potthoff, A. Implications of the stability behavior of zinc oxide nanoparticles for toxicological studies. *Int. Nano Lett.* **4,** 116 (2014).

24. Ren, G. *et al.* Characterisation of copper oxide nanoparticles for antimicrobial applications. *Int. J. Antimicrob. Agents* (2009). doi:10.1016/j.ijantimicag.2008.12.004

25. Rubilar, O. *et al.* Biogenic nanoparticles: Copper, copper oxides, copper sulphides, complex copper nanostructures and their applications. *Biotechnology Letters* (2013). doi:10.1007/s10529-013-1239-x

26. Nations, S. *et al.* Subchronic and chronic developmental effects of copper oxide (CuO) nanoparticles on Xenopus laevis. *Chemosphere* (2015). doi:10.1016/j.chemosphere.2015.03.078

27. Cronholm, P. *et al.* Intracellular uptake and toxicity of Ag and CuO nanoparticles: A comparison between nanoparticles and their corresponding metal ions. *Small* (2013). doi:10.1002/smll.201201069

28. Thit, A., Selck, H. & Bjerregaard, H. F. Toxic mechanisms of copper oxide nanoparticles in epithelial kidney cells. *Toxicol. Vitr.* (2015). doi:10.1016/j.tiv.2015.03.020

29. Ortelli, S. & Costa, A. L. Nanoencapsulation techniques as a “safer by (molecular) design” tool. *Nano-Structures and Nano-Objects* (2018). doi:10.1016/j.nanoso.2016.03.006

30. Ortelli, S., Poland, C. A., Baldi, G. & Costa, A. L. Silica matrix encapsulation as a strategy to control ROS production while preserving photoreactivity in nano-TiO2. *Environ. Sci. Nano* (2016). doi:10.1039/c6en00009f

31. Gardini, D. *et al.* Silica-coating as protective shell for the risk management of nanoparticles. *J. Phys. Conf. Ser.* **429,** (2013).

32. Sun, B. *et al.* Reduction of Acute Inflammatory Effects of Fumed Silica Nanoparticles in the Lung by Adjusting Silanol Display through Calcination and Metal Doping. *ACS Nano* (2015). doi:10.1021/acsnano.5b03443

33. Petros, R. A. & Desimone, J. M. Strategies in the design of nanoparticles for therapeutic applications. *Nature Reviews Drug Discovery* (2010). doi:10.1038/nrd2591

34. OECD. OECD 203 Fish Acute Toxicity Test. *OECD Guidel. Test. Chem. Sect. 2,* (1992). doi:10.1787/20745761

35. Developed by Subcommittee: D19.02. in *Book of Standards Volume: 11.02* (2013).

36. Wick, P. *et al.* The degree and kind of agglomeration affect carbon nanotube cytotoxicity. *Toxicol. Lett.* (2007). doi:10.1016/j.toxlet.2006.08.019

37. Rivera-Gil, P. *et al.* The challenge to relate the physicochemical properties of colloidal nanoparticles to their cytotoxicity. *Acc. Chem. Res.* (2013). doi:10.1021/ar300039j

38. Goodman, C. M., McCusker, C. D., Yilmaz, T. & Rotello, V. M. Toxicity of gold nanoparticles functionalized with cationic and anionic side chains. *Bioconjug. Chem.* (2004). doi:10.1021/bc049951i

39. McFarlane, N. L., Wagner, N. J., Kaler, E. W. & Lynch, M. L. Poly(ethylene oxide) (PEO) and poly(vinyl pyrolidone) (PVP) induce different changes in the colloid stability of nanoparticles. *Langmuir* (2010). doi:10.1021/la101907s

40. Liu, X. & Chen, K. L. Aggregation and interactions of chemical mechanical planarization nanoparticles with model biological membranes: Role of phosphate adsorption. *Environ. Sci. Nano* (2016). doi:10.1039/c5en00176e

41. Karimi, I., Hashemi, B., Javidi, M. & Azadani, S. N. Studying effect of various stabilisers on sol electrophoretic deposition of titania. *Surf. Eng.* **28,** 737–742 (2012).

42. Xia, T., Kovochich, M., Liong, M., Zink, J. I. & Nel, A. E. Cationic polystyrene nanosphere toxicity depends on cell-specific endocytic and mitochondrial injury pathways. *ACS Nano* (2008). doi:10.1021/nn700256c

43. Guerrero-Garc??a, G. I., Gonz??lez-Tovar, E. & Olvera De La Cruz, M. Effects of the ionic size-asymmetry around a charged nanoparticle: Unequal charge neutralization and electrostatic screening. *Soft Matter* (2010). doi:10.1039/b924438g

44. Karlsson, H. L. *et al.* Cell membrane damage and protein interaction induced by copper containing nanoparticles-Importance of the metal release process. *Toxicology* (2013). doi:10.1016/j.tox.2013.07.012

45. Ji, Z. *et al.* Dispersion and stability optimization of TiO2 nanoparticles in cell culture media. *Environ. Sci. Technol.* (2010). doi:10.1021/es100417s

46. Catalano, F. *et al.* Factors Ruling the Uptake of Silica Nanoparticles by Mesenchymal Stem Cells: Agglomeration Versus Dispersions, Absence Versus Presence of Serum Proteins. *Small* (2015). doi:10.1002/smll.201400698

47. Midander, K. *et al.* Surface characteristics, copper release, and toxicity of nano- and micrometer-sized copper and copper(II) oxide particles: A cross-disciplinary study. *Small* **5,** 389–399 (2009).

48. Semisch, A., Ohle, J., Witt, B. & Hartwig, A. Cytotoxicity and genotoxicity of nano - and microparticulate copper oxide: Role of solubility and intracellular bioavailability. *Part. Fibre Toxicol.* (2014). doi:10.1186/1743-8977-11-10

49. Mitrano, D. M. *et al.* Tracking dissolution of silver nanoparticles at environmentally relevant concentrations in laboratory, natural, and processed waters using single particle ICP-MS (spICP-MS). *Environ. Sci. Nano* **1,** 248–259 (2014).

Chapter 3

CuO vs $Cu_2CO_3(OH)_2$ in human toxicity tests

The raising concerns about potential exposure to Cu-ENMs on human health and environment, pushed the global community to invest a lot of money and resource for investigating the problems involved in the use of this new materials in commercial products. Following the principles of Safe by Design, within the European project SUN, several (eco)toxicological tests have been conducted to evaluate the real hazard associated to these materials and to find a way for reducing their toxicity, without altering their properties.

In this context, in order to evaluate the toxicological effects of Cu-ENMs in different exposure route, in-vivo oral and inhalation tests have been conducted, evaluating also the effects of different Cu-ENMs ($Cu_2CO_3(OH)_2$, CuO, and modify CuO).

3.1) Short-Term Inhalation Study (STIS) of modified CuO in rats ([c])

Gosens et al.(2016)[1] reported the pulmonary toxicity of nano-sized copper (II) oxide particles after short-term inhalation exposure in order to evaluate the intrinsic hazard related to inhalation of Cu-ENMs. From this study, emerges that a dose-dependent increase in lung inflammation, and both cellular damage and nose epithelium degeneration appear after 5 days of consecutive exposure to CuO ENMs. Starting from these results, a new series of experiments was conducted by using CuO ENMs modified with polyethylenimine and sodium ascorbate, whose characterization is reported in Chapter 2 section *"Colloidal characterization of CuO nanoparticles in biological and environmental media"*.

3.1.1 Materials and methods

The short-term inhalation study was performed by the National Institute for Public Health and the Environment RIVM (partner of SUN project). Pristine CuO ENMs and two modified CuO samples were chosen by RIVM for carried out the tests using already described protocols.[1]

The acid mixture used for samples mineralization included HNO_3 (TRACE SELECT ULTRA 69%, Sigma-Aldrich <0.5µg/Kg), H_2O_2 (TRACE SELECT ULTRA 30%, Sigma-Aldrich <0.05µg/Kg), in a 2:1 ratio. The microwave system ETHOS 1600 (Milestone), was used to digest the samples, following the procedure reported in Table 1. Afterwards, the samples were allowed to cool down for 30 minutes at room temperature. The obtained solutions were transferred in PTFE tubes and diluted to 25 mL with MilliQ water.

[c] My contribution in this section is related to the optimization of the microwave digestion, the ICP-MS analysis and the data treatment.

Table 1 Heating program for acid digestion

STAGE	RAMP TIME (min)	POWER (Watt)
1	1	250
2	1	0
3	5	250
4	3	400
5	3	600

An aliquot of each sample solution was properly diluted and analyzed by inductively coupled plasma mass spectrometry equipped with double channel Universal Cell (sp-ICP-MS NexION 350D, Perkin Elmer).

For the quantification of Copper, isotope ^{65}Cu was selected because of the less polyatomic interferences (e.g. $^{40}Ar^{23}Na$) than isotope ^{63}Cu. Samples were quantified by external calibration method using a multi-point curve (blank and 10 points over the concentration range 10 µg/L to 300 µg/L). Yttrium at 5 µg/L was used as internal standard.[2]

Potential contamination from the laboratory was controlled by adding at least one reagent blank during each digestion session.

The limit of detection and the limit of quantification were calculated for each sample set as the average of blanks + 3 standard deviation (SD) and as the average of blanks + 10 SD, respectively.

In order to verify the accuracy and repeatability of the method, 6 aliquots of the standard reference material (SRM) NIST 1577c (bovine liver) were analysed every 10 samples.[3] The average Cu concentration detected in the SRM was 277 ± 5 mg/Kg, in satisfactory agreement with the reference value (267 ± 6 mg/Kg); with respect to the certified value, the recovery of Cu ranged from 90 to 101%.

The Background Equivalent Concentration signal (BEC, providing the actual magnitude of noise) detected was 0.033 ng/L. Average blank values, LOD and LOQ were calculated by considering both the reagent and the control blanks. Detected LOD and LOQ value were, respectively, 153 ng/L and 461 ng/L.

3.1.2 Results

Previous characterization of CuO ENMs in different media, showed that in the biological media (DMEM) all the samples, pristine and modified nanomaterials, were partially dissolved after 24 h.[4] Though the information related to the possible presence of Cu-ENMs in the biological tissue can be very useful for understanding the mechanisms involved in the inflammation processes, the experimental design provide only the copper burden into organs, without any speciation between particles and dissolved form. Taking into account this consideration, a strong acid digestion was carried out, by using a moisture of nitric acid and hydrogen peroxide, under microwave condition.

Table 2 Experiment Plan, flux in m^3/h of ENM for STIS

	1day after exposion				22day after exposion			
*Pristine	0	0,5	2,9	11,6	0	0,5	2,9	11,6
PEI	0	1,7	15		0	1,7	15	
ASC	0	2,2	20		0	2,2	20	

As shown in Table 2, the rats were exposed to different experimental conditions, such as different concentrations of CuO in the inhalation atmosphere, day in which the autopsy was made and type of ENM tested (four rats for each experiment). For each rat six different organs were analyzed, in detail: liver, brain, spleen, lungs, heart, kidneys.

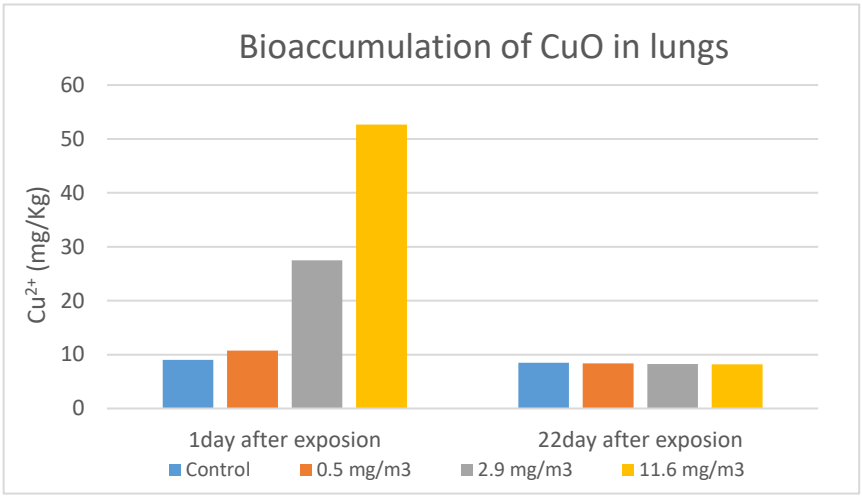

Graph 1 Cu^{2+} Bioaccumulation in lungs from CuO ENM pristine after 1 and 22 days with different flux (from Gosens et al. 2016)[1]

In the Graph 1, the bioaccumulation of Cu^{2+} in the lungs of rats is reported. As it can be seen, the measured lung burden was linear with the increasing equivalent concentration, but after 22 days from the last exposure, the Cu^{2+} was cleared completely from the lungs and levels returned to baseline.[1]

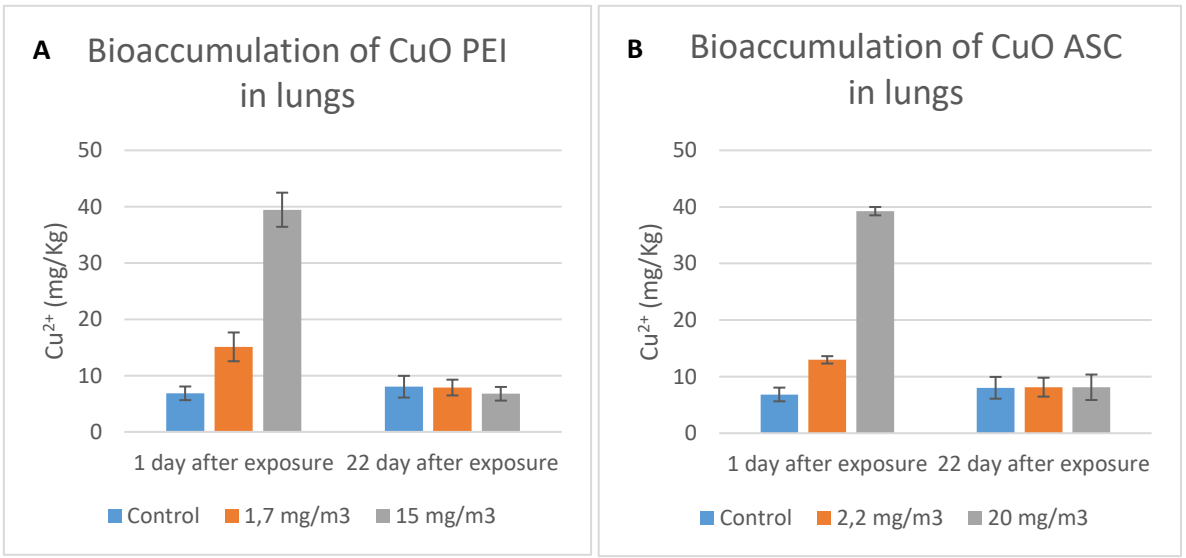

Graph 2 Cu^{2+} Bioaccumulation in lungs from CuO ENM PEI modify and ASC modify after 1 and 22 days using different flux

In Graph 2, the bioaccumulation of Cu^{2+} in the lungs of rats after inhalation of CuO ENMs modified with PEI [A] and with ASC [B] is reported. In both experiments, after 22 days the lungs are completely cleaned from Cu^{2+}. However, from the bioaccumulation experiments performed at day 1, the concentration of Cu^{2+} in the lungs of rats exposed to both CuO-PEI and CuO-ASC resulted slightly lower than those obtained for pristine (moving from 51 mg/Kg for pristine to 39 mg/Kg for functionalized CuO ENMs). Furthermore, a correlation between dose and copper bioaccumulation was observed for all the samples investigated.

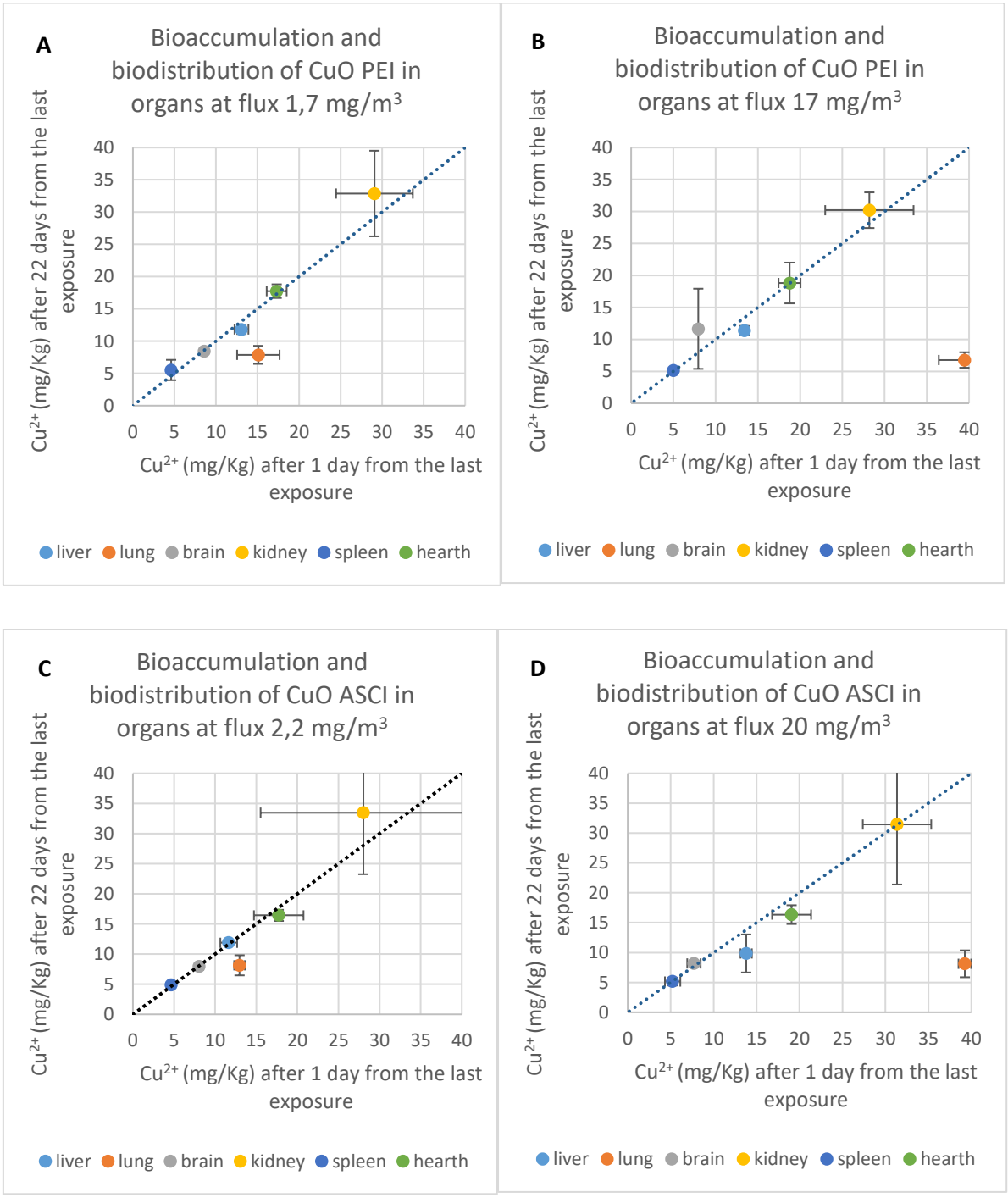

Graph 3 Bioaccumulation and biodistribution in different organs are reported, A) CuO PEI 1.7 mg/m³, B) CuO PEI 17 mg/m³, C) CuO ASC 2.2 mg/m³, D) CuO ASC 20 mg/m³. Values located away from the diagonal shows bioaccumulation

In Graph 3 the complete screening of the organs analyzed is reported; for all organs after 22 days, the Cu^{2+} value found in the tissue is comparable with the control value. Values distributed along the diagonal indicate no bioaccumulation, while values located away from the diagonal indicated organs subject to bioaccumulation.

3.1.3 Conclusion

From this study emerge that, as reported by Goosen et al. (2016)[1] in CuO STIS, both CuO ASC and CuO PEI show an initial increment in lung's copper concentration (c.a 15 mg/Kg for low flow and 40 mg/Kg for high flow) followed by a total "cleaning" of the organs. Moreover, it resulted clear that the main target organs involved in these processes are the lungs for the direct contact with the aerosol, and liver and kidneys for the detoxification process. The constant concentration of Cu^{2+} in the brain suggested, according to the data present in the literature, that blood-brain barrier is preventing its accumulation in this organ.[5]

3.2) Toxicity of Copper oxide and basic copper carbonate nanoparticles after short-term oral exposure in rats ([d])

In this section a part of the paper "Toxicity of Copper oxide and basic copper carbonate nanoparticles after short-term oral exposure in rats" published on the journal Nanotoxicology is reported; In summary, has been evaluated the toxicity in Short Term Oral Exposure (STOS) studies between CuO and $Cu_2CO_3(OH)_2$ after 1 and 21 days of oral administration is compared. These tests are useful to understand the relative toxicity of $Cu_2CO_3(OH)_2$ used in fungi wood protection.

Authors: De Jong W.H., De Rijk E., Bonetto A., Wohlleben W., Stone V., Brunelli A., Badetti E., Marcomini A., Gosensn I., Cassee F.

3.2.1 Introduction

Materials such as wood need to be protected against degradation induced by fungi, bacteria and insects in order to prolong their use duration. Copper (Cu) is the most widely used fungicide for treating wood in contact with the soil, with no satisfactory alternative available since it is the only biocide that shows significant effects against soft rot fungi and other soil borne fungi. Cu is compulsory for in-ground timber structures (use class 4 i.e. timber treated to make it suitable to be used in direct soil or water contact) and is a preferred antimicrobial wood preservative due to its minimal effect on mammals, including humans even if it shows a relatively high toxicity against aquatic communities. [6,7] Application occurs via impregnation techniques under high pressure and via non-pressure techniques like brushing, spraying and coat-cutting.[7] Solid copper carbonate ($Cu_2CO_3(OH)_2$) needs to be micronized by milling to generate particle sizes able to penetrate depths in the order of centimetres into the wood during pressure treatment. The resulting size distributions of micronized copper formulations contain a considerable fraction of nanoparticles. Woods impregnated with micronized Cu release any other Cu species than ions. At equal Cu loading per cubic meter of wood, form and rate of release are comparable to wood impregnated with molecular Cu−amine but slightly more stable throughout aging; this finding was attributed to the transformations during the wood use.[8] In comparison to solutions of Aqueous Copper amine (ACA) treated woods, the micronized copper treated woods feature a lower corrosive potential, a natural wood colour, and at least the same effectiveness of protection against fungal decomposition.[6,7,9–11] However, the use of nanoparticle-containing copper formulations has led to concerns regarding their safety in general [12–15] and specifically by hand-to-mouth transfer during installation or use of wooden installations.[11] To the best of our knowledge, there are no publication on oral toxicity of micronized $Cu_2CO_3(OH)_2$, whereas the oral toxicity of Cu ions is extremely well known with an acceptable drinking water standard of 1.3 mg/L.[16] Potential transformation between particulate and ionic forms of copper is likely, because leaching

[d] My contribution in this paper is related to the quantification of Copper in biological tissues, in particular biodistribution and bioaccumulation have been evaluated by using ICP-MS. I was also involved in the data treatment and in the optimization of the analysis methods.

studies indicated that the very acidic stomach fluids extract exclusively Cu ions from wood treated with micronized copper.[17,18]

Results from *in vivo* studies indicate that lung inflammation / toxicity after inhalation of copper oxide nanoparticles (CuO ENMs) resolved over 3 weeks[1] indicating a rapid recovery and very little if any Cu was left in the body of these animals. In addition, systemic organ toxicity was observed after repeated intraperitoneal administration of copper oxide nanoparticles.[19] For copper nanoparticles *in vivo* toxicity was reported in mice and rats after oral administration.[20–23] The aim of this study was to compare the toxicity of CuO ENMs and $Cu_2CO_3(OH)_2$ ENMs following short term repeated oral exposure.

3.2.2 Materials and Methods

3.2.2.1 Test material

CuO nanoparticles (CuO-ENMs) were obtained as a black powder from PlasmaChem, GmbH (Berlin, Germany). The crystalline material exhibited a size of 15-20 nm, a specific surface area of 47 m^2/g as assessed by the Brunauer–Emmett–Teller (BET) method and a density of 6.3 g/cm^3 according to the manufacturer's datasheet. The particles were crystalline with a density little below bulk (6.3 g/cm^3). An extensive characterization is presented in Pantano et al. (2018).[8] $Cu_2CO_3(OH)_2$ ENMs were obtained as an aqueous dispersion from BASF SE, identification number LP 17206 (30% Cu), lot nr VM3041, best before date 05.02.2017.

3.2.2.2 CuO ENMs and $Cu_2CO_3(OH)_2$ ENMs dispersions

CuO ENM powder and $Cu_2CO_3(OH)_2$ ENM suspensions were dispersed (CuO ENM) or further diluted ($Cu_2CO_3(OH)_2$ ENM) in Milli-Q water before sonication for 16 minutes in a waterbath (Elmasonic S100) at room temperature to optimize dispersion quality. Before each administration the nanoparticle dispersion was evaluated by CPS Disc Centrifuge™ (CPS Instruments Europe, Oosterhout, The Netherlands) to determine nanoparticle size and size distribution. Both the CuO ENM and the $Cu_2CO_3(OH)_2$ ENM dispersions remained stable up to 24 and 72 hours, respectively, after preparation of the dispersion.

3.2.2.3 Dissolution of CuO ENM and $Cu_2CO_3(OH)_2$ ENMs

A dynamic flow-through system (Wohlleben et al. 2017) was used to determine the dissolution rate of both CuO ENM and $Cu_2CO_3(OH)_2$ ENM far from equilibrium. The solid mass of 1mg of Cu (that is 1.25 mg of CuO powder or 3.47 mg of the $Cu_2CO_3(OH)_2$ suspension), was weighed onto a membrane (cellulose triacetate, Sartorius Stedim Biotech GmbH, Goettingen, Germany: 47 mm diameter, 5 kDa pore size), topped by another identical membrane, and enclosed in flow-through cells. Two complex buffers with standardized composition were used to mimic the stomach and intestine conditions at 37 ± 0.5 °C, all values in mM.[24] For the stomach conditions, the buffer was pH 1.6 and consisted of: sodium taurocholate 0.08 mM; lecithin 0.02 µM; pepsin 0.1 mg/mL and sodium chloride 34.2 mM. For the intestine conditions, the buffer was pH 5.8 and consisted of Fed-State Simulated Intestinal Fluid (FeSSIF):[25] Sodium taurocholate 10 mM, lecithin 2 mM, maleic acid 55.02 mM, sodium

hydroxide 81.65 mM, sodium chloride 125.5 mM, glyceryl monocholate 5 mM and sodium oleate 0.8 mM.

The eluates were determined by inductively coupled plasma-optical emission spectrometry (ICP-OES, Agilent 5100). After the experiment the remaining solids were rinsed off the membrane by particle-free water (Milli-Q). The resulting suspension was then pelleted onto a TEM grid held at the bottom of a centrifuge vial within 1h, then dried, so that the remaining solids morphology could be inspected without interference from drying artifacts of bile salts, which are removed by this preparation. The remaining solids were analyzed by 200 keV bright-field TEM (Tecnai G2-F20ST or Tecnai Osiris, FEI Company, Hillsboro, USA).

3.2.2.4 Experimental design

Male specific pathogen free rats (RjHan:WI,) aged 8-9 weeks were obtained from Janvier Labs (Le Genest-Saint-Isle, Saint Berthevin , France). The animals were treated via oral gavage for 5 days (days 1 to 5). The ENMs were administered by oral gavage using a bulb tipped gavage needle attached to a syringe. Each treatment was administered as 0.1 mL per 20 g (1 mL per 200 g). For both CuO ENMs and $Cu_2CO_3(OH)_2$ ENMs, each dose group consisted of 8 animals of which 4 were sacrificed at day 6 (1 day after the last treatment) and 4 were sacrificed at day 26 (21 days after the last treatment). The day 26 time point was included in order to evaluate recovery, possible persistence of effects or progression of effects induced by the ENMs. See Supplementary Table 1 for the experimental design of the study.

Assuming that the CuO ENMs would be largely dissolved in the acid environment of the stomach a starting dose of CuO ENMs was selected based on the literature for dissolved $CuSO_4$. The no-observed-adverse-effect-level (NOAEL) for $CuSO_4$ was reported to be 16.3 mg/Kg b.w. (ECHA 2008). A pilot study was conducted with 2 animals with a dose of 64 mg/Kg b.w. (day 1-5 daily). Based upon observations from the pilot study, the doses administered in the subsequent study were: vehicle control, 1, 2, 4, 8, 16, and 32 mg/Kg b.w. CuO ENMs. These doses were selected to be below and above the reported NOAEL for $CuSO_4$.[26] In an additional study one group of animals (n=4) was treated with a high dose of 512 mg/Kg b.w.

For $Cu_2CO_3(OH)_2$ ENMs a pilot study according to OECD TG 425 was performed to determine the starting dose in the 5 days oral gavage toxicity study.[27] One animal was treated orally with a single dose of $Cu_2CO_3(OH)_2$-ENM. If no toxicity was observed the dose was increased in the next animal until a toxic response was noted. When a single animal showed a toxic response an additional 4 animals were administered with the same dose. The highest dose chosen for $Cu_2CO_3(OH)_2$ ENM was 128 mg/Kg b.w. $Cu_2CO_3(OH)_2$ ENMs were administered via gavage in the 5 days oral study as vehicle control, 4, 8, 16, 32, 64 and 128 mg/Kg b.w.

3.2.2.5 Histopathology

At day 6 and day 26 animals were killed by exsanguination from the abdominal aorta during anaesthesia by isoflurane (3.5% in oxygen) inhalation. General macroscopic post mortem examinations were performed on all animals. At the time of necropsy, the following tissues

and organs were collected and fixed in 4% neutral buffered formaldehyde (10% formalin): heart, lung, thymus, liver, spleen, kidney, testes, brain, mesenteric lymph node, adrenal glands, pancreas, prostate, seminal vesicles, epididymis, thyroid gland, skeletal muscle - quadriceps, stomach, duodenum, jejunum, ileum, Peyer's patches, cecum, colon, rectum, skin, popliteal lymph node, femur with bone marrow, and peripheral nerve.

Microscopic examination of routinely prepared hematoxylin-eosin stained paraffin sections was performed on heart, lungs, thymus, stomach, duodenum, jejunum, ileum, Peyer's patches, cecum, colon, rectum, liver, spleen, mesenteric lymph nodes, kidneys, adrenal glands, brain, testis (unilateral), and femur with bone marrow. Microscopy was performed on all control groups and 32, 64 and 512 mg/Kg b.w. CuO ENMs treated animals and for 64 and 128 mg/Kg b.w. $Cu_2CO_3(OH)_2$ ENMs treated animals.

The animal data and macroscopic findings were manually entered into the computer system PathData®. Histopathological changes of examined sections were described according to distribution, severity and morphological character.

3.2.2.6 Cu^{2+} determination in organs

The acid mixture used for organ sample digestion included HNO_3 (trace select ultra 69%, Sigma-Aldrich <0.5µg/Kg), and H_2O_2 (trace select ultra 30%, Sigma-Aldrich <0.05µg/Kg), in a 2:1 ratio. The microwave system ETHOS 1600 (Milestone S.r.l., Sorisole, Italy) was used to digest the samples, following a dedicated heating program (1 minute 250 watt, 1 minute 0 Watt, 5 minutes 250 Watt, 3 minutes 400 Watt, and 3 minutes 600 Watt). Afterwards, the samples were allowed to cool down for 30 minutes at room temperature. The obtained solutions were transferred in PTFE tubes and diluted to 25 mL with MilliQ water. For determination of the Cu content an aliquot of each sample solution was properly diluted and analyzed by inductively coupled plasma mass spectrometry equipped with single channel Universal Cell (sp-ICP-MS NexION 350D, Perkin Elmer). Isotope ^{65}Cu was selected to quantify Cu because of the less polyatomic interferences (e.g. $^{40}Ar^{23}Na$) than isotope ^{63}Cu. Moreover, to decrease interferences Kinetic Energy Discrimination (KED) was employed, using He as collision gas. Samples were quantified by external calibration method using a multi-point curve (blank and 10 points over the concentration range from 0.5 µg/L to 5000 µg/L). Yttrium at 5 µg/L was used as internal standard.[2]

Potential contamination from the laboratory was controlled by adding at least one reagent blank during each digestion session. The limit of detection and the limit of quantification were calculated for each sample, set as the average of blanks + 3 standard deviation and as the average of blanks + 10 SD, respectively. In order to verify the accuracy and repeatability of the method, 6 aliquots of the Standard Reference Material (SRM) bovine liver (NIST 1577c, National Institute of Standards and Technology, Gaithersburg, Maryland, USA) were analysed every 10 samples.[3] The average Cu concentration detected in the SRM was 277 ± 5 mg/Kg, in satisfactory agreement with the reference value (262 ± 2 mg/Kg). Average blank values, LOD and LOQ were calculated by considering both the reagent and the control blanks. Detected

LOD and LOQ value were 20 ng/L and 68 ng/L, respectively. Copper concentration in tissues and organs from rats exposed to CuO ENMs and $Cu_2CO_3(OH)_2$ ENMs, are expressed on a dry weight basis,

3.2.3 Results

3.2.3.1 Particle Dissolution and Transformation

CuO ENM and $Cu_2CO_3(OH)_2$ ENM dissolve completely under stomach conditions at pH1.6 within 72h (Figure 2). During that time, the ion-resolved dissolution rate was very similar for both materials with 50% dissolved after about 16h for both materials. As this time is longer than the residence time in the stomach, we tested independently the dissolution under pH5.8 intestine conditions. Here we observed that the dissolution is incomplete, although transformation of the particles is clearly observed in the TEM (Figure 1f): the primary particles shrink, but agglomerate at the same time to large structures. The time to 50% dissolution is 20h for micronized copper carbonate ($Cu_2CO_3(OH)_2$ ENMs) but 50h for CuO ENMs. Adding to this interesting difference, we observed that dissolution occurs at much lower rates in the simple GI-tract simulant medium with the $NaNO_3$ buffer at pH5.3 compared to the complex GI-tract simulant FeSSIF-V2 (pH 5.8) . Thus, the dissolution in the intestine is not only pH driven but is likely to be accelerated by the bile salts and other physiological substances, in complete analogy to the interactions observed under environmental dissolution and transformation of Cu ENMs.[28,29] The dissolution kinetics of the ENMs in stomach fluid simulant is presented in Figure 2. Dissolution in gastro-intestinal fluid simulant and simple medium is shown in Supplementary Figures 2 and 3. Transformation of the CuO ENM and $Cu_2CO_3(OH)_2$ ENM is shown in Figure 1.

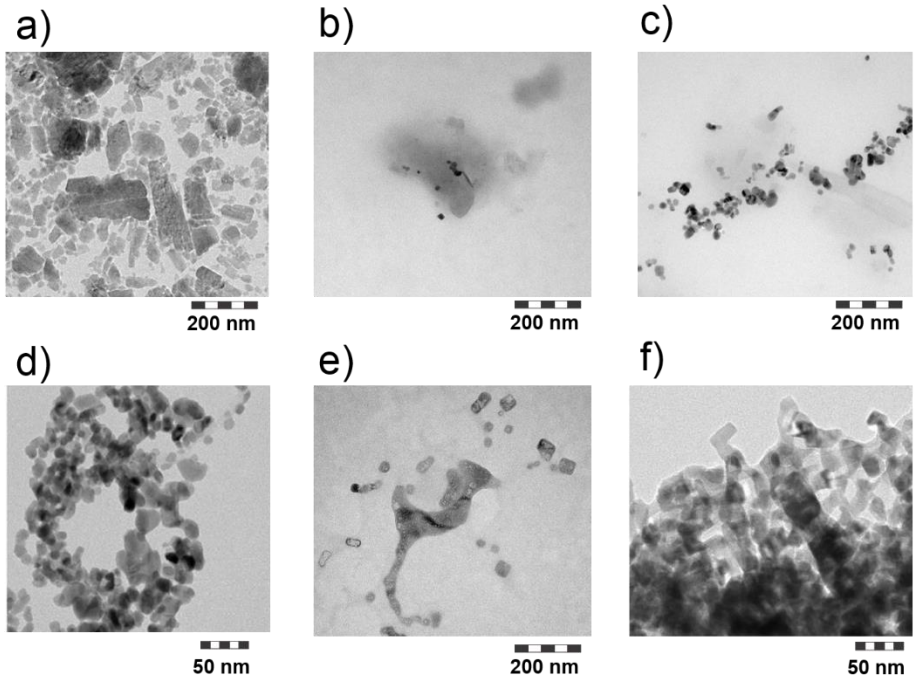

Figure 1 Morphology of pristine and transformed ENMs by transmission electron microscopy (TEM): $Cu_2CO_3(OH)_2$ ENMs (top row = a,b,c) and CuO NPs (bottom row = d, e, f) before (a,d) and after dissolution testing at 37°C in pH1.6 stomach simulant (b,e) and independently in pH5.8 FeSSIF-V2 middle intestine simulant (c,f.). EDXS finds no Cu content in the b,e structures.

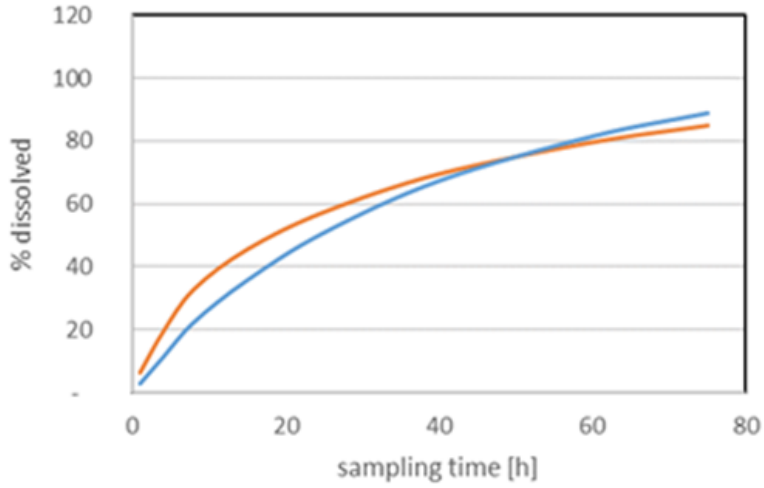

Figure 2 Dissolution of $Cu_2CO_3(OH)_2$ ENMs (blue) and CuO ENMs (orange) during flow-through testing at 37°C with pH 1.6 stomach simulant. Quantification of ions by ICP-OES.

3.2.3.2 General observations

CuO ENM: During the study no signs of toxicity were noted and there were no premature deaths in the study. There was no reduction in body and organ weights for CuO ENMs treated animals (Supplementary Tables 2A and 2B). No treatment related findings were observed at the macroscopic observation at autopsy. Due to the lack of effects observed at doses up to 32 mg/Kg b.w. also a high dose of 512 mg/Kg b.w. was tested. The 512 mg/Kg b.w. dose induced slight weight loss in one animal after two days of treatment and diarrhoea after three administrations. After four administrations two animals showed diarrhoea.

$Cu_2CO_3(OH)_2$ ENM: Repeated oral administration of a dose of 128 mg/Kg b.w. $Cu_2CO_3(OH)_2$ ENMs induced severe toxic responses in the animals as indicated by the behavior of the animals, including frequent washing and piloerection. Therefore, the animals scheduled for autopsy after a recovery period at day 21 after treatment were autopsied prematurely at days 6 and 7, respectively 24h and 48h after the last (day 5) treatment. A decrease in organ weight was observed for heart, liver, spleen, and thymus whereas the adrenal glands showed an increase in weight (Figure 3, Supplementary Table 2C). The most severe decrease in organ weight was noted for the spleen and thymus, respectively with approximately 45% and 70%. For doses up to 64 mg/Kg b.w. body and organ weight determined at day 26 after a three week recovery period showed no changes compared to the vehicle treated animals (Supplementary Table 2D).

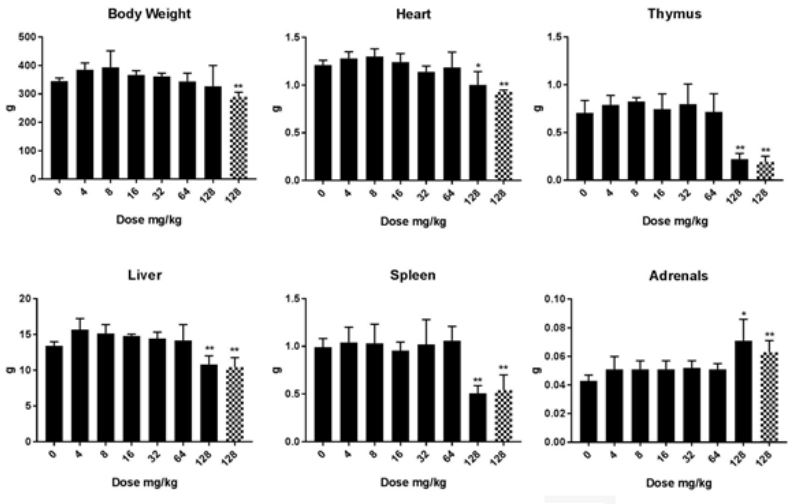

*Figure 3 Body and organ weight (g) in male rats at after 5 days consecutive oral administration of $Cu_2CO_3(OH)_2$ ENMs - At day 6/7 (24/48 hours after the last administration). The number of animals per group is 4 (n=4). Two groups of dose group of 128 mg/Kg b.w. are presented for autopsy at days 6/7 after treatment. For one group (blocked column) an unscheduled autopsy was done of in view of poor condition of the animals intended for recovery. Significant differences compared to vehicle treated animals. *p<0.05, **P<0.01 (ANOVA).*

3.2.3.3 Histopathology

CuO ENM: There were no test item-related microscopic observations in the initial dose response study at the highest dose of 64 mg/Kg b.w. of CuO ENMs evaluated (data not shown). All of the recorded microscopic findings were within the range of background histopathology encountered in rats of this age and strain. For animals treated with a dose of 512 mg/Kg b.w. CuO ENMs and evaluated at day 6 alterations were observed in the histopathology of stomach, liver, and bone marrow. In the stomach an increased incidence and severity of submucosal glandular inflammation with eosinophilic granulocytes was observed. The liver exhibited slight Kupffer cell hypertrophy/hyperplasia, inflammation composed of mixed inflammatory cells, hepatocellular hypertrophy, hepatocellular necrosis and single cell necrosis (above the background level of minimal).

$Cu_2CO_3(OH)_2$ ENM: Test item-related microscopic findings were observed in a number of organs examined after treatment with 64 or 128 mg/Kg b.w. $Cu_2CO_3(OH)_2$ ENMs. After five day oral administration of $Cu_2CO_3(OH)_2$ ENMs in the stomach an increased incidence and severity of submucosal glandular inflammation with eosinophilic granulocytes was observed on day 6 (Figure 4) which was still present in some animals after the 3 week recovery period. In other parts of the GI-tract effects were only seen at the dose of 128 mg/Kg b.w. Ulceration was observed in the cecum, colon and rectum.

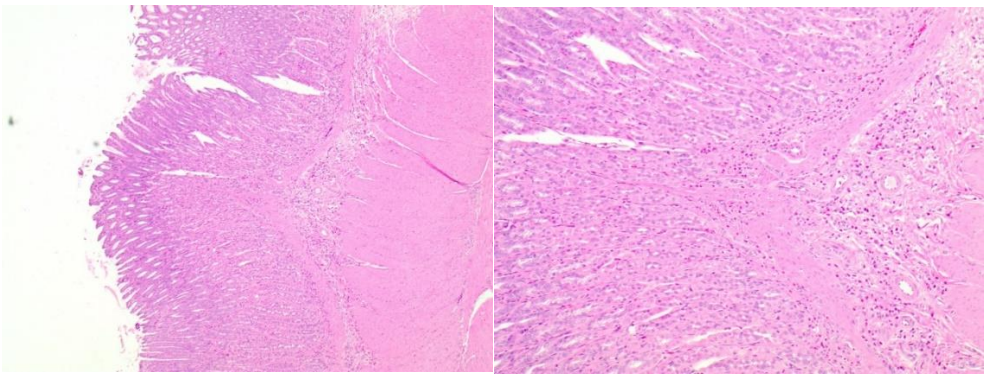

Figure 4 Presence of inflammation (arrows) in the submucosa of the stomach in a rat treated with a dose of 64 mg/Kg b.w. of $Cu_2CO_3(OH)_2$ NP for 5 consecutive days. Autopsy at day 6, 1 day after the last $Cu_2CO_3(OH)_2$ NP administration. Left overview, right detail of inflammatory cells (arrows)

Figure 5 shows ulceration of colon after 5 days treatment with 128 mg/Kg b.w. $Cu_2CO_3(OH)_2$ ENMs. Other lesions observed in the GI-tract were apoptosis (duodenum, ileum and cecum) and edema (colon, rectum).

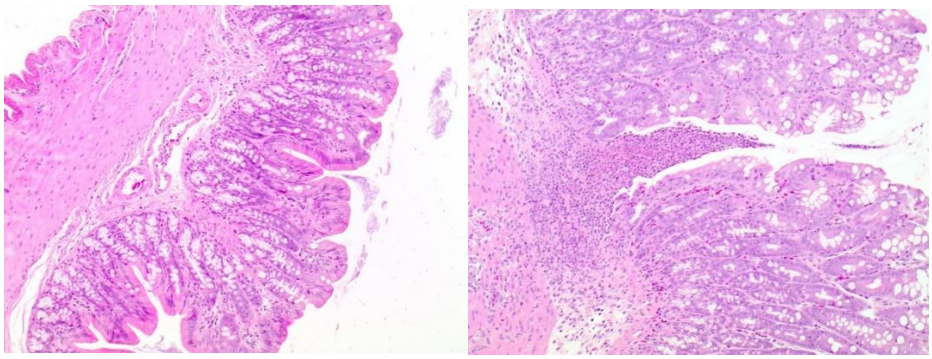

Figure 5 Presence of ulceration of colon mucosa (arrows, figure on the right) of rat treated with 128 mg/Kg b.w. of $Cu_2CO_3(OH)_2$ ENMs for 5 consecutive days. Note severe inflammation and loss of colon epithelium above inflammation. Autopsy at day 6, 1 day after the last $Cu_2CO_3(OH)_2$ ENMs administration. Left colon of vehicle treated control animal.

In the liver inflammation composed of mixed inflammatory cells (Figure 6) occurred at day 6 in rats treated at 64 mg/Kg and at 128 mg/Kg. In animals treated at 64 mg/Kg and 128 mg/Kg occurred hepatocellular necrosis, single cell necrosis, increased mitosis, liver and Kupffer cell hypertrophy.

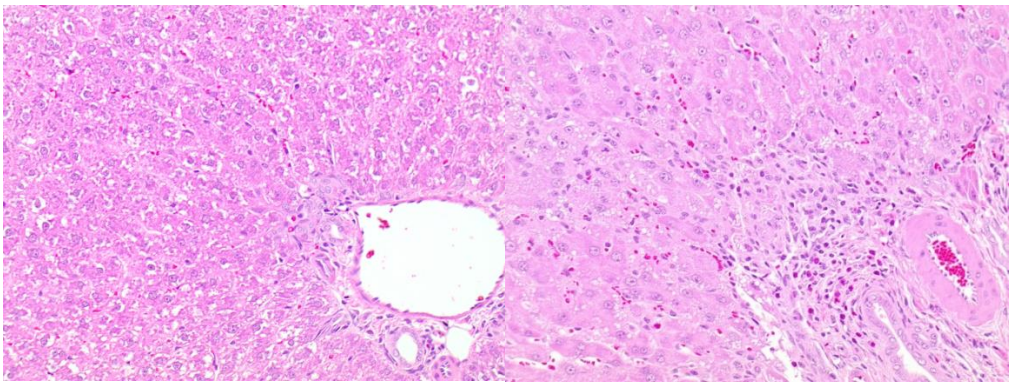

Figure 6 Presence of toxic effects in the liver. Top left, liver of vehicle control treated animal. Top right presence of inflammation(arrows) and vacuolisation (asterisks) of liver parenchyma cells. Bottom single cell necrosis of liver cells (arrows). Autopsy at day 7, 2 days after the last $Cu_2CO_3(OH)_2$ ENMs administration. Animal treated with 128 mg/Kg b.w. of $Cu_2CO_3(OH)_2$ ENMs for 5 consecutive days (days 1-5).

3.2.3.4 Organ burden

CuO ENM: At 32 and 64 mg/Kg b.w. the liver ($p<0.05$) and at 64 mg/Kg b.w. the mesenteric lymph node (MLN) ($p<0.001$) exhibited an increase in Cu content (Table 3). At day 6 one day after the last administration there is an increase in Cu level only the mesenteric lymph node for the doses of 64 mg/Kg b.w., and in the liver for the doses of 32 and 64 mg/Kg b.w. The dose of 512 mg/Kg b.w. that was not administered in the dose response study but at later in time, shows an increased Cu level in liver, lung, kidney, spleen, thymus and mesenteric lymph node when compared to non-treated control animals of the dose response study. At day 26 the increased levels of Cu in liver and also kidney were returned to levels equivalent to the control animals.

*Table 3 Cu^{2+} in organs of male rats after 5 days consecutive oral administration of CuO ENMs a) Cu^{2+} content in organs (µg/g tissue) at day 6 and day 26 after oral administration on 5 consecutive days (days 1-5) with CuO NPs. Results are presented as mean ± SD, n=4 unless otherwise indicated within brackets. ND, not done. Significant differences compared to vehicle treated animals. *<0.05, ***<0.001 students t-test, one sided.*

	Day 6				Day 26	
Dose (mg/Kg)	0	32	64	512	0	32
Organ						
Liver	13±0.4[a]	42±16[*]	75±4	914±541	14±3	12±1.5
Lung	6±1	6±1	5 (2)	70±69	7±0.2	6±1.3
Kidney	41±6	62±14	64 (1)	76±42	62±9	52±4 (3)
Spleen	6±0.4	6±0.3	6±1 (2)	10±5	6±0.6	5±1
Thymus	4±0.3	5±1 (3)	8±4 (2)	10±7	5±1	5±2
MLN	5±1	8±2 (3)	10±0.3 (2)***	26±11	4±2	5±2
Testis	11±0.3	11±0.1	11±0.3 (2)	12±1	12±1	11±1
Brain cortex	9±0.1	9±0.5	ND	10±1	10±3	9±0.4

$Cu_2CO_3(OH)_2$ ENM: Cu content of tissues after 5 consecutive days of $Cu_2CO_3(OH)_2$ ENMs oral administration is presented in Table 4. At the lower dose investigated (64 mg/Kg b.w.) an increase in Cu content was noted in liver, kidney, testes, brain and thymus only. For the highest dose (128 mg/Kg b.w.) increases in Cu content were observed in all organs evaluated. At day 26 the increased levels of Cu in liver, thymus and kidney for the dose of 64 mg/Kg b.w. were returned to background levels whereas for the liver and testes they were still increased ($p<0.05$ and $p<0.01$, respectively), although the increase was limited compared to day 6.

*Table 4 Cu in organs of male rats after 5 days consecutive oral administration of $Cu_2CO_3(OH)_2$ ENMs. a) Dose of 128 mg/Kg b.w. $Cu_2CO_3(OH)_2$ ENMs determination at days 6 and day 7 after start of experiment. Animals received $Cu_2CO_3(OH)_2$ ENMs by oral administration at days 1 –5. Recovery animals were taken out of the study in view of poor condition (day 7 being day 2 after last $Cu_2CO_3(OH)_2$ ENMs administration). b) Cu^{2+} content in organs (µg/g tissue) at day 6 and day 26 after oral administration on 5 consecutive days (days 1-5) with $Cu_2CO_3(OH)_2$ NPs. Results are presented as mean ± SD, n=4 unless otherwise indicated within brackets. Significant differences compared to vehicle treated animals. *<0.05, **<0.01, ***<0.001 students t-test, one sided.*

	Day 6			**Day 26**	
Dose (mg/Kg)	0	64	128	0	64
Organ					
Liver	13±0.5[b]	451±58***	1399±307***	13±1	29±9*
Lung	8±0.4	9±3	259±335 (8)*	7±0.3	7±06
Kidney	29±6	55±13	810±369 (8)***	36±17	28±4
Spleen	5±0.2	6±0.6	35±26 (7)*	5±0.2	5±0.3
Thymus	4±0.5	6±0.6***	29±20 (8)***	3±0.3	3±0.4
MLN	6±1	7±1	48±23 (8)**	6±3	6±2
Testis	11±0.3	12±0.2*	15±0.3 (8)**	11±0.2	13±1**
Brain cortex	9±0.2	10±0.4*	11±1 (8)***	9±0.5	10±7

3.2.4 Discussion

We investigated the potential toxicity of two Cu-nanoformulations used for the preservation of wood products in a repeated dose oral toxicity study. Our results show that both CuO ENMs and $Cu_2CO_3(OH)_2$ ENMs exhibited approximately 50% dissolution at 16 h of incubation in stomach fluid simulant. During flow through conditions, which are more realistic of the strong dilution in the stomach environment, approximately 50% dissolution was reached at 24 h. Emptying of the stomach in rats may be reached within 6h,[30] suggesting that part of the oral dose will reach the intestines in particulate nanoform. Imaging of the particles after dissolution under intestinal conditions with a pH5.8 suggested morphological changes such as shrinking and agglomeration. This data would suggest that it is relevant to consider the possible toxicological effects of both the Cu^{2+} ions and the nanoparticles. The $Cu_2CO_3(OH)_2$ ENMs showed similar dissolution characteristics to CuO ENMs in simulated stomach conditions, but $Cu_2CO_3(OH)_2$ ENMs dissolved faster in simulated intestine conditions.

Based on the dissolution experiments, we speculate that if any particles last the fast and pH-driven dissolution in the stomach passage, they would transform and $Cu_2CO_3(OH)_2$ ENMs would shed Cu^{2+} ions earlier or more during intestine passage than CuO ENMs. A more sophisticated protocol would be to use sequential buffers [31] and/or simulated full diets.[32] One might even imagine to combine flow-through-testing (for ease of retrieving transformed ENMs, for fast time resolution on ions) with sequential buffers (for added physiological realism), but that was beyond scope of the present investigation. Although we tested at low concentration and out of equilibrium, saturation may have suppressed dissolution rates below the *in vivo* rates. Investigating the release of Cu^{2+} ions from wood treated with $Cu_2CO_3(OH)_2$ ENMs, revealed more than 80% dissolution after 1h at room temperature in a simple glycine

simulant with pH1.5,[18] and only slightly longer times were suggested under environmental unsaturated conditions.[33,34] So, the use of Cu-nanomaterial as a wood preservative will result in both human and environmental exposure to Cu^{2+} ions which can be considered responsible for the induced toxic effects.

In terms of biodistribution, the treatment doses below 512 mg/Kg b.w. CuO ENMs resulted in a detectable increase in the Cu content of the liver only, while at the high 512 mg/Kg b.w. dose increased copper levels were observed in all evaluated organs (Table 1). The partial dissolution in the stomach might explain why the doses of CuO ENMs up to 32 mg/Kg b.w. had limited toxic impacts compared to the reported toxicity of soluble Cu formulations such as $CuSO_4$ (NOAEL of 16.3 mg/Kg).[26] The high dose of 512 mg/Kg b.w. CuO ENMs induced histopathological alterations in stomach, liver and bone marrow. In view of the solubility and dissolution characteristics of Cu nanomaterials also the Cu ion may play an important role for the Cu nanomaterial toxicity.

$Cu_2CO_3(OH)_2$ ENMs were more toxic than CuO ENMs when compared on the basis of a dose in mg/Kg b.w. Animals dosed with 128 mg/Kg b.w. showed after five days of repeated dosing overt signs of toxicity leading to a preliminary removal of the dose group intended for the recovery period from the study. Both haematology and clinical chemistry indicated toxic effects at the 64 and 128 mg/Kg b.w. doses. Treatment with $Cu_2CO_3(OH)_2$ ENM also induced inflammation in the stomach, apoptosis in duodenum, ileum, and cecum, and ulceration in the large intestines (cecum, colon, rectum). In the liver inflammation, apoptosis, necrosis, and hypertrophy as potential repair of the liver damage were observed. In addition kidney degeneration/regeneration and necrosis was observed. There was a marked lymphoid atrophy after the five day oral treatment with $Cu_2CO_3(OH)_2$ ENM in spleen and thymus accompanied by an increase in myeloid activity in the bone marrow. After oral $Cu_2CO_3(OH)_2$ ENMs treatment increased Cu levels could be detected in almost all organs investigated (liver, lung, kidney, spleen, thymus, mesenteric lymph node, testes, brain). For CuO ENMs histopathology was only performed on animals with the high extra dose of 512 mg/Kg b.w. In these animals in the stomach, liver and bone marrow similar pathological lesions were observed as for the $Cu_2CO_3(OH)_2$ ENMs induced lesions, although lymphoid depletion in spleen and thymus was absent. Overall, the pathology in terms of organ damage in the GI-tract, kidney and the lymphoid organs (spleen, thymus) was more severe for $Cu_2CO_3(OH)_2$ ENM compared to CuO ENM administration.

Cu^{2+} accounts for about 80% of the CuO mass, about 60% in $Cu_2CO_3(OH)_2$ and about 40% in $CuSO_4$. Dissolution of the ENMs in the stomach environment was about 50%, with a faster rate of Cu^{2+} ions dissolution from the remaining $Cu_2CO_3(OH)_2$ particles in intestine, whereas for $CuSO_4$ dissolution was complete already in stomach conditions. None of the ENMs showed significant transformation to other particulate species, such that a potential toxic effect via newly formed particles is improbable. Based on this mass and solubility data, a certain mass dose for both CuO ENMs and $Cu_2CO_3(OH)_2$ ENMs would be associated with a similar amount of Cu^{2+} ion release as that from $CuSO_4$ in the stomach (i.e. about 40% Cu mass for CuO ENMs,

30% Cu mass for $Cu_2CO_3(OH)_2$ ENMs, and about 40% Cu mass for $CuSO_4$, considering 50% dissolution for CuO ENMs and $Cu_2CO_3(OH)_2$ ENMs and 100% dissolution for $CuSO_4$). $Cu_2CO_3(OH)_2$ ENMs would have higher toxicity via ions originating in the intestine in view of its high dissolution in simulant intestinal fluids.

Privalova et al. (2014)[19] using intraperitoneal administration of CuO ENMs (diameter 20 nm) in rats for three times a week applying 19 injections up to a total dose of approximately 10 mg/Kg b.w. mainly described induction of kidney lesions. In contrast to that study, we did not observe histopathological lesions in kidney and spleen by CuO ENMs but did note lesions in stomach, liver and bone marrow after 5 days repeated oral administration of 512 mg/Kg b.w. In view of the very fast dissolution of the CuO ENMs used by Privalova et al. (2014)[19] it might be assumed that Cu ions are responsible for the observed toxicity. In this respect our results on $Cu_2CO_3(OH)_2$ ENMs show a more widespread organ toxicity including severe cellular depletion of spleen and thymus, and kidney lesions which might be related to the more complete dissolution in the GI-tract and the resulting higher internal Cu^{2+} ion dose at organ level.

Toxicity of CuO ENMs presumably due to the release of Cu^{2+} ions, was previously demonstrated in *in vitro* cellular toxicity tests for various lung derived cells such as A549 cells, 16-HBE cells, and BEAS-2B cells.[35–38] CuO ENMs were found to be more toxic compared to microCuO particles (CuO-MP) and $CuCl_2$ when comparing doses as mass per mL in the cell culture medium.[37] The toxic effect was explained by a much higher Cu content in the cell (cellular cytoplasm and nucleus) after exposure to the CuO ENMs compared to CuO MP and $CuCl_2$ followed by intracellular Cu^{2+} ion release. Both for Ag ENMs and CuO ENMs a higher cellular content of metal (Ag^+ and Cu^{2+}) ions was observed in A549 and BEAS-2B cells compared with exposure to Ag^+ and Cu^{2+} ions in the form of $AgNO_3$ or $CuCl_2$, respectively. [39]

Our data also identified that the immune system may also be severely affected by the Cu^{2+} ions released from the Cu containing nanomaterials as shown by the severe lymphoid cell depletion in spleen and thymus. This may have consequences for the functionality of the immune system as was recently demonstrated by us for silver nanoparticles.[40,41] In view of the potential high migration to the spleen the immune system maybe a target for nanomaterial toxicity and needs consideration for a more a more specific toxicity evaluation.[42,43] So, an evaluation of the immune system function exposed to $Cu_2CO_3(OH)_2$ ENMs may be warranted.

3.2.5 Conclusion

In conclusion, we observed a marked difference in the severity of the pathological lesions in various organs (e.g. GI-tract, kidney, spleen, and thymus) between CuO ENMs and $Cu_2CO_3(OH)_2$ ENMs after oral exposure comparing dose effects in our rat study. For $Cu_2CO_3(OH)_2$ ENMs body weight and severe organ weight loss was observed. In spleen and thymus the severe weight loss was accompanied by lymphoid depletion that warrants further immunotoxicological evaluation. However, for risk assessment the Bench Mark Dose (BMD) with a 5% deviation of the vehicle control, is surprisingly similar for the serum liver enzyme

AST as a first indication for liver toxicity, being 26.2 mg/Kg for CuO ENMs and 30.8 mg/Kg for $Cu_2CO_3(OH)_2$ ENMs, respectively. These data may be useful for deriving an acceptable daily intake for these toxic wood preservatives which may then be used for a risk assessment including exposure scenarios.

3.3) Open issues

In both STOS and STIS, the copper burden in organs is measured as total Cu^{2+}, without any information regarding the physical form (ionic or particle). As it is reported, Cu-ENMs undergo to a dissolution process in biological media, that means that the Cu^{2+} can be present in the tissues as ionic copper and/or in nanoform. This information will be useful to understand the mechanisms involved in the inflammation process and consequent detoxification. Moreover, additional information on size distribution and their spatial location within the cells can help to understand the transport dynamics from the blood vessel towards biological targets, and as consequence the efficiency of the biological barrier. It has to be remarked that information on biological barriers and transport mechanisms inside biological tissues is extremely important in the field of nanotoxicology, nanomedicine and in the development of new Cu-ENMs modified by following the principles of safe by design. For this reason, the application of advance techniques for the detection and quantification of ENMs in these complex matrices should be considered in future studies.

3.4) References

1. Gosens, I. *et al.* Organ burden and pulmonary toxicity of nano-sized copper (II) oxide particles after short-term inhalation exposure. *Nanotoxicology* (2016). doi:10.3109/17435390.2016.1172678

2. Hsiung, C.-S. S., Andrade, J. D., Costa, R. & Ash, K. O. Minimizing interferences in the quantitative multielement analysis of trace elements in biological fluids by inductively coupled plasma mass spectrometry. *Clin. Chem.* (1997).

3. Nomura, C. S., Silva, C. S., Nogueira, A. R. A. & Oliveira, P. V. Bovine liver sample preparation and micro-homogeneity study for Cu and Zn determination by solid sampling electrothermal atomic absorption spectrometry. *Spectrochim. Acta - Part B At. Spectrosc.* (2005). doi:10.1016/j.sab.2005.02.021

4. Ortelli, S. *et al.* Colloidal characterization of CuO nanoparticles in biological and environmental media. *Environ. Sci. Nano* **4,** (2017).

5. Zheng, W. & Monnot, A. D. Regulation of brain iron and copper homeostasis by brain barrier systems: Implication in neurodegenerative diseases. *Pharmacol. Ther.* (2012). doi:10.1016/j.pharmthera.2011.10.006

6. Freeman, B. M. H. & McIntyre, C. R. A Comprehensive Review of Copper-Based Wood Preservatives with a focus on new micronized or dispersed copper systems. *For. Prod. J.* (2008).

7. Lebow, S. & Foster, D. Environmental concentrations of copper, chromium, and arsenic released from a chromated-copper-arsenate- (CCA-C-) treated wetland boardwalk. *For. Prod. J.* (2005).

8. Pantano, D. *et al.* Transformations of Nanoenabled Copper Formulations Govern Release, Antifungal Effectiveness, and Sustainability throughout the Wood Protection Lifecycle. *Environ. Sci. Technol.* (2018). doi:10.1021/acs.est.7b04130

9. Cookson, L. J., Creffield, J. W., McCarthy, K. J. & Scown, D. K. Trials on the Efficacy of Micronized Copper in Australia. *For. Prod. J.* (2010). doi:10.13073/0015-7473-60.1.6

10. Akhtari, M., Taghiyari, H. R. & Kokandeh, M. G. Effect of some metal nanoparticles on the spectroscopy analysis of Paulownia wood exposed to white-rot fungus. *Eur. J. Wood Wood Prod.* (2013). doi:10.1007/s00107-013-0676-5

11. Platten, W. E. I. *et al.* Release of Micronized Copper Particles from Pressure-treated Wood. 45 (2014).

12. Clausen, C. A. Nanotechnology: Implications for the Wood Preservation Industry. *38th Annu. Meet. Int. Res. Gr. Wood Preserv.* (2007).

13. Evans, P., Matsunaga, H. & Kiguchi, M. Large-scale application of nanotechnology for wood protection. *Nature Nanotechnology* (2008). doi:10.1038/nnano.2008.286

14. Kartal, S. N., Green, F. & Clausen, C. A. Do the unique properties of nanometals affect leachability or efficacy against fungi and termites? *Int. Biodeterior. Biodegrad.* (2009). doi:10.1016/j.ibiod.2009.01.007

15. Civardi, C. *et al.* Release of copper-amended particles from micronized copper-pressure-treated wood during mechanical abrasion. *J. Nanobiotechnology* (2016). doi:10.1186/s12951-016-0232-7

16. Astdr. Toxicological profile for Copper. *U.S Public Heal. Serv. Agency Toxic Subst. Dis. Regist.* (2004). doi:doi:10.1201/9781420061888_ch106

17. Wang, Z., Von Dem Bussche, A., Kabadi, P. K., Kane, A. B. & Hurt, R. H. Biological and environmental transformations of copper-based nanomaterials. *ACS Nano* **7,** 8715–8727 (2013).

18. Santiago-Rodríguez, L. *et al.* Assessment of the bioaccessibility of micronized copper wood in synthetic stomach fluid. *Environ. Nanotechnology, Monit. Manag.* (2015). doi:10.1016/j.enmm.2015.07.003

19. Privalova, L. I. *et al.* Subchronic toxicity of copper oxide nanoparticles and its attenuation with the help of a combination of bioprotectors. *Int. J. Mol. Sci.* (2014). doi:10.3390/ijms150712379

20. Chen, Z. *et al.* Acute toxicological effects of copper nanoparticles in vivo. *Toxicol. Lett.* (2006). doi:10.1016/j.toxlet.2005.10.003

21. Lei, R. *et al.* Integrated metabolomic analysis of the nano-sized copper particle-induced hepatotoxicity and nephrotoxicity in rats: A rapid in vivo screening method for nanotoxicity. *Toxicol. Appl. Pharmacol.* (2008). doi:10.1016/j.taap.2008.06.026

22. Sarkar, A., Das, J., Manna, P. & Sil, P. C. Nano-copper induces oxidative stress and apoptosis in kidney via both extrinsic and intrinsic pathways. *Toxicology* (2011). doi:10.1016/j.tox.2011.09.086

23. Liao, M. & Liu, H. Gene expression profiling of nephrotoxicity from copper nanoparticles in rats after repeated oral administration. *Environ. Toxicol. Pharmacol.* (2012). doi:10.1016/j.etap.2011.05.014

24. Marques, M. R. C., Loebenberg, R. & Almukainzi, M. Simulated biological fluids with possible application in dissolution testing. *Dissolution Technologies* (2011). doi:10.14227/DT180311P15

25. Jantratid, E., Janssen, N., Reppas, C. & Dressman, J. B. Dissolution media simulating conditions in the proximal human gastrointestinal tract: An update. *Pharm. Res.* (2008). doi:10.1007/s11095-008-9569-4

26. Hebert, C. NTP technical report on the toxicity studies of Cupric Sulfate (CAS No. 7758-99-8) Administered in Drinking Water and Feed to F344/N Rats and B6C3F1 Mice. *Toxic. Rep. Ser.* (1993).

27. OECD. OECD Guidelines for the Testing of Chemicals, Section 4, Test No. 425: Acute Oral Toxicity - Up-and-Down Procedure. *Guidel. Test. Chem.* (2001). doi:10.1787/9789264071049-en

28. Keller, A. A. *et al.* Comparative environmental fate and toxicity of copper nanomaterials. *NanoImpact* (2017). doi:10.1016/j.impact.2017.05.003

29. Adeleye, A. S., Conway, J. R., Perez, T., Rutten, P. & Keller, A. A. Influence of extracellular polymeric substances on the long-term fate, dissolution, and speciation of copper-based nanoparticles. *Environ. Sci. Technol.* (2014). doi:10.1021/es5033426

30. Qualls-creekmore, E., Tong, M. & Holmes, G. M. Time-course of recovery of gastric emptying and motility in rats with experimental spinal cord injury. *NEurogastroenterol Motil* **22,** 62-e28 (2011).

31. Bove, P. *et al.* Dissolution test for risk assessment of nanoparticles: A pilot study. *Nanoscale*

(2017). doi:10.1039/c6nr08131b

32. DeLoid, G. M. *et al.* An integrated methodology for assessing the impact of food matrix and gastrointestinal effects on the biokinetics and cellular toxicity of ingested engineered nanomaterials. *Part. Fibre Toxicol.* (2017). doi:10.1186/s12989-017-0221-5

33. Kent, R. D. & Vikesland, P. J. Dissolution and Persistence of Copper-Based Nanomaterials in Undersaturated Solutions with Respect to Cupric Solid Phases. *Environ. Sci. Technol.* (2016). doi:10.1021/acs.est.5b04719

34. Vencalek, B. E. *et al.* In Situ Measurement of CuO and Cu(OH)2Nanoparticle Dissolution Rates in Quiescent Freshwater Mesocosms. *Environ. Sci. Technol. Lett.* (2016). doi:10.1021/acs.estlett.6b00252

35. Cho, W.-S. *et al.* Predictive value of in vitro assays depends on the mechanism of toxicity of metal oxide nanoparticles. *Part. Fibre Toxicol.* (2013). doi:10.1186/1743-8977-10-55

36. Jing, X., Park, J. H., Peters, T. M. & Thorne, P. S. Toxicity of copper oxide nanoparticles in lung epithelial cells exposed at the air-liquid interface compared with in vivo assessment. *Toxicol. Vitr.* (2015). doi:10.1016/j.tiv.2014.12.023

37. Strauch, B. M., Niemand, R. K., Winkelbeiner, N. L. & Hartwig, A. Comparison between micro- and nanosized copper oxide and water soluble copper chloride: Interrelationship between intracellular copper concentrations, oxidative stress and DNA damage response in human lung cells. *Part. Fibre Toxicol.* (2017). doi:10.1186/s12989-017-0209-1

38. Ude, V. C. *et al.* Impact of copper oxide nanomaterials on differentiated and undifferentiated Caco-2 intestinal epithelial cells; assessment of cytotoxicity, barrier integrity, cytokine production and nanomaterial penetration. *Part. Fibre Toxicol.* (2017). doi:10.1186/s12989-017-0211-7

39. Cronholm, P. *et al.* Intracellular uptake and toxicity of Ag and CuO nanoparticles: A comparison between nanoparticles and their corresponding metal ions. *Small* (2013). doi:10.1002/smll.201201069

40. De Jong, W. H. *et al.* Systemic and immunotoxicity of silver nanoparticles in an intravenous 28 days repeated dose toxicity study in rats. *Biomaterials* (2013). doi:10.1016/j.biomaterials.2013.06.048

41. Vandebriel, R. J. *et al.* Immunotoxicity of silver nanoparticles in an intravenous 28-day repeated-dose toxicity study in rats. *Part. Fibre Toxicol.* (2014). doi:10.1186/1743-8977-11-21

42. Dobrovolskaia, M. A., Shurin, M. & Shvedova, A. A. Current understanding of interactions between nanoparticles and the immune system. *Toxicol. Appl. Pharmacol.* (2016). doi:10.1016/j.taap.2015.12.022

43. Dusinska, M. *et al.* Immunotoxicity, genotoxicity and epigenetic toxicity of nanomaterials: New strategies for toxicity testing? *Food Chem. Toxicol.* (2017). doi:10.1016/j.fct.2017.08.030

Chapter 4

Detection of CuO and $Cu_2CO_3(OH)_2$ nanoparticles in rats after short-term oral exposure ([e])

In Chapter 3 has been discussed the toxicological results related to the oral exposure of CuO and $Cu_2CO_3(OH)_2$ in rats. It has been reported that the oral administration of $Cu_2CO_3(OH)_2$ to rats, lead to a severe reduction in body weight and organs weight loss, in comparison to CuO administration. Moreover, histopathological analysis shows that the assumption of Cu-ENMs lead to a substantial liver and lymphatic tissue damage, showing also high copper bioaccumulation.

In this chapter, is reported an "on-preparation" manuscript focused on the detection of Cu-ENMs in rat tissues, with the aim to provide more information on the fate of Cu-ENMs in biological matrices. In particular Transmission Electron Microscopy (TEM) and single particle Inductive Coupled Plasma Mass Spectrometry (sp-ICP-MS) were used with the aim to detect and quantify CuO and $Cu_2CO_3(OH)_2$ nanoparticles Cu-ENMs in rat organs. Liver was the organ selected as it contains for both nanoparticles (NPs) exposure, the highest total copper concentrations (~1 g/Kg). Tissues were processed for 4h at 37°C by an enzymatic digestion in order to be analysed by sp-ICP-MS. In addition, both liver samples and the suspension obtained after the enzymatic digestion were analysed by TEM. The resulting images showed in all cases a large number of NPs with a smaller size (~ 8 nm in liver thin layer and ~10 nm after the enzymatic digestion) compared to that of pristine particles (12 nm for CuO, and 40 nm for $Cu_2CO_3(OH)_2$). The decrease in size of NPs present in liver thin layer can confirm the dissolution process hypothesized by De Jong et al. (2018).[1] After the enzymatic digestion particles seem increased in size, in reality by a deep analysis of size distributions determined by TEM, it results that small NPs dissolved faster, leaving in the sample prevalently larger particles and aggregates. Unfortunately, the dissolution process has led to NPs with dimensions that are close to or below the detection limits of the sp-ICP-MS, making therefore difficult their detection. Only a partial quantification was then achieved by using this technique, since shrunk primary particles could not be detected but only agglomerates with dimensions greater than 13 nm.

Authors: Bonetto A., Badetti E., Ambrosi E., De Jong W.H., Marcomini A.

4.1) Introduction

Copper-based systems are widely used as antimicrobial agent for protecting wood in contact with soil against the degradation induced by fungi, bacteria and insects. They are applied via impregnation under high-pressure techniques or by brushing, spraying and coat-cutting techniques. Although these compounds show a relatively high toxicity towards aquatic communities, [2,3] they cause minimal effect on mammals, including humans, and no efficacy

[e] This work is mainly developed by myself, starting from the problem formulation, the sp-ICP-MS analysis, the processing of the results, up to the drafting of the manuscript

alternative biocide are available on the market. Recently, Cu-ENMs have been also largely considered since their nano-size allow to better penetrate into the wood, especially during the pressure treatments, leading to material which showed better performances with respect to the corresponding bulk material (solutions of ACA).

Once applied on the wood to be preserved, these nano-based materials can be released together with the copper ionic fraction, and they can be accidentally ingested by a possible transfer occurring from hand to mouth. Concern on human health is therefore associated both to the application (occupational hazard) and post-application phase (hazard related to the use of treated wooden installations). However, while the oral toxicity of Cu ions is extremely well known,[4] to the best of our knowledge, only few studies on Cu-ENMs are available.[1] For this reason, the development of analytical techniques for characterize and quantify Cu-ENMs in biological tissues is highly desirable as it can help to better elucidate the potential risk for humans associated with Nanoparticles (NPs) exposure.[5]

Electron microscopy techniques are commonly used to characterize ENMs into cells and tissues after an appropriate treatment of the samples, giving information about their fate and uptake [6] but not on their quantification. The analytical approaches currently available to quantify NPs in biological tissues are involving separation techniques such as hydrodynamic chromatography and field flow fractionation combined with detectors like Multiple Angle Light Scattering and inductive coupled plasma mass spectrometry.[7–10] A limitation to these approaches can be the detection limit of these combined techniques which can often require a pre-treatment of the sample (e.g. concentration of the analyte) before the instrumental analysis. Other approaches for the detection of ENMs from biological tissues combine conventional or single particle ICP-MS (sp-ICP-MS) with tissue extraction. Gray et al. (2013)[11] for example, investigated silver and gold ENMs from ground beef via sp-ICP-MS after an alkaline digestion of the tissues (using tetramethylammonium hydroxide) spiked with the desired NPs. The method was then verified in actual conditions by exposing to ENMs both Daphnia magna and Lumbriculus variegatus. Silver nanoparticles in chicken meat (spiked) were investigated by Loeschner et al. (2013) [12] by performing an enzymolysis of the tissues with Proteinase K, followed by asymmetric flow field flow fractionation with detection by conventional or single particle ICP-MS. Shortly after, Peters et al. published a similar approach for the sizing and quantitative determination of nano-silver in chicken meat by using an enzymatic digestion of the sample material as Loeschner et at. (2013),[12] but in this case the digest was analysed directly by sp-ICP-MS after a simple dilution. A comparison between the use of alkaline or enzymatic sample pre-treatment for characterization of ENMs in biological tissues prior to characterization by sp-ICP-MS was then performed for the detection of gold NPs in animal tissue[6,13] and of silver NPs in human tissue.[14] These studies show that the alkaline digestion is probably restricted to NPs that do not degrade and can be stabilized in such alkaline conditions, and that the enzymatic digestion can lead to the presence of hydrolysed sample residues which can reduce the number of detected NPs by sp-ICP-MS. As it can be understood from these results, the selection of the most suitable digestion process depends from the nature of the NPs to be analysed.

In a recent work reported by some of us, the potential toxicity of two Cu-based nanoparticles in a short term repeated oral exposure was investigated.[1] Male rats were fed by gavage with different concentrations (from 32 to 512 mg/Kg) of CuO and $Cu_2CO_3(OH)_2$ NPs for several days, and the distribution of total copper in the different organs tissue samples was determined by ICP-MS, after total digestion in HNO_3/H_2O_2. The presence of Cu still in the nanoform was only hypothesized, since it was not the scope of the study, by considering the results from dissolution and transformation studies performed in stomach and intestinal simulant fluids. From these studies emerge that both ENMs exhibited approximately 50% dissolution at 16h of incubation in stomach fluid simulant and considering the flow through conditions, and the time needed to empty the stomach (6h), it was supposed that part of the oral dose should reach the intestines and then the other organs in particulate nanoform. In this context, the aim of this work was to detect the presence of still undissolved NPs in liver samples for confirming the hypothesis of our previous study, and to investigate their transformations in terms of size and shape. Moreover, it has been attempted to quantify them by sp-ICP-MS by following the analytical methodologies already reported in the literature for other metals, performing a pre-treatment of the samples through an enzymatic digestion.[12,13,15] It has to be remarked that the studies conducted so far are always considering NPs such as Au or Ag, which present a highest stability than the Cu-ENMs investigated in this study. In addition, in all the cases NPs are spiked into the meat tissue samples to be analysed so that processes such as the digestion as well as the migration towards the different organs is never considered.

4.2) Materials and Methods

4.2.1 Materials

CuO nanoparticles (CuO-NPs) were obtained from PlasmaChem (Berlin, Germany) as a black powder. According to the manufacturer's datasheet, CuO-NPs exhibited a primary size of 15-20 nm, a specific surface area of 47 m^2/g determined by Brunauer-Emmett-Teller (BET) method and a density of 6.3 g/cm^3. Further characterization is reported in Pantano et al (2018). [16]

$Cu_2CO_3(OH)_2$ NPs were obtained from BASF SE as aqueous dispersion. Identification number LP 17206 (30% Cu), lot nr VM3041, best before date 05.02.2017. A more extensive characterization is reported in De Jong et al.[1] FE-SEM images of CuO and $Cu_2CO_3(OH)_2$ NPs previously dispersed in ethanol are reported in Figure 1.

Gold NPs as reference material for sp-ICP-MS were purchased from Sigma-Aldrich and consists in two suspension of spherical gold NPs with a diameter of 50 and 100 nm having a particle concentration of $3.5*10^{10}$ and $3.8*10^9$ respectively, stabilized in citrate buffer. Gold and Copper pure single-element as ionic standard (1000 µg/L) were obtained from Perkin-Elmer (for trace analysis).

The mixture used for organ sample enzymatic digestion included Proteinase K from Tritirachium album (lyophilized powder ≥ 30 units/mg), Triton X-100 solution (BioUltra, 10% in water), calcium acetate hydrate (ReagentPlus 99%) and tris buffer Trizma base (traceSELECT) from Sigma-Aldrich (St. Louis, MO, USA). The acid mixture used for organ sample

digestion included HNO_3 (trace select ultra 69%, Sigma-Aldrich <0.5µg/Kg), and H_2O_2 (trace select ultra 30%, Sigma-Aldrich <0.05µg/Kg). MilliQ water used for sample dilution was obtained from a Millipore Milli-Q-Plus ultrapure water system (Amsterdam, The Netherlands). Bovine liver (NIST 1577c, National Institute of Standards and Technology, Gaithersburg, Maryland, USA) was used as standard reference material.

4.2.2 Biological materials

Livers of rats after oral exposure tests derived from FP-7 SUN project and the experimental design (short-term exposure to CuO and $Cu_2CO_3(OH)_2$ NPs) is fully described in Jong et al (2018)[1]. Briefly, Cu-ENMs were administrated by oral gavage to male rats of 8-9 weeks old in the concentration range from 32-512 mg/Kg b.w. for CuO-NPs and 64-128 mg/Kg b.w. for $Cu_2CO_3(OH)_2$ NPs. Rats were sacrificed at day 6 (1 day after the last treatment) and at day 26 (21 days after the last treatment). Day 26 was chosen to evaluate recovery and possible persistence of effects or progression of effects induced by NPs.

4.2.3 Enzymatic digestion

According to Peters et al (2014 Anal Bioanal Chem) the digestion buffer was prepared by mixing 10 mmol of Trizma, 1% of TritonX-100 and 1 mmol of calcium acetate hydrate. 3 ml of digestion buffer were added to an aliquot of freeze and dry homogenized sample (~150mg) in a 12 ml PE test tube. The sample was vortexed and homogenized with an ultrasonic probe (UP-200S Hielscher Ultrasonics GmbH, Germany) in an ice bath, delivering a power of 200 W for 5 min using a pulsed 80% mode. Proteinase K (~0.1 units/mg) was then added to the mixture, which was incubated for 3 hours at 37 °C.

4.2.4 sp-ICP-MS analysis

The samples digested with the enzymatic buffer were diluted 1:10000 in MilliQ water and analysed by an inductively coupled plasma mass spectrometry equipped with double channel Universal Cell (sp-ICP-MS NexION 350D, Perkin Elmer).
According to the particle size method, the Transport Efficiency (TE) was determined by the Software Syngistix-Nano (Perkin Elmer) through two calibration curves. The first calibration curve was performed for ionic Au standards by determining the average of ^{197}Au signal intensity at 0, 0.5, 1, 2, 5, 10 and 20 g/L. The second calibration curve was created for the reference Au NPs (50 and 100 nm), relating ^{197}Au signal intensity (maximum of the intensity distribution peak) to the particle mass. For the analysis, it was set a Dwell time of 100 µs and an acquisition time of 60 seconds.
Considering the primary size of the Cu-ENMs used in this study, isotope ^{63}Cu was selected to reach the low DL_S of 15 nm for CuO and 18 nm for $Cu_2CO_3(OH)_2$. The copper mass was quantified using a multi-point curve in the concentration range from 0.5 to 20 µg/L.

4.2.5 Ultrafiltration experiment

Pristine CuO and $Cu_2CO_3(OH)_2$ has been subjected to the enzymatic digestion described above. After 3 hours at 37 °C, 500 µL of the mixture was transferred into ultrafiltration vials (Millipore

Amicon Ultra 2, Ultracel 3, cut-off 3K Dalton) and centrifuged for 30 minutes at 12000 rpm. After centrifugation, 100 µL of the filtrated solution was diluted and directly analysed by ICP-MS. For comparison, an aliquot of the enzymatic digested mixture has been mineralized as described below and analysed by ICP-MS.

4.2.6 Acidic Digestion

Samples digested with the enzymatic buffer were then mineralized in a mixture of HNO_3 and H_2O_2 (in a 2:1 ratio). A microwave system (Discovery SD, CEM) was used to mineralize an aliquot (1ml) of the enzymatic digested samples. The heating program used for the acid digestion has been: TMAX = 175°C, Ramp Time = 5 min, Hold Time = 4 min, Power = 300 W. The obtained solutions were transferred in PE tubes and diluted to 15 mL with MilliQ water.

4.2.7 ICP-MS analysis

An aliquot of each sample solution was properly diluted and analysed by inductively coupled plasma mass spectrometry equipped with double channel Universal Cell (sp-ICP-MS NexION 350D, Perkin Elmer). For the quantification of Copper, isotope ^{63}Cu was selected because more abundant than isotope ^{65}Cu (69.15 vs 30.85%). In order to remove the polyatomic interference in the mass ^{63}Cu (e.g. $^{40}Ar^{23}Na$), the analysis was performed in KED mode as He as carrier gas. Samples were quantified by external calibration method using a multi-point curve (blank and 10 points over the concentration range 0.5 µg/L to 500 µg/L). Yttrium at 5 µg/L was used as internal standard.[17] ICP-MS parameter are reported in Table 1.

Table 1 ICP-MS parameters

Component Parameter	**Type/Value/Mode**
Nebulizer	Meinhard quartz microconcentric
Spry Chamber	Quartz cyclonic
Triple Cone Interface Material	Nickel/Aluminum
Plasma Gas Flow	18 L/min
Auxiliary Gas Flow	1.2 L/min
Nebulizer Gas Flow	0.96 L/min
Sample Uptake Rate	200-250 uL/min
RF Power	1600 W
Collision Gas flow (Helium)	4.4 ml/min

Potential contamination from the laboratory was controlled by adding at least one reagent blank during each digestion session.

In order to verify the accuracy and repeatability of the method, 3 aliquots of the standard reference material Bovine liver NIST 1577c (National Institute of Standard and Technology) were analysed.[18]

4.2.8 Microscope Analysis

Fate and uptake of Cu-ENMs into tissues were investigated by a Tecnai G2 (FEI) Transmission Electron Microscope operating at 100 kV and the images were captured with a Veleta (Olympus Soft Imaging System) digital camera.
Tissues digested using Proteinase K were directly analyzed by placing one drop of the mixture (about 25µL) on 400 mesh holey film grid which was dried at air before the measurement.
For the analysis of ENMs embedded in liver and kidneys samples, small tissue fragments (about 1 mm^3) were fixed in 2.5% glutaraldehyde in 0.1M sodium cacodylate buffer (pH 7.4 overnight), at 4°C, post fixed in osmium tetroxide 1% in 0.1M sodium cacodylate buffer for 1 hour at 4° and embedded in an Epon-Araldite mixture. Semithin sections were stained with toluidine blue. Ultrathin sections (60-70 nm) were obtained with an Ultrotome V (LKB) ultramicrotome and placed on 400 mesh holey film grid for the measurement. When needed samples were counterstained with uranyl acetate and lead citrate.

4.3) Results and Discussion

4.3.1 TEM and SEM analysis

CuO and $Cu_2CO_3(OH)_2$ ENMs were analysed by SEM (Figure 1). As already reported for these materials,[1] CuO ENMs present spherical particles with diameters of around 15-20 nm while $Cu_2CO_3(OH)_2$ ENMs shows particles with irregular shapes, with a mean size of 40 nm. The shapes of the latter are related to the micronization of solid copper carbonate by milling, performed to obtain the desired fraction of nano-sized particles.

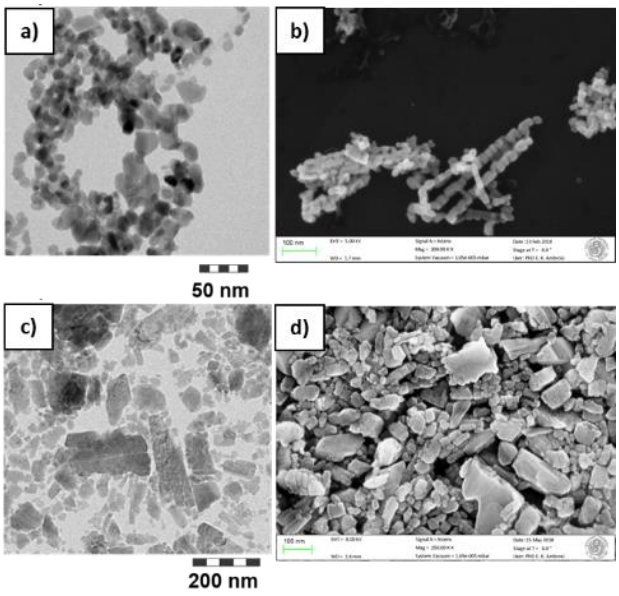

Figure 1 a) TEM images of pristine CuO ENMs, b) SEM images of pristine CuO ENMs and c) TEM images of pristine $Cu_2CO_3(OH)_2$ ENMs, d) SEM images of pristine $Cu_2CO_3(OH)_2$ ENMs.

These pristine materials were both used within SUN FP7 project, by the Institute for Public Health and the Environment, for conducting a short-term oral toxicity study.[1] In detail, male rats were fed by gavage for 5 consecutive days and the autopsy was done on day 1 and 21 after the last oral administration. The doses administrated ranged from1 to 512 mg/Kg body

weight for CuO ENMs and from 4 to 128 mg/Kg for $Cu_2CO_3(OH)_2$ ENMs. Liver was found to contain a highest concentration of copper than the other organs examined, as determined by ICP-MS analysis (~ 1 g/Kg). In this study, two samples of liver taken from rats fed with 512mg/Kg of CuO and 128 mg/Kg of $Cu_2CO_3(OH)_2$ ENMs respectively, were analysed by TEM. Images from semithin sections of liver are reported in Figure 2 and 3. As expected from our previous study, a large number of NPs were detected in both cases.

Surprisingly, these particles showed similar size and shape. In detail, spherical NPs with a most frequency size of 7.6 nm (mean size of 9.1 ± 11 nm) were detected for the liver of rats fed with CuO (Figure 2) while 7.4 nm were founded for $Cu_2CO_3(OH)_2$ NPs (mean size of 7.4 ± 2.3 nm) (Figure 6). In both samples analysed, some groups of NPs arranged in circular shapes of around 100 nm were detected. This could be ascribed to the inclusion of NPs in some organelle/vesicle, even if we have no certainty from the experimental point of view.

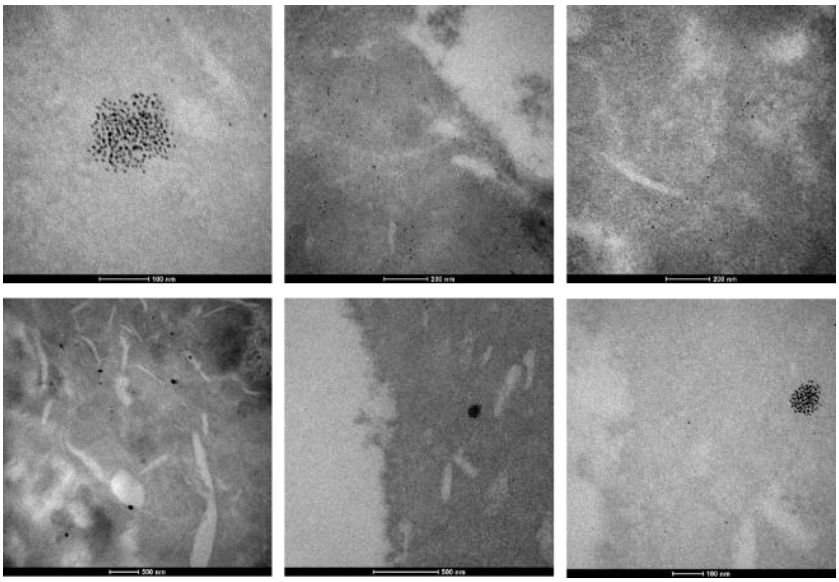

Figure 2 TEM images of liver tissues (semithin section) from one of the rats fed with 512 mg/Kg of CuO ENMs for 5 days.

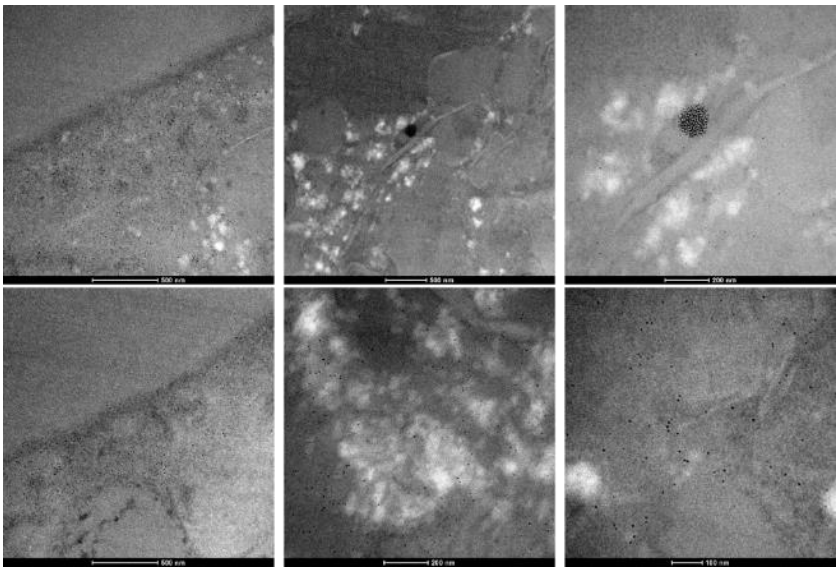

Figure 3 TEM images of liver tissues (semithin section) from one of the rats fed with 128 mg/Kg of $Cu_2CO_3(OH)_2$ ENMs for 5 days

A semithin section of liver of one of the rats fed with $Cu_2CO_3(OH)_2$ ENMs was then counterstained with uranyl acetate and lead citrate for investigating also the biological part of the samples. Some TEM images are reported in Figure 4 and as it can be observed, after colour contrasting, it results quite difficult to distinguish ENMs from the cellular structure. NPs with the same size of those detected without contrasting are present within the mitochondria, however it is not clear how these particles are distributed in other zones of the tissue.

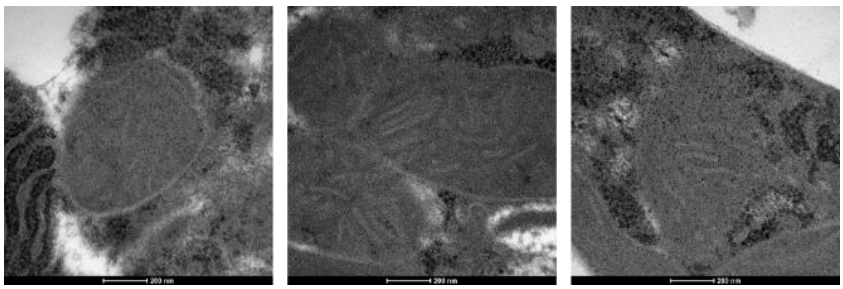

Figure 4 TEM images of liver tissues (semithin section) from one of the rats fed with 128 mg/Kg of $Cu_2CO_3(OH)_2$ ENMs for 5 days, after counterstained with uranyl acetate and lead citrate

The samples were then pre-treated for sp-ICP-MS analysis by an enzymatic digestion, in the attempt to quantify ENMs in rat's liver. As reported in the literature,[15] liver samples were digested in an enzymatic buffer after 3 hours at 37°C. A drop of each of these mixtures was analyzed by TEM, the images obtained are reported in Figure 4 and 5. As expected, the detected sizes are smaller than those observed for the same sample liver analysed before the enzymatic digestion. In detail, particles with a most frequency size of 5 nm (mean size of 10.6 ± 8.6 nm) were detected for rats fed with CuO ENMs and 8.9 nm for $Cu_2CO_3(OH)_2$ ENMs (mean size of 10.8 ± 5.4 nm). Size distributions of both ENMs, before and after the enzymatic digestion, were obtained by considering at list 1000 particles for each of the sample investigated (Figure 5 and 6).

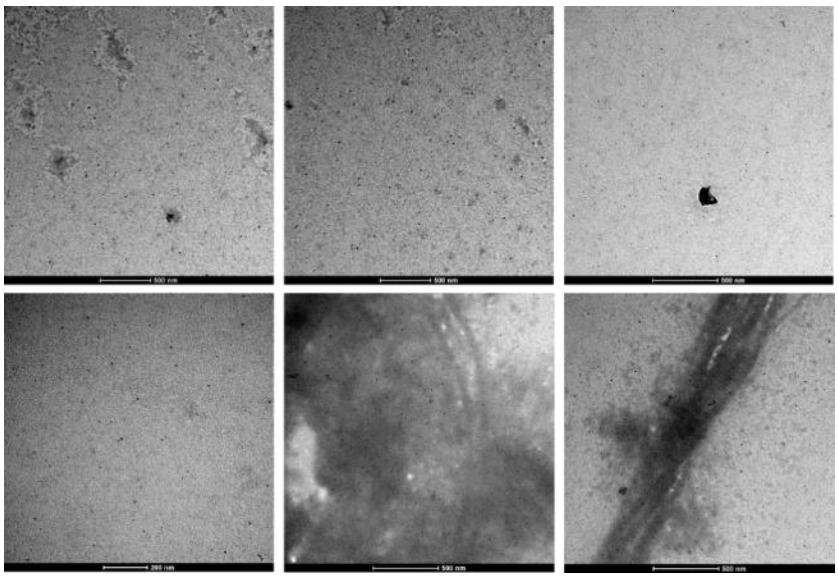

Figure 5 TEM images of liver tissues from rats fed with 512 mg/Kg of CuO ENMs for 5 days after digestion with Proteinase K (3 hours at 37°C)

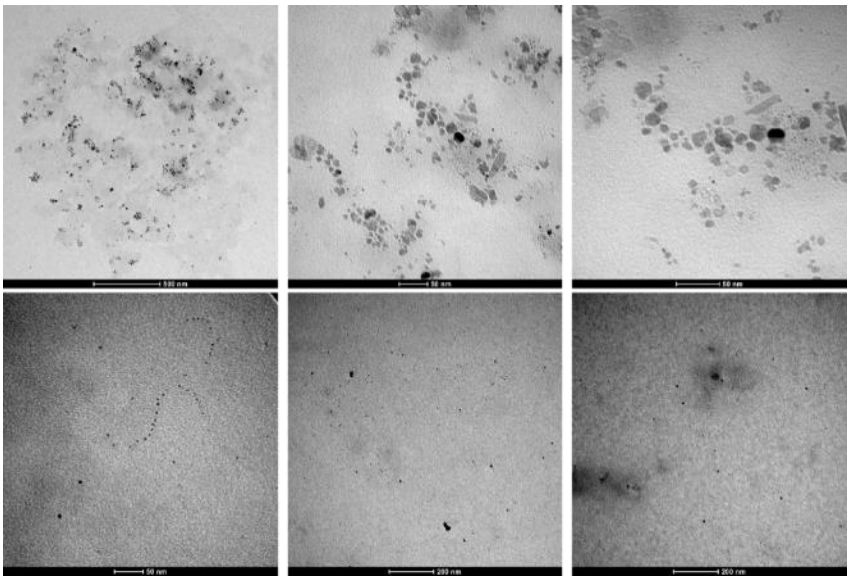

Figure 6 TEM images of liver tissues from rats fed with 128 mg/Kg of $Cu_2CO_3(OH)_2$ ENMs for 5 days after digestion with Proteinase K (3 hours at 37°C)

4.3.2 Possible transformations

A detailed analysis of the particle size distribution determined by TEM, combined with sp-ICP-MS results, has allowed us to hypotheses, by describing the experimental data obtained, the possible transformations occurring to Cu-ENMs in in-vivo samples. A schematic of the different steps is reported below (Scheme 1).

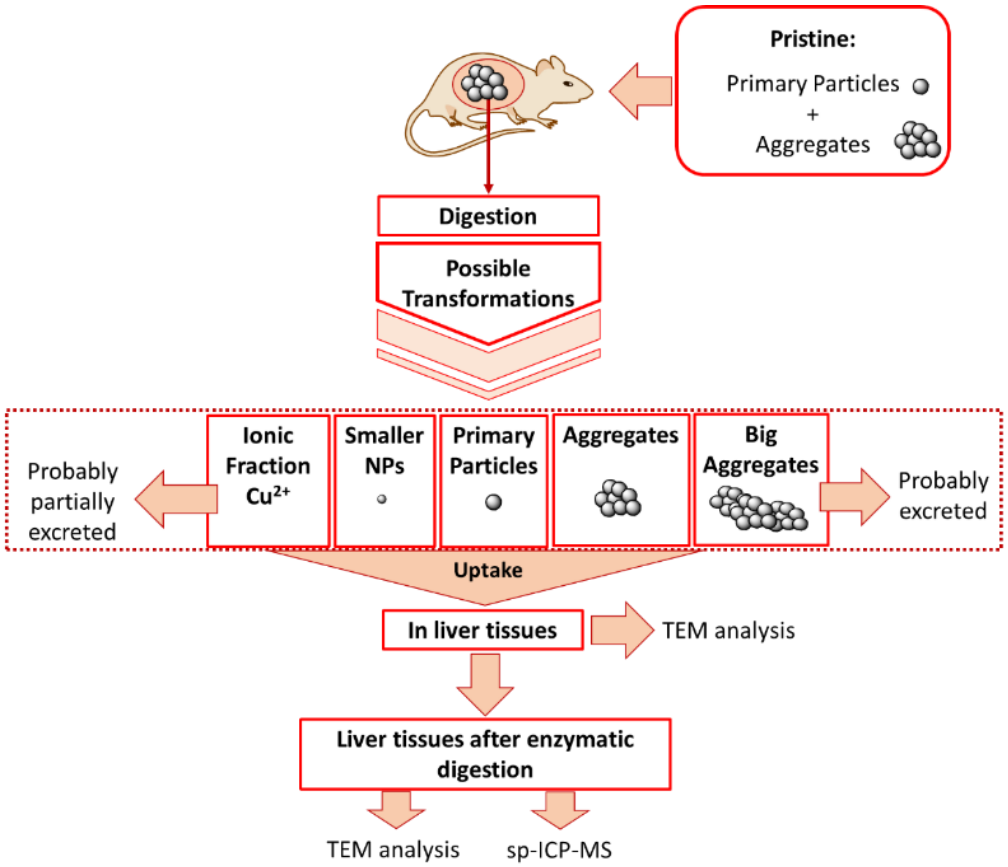

Scheme 1 Schematic of possible Cu-ENMs transformations and analytical techniques employed.

4.3.3 Dissolution process and liver uptake

Both pristine CuO and $Cu_2CO_3(OH)_2$ ENMs are composed by primary particles and aggregates (Figure 1). As reported by De Jong et al. (2018),[1] dissolution studies in stomach and intestinal simulant fluid indicate as these ENMs are subjected to partial dissolution under these conditions. This phenomenon should be accompanied by shrinking of particles, where primary particles are expected to dissolve faster than aggregates (highest surface area to volume ratio). Considering these experimental evidences, it is expected that once the Cu-ENMs are ingested by rats, dissolution among other transformation processes may occur, and a certain fraction will be excreted by the organism. In particular, a part of the resulting ionic fraction as well as particles with a certain size, especially big aggregates (already present in the pristine or formed during the digestive process), are probably excreted by the organism. As reported by Shang et el. (2014)[19] NPs size play a key role in the internalization processes, and it is expected that within organs the internalization mechanisms act as a sort of sieve where only particles with a certain size will be easily uptake. The size exclusion mechanism can be somehow confirmed by TEM images reported in Figures 2 and 3, in which only particles of around 9 and 7 nm for CuO and $Cu_2CO_3(OH)_2$ ENMs respectively, are encountered within liver tissues.

4.3.4 Enzymatic digestion and characterization of digested samples

The liver samples were then treated by enzymatic digestion, this pre-treatment procedure should lead to samples which can be directly analysed by sp-ICP-MS without altering the intrinsic characteristics of NPs too much. To confirm the efficacy of the enzymatic digestion already reported in the literature for other metallic NPs,[13,15] a deep characterization of the ENMs embedded in the digested mixture was performed. A drop of these mixtures was deposited on grids and they were directly analysed by TEM (Figure 5 for CuO ENMs and Figure 6 for $Cu_2CO_3(OH)_2$). As observed by TEM images, the digested livers show particles with similar sizes for both the ENMs investigated. For rats fed with CuO, ENMs detected showed a most frequency diameter of ~ 5 nm (mean size 10.6 ± 8.6), while in the case of $Cu_2CO_3(OH)_2$, ~ 9 nm (mean size 10.8 ± 5.4 nm) were obtained. Although by considering NPs mean sizes it seems that their dimensions have increased after the enzymatic digestion, by comparing the size distribution graphs reported in Figure 7, it appears clear from both the most frequency size and the data distribution, that a dissolution process has occurred. In detail, for CuO ENMs the most frequency size is shifted towards a smaller diameter and this clearly indicates partial dissolution of the NPs. In the case of $Cu_2CO_3(OH)_2$ ENMs, the increased NPs mean size observed by TEM can be explain by the faster dissolution of smallest NPs with respect to aggregates, which probably need more time to get dissolved.

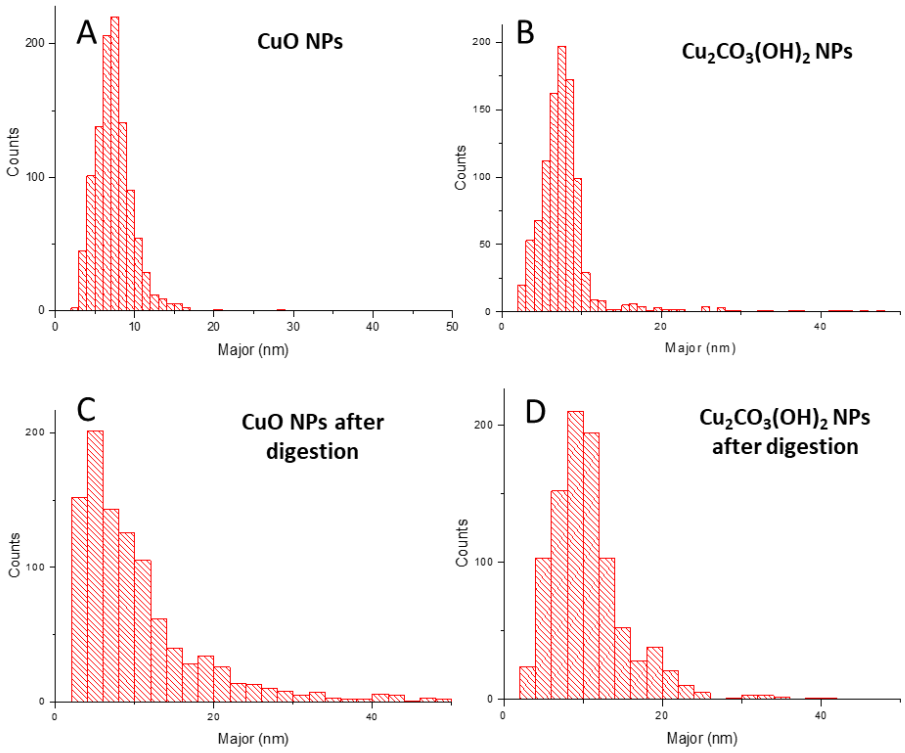

Figure 7 Distribution size of a) CuO NPs in liver after resin embedding b) CuO NPs in liver after enzymatic digestion, c) $Cu_2CO_3(OH)_2$ NPs in liver after resin embedding d) $Cu_2CO_3(OH)_2$ NPs in liver after enzymatic digestion

To gather more information on the dissolution of both CuO and $Cu_2CO_3(OH)_2$ ENMs under digestion conditions, both pristine materials have been treated with the same enzymatic digestion buffer used for the tissue's digestion: after 3 h at 37°C the samples were ultra-filtrate and dissolved Cu^{2+} was quantified by ICP-MS. As is reported in Table 2, copper oxide showed a dissolution of 37% while copper carbonate NPs are totally dissolved under these experimental conditions, because of the presence of the enzyme. It has to be considered that when these Cu-ENMs are embedded in tissues, they are probably covered by a shell of proteins and biomolecules that are limiting the dissolution phenomenon. On the contrary, when pristine Cu-ENMs are directly dispersed in the digestion buffer, the dissolution occurred fastest due to the lack of the shielding effect. This can explain why $Cu_2CO_3(OH)_2$ ENMs are still present in TEM images (Figure 5-6) after the enzymatic digestion.

Table 2 Percentage of dissolution of $Cu_2CO_3(OH)_2$ and CuO in MilliQ water and digestion buffer

ENMs	MillQ water (%)	Digestion buffer (%)
CuO	1,9 ± 0,3	37 ± 4
$Cu_2CO_3(OH)_2$	0,99 ± 0,09	102 ± 5

4.3.5 sp-ICP-MS

The size detection limits (DL_S) for CuO and $Cu_2CO_3(OH)_2$ ENMs by sp-ICP-MS were estimated of 13nm and 18 nm respectively. Considering the sizes of pristine materials, both NPs are in the range of detection of the instrument or slightly below it. However, after ingestion and

uptake in liver, as well as after the enzymatic digestion, these particles went below the DL_S and this is obviously affecting the mass balance calculation. Unfortunately, this means that by sp-ICP-MS, only particles and aggregates over these DL_S can be detected and quantified. Taking into account these considerations and aware that TEM images showed the presence of agglomerates over this size limit, sp-ICP-MS was used to screen their presence in liver of rats dosed with different Cu-ENMs concentrations. In detail, we analysed livers of rats fed with 32, 64 and 512 mg/Kg for CuO and sacrificed at day 6, and liver of rats dosed with 32 mg/Kg and scarified 26 days after the last oral administration. For $Cu_2CO_3(OH)_2$ ENMs, liver of rats dosed with 64 and 128 mg/Kg were investigated after 6 days from the last administration, as well as 64 mg/Kg at day 26. The overall data obtained by sp-ICP-MS are reported in Table 3, together with the total copper determined by ICP-MS after an acidic digestion.

Table 3 Total copper determined by ICP-MS after an acidic digestion, particle concentration, and the most frequent size both determined by sp-ICP-MS

Analyte	Dose/Autopsy (mg/day)	Cu^{2+} (mg/Kg)	Particle Concentration (parts*10^5/mg)	Most Frequent Size (nm)
CuO	512/5	757	2294	19
	32/6	36	42	19
	64/7	78	152	24
	32/26	13	4	17
$Cu_2CO_3(OH)_2$	64/5	367	1758	23
	128/5	1231	3133	29
	64/26	42	415	23

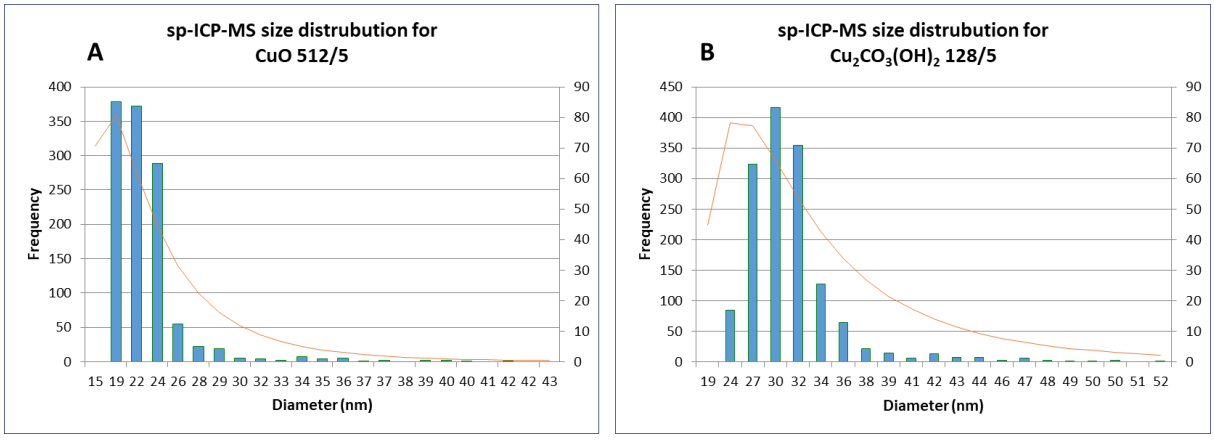

Figure 8 sp-ICP-MS size distribution for A) CuO 512/5, B) $Cu_2CO_3(OH)_2$ 128/5

Data from sp-ICP-MS analysis of the digested mixtures revealed the presence of Cu-ENMs in all the samples investigated, except for rats dosed with 32 mg/Kg of CuO and scarified 26 days after the last administration, in which no significant size distribution was measured. This confirms, as already reported by De Jong et al. (2018)[1], that this doses of CuO ENMs is totally excreted by rats after 26 days. Moreover, from these data emerged that to high value of ionic copper concentration (measured after the acidic digestion) always corresponds a high particle concentration value. Finally, the samples analysed showed an average most frequency size of

around 20 nm for CuO and 25 nm $Cu_2CO_3(OH)_2$ ENMs (Table 3). Two examples of the nanoparticles size distribution determined by sp-ICP-MS are reported in Figure 8, and the DL_s of the instrument for the two materials investigated is shown (~ 15 nm for CuO ENMs, and ~ 19 nm for $Cu_2CO_3(OH)_2$ ENMs). Unfortunately, these results indicate that by sp-ICP-MS, all the information concerning particles below the DL_S is missed This approach can be therefore useful only for a qualitative characterization of the samples, as it allows to detect only the particle/aggregates over the instrumental DL_S.

4.4) Conclusions

In conclusion, from this work emerges that CuO and $Cu_2CO_3(OH)_2$ NPs used to feed rats in the short-term oral study conducted by Wim et al. are, in liver tissues, still in the nanoform 1 day after the last oral administration. To the best of our knowledge, this is the first time in which copper-based NPs are detected in organs of rats exposed to these nanomaterials, and an attempt to understand the transformations to which they are subjected have been herein reported. Unfortunately, the dissolution processes occurring within rat's organism, as well as the enzymatic digestion of the tissues, has led to NPs with sizes below the LOD_{SIZE} of sp-ICP-MS and it was possible to quantify only the aggregates with sizes over this limit of detection values. The quantification of nanomaterials in the nanoform, in particular of those kinetically unstable, remains therefore a challenge for researchers. The toxicological effects of nanomaterials in fact, are always associated to the exposure doses expressed in mass units (as for bulk materials) instead of particle number. The specific surface area is only poorly considered. As already reported in the literature,[20] this information could be helpful to better interpret the results from nanotoxicology studies, especially with respect to dose/effect relationship.

4.5) References

1. De Jong W.H., De Rijk E., Bonetto A., Wohlleben W., Stone V., Brunelli A., Badetti E., Marcomini A., Gosensn I., C. F. Toxicity of copper oxide and basic copper carbonate nanoparticles after short-term oral exposure in rats. *Nanotoxicology* **accepted,** (2018).

2. Freeman, B. M. H. & McIntyre, C. R. A Comprehensive Review of Copper-Based Wood Preservatives with a focus on new micronized or dispersed copper systems. *For. Prod. J.* (2008).

3. Lebow, S. & Foster, D. Environmental concentrations of copper, chromium, and arsenic released from a chromated-copper-arsenate- (CCA-C-) treated wetland boardwalk. *For. Prod. J.* (2005).

4. Astdr. Toxicological profile for Copper. *U.S Public Heal. Serv. Agency Toxic Subst. Dis. Regist.* (2004). doi:doi:10.1201/9781420061888_ch106

5. Richman, E. K. & Hutchison, J. E. The nanomaterial characterization bottleneck. *ACS Nano* (2009). doi:10.1021/nn901112p

6. Soto-Alvaredo, J. *et al.* Speciation of gold nanoparticles and low-molecular gold species in Wistar rat tissues by HPLC coupled to ICP-MS. *J. Anal. At. Spectrom.* (2017). doi:10.1039/c6ja00248j

7. Hassellöv, M., Readman, J. W., Ranville, J. F. & Tiede, K. Nanoparticle analysis and characterization methodologies in environmental risk assessment of engineered nanoparticles. *Ecotoxicology* **17,** 344–361 (2008).

8. Ottofuelling, S., Von Der Kammer, F. & Hofmann, T. Commercial titanium dioxide nanoparticles in both natural and synthetic water: Comprehensive multidimensional testing and prediction of aggregation behavior. *Environ. Sci. Technol.* **45,** 10045–10052 (2011).

9. von der Kammer, F. *et al.* Analysis of engineered nanomaterials in complex matrices (environment and biota): General considerations and conceptual case studies. *Environmental Toxicology and Chemistry* (2012). doi:10.1002/etc.723

10. Dekkers, S. *et al.* Presence and risks of nanosilica in food products. *Nanotoxicology* (2011). doi:10.3109/17435390.2010.519836

11. Gray, E. P. *et al.* Extraction and Analysis of Silver and Gold Nanoparticles from Biological Tissues Using Single Particle Inductively Coupled Plasma Mass Spectrometry. *Environ. Sci. Technol.* **47,** 14315–14323 (2013).

12. Loeschner, K. *et al.* Detection and characterization of silver nanoparticles in chicken meat by asymmetric flow field flow fractionation with detection by conventional or single particle ICP-MS. *Anal. Bioanal. Chem.* **405,** 8185–8195 (2013).

13. Loeschner, K., Brabrand, M. S. J., Sloth, J. J. & Larsen, E. H. Use of alkaline or enzymatic sample pretreatment prior to characterization of gold nanoparticles in animal tissue by single-particle ICPMS Characterisation of Nanomaterials in Biological Samples. *Anal. Bioanal. Chem.* **406,** 3845–3851 (2014).

14. Vidmar, J., Buerki-Thurnherr, T. & Loeschner, K. Comparison of the suitability of

alkaline or enzymatic sample pre-treatment for characterization of silver nanoparticles in human tissue by single particle ICP-MS. *J. Anal. At. Spectrom.* **33,** 752–761 (2018).

15. Peters, R. J. B. *et al.* Development and validation of single particle ICP-MS for sizing and quantitative determination of nano-silver in chicken meat Characterisation of Nanomaterials in Biological Samples. *Anal. Bioanal. Chem.* **406,** 3875–3885 (2014).

16. Pantano, D. *et al.* Transformations of Nanoenabled Copper Formulations Govern Release, Antifungal Effectiveness, and Sustainability throughout the Wood Protection Lifecycle. *Environ. Sci. Technol.* (2018). doi:10.1021/acs.est.7b04130

17. Hsiung, C.-S. S., Andrade, J. D., Costa, R. & Ash, K. O. Minimizing interferences in the quantitative multielement analysis of trace elements in biological fluids by inductively coupled plasma mass spectrometry. *Clin. Chem.* (1997).

18. Nomura, C. S., Silva, C. S., Nogueira, A. R. A. & Oliveira, P. V. Bovine liver sample preparation and micro-homogeneity study for Cu and Zn determination by solid sampling electrothermal atomic absorption spectrometry. *Spectrochim. Acta - Part B At. Spectrosc.* (2005). doi:10.1016/j.sab.2005.02.021

19. Shang, L., Nienhaus, K. & Nienhaus, G. U. Engineered nanoparticles interacting with cells: Size matters. *Journal of Nanobiotechnology* (2014). doi:10.1186/1477-3155-12-5

20. Sager, T. M. & Castranova, V. Surface area of particle administered versus mass in determining the pulmonary toxicity of ultrafine and fine carbon black: Comparison to ultrafine titanium dioxide. *Part. Fibre Toxicol.* (2009). doi:10.1186/1743-8977-6-15

5) Conclusion

The thesis work on Cu-ENMs behaviour in environmental media, and on their effects and biodistribution in organisms after toxicological testing, provided important information for the interpretation of nano-bio/eco interactions and to establish the basis for safer copper-based products design and use.

The thesis results have shown that many variables may influence particle transformation, especially when dissolution phenomena are involved. Since dissolution is a multi-parameter transformation also affected by particles diameter, the results obtained demonstrated that pH plays a key role in Cu-based ENMs dissolution, with respect to other water and biological variables (e.g. ionic strength, DNOM, proteins). However, since ENMs are subjected to continuous transformations, it is not only important to consider the chemical properties of the media in which they are dispersed, but also the nanoparticles concentration. The latter in fact is crucial to interpret all the processes involved, i.e. dissolution, agglomeration and sedimentation phenomena.

Regarding the biological interactions, the investigation carried out during the thesis showed that the short-term inhalation/oral exposure tests of Cu-based ENMs on rats led to severe pathological lesions in various organs, related to a high bioaccumulation and to a targeted biodistribution (lungs for inhalation tests and liver and kidneys for the oral exposure test). After 3 weeks from the last exposure to the Cu-ENMs, the copper concentration in the rats' organs was found to return to ordinary values, but the pathological lesions remain visible. Additional information on Cu-based ENMs size distribution and their spatial location within the biological tissues, helped to understand the transport dynamics from the blood vessel towards biological targets, and to understand the inflammation and detoxification processes involved. These results can be very important in the field of nanotoxicology for Cu-based ENMs, and they can also be applied in nanomedicine and for the development of new safer Cu-based ENMs products.

To date, studying the transformations of ENMs in real environmental samples still represent an analytical challenge, mainly because of high background levels and low ENMs concentration, which is complicated also by the fact that the conventional instrumental techniques does not allow to reach appropriate detection/quantification levels. In the case of biological samples, the intrinsic instability of the starting materials and/or the sample pre-treatment can drastically change the original characteristics of the ENMs under study thus introducing significant analytical bias.

ANNEX I

Colloidal characterization of CuO nanoparticles in biological and environmental media

Volume 4 | Number 6 | June 2017 | Pages 1201–1420

Environmental Science Nano

rsc.li/es-nano

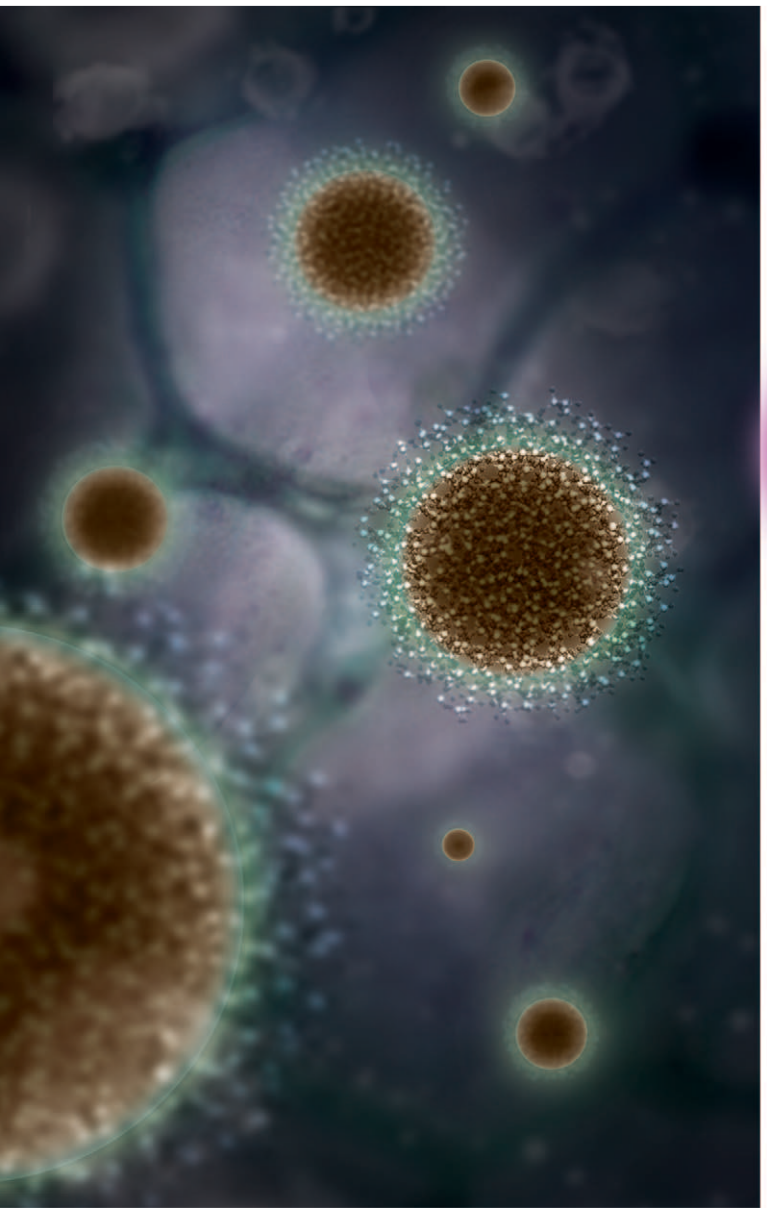

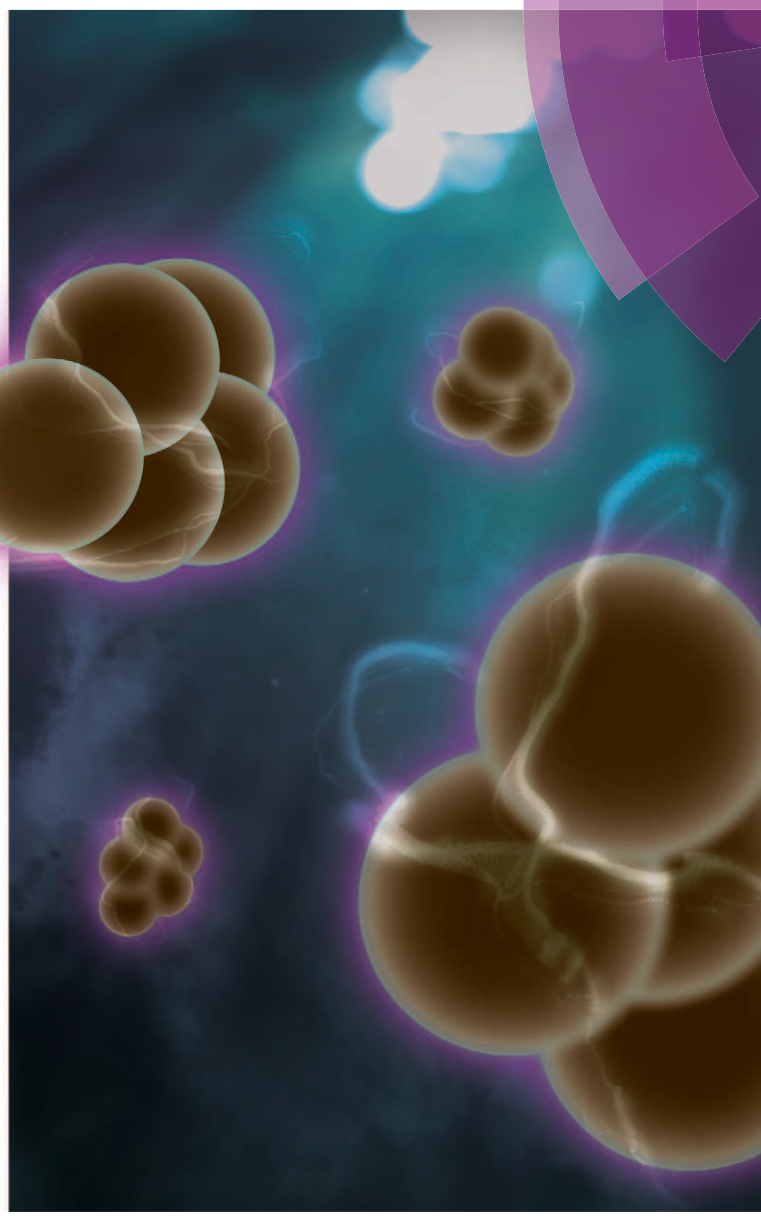

ISSN 2051-8153

ROYAL SOCIETY OF CHEMISTRY

PAPER

Simona Ortelli *et al.*

Colloidal characterization of CuO nanoparticles in biological and environmental media

Environmental Science Nano

PAPER

View Article Online
View Journal | View Issue

Cite this: *Environ. Sci.: Nano*, 2017, 4, 1264

Colloidal characterization of CuO nanoparticles in biological and environmental media†

Simona Ortelli,[a] Anna Luisa Costa,*[a] Magda Blosi,[a] Andrea Brunelli,[b] Elena Badetti,[b] Alessandro Bonetto,[b] Danail Hristozov[b] and Antonio Marcomini[b]

Received 24th November 2016,
Accepted 21st March 2017

DOI: 10.1039/c6en00601a

rsc.li/es-nano

The relationships between the physicochemical properties of engineered nanomaterials (ENMs) and their adverse health and environmental effects are still unclear. In order to understand key nano-bio/eco interactions and to convert this knowledge into "Safety by Design" ($S_{by}D$) strategies, it is essential to study the colloidal properties of ENMs in nano(eco)toxicology-relevant media. In the frame of such a $S_{by}D$ approach, this paper investigates the dispersion stability of copper oxide NPs surface-modified by means of four stabilizing agents, namely, [polyethylenimine (PEI), sodium ascorbate (ASC), sodium citrate (CIT), and polyvinylpyrrolidone (PVP)], which were used to achieve positive (PEI), negative (ASC, CIT), and neutral (PVP) surface charging of the NPs. The effects of these four stabilizers on the CuO NPs' physicochemical properties were investigated in different biological and environmental media by combining dynamic and electrophoretic light scattering (DLS and ELS), centrifugal separation analysis (CSA) and inductively coupled plasma optical emission spectroscopy (ICP-OES). The results showed improved dispersion stability for CuO-CIT, CuO-ASC, and CuO-PEI in both Milli-Q and phosphate buffered saline (PBS) as compared to pristine CuO and CuO-PVP. The increased ionic strength of artificial fresh (AFW) and marine (AMW) waters strongly destabilized all the CuO NP suspensions, except for CuO-PEI dispersed in AFW. The presence of proteins and amino acids in the test media had a strong influence on the colloidal stability of all the dispersions. Characterization of colloidal properties and ion release rates in (eco)toxicological testing media will help to correlate some of these properties with (eco)toxicological responses, thus enabling prediction of the behavior of NPs in real environments.

Environmental significance

The relationships between the physicochemical properties of engineered nanomaterials (ENMs) and their adverse health and environmental effects are still unclear. In order to understand key nano-bio/eco interactions and to convert this knowledge into design criteria for the development of "Safety by Design" ($S_{by}D$) strategies, it is essential to study the colloidal properties of ENMs in media relevant for nano(eco)toxicology. An accurate measurement of such properties allows the prediction of ENM release, uptake, biokinetics and toxicity and represents a key step for grouping and read-across in a risk assessment and management framework.

1. Introduction

There are already many engineered nanomaterials (ENMs) on the market, and their number continues to increase. These materials are optimized with respect to a variety of properties (*e.g.* size, morphology, purity, and surface coating) that enables their application in different consumer products (nanodb.dk). This enormous complexity of nanoforms has made the analysis of their environmental health and safety implications impossible without highly demanding case-by-case testing, which poses a huge problem to the regulation of their risks.[1–3] It is widely accepted by regulators, industries, and scientists, that grouping and read-across can address this issue, as these are useful approaches to reducing costs and enhancing the efficiency of testing for risk assessment and safer product design.[4,5] In order to develop such approaches for ENMs, it is essential to gain fundamental understanding of which intrinsic and extrinsic (and combinations thereof) structural and physicochemical characteristics of ENMs dispersed in environmental or biological media, or embedded in product matrices, affect their release, uptake,

[a] *CNR-ISTEC, Institute of Science and Technology for Ceramics – National Research Council of Italy, Via Granarolo 64, I-48018 Faenza, RA, Italy. E-mail: anna.costa@istec.cnr.it; Tel: +39 0546 699718*

[b] *DAIS - Dept. of Environmental Sciences, Informatics and Statistics, University Ca' Foscari of Venice, Via delle Industrie 21/8 c/o INCA - VEGAPARK, I-30175 Marghera, VE, Italy*

† Electronic supplementary information (ESI) available. See DOI: 10.1039/c6en00601a

biokinetics, and toxicity. This involves the investigation of key interactions at the interface between ENMs and environmental or biological media,[6] which depend on both the physicochemical properties of ENMs and the characteristics of the surrounding media.[7,8] Therefore, any testing strategies for the purpose of risk assessment and safer product design should also consider the interactions between ENMs and other compounds present in a medium, regardless of whether they are biological (*e.g.* proteins and amino acids) or environmental (*e.g.* natural organic matter or extracellular polymeric substances). Many studies investigated such interactions,[9–12] focusing on *core* intrinsic properties (*i.e.* chemical composition, size, shape, coating), *shell* evolution (*i.e.* agglomeration/aggregation, charge, corona formation) in testing and life-cycle media,[13,14] and *specific reactivity* (*i.e.* potential generation of reactive oxygen species (ROS) or release of toxic metal ions). Most of these studies concluded that ENMs should be considered as dynamic entities that undergo chemical and physical transformations once embedded in product matrices and exposed to environmental and biological stressors.[15,16]

This study focuses on the physicochemical characterization of copper oxide nanoparticles (CuO NPs), performed in the frame of the EU FP7 SUN project, in order to support the interpretation of (eco)toxicological data from *in vivo* and *in vitro* testing. In fact, the exposure route by which these contaminants enter an organism after contact, can strongly depend on ENM dispersion stability (*i.e.* NPs that quickly settle from the water column can increase the interaction with benthic species).[17]

Nanoscale CuO was chosen as a case study because it is widely used, owing to its antibacterial properties, in wood preservation, paints and textiles.[18–20] Timber preservation applications include outdoor residential decking, gardening, fencing, and playground equipment. Specifically, the SUN case study involves CuO-based paint, which, in addition to wood preservation, also provides aesthetic functionality to softwood cladding. Pristine CuO NPs were mixed with an acrylic base to produce the paint according to a specified composition. The fixation mechanism of this formulation involves reaction of the cupric ion with carboxylic and phenolic groups from cellulose, hemicellulose and lignin. This leads to the homogenous distribution of the ions in the wood cells, including penetration through cell wall voids. Once the wood is saturated, the remaining copper precipitates as basic copper carbonate and can be released into the environment through leaching, which leads to exposure of ecosystems and humans.

This may pose health and environmental risks as CuO is considered a toxic substance.[21,22] In order to prevent those, we modified the surface of the CuO NPs by a "Safety by Design" ($S_{by}D$) approach.[23–27] Surface modification involved the attachment of four non-hazardous modifying agents to obtain different surface charges [negative for sodium citrate (CIT) and sodium ascorbate (ASC), positive for branched polyethylenimine (PEI), neutral for polyvinylpyrrolidone (PVP)]. Key properties (*i.e.* colloidal stability including surface charge and ion release) of pristine and modified CuO NPs were investigated in Milli-Q water, phosphate buffered saline (PBS), and biological and environmental media. We studied their evolution at increasing levels of complexity of the embedding matrices (from distilled water to biological fluids) to understand how the intrinsic identity of the NPs is affected by the extrinsic characteristics of the media (*i.e.* pH, ionic strength, presence of biomolecules). The obtained results are highly relevant for hypothesizing key nano-bio/eco interactions in relation to modes of toxicological action in order to derive criteria and guiding principles for grouping and read-across.

2. Materials and methods

2.1 Materials

Commercial CuO nanopowder (average particle diameter: 12 ± 4 nm) was provided by PlasmaChem GmbH (Germany). Minimum Essential Medium (MEM), Dulbecco's Modified Eagle Medium (DMEM – high glucose), fetal bovine serum (FBS) and penicillin/streptomycin (Pen–Strep) were purchased from Life Technologies Corporation (Carlsbad, USA). Dulbecco's phosphate buffered saline (PBS), sodium citrate (CIT), sodium ascorbate (ASC), polyvinylpyrrolidone (PVP – MW 29000), branched polyethylenimine (PEI – solution 50% in H_2O) and nitric acid 70% (redistilled, 99.99% trace metal basis) were purchased from Sigma-Aldrich. Artificial fresh water (AFW) and artificial marine water (AMW) were prepared according to standardized protocols.[28,29] All inorganic salts were of analytical grade and purchased from Sigma-Aldrich (St. Louis, MI, USA).

2.2 Methods

A CuO pristine stock suspension at a concentration of 10 g L^{-1} of Cu (1 wt%) was prepared by dispersing CuO powder in PBS (total phosphate concentration: 0.05 M, pH = 7.4). Starting from the stock suspension, modified CuO dispersions were prepared by adding 10 wt% modifying agents (*i.e.* CIT, ASC, PEI and PVP) (Fig. 1) with respect to the total amount of copper oxide. This amount was estimated by titrating the pristine CuO NPs while adding the stabilizers by means of an electroacoustic technique (Acoustosizer, Colloidal Dynamics, USA) (see the ESI†). As a result, for each kind of stabilizer, we observed that an amount of 10 wt% guarantees a complete covering on CuO NPs. Both the pristine and modified stock suspensions were mixed *via* ball milling (BM) with 3 mm zirconia spheres over 95 h. Five different stock suspensions were thus obtained: pristine (CuO-pristine), sodium citrate-modified (CuO-CIT), sodium ascorbate-modified (CuO-ASC), polyethylenimine-modified (CuO-PEI), and polyvinylpyrrolidone-modified (CuO-PVP) CuO nanoparticles.

Colloidal characterization was performed using diluted CuO stock suspensions (Cu content 100 mg L^{-1}) mixed with: diluted PBS (1 : 10 dilution to reach the same ionic strength (16 mM) as those of the biological media tested); "complete" DMEM and MEM (*i.e.* either MEM or DMEM to

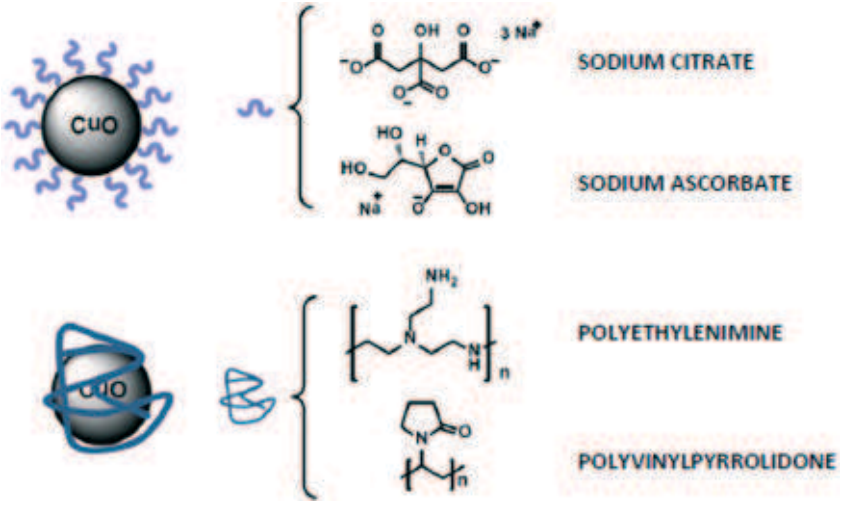

Fig. 1 Schematic representation of the $S_{by}D$ strategy applied: introduction of modifying agents (*i.e.* CIT, ASC, PEI and PVP) by self-assembling.

which 10% v/v FBS and 1% v/v Pen–Strep were added), and AFW and AMW (simulating media usually used for ecotoxicological testing; ionic strength of 2 and 630 mM, respectively). The compositions of all the media are reported in the ESI.†

2.3 Characterization

Morphological characterization of pristine CuO NPs was performed by scanning transmission electron microscopy (STEM) analysis using a field emission-scanning electron microscopy (FE-SEM) instrument (Carl Zeiss Sigma NTS Gmbh, Oberkochen, DE). One drop of the CuO NP suspension (100 mg L^{-1}) diluted in Milli-Q water was deposited on a film-coated copper grid and then dried in air. Image analysis was performed on more than 50 particles to estimate the particle size distribution. The hydrodynamic diameter (d_{DLS}) was determined by dynamic light scattering (DLS) measurements, performed using a Zetasizer nano ZSP (model ZEN5600, Malvern Instruments, UK). Zeta potential (ζ-pot_{ELS}) measurements were performed by electrophoretic light scattering (ELS). The Smoluchowski equation was applied to convert the electrophoretic mobility to zeta potential. pH measurements were carried out in diluted (100 mg L^{-1}) suspensions after 24 hours to allow colloidal stabilization. Sedimentation velocity data of the colloidal dispersions were obtained from centrifugal separation analysis (CSA), using the multi-wavelength dispersion analyzer LUMiSizer 651® based on STEP™ technology (space-and-time-resolved extinction profiles), according to ISO/TR 13097:2013. The separation of different components in the dispersions, performed by CSA, was accelerated by applying relative centrifugal force (RCF), which accelerates settling of materials up to 2325 times compared to gravity settling. Sedimentation velocity data were calculated from the percent transmittance values at 470 nm, measured over time at three different positions (115, 120 and 125 mm far from the rotor) along the longitudinal axis of the cuvette. The sedimentation velocity at unit gravity was then extrapolated after verifying the linear correlation between RCF and sedimentation velocity at the selected RCF (2325).

Copper ion release was calculated as the ratio between the dissolved copper ions and the total copper oxide present in suspension. The quantification of copper ions dissolved in each medium was performed by centrifuging 15 mL of each working stock suspension at 5000 rpm and a spin time of 30 min, using an ultra-centrifugal filter (UCF) unit (Amicon Ultra-15, 10 kDa, Millipore). The filtered solution (10 mL) was analyzed by inductively coupled plasma optical emission spectrometry using an ICP-OES 5100 – vertical dual view apparatus (Agilent Technologies, Santa Clara, CA, USA). The total copper was quantified in each diluted suspension, which was previously treated with 2 mL of ultrapure HNO_3 to ensure complete digestion. According to the experimental conditions typical of toxicological and ecotoxicological testing, the ion release experiments were performed at 37 °C after 24 h in biological media and at 25 °C in Milli-Q, PBS, and environmental media. The results from DLS, ELS, LUMiSizer and ICP-OES were reported as the average of three independent measurements.

3. Results and discussion

The morphological characterization of pristine CuO NPs by STEM analysis showed the presence of spherical and monodispersed CuO NPs (Fig. 2). The magnified image (Fig. 2b) highlights the presence of well dispersed NPs with a primary nanoparticle average diameter of 12 ± 8 nm, consistent with supplier specifications. As expected, some agglomerated NPs have also been detected (Fig. 2a and c).

Colloidal stability, which has been reported in the literature as strongly affecting the outcome of toxicological tests,[30–33] was investigated by measuring the hydrodynamic size, ζ-potential, and sedimentation velocity of both pristine and modified CuO NPs. The influence of the modifying agents on the CuO NP stability and agglomeration when

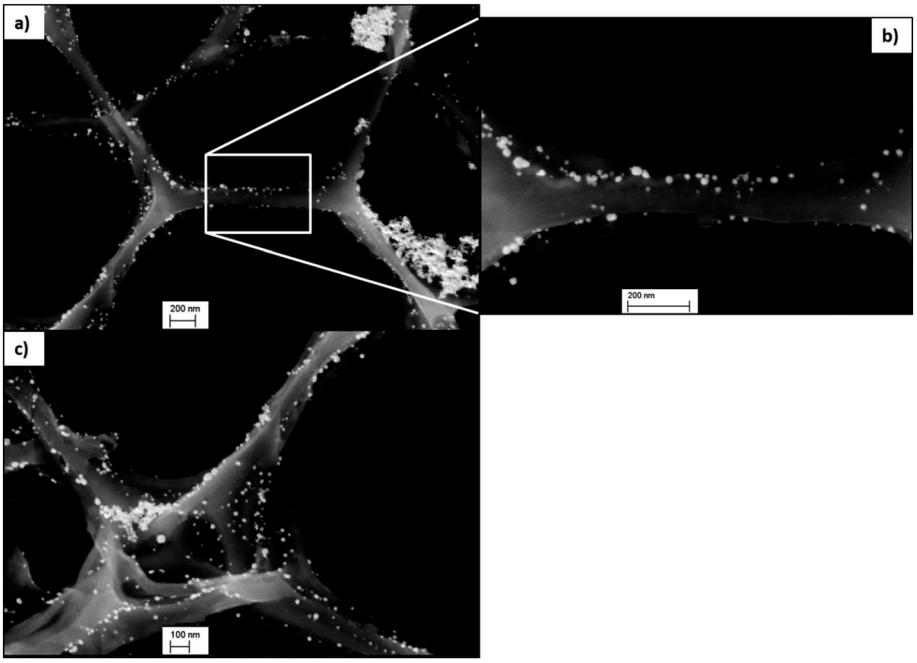

Fig. 2 STEM images (a and c) and magnified image (b) of pristine CuO NPs in Milli-Q water (100 mg L^{-1}).

Table 1 Hydrodynamic diameters (nm) of pristine and modified CuO samples dispersed in different media: Milli-Q water, PBS, MEM, DMEM, AFW and AMW

	Hydrodynamic diameter (nm)					
	Milli-Q	PBS	MEM	DMEM	AFW	AMW
CuO-pristine	1093 ± 50	2756 ± 347	47 ± 6	55 ± 16	1663 ± 210	1281 ± 393
CuO-CIT	368 ± 10	271 ± 43	89 ± 5	37 ± 2	1050 ± 16	1062 ± 159
CuO-ASC	122 ± 1.4	1314 ± 525	52 ± 4	73 ± 21	1293 ± 278	1234 ± 25
CuO-PEI	247 ± 14	209 ± 16	46 ± 4	45 ± 14	675 ± 199	1281 ± 168
CuO-PVP	797 ± 84	2765 ± 432	44 ± 2	53 ± 25	1159 ± 256	1661 ± 580

dispersed in different biological and environmental media was assessed. The DLS results for pristine and modified CuO NPs diluted in Milli-Q water, PBS, MEM, DMEM, AFW and AMW are reported in Table 1.

Data collected in Milli-Q water confirmed the expected effect of surface modifier addition. An improvement of the colloidal dispersion with respect to the pristine one was observed for samples coated by ionic agents (negative CIT and ASC, positive PEI), with a significant decrease of the average hydrodynamic diameter. On the other hand, neutral PVP did not significantly improve the dispersion of CuO NPs. The long aliphatic chains probably force NP aggregation by depletion flocculation.[34] In comparison with Milli-Q water, data collected in PBS showed an increase of the hydrodynamic diameter for CuO-pristine as well as for CuO-ASC and CuO-PVP. This is correlated to aggregation phenomena and justified by the increase of ionic strength due to the salt content in Dulbecco's phosphate buffered saline (PBS) medium. It was previously reported that dissolved salts screen the charge on the NP surface, reducing electrostatic repulsion.[35] However, CuO-CIT and CuO-PEI modified samples were not affected by the presence of salts in solution, showing hydrodynamic size values comparable with those measured in Milli-Q water. From DLS measurements, CuO-PEI resulted in the best dispersed system in both Milli-Q water and in a higher ionic strength medium (PBS). A possible explanation could be related to the electrosteric action of polyethylenimine.[36] Results indicate that ascorbate and citrate salts improve only the repulsive potential due to the negative charge transferred to the particle surface, while PEI provides both electrostatic (due to its positive charge) and steric contributions, due to PEI's polymeric structure.

All DLS data collected in MEM and DMEM cell culture media showed very similar values. The biological components (amino acids and proteins) of the *milieu* seem to strongly level the hydrodynamic size data regardless of the stabilizers used. However, in the case of the samples dispersed in AFW and AMW, an increase of the hydrodynamic diameters was observed for both the pristine and modified NPs. Salts present in environmental media, in particular divalent cations (*e.g.* Ca(II) and Mg(II)), can be adsorbed onto the nanoparticle surface and induce particle agglomeration. This phenomenon was already observed in AFW, whose ionic strength is ten times lower than that of AMW. Agglomeration in AFW seems

to be prevented only by PEI, which loses its efficacy in AMW, *i.e.* at the highest ionic strength.[6]

ζ-potential represents another important parameter directly affecting colloidal stability and interaction of NPs with the surrounding medium.[12,37] Basically, the charge is often quantified in terms of ζ-potential which depends on the *milieu* in which the NPs are dispersed and is therefore strongly correlated to the pH.[38] ζ-potentials of biological media were measured at around pH 8, and values of −9.9 ± 0.2 mV and −10.6 ± 0.3 mV were obtained for MEM and DMEM, respectively. The results collected for the pristine and modified samples are listed in Table 2.

Pristine CuO NPs diluted in Milli-Q water had a negative ζ-potential, despite the positive value expected for copper oxide and, more generally, for basic metal oxides dispersed in water.[39,40] The reversal of the CuO pristine surface charge sign is due to the presence of phosphate ions (PO_4^{3-}) used in the sample preparation, which are specifically adsorbed onto the CuO NPs surface (Fig. 3a). The key role of phosphate adsorption has already been reported in the literature.[35,40] The modified samples diluted in Milli-Q water showed values coherent with the charge carried by the stabilizers, confirming the preferred interaction of CuO NPs with the aforementioned modifiers over that with phosphate ions (Fig. 3b). As expected, the addition of a neutral PVP coating did not modify the ζ-potential of the pristine samples. An increase of ionic strength induced colloidal destabilization in PBS, as confirmed by both the increased agglomeration rate (Table 1) and ζ-pot decrease (Table 2). The ζ-pot values of CuO-pristine and CuO-PVP are close to zero, indicating proximity to the isoelectric point (pH_{IEP}). The correlation between the NP size and ζ-potential results confirmed that DLS coupled with ELS represents an effective tool for colloidal stability evaluation. In DMEM and MEM, the ζ-potential data level off at the value measured for the biological media without NPs (negative ζ-pot, around −10 mV, see Table 2 and Fig. 3c). This can be in agreement with the protein-corona theory, in which NPs are probably covered by proteins upon contact with a biological medium.[40,41] As a result, amino acids and proteins seemed to overwhelm the effects of surface-modifying agents in driving colloidal stability.

On the other hand, particles dispersed in AFW showed ζ-pot values similar to those in PBS, while a slight increase was observed when the stabilization was driven by polymers. According to the media preparation specifications, the ionic strengths of AFW and PBS were comparable. Positive ζ-pot values were detected for all the samples dispersed in AMW (Fig. 3d). As already described in the literature, inorganic divalent cations seem to get adsorbed onto the NP surface, and to control the electrical double layer formation.[6]

A hypothetical scheme on how the different coatings (*i.e.* phosphate ions, modifiers, divalent cations, amino acids and proteins) affect, in terms of aggregation and surface charge, the colloidal stability of pristine and CuO-modified NPs, is reported in Fig. 3.

Colloidal stability was also investigated through CSA by means of a LUMiSizer, calculating the sedimentation velocity of the CuO NPs previously dispersed at 100 mg L^{-1} in MQ, PBS, MEM, DMEM, AFW and AMW. Fig. 4 shows the average sedimentation velocity data for pristine and modified CuO NPs dispersed in the six different media selected, highlighting a correlation with the hydrodynamic diameter determined by DLS (Table 1) for almost all the samples investigated. The main differences observed could be ascribed to the principles on which the techniques employed are based. The sedimentation velocity distributions are shown in Fig. 5. In general, it was confirmed that the modifying agents improved the colloidal stability of the dispersions, preventing or decreasing the formation of CuO aggregates with respect to pristine CuO NPs. In particular, for Milli-Q and PBS media, the sedimentation velocity distribution decreased for all the modified suspensions compared to pristine CuO NPs. The sedimentation velocity rate in these two aqueous media followed the same trend observed for the hydrodynamic diameter data in Milli-Q (Table 1), in which pristine and CuO-PVP suspensions are less stable than CuO-CIT, followed by CuO-PEI and CuO-ASC. The correlation between the LUMiSizer and DLS data was also noticed for CuO-pristine and CuO-PVP dispersed in PBS, showing both the highest sedimentation velocity values and agglomeration rates. Surprisingly, the CuO-ASC dispersion displayed the lowest sedimentation velocity values in PBS, but a high average hydrodynamic diameter (>1 μm). Taking into account the two different biological media, the results from LUM and DLS suggest that proteins and amino acids enhance the stability rate of the dispersions, both for pristine as well as for modified CuO. The only exception is represented by the slightly higher sedimentation velocity values of CuO-PEI than those of the other dispersions. However, more precise analysis of the sedimentation rates can be achieved by considering LUMiSizer numerical data through their quartiles, using a box plot as a graphical descriptive statistic (Fig. 5).

Table 2 ζ-potentials (mV) of pristine and modified CuO samples dispersed in different media: Milli-Q water, PBS, DMEM, MEM, AFW and AMW

	ζ-pot (mV)					
	Milli-Q (pH = 6.5)	PBS (pH = 7.4)	MEM (pH = 7.9)	DMEM (pH = 8.2)	AFW (pH = 8.1)	AMW (pH = 8.1)
CuO-pristine	−9.1 ± 0.4	−2.3 ± 2.1	−10.1 ± 0.5	−8.2 ± 0.4	−3.5 ± 0.4	+7.6 ± 0.4
CuO-CIT	−18.0 ± 0.3	−3.4 ± 1.2	−10.5 ± 0.2	−9.7 ± 0.6	−3.6 ± 0.4	+4.5 ± 0.7
CuO-ASC	−17.4 ± 0.3	−8.1 ± 0.1	−9.5 ± 0.2	−9.2 ± 0.2	−8.1 ± 0.4	+2.7 ± 0.6
CuO-PEI	+28.3 ± 0.7	+13.8 ± 0.1	−10.5 ± 0.9	−10.1 ± 0.7	+20.9 ± 0.9	+10.1 ± 1.1
CuO-PVP	−8.1 ± 2.3	−0.9 ± 0.7	−10.1 ± 0.4	−9.4 ± 0.8	+1.6 ± 0.3	+6.5 ± 1.5

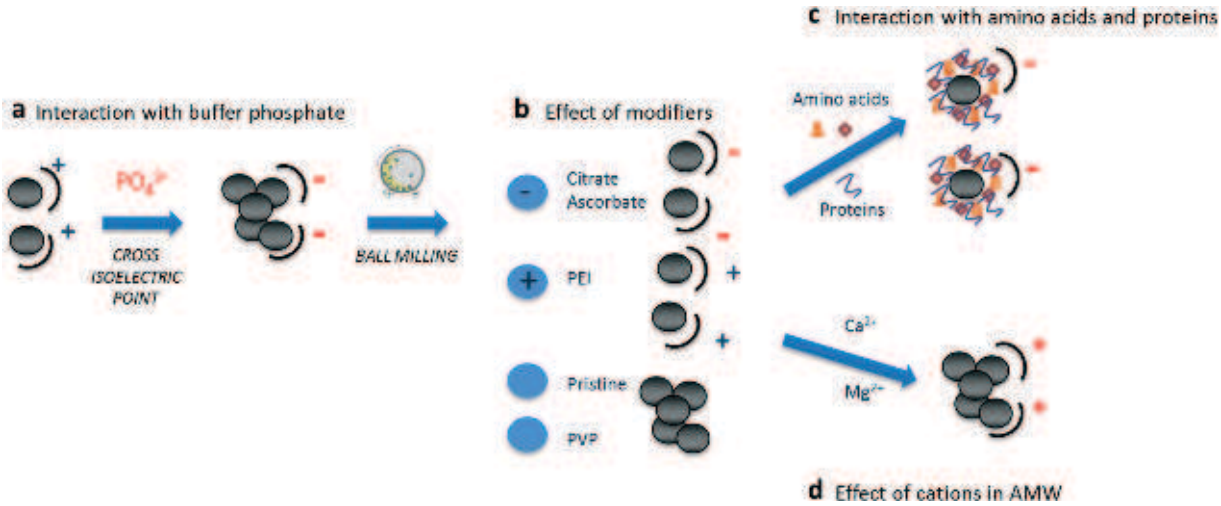

Fig. 3 Hypothetical scheme of the interactions between CuO NPs and different coatings.

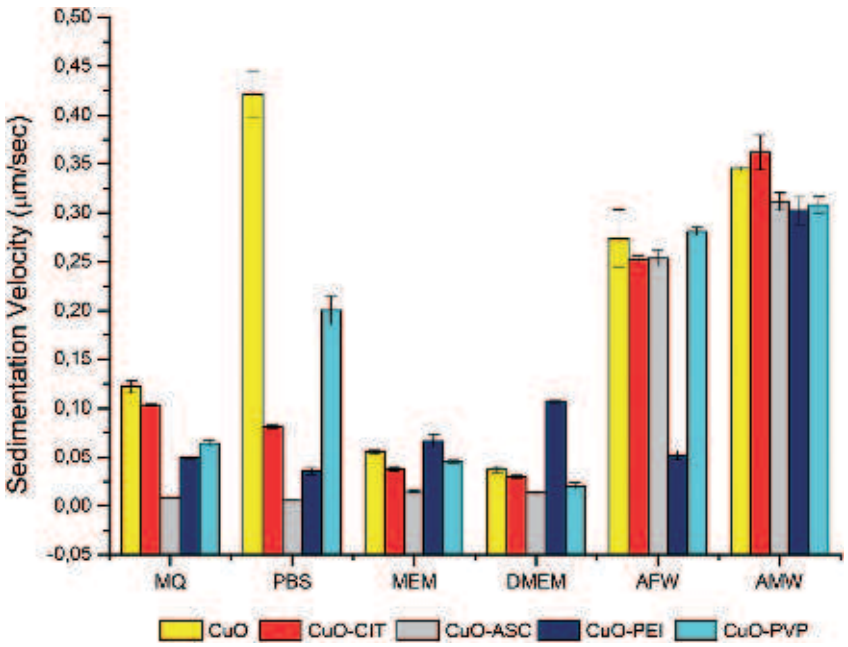

Fig. 4 Average sedimentation velocity data for pristine and modified CuO NPs dispersed in Milli-Q, PBS, MEM, DMEM, AFW and AMW.

Knowledge of the degree of dispersion (spread), the skewness in the data and the outliers allow the obtainment of more accurate information on the colloidal stability of the different dispersions with respect to the DLS data previously obtained. For example, CuO-ASC, despite the high hydrodynamic diameter detected by DLS in PBS, shows a very narrow distribution of data (due to the homogeneity of the NPs) and in general the best suspension stability in all the media analyzed. Finally, NPs dispersed in environmental media fit the same ranking determined by DLS. An increase in instability was shown for all the samples in both AFW and AMW, except for CuO-PEI, which showed higher stability in AFW in agreement with hydrodynamic size and ζ-pot values (see Tables 1 and 2).

Ion release data, determined using the dissolved ionic copper to total copper ratio obtained by means of ultracentrifugation followed by ICP-OES analysis, are presented in Table 3. As can be observed from the data collected in MEM and DMEM, the dissolution greatly increased in both biological media compared to values in Milli-Q, PBS, AFW and AMW media. Taking into account the dissolution experiments for all the dispersions performed in DMEM, the $Cu_{dissolved}/CuO_{total}$ ratio reached values between 65 and 69% after 24 h. As for the dissolution experiments in MEM, the dissolution grade was slightly lower compared with that in DMEM, ranging from 34 to 59% after 24 h. One of the reasons for the high dissolution of CuO NPs in the biological media can be

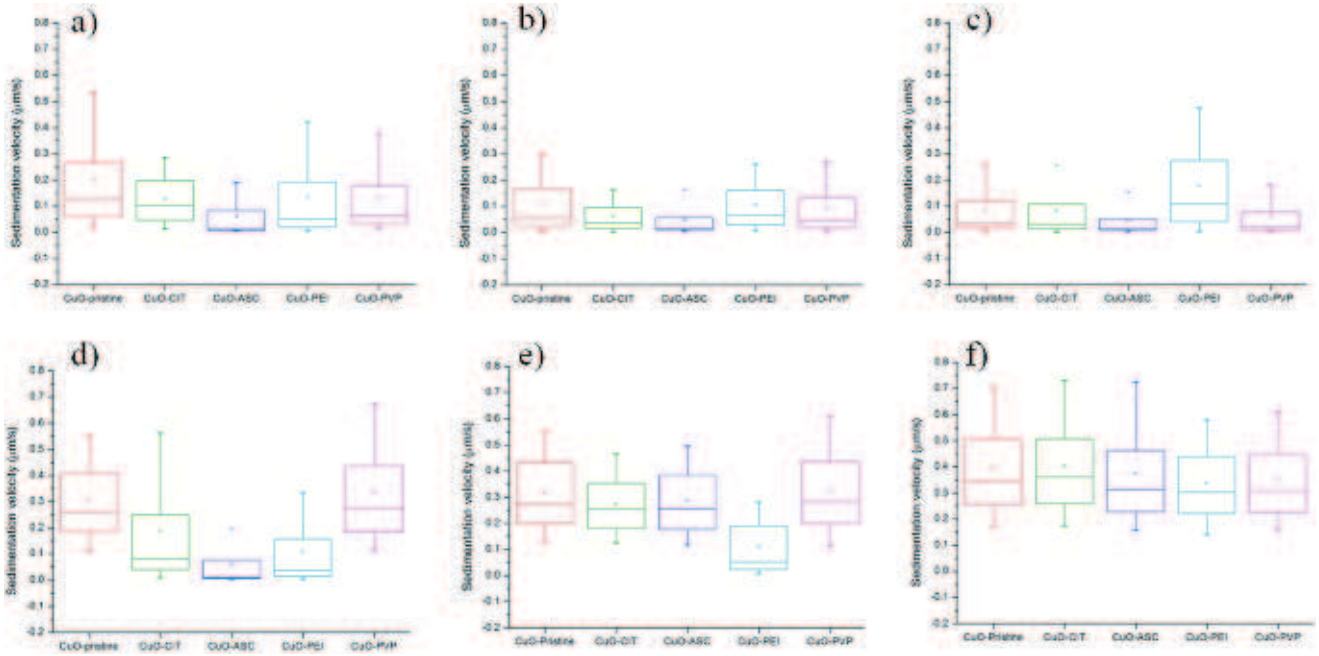

Fig. 5 Sedimentation velocity distribution of pristine and modified CuO NPs dispersed in a) Milli-Q, b) MEM, c) DMEM, d) PBS e) AFW and f) AMW.

Table 3 $Cu_{dissolved}/CuO_{total}$ weight ratio (%) of pristine and modified CuO samples dispersed in different media after 24 h at 25 °C (in Milli-Q, PBS and environmental media) and at 37 °C (in biological media)

	$Cu_{dissolved}/CuO_{total}$ weight ratio (%)					
	Milli-Q (rsd%)	PBS (rsd%)	MEM (rsd%)	DMEM (rsd%)	AFW (rsd%)	AMW (rsd%)
CuO-pristine	0.2 (1.1)	<0.3 (0.1)	60 (0.7)	67 (0.5)	0.3 (5.5)	0.3 (5.8)
CuO-CIT	2 (0.5)	1.8 (0.4)	55 (0.5)	69 (1.0)	2.1 (0.7)	2.4 (0.6)
CuO-ASC	2 (0.5)	<0.3 (0.1)	48 (0.3)	65 (0.4)	0.7 (0.7)	0.7 (1.1)
CuO-PEI	2.8 (0.6)	2.5 (0.6)	34 (0.4)	67 (0.5)	6.3 (0.9)	7.4 (0.5)
CuO-PVP	0.2 (1.0)	<0.3 (0.1)	43 (0.3)	66 (1.3)	0.1 (2.8)	0.1 (1.6)

ascribed to the chelating effect of amino acids and proteins.[42,43] Taking into account the different compositions of the tested media, the generally low CuO NPs solubility rate observed in both Milli-Q and PBS (dissolution below 3%) as well as in AFW and AMW (dissolution below 8%) further confirms the primary role of protein components in promoting dissolution. Among all the media, the extent of CuO NP dissolution was at its highest in DMEM because glucose, amino acids and the vitamin content are approximately fourfold those in MEM.

In the case of the media without amino acids and proteins (Milli-Q, PBS, AFW and AMW), it was observed that the highest dissolution rates were found for the CuO-CIT and CuO-PEI dispersions. This confirms that the particle dissolution behavior depends on the CuO NP characteristics as well as on the chemical composition of the medium surrounding the NPs, unless the features of the medium do not prevail in the complete system.[44] Furthermore, in support of this, size-dependent solubility is shown in the samples dispersed in Milli-Q and PBS. A low aggregation rate corresponds to a high solubility (CuO-CIT and CuO-PEI). On the other hand, samples that were found to be more aggregated (CuO-pristine, CuO-PVP and CuO-ASC) displayed very low values of the $Cu_{dissolved}/CuO_{total}$ weight ratio (%).

4. Conclusions

Four different non-hazardous modifying agents, namely, sodium citrate (CIT), sodium ascorbate (ASC), polyethylenimine (PEI) and polyvinylpyrrolidone (PVP), were added to CuO NP suspensions to promote the *in situ* coating of particles within a $S_{by}D$ approach. Comprehensive colloidal characterization was performed to study the evolution of pristine and modified CuO NP properties with increasing complexity of the selected media, from Milli-Q water to biological and environmental fluids. The good agreement among NP size, ζ-pot, sedimentation velocity and dissolution results confirmed that light scattering techniques combined with ICP-OES represent an effective tool for the assessment of NPs' risk-relevant properties, providing useful information for reading-across hazard

and exposure potentials. The overall results clearly show that the four modifying agents strongly affect CuO NP dispersion stability only in media with ionic strength <16 mM and in the absence of biological components, *i.e.* Milli-Q, PBS and AFW. However, amino acid- and protein-rich media such as MEM and DMEM, and high-ionic-strength media containing divalent cations from inorganic salts, like AMW, totally control colloidal stability regardless of the coating agent employed.

The obtained results contribute to the understanding of the interactions between NPs and media components such as amino acids, proteins, divalent cations and phosphates. We expect that these results will facilitate the interpretation of (eco)toxicological data and will contribute to our knowledge of key nano-bio/eco interactions and modes of action as the basis to establish criteria and guiding principles for grouping and read-across for the purposes of risk assessment and safer product design.

Acknowledgements

The research leading to these results has received funding from the European Union Seventh Framework Programme [FP7/2007–2013] under EC-GA No.604305 'SUN'.

References

1 D. Hristozov, S. Gottardo, E. Semenzin, A. Oomen, P. Bos, W. Peijnenburg, M. van Tongeren, B. Nowack, N. Hunt, A. Brunelli, J. J. Scott-Fordsmand, L. Tran and A. Marcomini, *Environ. Int.*, 2016, **95**, 36–53.

2 D. Hristozov, S. Gottardo, A. Critto and A. Marcomini, *Nanotoxicology*, 2012, **6**, 880–898.

3 D. Hristozov and I. Malsch, *Sustainability*, 2009, **1**, 1161–1194.

4 G. A. Oomen, A. E. Bleeker, M. P. Bos, F. van Broekhuizen, S. Gottardo, M. Groenewold, D. Hristozov, K. Hund-Rinke, M.-A. Irfan, A. Marcomini, W. J. G. M. Peijnenburg, K. Rasmussen, A. Sánchez Jiménez, J. J. Scott-Fordsmand, M. van Tongeren, K. Wiench, W. Wohlleben and R. Landsiedel, *Int. J. Environ. Res. Public Health*, 2015, **12**, 13415–13434.

5 V. Stone, S. Pozzi-Mucelli, L. Tran, K. Aschberger, S. Sabella, U. Vogel, C. Poland, D. Balharry, T. Fernandes, S. Gottardo, S. Hankin, M. G. J. Hartl, N. Hartmann, D. Hristozov, K. Hund-Rinke, H. Johnston, A. Marcomini, O. Panzer, D. Roncato, A. T. Saber, H. Wallin and J. J. Scott-Fordsmand, *Part. Fibre Toxicol.*, 2014, **11**, 9.

6 I. A. Mudunkotuwa and V. H. Grassian, *Environ. Sci.: Nano*, 2015, **2**, 429–439.

7 S. K. Sohaebuddin, P. T. Thevenot, D. Baker, J. W. Eaton and L. Tang, *Part. Fibre Toxicol.*, 2010, **7**, 22.

8 D. Docter, D. Westmeier, M. Markiewicz, S. Stolte, S. K. Knauer and R. H. Stauber, *Chem. Soc. Rev.*, 2015, **44**, 6094–6121.

9 B. Fadeel and A. E. Garcia-Bennett, *Adv. Drug Delivery Rev.*, 2010, **62**, 362–374.

10 I. Lynch, C. Weiss and E. Valsami-Jones, *Nano Today*, 2014, **9**, 266–270.

11 E. Bergamaschi, F. Murphy, C. A. Poland, M. Mullins, A. L. Costa, E. McAlea, L. Tran and S. A. M. Tofail, *WIREs Nanomedicine and Nanobiotechnology*, 2015, **7**, 839–855.

12 Z. J. Deng, M. Liang, M. Monteiro, I. Toth and R. F. Minchin, *Nat. Nanotechnol.*, 2011, **6**, 39–44.

13 Macromolecular Coronas and Their Importance in Nanotoxicology and Nanoecotoxicology, in *Frontiers of Nanoscience*, ed. I. Lynch, K. A. Dawson, J. R. Lead and E. Valsami-Jones, Elsevier, 2014, pp. 127–156.

14 T. L. Moore, L. Rodriguez-Lorenzo, V. Hirsch, S. Balog, D. Urban, C. Jud, B. Rothen-Rutishauser, M. Lattuada and A. Petri-Fink, *Chem. Soc. Rev.*, 2015, **44**, 6287–6305.

15 B. Nowack, J. F. Ranville, S. Diamond, J. A. Gallego-Urrea, C. Metcalfe, J. Rose, N. Horne, A. A. Koelmans and S. J. Klaine, *Environ. Toxicol. Chem.*, 2012, **31**, 50–59.

16 E. Asmatulu, J. Twomey and M. Overcash, *J. Nanopart. Res.*, 2012, **14**, 1–8.

17 T. Meiβner, K. Oelschlägel and A. Potthoff, *Int. Nano Lett.*, 2014, **4**, 116.

18 G. Ren, D. Hu, E. W. C. Cheng, M. A. Vargas-Reus, P. Reip and R. P. Allaker, *Int. J. Antimicrob. Agents*, 2009, **33**, 587–590.

19 O. Rubilar, M. Rai, G. Tortella, M. C. Diez, A. B. Seabra and N. Durán, *Biotechnol. Lett.*, 2013, **35**, 1365–1375.

20 S. Nations, M. Long, M. Wages, J. D. Maul, C. W. Theodorakis and G. P. Cobb, *Chemosphere*, 2015, **135**, 166–174.

21 P. Cronholm, H. L. Karlsson, J. Hedberg, T. A. Lowe, L. Winnberg, K. Elihn, I. Odnevall Wallinder and L. Möller, *Small*, 2013, **9**, 970–982.

22 A. Thit, H. Selck and H. F. Bjerregaard, *Toxicol. In Vitro*, 2015, **29**, 1053–1059.

23 S. Ortelli and A. L. Costa, Nanoencapsulation techniques as a "safer by (molecular) design" tool, *Nano-Struct. Nano-Objects*, 2016, DOI: 10.1016/j.nanoso.2016.03.006.

24 S. Ortelli, C. A. Poland, G. Baldi and A. L. Costa, *Environ. Sci.: Nano*, 2016, **3**, 602–610.

25 D. Gardini, M. Blosi, C. Delpivo, S. Ortelli and A. L. Costa, *J. Phys.: Conf. Ser.*, 2013, **429**, 012052.

26 B. Sun, S. Pokhrel, D. R. Dunphy, H. Zhang, Z. Ji, X. Wang, M. Wang, Y.-P. Liao, C. Hyun Chang, J. Dong, R. Li, L. Mädler, C. Jeffrey Brinker, A. E. Nel and T. Xia, *ACS Nano*, 2015, **9**, 9357–9372.

27 R. A. Petros and J. M. DeSimone, *Nat. Rev. Drug Discovery*, 2010, **9**, 615–627.

28 OECD Guidelines for Testing of Chemicals No. 203. Fish, Acute Toxicity Test (Annex 2 Composition of the recommended reconstituted water), 1992.

29 ASTM D1141-98, Standard Practice for the Preparation of Substitute Ocean Water, Re-approved 2003.

30 P. Wick, P. Manser, L. K. Limbach, U. Dettlaff-Weglikowska, F. Krumeich, S. Roth, W. J. Stark and A. Bruinink, *Toxicol. Lett.*, 2007, **168**, 121–131.

31 P. Rivera-Gil, D. Jimenez de Aberasturi, V. Wulf, B. Pelaz, P. del Pino, Y. Zhao, J. M. de la Fuente, I. Ruiz de Larramendi, T. Rojo, X. J. Liang and W. J. Parak, *Acc. Chem. Res.*, 2013, **46**, 743–749.
32 C. M. Goodman, C. D. McCusker, T. Yilmaz and V. M. Rotello, *Bioconjugate Chem.*, 2004, **15**, 897–900.
33 G. Roebben, S. Ramirez-Garcia, V. A. Hackley, M. Roesslein, F. Klaessig, V. Kestens, I. Lynch, C. M. Garner, A. Rawle, A. Elder, V. L. Colvin, W. Kreyling, H. F. Krug, Z. A. Lewicka, S. McNeil, A. Nel, A. Patri, P. Wick, M. Wiesner, T. Xia, G. Oberdörster and K. A. Dawson, *J. Nanopart. Res.*, 2011, **13**, 2675–2687.
34 N. L. McFarlane, N. J. Wagner, E. W. Kaler and M. L. Lynch, *Langmuir*, 2010, **26**, 13823–13830.
35 X. Liua and K. L. Chen, *Environ. Sci.: Nano*, 2016, **3**, 146–156.
36 I. Karimi, B. Hashemi, M. Javidi and S. N. Azadani, *Surf. Eng.*, 2012, **28**, 737–742.
37 T. Xia, M. Kovochich, M. Liong, J. I. Zink and A. E. Nel, *ACS Nano*, 2007, **2**, 85–96.
38 G. I. Guerrero-García, E. Gonzalez-Tovar and M. Olvera de la Cruz, *Soft Matter*, 2010, **6**, 2056–2065.
39 H. L. Karlsson, P. Cronholm, Y. Hedberg, M. Tornberg, L. De Battice, S. Svedhem and I. O. Wallinder, *Toxicology*, 2013, **313**, 59–69.
40 Z. X. Ji, X. Jin, S. George, T. A. Xia, H. A. Meng, X. Wang, E. Suarez, H. Y. Zhang, E. M. V. Hoek, H. Godwin, A. E. Nel and J. I. Zink, *Environ. Sci. Technol.*, 2010, **44**, 7309–7314.
41 F. Catalano, L. Accomasso, G. Alberto, C. Gallina, S. Raimondo, S. Geuna, C. Giachino and G. Martra, *Small*, 2015, **11**, 2919–2928.
42 K. Midander, P. Cronholm, H. L. Karlsson, K. Elihn, L. Möller, C. Leygraf and I. Odnevall Wallinder, *Small*, 2009, **5**, 389–399.
43 A. Semisch, J. Ohle, B. Witt and A. Hartwig, *Part. Fibre Toxicol.*, 2014, **11**, 10.
44 P. Cronholm, H. L. Karlsson, J. Hedberg, T. A. Lowe, L. Winnberg, K. Elihn, I. Odnevall Wallinder and L. Möller, *Small*, 2013, **9**, 970–982.

ANNEX II

Toxicity of Copper Oxide and Basic Carbonate Nanoparticles after short-term oral exposure in rats

TOXICITY OF COPPER OXIDE AND BASIC COPPER CARBONATE NANOPARTICLES AFTER SHORT-TERM ORAL EXPOSURE IN RATS

Wim H. De Jong[1a], Eveline De Rijk[2], Alessandro Bonetto[3], Wendel Wohlleben[4], Vicki Stone[5], Andrea Brunelli[3], Elena Badetti[3], Antonio Marcomini[3], Ilse Gosens[1], Flemming R. Cassee[1,6]

(1) National Institute for Public Health and the Environment (RIVM), Bilthoven, Netherlands.
(2) Charles River Laboratories, Den Bosch, Netherlands.
(3) DAIS - Dept. of Environmental Sciences, Informatics and Statistics, University Ca' Foscari of Venice, Venice, Italy.
(4) BASF SE, Dept. of Material Physics and Dept. of Experimental Toxicology, Ludwigshafen am Rhein, Germany.
(5) Institute of Biological Chemistry, Biophysics and Bioengineering, School of Engineering and Physical Sciences, Heriot-Watt University, Edinburgh, UK.
(6) Institute for Risk Assessment Studies, Utrecht University, Utrecht, Netherlands.

a) Corresponding author: Tel: +31 30 2742311; E-mail: wim.de.jong@rivm.nl

KEYWORDS:

Benchmark dose modelling; copper oxide nanoparticles; copper carbonate nanoparticles; oral toxicity, dissolution and transformation

Abstract

Copper oxide nanoparticles (CuO NPs) and copper carbonate nanoparticles ($Cu_2CO_3(OH)_2$ NPs) have applications as antimicrobial agents and wood preservatives, with possible oral ingestion via hand to mouth transfer. For both Cu-nanoparticles a short-term oral toxicity study was conducted in rats by oral gavage for five consecutive days followed by autopsy on day 1 and day 21 after the last oral administration. For CuO NPs doses ranging from 1 to 512 mg/kg body weight were administered, and indications of toxicity were observed including increased (at the 512 mg/kg b.w. dose) white blood cell (WBC) and red blood cell (RBC) parameters, and clinical chemistry markers indicative of liver damage (increased alanine aminotransferase (ALT) and lactate dehydrogenase (LDH)). Histopathology revealed alterations in bone marrow, stomach and liver consisting of inflammation, ulceration and degeneration.

$Cu_2CO_3(OH)_2$ NPs, administered in doses ranging from 4 to 128 mg/kg body weight, induced an increase in WBCs indicating some inflammatory response, whereas clinical chemistry parameters (increase in AST, ALT) indicated liver damage. Histopathology occurred at low doses in the stomach and liver and at high doses in liver, stomach, intestines, spleen, thymus, kidneys, and bone marrow. In spleen and thymus lymphoid depletion was noted that warrants further immunotoxicological evaluation. Dissolution and transformation studies in stomach and intestinal simulant fluids indicate partial dissolution of the NPs in the stomach followed by shrinking of the primary particles and agglomeration to large structures under intestinal conditions, but the NPs eventually dissolve completely. So, both copper ions and the particulate nanoforms should be considered as cause for the observed toxicity.

Regarding organ damage for $Cu_2CO_3(OH)_2$ NPs more severe histopathology was observed compared to CuO NPs administration. For risk assessment the bench mark dose (BMD) with a 5% deviation of the vehicle control, is surprisingly similar for the serum liver enzyme AST as indication for liver toxicity, being 26.2 mg/kg for CuO NPs and 30.8 mg/kg for $Cu_2CO_3(OH)_2$ NPs, respectively.

Introduction

Materials such as wood need to be protected against degradation induced by fungi, bacteria and insects in order to prolong their use duration. Copper (Cu) is the most widely used fungicide for treating wood in contact with the soil, with no satisfactory alternative available since it is the only biocide that shows significant effects against soft rot fungi and other soil borne fungi. Cu is compulsory for in-ground timber structures (use class 4 i.e. timber treated to make it suitable to be used in direct soil or water contact) and is a preferred antimicrobial wood preservative due to its minimal effect on mammals, including humans even if it shows a relatively high toxicity against aquatic communities (Freeman et al. 2008; Lebow et al. 2005). Application occurs via impregnation techniques under high pressure and via non-pressure techniques like brushing, spraying and coat-cutting (Lebow et al. 2005). Solid copper carbonate ($Cu_2CO_3(OH)_2$) needs to be micronized by milling to generate particle sizes able to penetrate depths in the order of centimetres into the wood during pressure treatment. The resulting size distributions of micronized copper formulations contain a considerable fraction of nanoparticles. Woods impregnated with micronized Cu release any other Cu species than ions. At equal Cu loading per cubic meter of wood, form and rate of release are comparable to wood impregnated with molecular Cu−amine but slightly more stable throughout aging; this finding was attributed to the transformations during the wood use (Pantano et al. 2018). In comparison to solutions of aqueous copper amine (ACA) treated woods, the micronized copper treated woods feature a lower corrosive potential, a natural wood colour, and at least the same effectiveness of protection against fungal decomposition (Lebow et al. 2005; Freeman et al. 2008; Cookson et al. 2010; Akhtari et al. 2013; Platten et al. 2014;). However, the use of nanoparticle-containing copper formulations has led to concerns regarding their safety in general (Clausen 2007; Evans et al. 2008, Kartal et al. 2009; Civardi et al. 2016) and specifically by hand-to-mouth transfer during installation or use of wooden installations.(Platten et al. 2016). To the best of our knowledge, there are no publication on oral toxicity of micronized $Cu_2CO_3(OH)_2$, whereas the oral toxicity of Cu ions is extremely well known with an acceptable drinking water standard of 1.3 mg/L (ATSDR, 2013). Potential transformation between particulate and ionic forms of copper is likely, because leaching studies indicated that the very acidic stomach fluids extract exclusively Cu ions from wood treated with micronized copper (Wang et al. 2013; Santiago-Rodríguez et al. 2015) .

Results from *in vivo* studies indicate that lung inflammation / toxicity after inhalation of copper oxide nanoparticles (CuO NPs) resolved over 3 weeks (Gosens et al. 2016) indicating a rapid recovery and very little if any Cu was left in the body of these animals. In addition, systemic organ toxicity was observed after repeated intraperitoneal administration of copper oxide nanoparticles (Privalova et al. 2014). For copper nanoparticles *in vivo* toxicity was reported in mice and rats after oral administration (Chen et al. 2006; Lei et al. 2008; Sarkar et al. 2011; Liao and Liu. 2012) .

The aim of this study was to compare the toxicity of CuO NPs and $Cu_2CO_3(OH)_2$ NPs following short term repeated oral exposure and to determine the low end of the Bench Mark Dose (BMDlow) for this short term exposure duration.

Materials and Methods

Test material.

CuO nanoparticles (CuO-NPs) were obtained as a black powder from PlasmaChem, GmbH (Berlin, Germany). The crystalline material exhibited a size of 15-20 nm, a specific surface area of 47 m^2/g as assessed by the Brunauer–Emmett–Teller (BET) method and a density of 6.3 g/cm^3 according to the manufacturer's datasheet. The particles were crystalline with a density little below bulk (6.3 g/cm^3). An extensive characterization is presented in Pantano et al (2018). $Cu_2CO_3(OH)_2$ NPs were obtained as an aqueous dispersion from BASF SE, identification number LP 17206 (30% Cu), lot nr VM3041, best before date 05.02.2017. Figure 1a-b show a representative example of CuO nanoparticles in water (Gosens et al. 2016) and Cu_2CO_3(OH)2 NPs in water .

CuO NP and $Cu_2CO_3(OH)_2$ NP dispersions

CuO NP powder and $Cu_2CO_3(OH)_2$ NP suspensions were dispersed (CuO NP) or further diluted ($Cu_2CO_3(OH)_2$ NP) in Milli-Q water before sonication for 16 minutes in a waterbath (Elmasonic S100) at room temperature to optimize dispersion quality. Before each administration the nanoparticle dispersion was evaluated by CPS Disc Centrifuge™ (CPS Instruments Europe, Oosterhout, The Netherlands) to determine nanoparticle size and size distribution. Both the CuO NP and the $Cu_2CO_3(OH)_2$ NP dispersions remained stable up to 24 and 72 hours, respectively, after preparation of the dispersion. Representative results are presented in Supplementary Figure 1.

Dissolution of CuO NP and $Cu_2CO_3(OH)_2$ NP

A dynamic flow-through system (Wohlleben et al. 2017) was used to determine the dissolution rate of both CuO NP and $Cu_2CO_3(OH)_2$ NP far from equilibrium. The solid mass of 1mg of Cu (that is 1.25 mg of CuO powder or 3.47 mg of the $Cu_2CO_3(OH)_2$ suspension), was weighed onto a membrane (cellulose triacetate, Sartorius Stedim Biotech GmbH, Goettingen, Germany: 47 mm diameter, 5 kDa pore size), topped by another identical membrane, and enclosed in flow-through cells. Two complex buffers with standardized composition were used to mimic the stomach and intestine conditions at 37 ± 0.5 °C, all values in mM: (Marques et al. 2011). For the stomach conditions, the buffer was pH 1.6 and consisted of: sodium taurocholate 0.08 mM; lecithin 0.02 µM; pepsin 0.1 mg/mL and sodium chloride 34.2 mM. For the intestine conditions, the buffer was pH 5.8 and consisted of Fed-State Simulated Intestinal Fluid (FeSSIF) (Jantratid et al. 2008): Sodium taurocholate 10 mM, lecithin 2 mM, maleic acid 55.02 mM, sodium hydroxide 81.65 mM, sodium chloride 125.5 mM, glyceryl monocholate 5 mM and sodium oleate 0.8 mM.

The eluates were determined by inductively coupled plasma-optical emission spectrometry (ICP-OES, Agilent 5100). After the experiment the remaining solids were rinsed off the membrane by particle-free water (Milli-Q). The resulting suspension was then pelleted onto a TEM grid held at the bottom of a centrifuge vial within 1h, then dried, so that the remaining solids morphology could be inspected without interference from drying artifacts of bile salts, which are removed by this preparation. The remaining solids were analyzed by 200 keV bright-field TEM (Tecnai G2-F20ST or Tecnai Osiris, FEI Company, Hillsboro, USA).

Experimental design.

Male specific pathogen free rats (RjHan:WI,) aged 8-9 weeks were obtained from Janvier Labs (Le Genest-Saint-Isle, Saint Berthevin , France). The animals were treated via oral gavage for 5 days (days 1 to 5). The NPs were administered by oral gavage using a bulb tipped gavage needle attached to a syringe. Each treatment was administered as 0.1 mL per 20 g (1 mL per 200 g). For both CuO NPs and $Cu_2CO_3(OH)_2$ NPs, each dose group consisted of 8 animals of which 4 were sacrificed at day 6 (1 day after the last treatment) and 4 were sacrificed at

day 26 (21 days after the last treatment). The day 26 time point was included in order to evaluate recovery, possible persistence of effects or progression of effects induced by the NPs. See Supplementary Table 1 for the experimental design of the study.

Assuming that the CuO NPs would be largely dissolved in the acid environment of the stomach a starting dose of CuO NPs was selected based on the literature for dissolved $CuSO_4$. The no-observed-adverse-effect-level (NOAEL) for $CuSO_4$ was reported to be 16.3 mg/kg b.w. (ECHA 2008). A pilot study was conducted with 2 animals with a dose of 64 mg/kg b.w. (day 1-5 daily). Based upon observations from the pilot study, the doses administered in the subsequent study were: vehicle control, 1, 2, 4, 8, 16, and 32 mg/kg b.w. CuO NPs. These doses were selected to be below and above the reported NOAEL for $CuSO_4$ (Hébert 1993). In an additional study one group of animals (n=4) was treated with a high dose of 512 mg/kg b.w.

For $Cu_2CO_3(OH)_2$ NPs a pilot study according to OECD TG 425 was performed to determine the starting dose in the 5 days oral gavage toxicity study (OECD 2008). One animal was treated orally with a single dose of $Cu_2CO_3(OH)_2$-NP. If no toxicity was observed the dose was increased in the next animal until a toxic response was noted. When a single animal showed a toxic response an additional 4 animals were administered with the same dose. The highest dose chosen for $Cu_2CO_3(OH)_2$ NP was 128 mg/kg b.w. $Cu_2CO_3(OH)_2$ NPs were administered via gavage in the 5 days oral study as vehicle control, 4, 8, 16, 32, 64 and 128 mg/kg b.w.

Histopathology

At day 6 and day 26 animals were killed by exsanguination from the abdominal aorta during anaesthesia by isoflurane (3.5% in oxygen) inhalation. General macroscopic post mortem examinations were performed on all animals. At the time of necropsy, the following tissues and organs were collected and fixed in 4% neutral buffered formaldehyde (10% formalin): heart, lung, thymus, liver, spleen, kidney, testes, brain, mesenteric lymph node, adrenal glands, pancreas, prostate, seminal vesicles, epididymis, thyroid gland, skeletal muscle - quadriceps, stomach, duodenum, jejunum, ileum, Peyer's patches, cecum, colon, rectum, skin, popliteal lymph node, femur with bone marrow, and peripheral nerve.

Microscopic examination of routinely prepared hematoxylin-eosin stained paraffin sections was performed on heart, lungs, thymus, stomach, duodenum, jejunum, ileum, Peyer's patches, cecum, colon, rectum, liver, spleen, mesenteric lymph nodes, kidneys, adrenal glands, brain, testis (unilateral), and femur with bone marrow. Microscopy was performed on all control groups and 32, 64 and 512 mg/kg b.w. CuO NPs treated animals and for 64 and 128 mg/kg b.w. $Cu_2CO_3(OH)_2$ NPs treated animals.

The animal data and macroscopic findings were manually entered into the computer system PathData®. Histopathological changes of examined sections were described according to distribution, severity and morphological character. Severity scores for histopathology were assigned as follows:

Present, Finding present, grading not scored; Grade 1, Minimal/very few/very small size; Grade 2, Slight/few/small size; Grade 3, Moderate/moderate number/moderate size; Grade 4, Marked/many/large size; Grade 5, Massive/extensive number/extensive size; N.A.D. No Abnormality Detected.

Haematology

On day 6 and day 26 blood was collected in EDTA-coated tubes. Haematological parameters included WBC count, RBC count, haemoglobin (Hb), heaematocrit (Ht), mean corpuscular volume (MCV), mean corpuscular haemoglobin (MCHC), and platelet (PLT) count. All haematology parameters in the blood samples were determined in an Advia 120 Hematology Analyzer (Siemens Health Care, Germany) according to the

manufacturer's instructions. In addition, blood smears were prepared for visual evaluation depending on the results obtained with the haematology analyser.

Bone marrow

Bone marrow cells were collected by flushing 4 ml Impuls Cytometer Fluid through the left femur. The concentration of nucleated cells was determined in a Coulter Counter.

Clinical chemistry

After collection of blood serum and storage at -20 ^{o}C the following parameters were determined: albumin (ALB), alkaline phosphatase (ALP), alanine aminotransferase (ALT), aspartate aminotransferase (AST), gamma-glutamyl transpeptidase (GGT), amylase (AMY), creatinin kinase (CK), lactate dehydrogenase (LDH), sodium (Na), potassium (K), glucose (GLU), urea, creatinin (CRE), cholesterol (CHOL) and total protein (TP). All clinical chemistry parameters in the serum samples were determined in an automatic analyser Unicel DxC 800 Synchron Clinical Systems (Beckman Coulter Nederland B.V., Woerden, The Netherlands).

Cu determination in organs

The acid mixture used for organ sample digestion included HNO_3 (trace select ultra 69%, Sigma-Aldrich <0.5µg/Kg), and H_2O_2 (trace select ultra 30%, Sigma-Aldrich <0.05µg/Kg), in a 2:1 ratio. The microwave system ETHOS 1600 (Milestone S.r.l., Sorisole, Italy) was used to digest the samples, following a dedicated heating program (1 minute 250 watt, 1 minute 0 Watt, 5 minutes 250 Watt, 3 minutes 400 Watt, and 3 minutes 600 Watt). Afterwards, the samples were allowed to cool down for 30 minutes at room temperature. The obtained solutions were transferred in PTFE tubes and diluted to 25 mL with MilliQ water. For determination of the Cu content an aliquot of each sample solution was properly diluted and analyzed by inductively coupled plasma mass spectrometry equipped with single channel Universal Cell (sp-ICP-MS NexION 350XXD, Perkin Elmer). Isotope ^{65}Cu was selected to quantify Cu because of the less polyatomic interferences (e.g. ^{40}Ar^{23}Na) than isotope ^{63}Cu. Moreover, to decrease interferences Kinetic energy discrimination (KED) was employed, using He as collision gas. Samples were quantified by external calibration method using a multi-point curve (blank and 10 points over the concentration range from 0.5 µg/L to 5000 µg/L). Yttrium at 5 µg/L was used as internal standard.

Potential contamination from the laboratory was controlled by adding at least one reagent blank during each digestion session. The limit of detection (LOD) and the limit of quantification (LOQ) were calculated for each sample, set as the average of blanks + 3 standard deviation (SD) and as the average of blanks + 10 SD, respectively. In order to verify the accuracy and repeatability of the method, 6 aliquots of the standard reference material (SRM) bovine liver (NIST 1577c, National Institute of Standards and Technology, Gaithersburg, Maryland, USA) were analysed every 10 samples. The average Cu concentration detected in the SRM was 277 ± 5 mg/kg, in satisfactory agreement with the reference value (262 ± 2 mg/kg). Average blank values, LOD and LOQ were calculated by considering both the reagent and the control blanks. Detected LOD and LOQ value were 20 ng/L and 68 ng/L, respectively. Copper concentration in tissues and organs from rats exposed to CuO NPs and $Cu_2CO_3(OH)_2$ NPs, are expressed on a dry weight basis,

Statistical analysis

Effects of the CuO NPs and $Cu_2CO_3(OH)_2$ NPs on various parameters in the orally exposed animals were initially compared with vehicle control animals using ANVOA for dose-response evaluation and a one sided Student's T-test for group differences. Further dose response analysis was performed with Bench Mark Dose

(BMD) evaluation using PROAST (version 60.1, www.rivm.nl/proast). Dose–response models were fitted to the data and a benchmark response (BMR) was defined. The 90%-confidence interval was derived from the fitted model as previously described (De Jong et al., 2013, Gosens et al., 2015), resulting in a lower and upper limit (BMDlow at 5% and BMDhigh at 95%, respectively) of the associated benchmark dose. The BMR or critical effect size (CES) for general and specific toxicity endpoints was chosen at 5% deviation of the control values, In this study consensus default BMR values were used as proposed by the European Food Safety Authority (EFSA 2009).

Results

Particle Dissolution and Transformation

CuO NP and $Cu_2CO_3(OH)_2$ NP dissolve completely under stomach conditions at pH1.6 within 72h (Figure 2). During that time, the ion-resolved dissolution rate was very similar for both materials with 50% dissolved after about 16h for both materials. As this time is longer than the residence time in the stomach, we tested independently the dissolution under pH5.8 intestine conditions. Here we observed that the dissolution is incomplete, although transformation of the particles is clearly observed in the TEM (Figure 1f): the primary particles shrink, but agglomerate at the same time to large structures. The time to 50% dissolution is 20h for micronized copper carbonate ($Cu_2CO_3(OH)_2$ NPs) but 50h for CuO NPs. Adding to this interesting difference, we observed that dissolution occurs at much lower rates in the simple GI-tract simulant medium with the $NaNO_3$ buffer at pH5.3 compared to the complex GI-tract simulant FeSSIF-V2 (pH 5.8) . Thus, the dissolution in the intestine is not only pH driven but is likely to be accelerated by the bile salts and other physiological substances, in complete analogy to the interactions observed under environmental dissolution and transformation of Cu NPs (Adeley et al. 2014; Keller et al. 2017). The dissolution kinetics of the NPs in stomach fluid simulant is presented in Figure 2. Dissolution in gastro-intestinal fluid simulant and simple medium is shown in Supplementary Figures 2 and 3. Transformation of the CuO NP and $Cu_2CO_3(OH)_2$ NP is shown in Figure 1.

General observations

CuO NP: During the study no signs of toxicity were noted and there were no premature deaths in the study. There was no reduction in body and organ weights for CuO NPs treated animals (Supplementary Tables 2A and 2B). No treatment related findings were observed at the macroscopic observation at autopsy. Due to the lack of effects observed at doses up to 32 mg/kg b.w. also a high dose of 512 mg/kg b.w. was tested. The 512 mg/kg b.w. dose induced slight weight loss in one animal after two days of treatment and diarrhoea after three administrations. After four administrations two animals showed diarrhoea.

$Cu_2CO_3(OH)_2$ NP: Repeated oral administration of a dose of 128 mg/kg b.w. $Cu_2CO_3(OH)_2$ NPs induced severe toxic responses in the animals as indicated by the behaviour of the animals, including frequent washing and piloerection. Therefore, the animals scheduled for autopsy after a recovery period at day 21 after treatment were autopsied prematurely at days 6 and 7, respectively 24h and 48h after the last (day 5) treatment. A decrease in organ weight was observed for heart, liver, spleen, and thymus whereas the adrenal glands showed an increase in weight (Figure 3, Supplementary Table 2C). The most severe decrease in organ weight was noted for the spleen

and thymus, respectively with approximately 45% and 70%. For doses up to 64 mg/kg b.w. body and organ weight determined at day 26 after a three week recovery period showed no changes compared to the vehicle treated animals (Supplementary Table 2D).

Haematology and Clinical chemistry

CuO NP: Haematology: An overview of haematological parameters as determined on day 6 that were affected by the 5 day oral administration of CuO NPs nanoparticles is presented in Figure 4, whereas the extended set of haematology parameters are presented in Supplementary Table 3A. At day 6 one day after the five day treatment the total WBC count was decreased at doses of 32 and 64 mg/kg b.w. whereas in increase was present at the dose of 512 mg/kg b.w. (Figure 4). In addition, in the animals treated with 64 mg/kg b.w. CuO NPs some red blood cell parameters (number of red blood cells, haemoglobin content, and haematocrit) were decreased. At day 21 after the five day treatment (day 26) all white and red blood cell parameters were similar to control vehicle treated animals for the doses evaluated up to 32 mg/kg b.w. (Supplementary Table 3B).

At day 6, one day after the five day treatment with CuO NPs there was no treatment related effect in the cellularity of the bone marrow (Supplementary Table 4).

CuO NP: Clinical chemistry: At day 6 alterations in the level of alkaline phosphatase (ALP) and aspartate aminotransferase (AST) enzymes indicated the presence of liver toxicity (Figure 5). At the highest dose of 512 mg/kg b.w. lactate dehydrogenase (LDH) levels were also increased indicating cell and organ damage. All clinical chemistry data are presented in Supplementary Table 5A. At day 26 only the ALP was significantly ($p<0.05$) decreased at the 2 mg/kg b.w. dose (Supplementary Table 5B). Animals treated with 512 mg/kg showed similar alterations in clinical chemistry (low level of alkaline phosphatase, high level of AST and high level of LDH thus supporting the data of the dose response study (Supplementary Table 5A). There was no treatment related effect in the cellularity of the bone marrow after treatment with CuO NPs (Supplementary Table 4).

$Cu_2CO_3(OH)_2$ NP: Haematology. Alterations in haematological parameters after five day oral administration of $Cu_2CO_3(OH)_2$-NPs are presented in Figure 6, whereas the extended set of haematology parameters are presented in Supplementary Table 3C and 3D. At day 6 an increase in WBC was present for doses of 64 mg/kg b.w., which increase in WBC was due to an increase in lymphocytes. At 128 mg/kg b.w. the increase in WBC was mainly due to an increase in neutrophilic granulocytes. The decrease in relative number of lymphocytes can be attributed to the increase in neutrophilic granulocytes. The absolute number of lymphocytes was not affected by the $Cu_2CO_3(OH)_2$ NPs treatment at the dose of 128 mg/kg b.w. Data for day 26 are shown in Supplementary Table 3D. At day 26 no alterations in haematological parameters were observed compared to vehicle treated animals for the highest dose investigated (64 mg/kg b.w.).

There was no treatment related effect in the cellularity of the bone marrow after treatment with $Cu_2CO_3(OH)_2$ NP (Supplementary Table 4). However, microscopic evaluation of the bone marrow after treatment with 128 mg/kg b.w. indicated a significant shift from erythroid cells into myeloid cells ($p<0.01$, $P<0.001$) that was confirmed by histopathology (Figure 7, Supplementary Table 4).

$Cu_2CO_3(OH)_2$ NP: Clinical chemistry. For $Cu_2CO_3(OH)_2$ NPs at day 6 ALP was decreased while AST, ALT, and LDH were increased (Figure 8). All clinical chemistry data are presented in Supplementary Tables 5C and

5D. The observed enzyme alterations in the blood indicate both liver and organ toxicity. In addition, free fatty acids, creatinine, iron and potassium levels in blood were increased. At day 26 only some incidental alterations were observed in clinical chemistry parameters and most parameters were back to levels similar to control vehicle treated animals, while those that did show an alteration did not show a dose response effect (Supplementary Table 5).

Histopathology

CuO NP: There were no test item-related microscopic observations in the initial dose response study at the highest dose of 64 mg/kg b.w. of CuO NPs evaluated (data not shown). All of the recorded microscopic findings were within the range of background histopathology encountered in rats of this age and strain. For animals treated with a dose of 512 mg/kg b.w. CuO NPs and evaluated at day 6 alterations were observed in the histopathology of stomach, liver, and bone marrow (Supplementary Table 6). In the stomach an increased incidence and severity of submucosal glandular inflammation with eosinophilic granulocytes was observed. The liver exhibited slight Kupffer cell hypertrophy/hyperplasia, inflammation composed of mixed inflammatory cells, hepatocellular hypertrophy, hepatocellular necrosis and single cell necrosis (above the background level of minimal). Bone marrow changes included slight increased myeloid elements and decreased erythroid elements.

$Cu_2CO_3(OH)_2$ NP: Test item-related microscopic findings were observed in a number of organs examined after treatment with 64 or 128 mg/kg b.w. $Cu_2CO_3(OH)_2$ NPs. An overview of the all data is presented in Supplementary Table 6. After five day oral administration of $Cu_2CO_3(OH)_2$ NPs in the stomach an increased incidence and severity of submucosal glandular inflammation with eosinophilic granulocyteswas observed on day 6 (Figure 9) which was still present in some animals after the 3 week recovery period (Supplementary Table 6). In other parts of the GI-tract effects were only seen at the dose of 128 mg/kg b.w. Ulceration was observed in the cecum, colon and rectum (Supplementary Table 6). Figure 10 shows ulceration of colon after 5 days treatment with 128 mg/kg b.w. $Cu_2CO_3(OH)_2$ NPs. Other lesions observed in the GI-tract were apoptosis (duodenum, ileum and cecum) and edema (colon, rectum).

In the liver inflammation composed of mixed inflammatory cells (Figure 11) occurred at day 6 in rats treated at 64 mg/kg and at 128 mg/kg. In animals treated at 64 mg/kg and 128 mg/kg occurred hepatocellular necrosis, single cell necrosis (Figure 11), increased mitosis, liver and Kupffer cell hypertrophy. In the kidneys at 128 mg/kg dose effects were observed including tubular necrosis, hyaline casts in the tubules, and tubular degeneration/regeneration (Supplementary Table 6).

$Cu_2CO_3(OH)_2$ NPs at 128 mg/kg b.w. induced severe lymphoid atrophy in the spleen (Figure 12) and thymus (Figure 12). In the bone marrow an increase in myeloid activity and decrease in erythroid activity was observed at 128 mg/kg treatment as already indicated by the evaluation of bone marrow cell populations (Figure 7 above, Supplementary Figure 4).

In the testes a moderate degeneration of germ cells (including slight multinucleated giant cells) and marked spermatid retention was observed at 128 mg/kg dose. Also at this dose decreased fluid was observed in the seminal vesicles of 8 out of 8 animals (Supplementary Table 6).

After the recovery period of 21 days at day 26 only in the stomach the submucosal glandular inflammation with eosinophilic granulocytes remained, whereas other histopathological alterations in the other organs were not

observed at the dose of 64 mg/kg b.w., the highest dose investigated after the recovery period (Supplementary Table 6).

Organ burden

CuO NP: At 32 and 64 mg/kg b.w. the liver ($p<0.05$) and at 64 mg/kg b.w. the mesenteric lymph node (MLN) ($p<0.001$) exhibited an increase in Cu content (Table 1A). At day 6 one day after the last administration there is an increase in Cu level only the mesenteric lymph node for the doses of 64 mg/kg b.w., and in the liver for the doses of 32 and 64 mg/kg b.w. The dose of 512 mg/kg b.w. that was not administered in the dose response study but at later in time, shows an increased Cu level in liver, lung, kidney, spleen, thymus and mesenteric lymph node when compared to non-treated control animals of the dose response study. At day 26 the increased levels of Cu in liver and also kidney were returned to levels equivalent to the control animals.

$Cu_2CO_3(OH)_2$ NP: Cu content of tissues after 5 consecutive days of $Cu_2CO_3(OH)_2$ NPs oral administration is presented in Table 1B. At the lower dose investigated (64 mg/kg b.w.) an increase in Cu content was noted in liver, kidney, testes, brain and thymus only. For the highest dose (128 mg/kg b.w.) increases in Cu content were observed in all organs evaluated. At day 26 the increased levels of Cu in liver, thymus and kidney for the dose of 64 mg/kg b.w. were returned to background levels whereas for the liver and testes they were still increased ($p<0.05$ and $p<0.01$, respectively), although the increase was limited compared to day 6.

Dose-response modelling

Tables 2 and 3 show a further statistical evaluation of the outcomes of the oral CuO NPs and $Cu_2CO_3(OH)_2$ NPs studies, respectively, by using the bench mark dose (BMD) approach with a 5% deviation of levels in vehicle control treated animals as bench mark. This analysis shows that for the liver enzyme AST and the red blood cell parameters (RBC, Hb, Ht) an effect could be demonstrated showing a 5% deviation from controls both for CuO NPs and $Cu_2CO_3(OH)_2$ NPs. Histopathology confirmed the liver toxicity at high doses. The complete BMD analysis is presented in Supplementary Table 7 and 8 for CuO NPs and $Cu_2CO_3(OH)_2$ NPs, respectively.

The lowest BMD for an effect of $Cu_2CO_3(OH)_2$ NPs is the effect on the liver enzyme AST with a dose of 30.8 mg/kg directly followed by the effect on liver weight (BMD 32.2 mg/kg b.w.)(Table 3). The accompanying BMDlow being the lower end of the 90% confidence interval that might be used for risk assessment is 18.8 mg/kg for an AST effect and 9.5 mg/kg b.w. for the liver weight effect.

Discussion

We investigated the potential toxicity of two Cu-nanoformulations used for the preservation of wood products in a repeated dose oral toxicity study. Our results show that both CuO NPs and $Cu_2CO_3(OH)_2$ NPs exhibited approximately 50% dissolution at 16 h of incubation in stomach fluid simulant. During flow through conditions, which are more realistic of the strong dilution in the stomach environment, approximately 50% dissolution was reached at 24 h. Emptying of the stomach in rats may be reached within 6h (Qualls-Creekmore et al. 2010), suggesting that part of the oral dose will reach the intestines in particulate nanoform. Imaging of the particles after dissolution under intestinal conditions with a pH5.8 suggested morphological changes such as shrinking

and agglomeration. This data would suggest that it is relevant to consider the possible toxicological effects of both the Cu ions and the nanoparticles. The $Cu_2CO_3(OH)_2$ NPs showed similar dissolution characteristics to CuO NPs in simulated stomach conditions, but $Cu_2CO_3(OH)_2$ NPs dissolved faster in simulated intestine conditions. Based on the dissolution experiments, we speculate that if any particles last the fast and pH-driven dissolution in the stomach passage, they would transform and $Cu_2CO_3(OH)_2$ NPs would shed Cu ions earlier or more during intestine passage than CuO NPs. A more sophisticated protocol would be to use sequential buffers (Bove et al. 2017) and/or simulated full diets (DeLoid et al. 2017). One might even imagine to combine flow-through-testing (for ease of retrieving transformed NPs, for fast time resolution on ions) with sequential buffers (for added physiological realism), but that was beyond scope of the present investigation. Although we tested at low concentration and out of equilibrium, saturation may have suppressed dissolution rates below the *in vivo* rates. Investigating the release of Cu ions from wood treated with $Cu_2CO_3(OH)_2$ NPs, revealed more than 80% dissolution after 1h at room temperature in a simple glycine simulant with pH1.5 (Santiago-Rodríguez et al. 2015), and only slightly longer times were suggested under environmental unsaturated conditions.(Kent and Vikesland 2016; Vencalek et al. 2016). So, the use of Cu-nanomaterial as a wood preservative will result in both human and environmental exposure to Cu ions which can be considered responsible for the induced toxic effects.

In terms of biodistribution, the treatment doses below 512 mg/kg b.w. CuO NPs resulted in a detectable increase in the Cu content of the liver only, while at the high 512 mg/kg b.w. dose increased Cu levels were observed in all evaluated organs (Table 1). The partial dissolution in the stomach might explain why the doses of CuO NPs up to 32 mg/kg b.w. had limited toxic impacts compared to the reported toxicity of soluble Cu formulations such as $CuSO_4$ (NOAEL of 16.3 mg/kg (Hébert 1993)). The high dose of 512 mg/kg b.w. CuO NPs induced histopathological alterations in stomach, liver and bone marrow. These alterations in the liver were accompanied by an increase of liver enzymes (ALT, AST) and WBC in the blood. Also for doses of CuO NPs not showing clear toxicity some alterations were noted for ALP and AST in serum as markers for liver damage. The histopathological observations in animals treated with 512 mg/kg b.w. concur with the clinical chemistry observations. However, such clinical chemistry effects were observed at lower doses (up to 64 mg/kg b.w. CuO NPs) for which histopathological alterations were not evaluated. So, when we consider liver toxicity liver enzyme levels in serum might be used as first indicators for adverse effects of nanomaterials.

The dose response effects for various toxicity indicators were further evaluated by using the BMD approach. The benchmark itself that was used, was a 5% alteration compared to the vehicle control, as suggested by EFSA (EFSA 2009). The BMDlow of 16.1 and 18.8 mg/kg b.w. for serum AST alteration induced by CuO NPs and $Cu_2CO_3(OH)_2$ NPs, respectively, is surprisingly similar to the NOAEL for $CuSO_4$. For $CuSO_4$ the Cu ion is likely the main toxicant. In view of the solubility and dissolution characteristics of Cu nanomaterials also the Cu ion may play an important role for the Cu nanomaterial toxicity. The derived BMD uses as lower end of the confidence interval a 5% deviation from vehicle treated controls that would normally not be detected in an experiment. This might explain why the BMDlow is at the same order of magnitude as the NOAEL of $CuSO_4$.

$Cu_2CO_3(OH)_2$ NPs were more toxic than CuO NPs when compared on the basis of a dose in mg/kg b.w. Animals dosed with 128 mg/kg b.w. showed after five days of repeated dosing overt signs of toxicity leading to a

preliminary removal of the dose group intended for the recovery period from the study. Both haematology and clinical chemistry indicated toxic effects at the 64 and 128 mg/kg b.w. doses. Similar to the high dose CuO NPs clinical chemistry results, the $Cu_2CO_3(OH)_2$ NPs increased levels of AST and ALT indicating liver toxicity, while LDH increases indicated cellular damage in general. Treatment with $Cu_2CO_3(OH)_2$ NP also induced inflammation in the stomach, apoptosis in duodenum, ileum, and cecum, and ulceration in the large intestines (cecum, colon, rectum). In the liver inflammation, apoptosis, necrosis, and hypertrophy as potential repair of the liver damage were observed. In addition kidney degeneration/regeneration and necrosis was observed. There was a marked lymphoid atrophy after the five day oral treatment with $Cu_2CO_3(OH)_2$ NP in spleen and thymus accompanied by an increase in myeloid activity in the bone marrow. In the spleen both T (periarteriolar lymphoid sheat, PALS) and B cell areas (follicles) were affected. After oral $Cu_2CO_3(OH)_2$ NPs treatment increased Cu levels could be detected in almost all organs investigated (liver, lung, kidney, spleen, thymus, mesenteric lymph node, testes, brain). Using a 5% deviation of control animals the lowest realistic BMD of 30.8 mg/kg (BMDlow of 18.8 mg/kg and a BMDhigh of 42.9 mg/kg) was observed for an increase of serum AST. For CuO NPs histopathology was only performed on animals with the high extra dose of 512 mg/kg b.w. In these animals in the stomach, liver and bone marrow similar pathological lesions were observed as for the $Cu_2CO_3(OH)_2$ NPs induced lesions, although lymphoid depletion in spleen and thymus was absent. Overall, the pathology in terms of organ damage in the GI-tract, kidney and the lymphoid organs (spleen, thymus) was more severe for $Cu_2CO_3(OH)_2$ NP compared to CuO NP administration.

Cu accounts for about 80% of the CuO mass, about 60% in $Cu_2CO_3(OH)_2$ and about 40% in $CuSO_4$. Dissolution of the NPs in the stomach environment was about 50%, with a faster rate of Cu ions dissolution from the remaining $Cu_2CO_3(OH)_2$ particles in intestine, whereas for $CuSO_4$ dissolution was complete already in stomach conditions. None of the NPs showed significant transformation to other particulate species, such that a potential toxic effect via newly formed particles is improbable. Based on this mass and solubility data, a certain mass dose for both CuO NPs and $Cu_2CO_3(OH)_2$ NPs would be associated with a similar amount of Cu ion release as that from $CuSO_4$ in the stomach (i.e. about 40% Cu mass for CuO NPs, 30% Cu mass for $Cu_2CO_3(OH)_2$ NPs, and about 40% Cu mass for $CuSO_4$, considering 50% dissolution for CuO NPs and $Cu_2CO_3(OH)_2$ NPs and 100% dissolution for $CuSO_4$). $Cu_2CO_3(OH)_2$ NPs would have higher toxicity via ions originating in the intestine in view of its high dissolution in simulant intestinal fluids.

Privalova et al. (2014) using intraperitoneal administration of CuO NPs (diameter 20 nm) in rats for three times a week applying 19 injections up to a total dose of approximately 10 mg/kg b.w. mainly described induction of kidney lesions. In contrast to that study, we did not observe histopathological lesions in kidney and spleen by CuO NPs but did note lesions in stomach, liver and bone marrow after 5 days repeated oral administration of 512 mg/kg b.w. In view of the very fast dissolution of the CuO NPs used by Privalova et al. (2014) it might be assumed that Cu ions are responsible for the observed toxicity. In this respect our results on $Cu_2CO_3(OH)_2$ NPs show a more widespread organ toxicity including severe cellular depletion of spleen and thymus, and kidney lesions which might be related to the more complete dissolution in the GI-tract and the resulting higher internal Cu ion dose at organ level.

Toxicity of CuO NPs presumably due to the release of Cu ions, was previously demonstrated in *in vitro* cellular toxicity tests for various lung derived cells such as A549 cells, 16-HBE cells,and BEAS-2B cells (Cho et al., 2013, Jing et al., 2015, Strauch et al., 2017, Ude et al. 2017). CuO NPs were found to be more toxic compared to microCuO particles (CuO-MP) and $CuCl_2$ when comparing doses as mass per mL in the cell culture medium (Strauch et al., 2017). The toxic effect was explained by a much higher Cu content in the cell (cellular cytoplasm and nucleus) after exposure to the CuO NPs compared to CuO MP and $CuCl_2$ followed by intracellular Cu ion release. Both for Ag NPs and CuO NPs a higher cellular content of metal (Ag and Cu) ions was observed in A549 and BEAS-2B cells compared with exposure to Ag and Cu ions in the form of $AgNO_3$ or $CuCl_2$, respectively (Cronholm et al., 2013)

Our data also identified that the immune system may also be severely affected by the Cu ions released from the Cu containing nanomaterials as shown by the severe lymphoid cell depletion in spleen and thymus. This may have consequences for the functionality of the immune system as was recently demonstrated by us for silver nanoparticles (De Jong et al. 2013, Vandebriel et al. 2014). In view of the potential high migration to the spleen the immune system maybe a target for nanomaterial toxicity and needs consideration for a more a more specific toxicity evaluation (Dobrovolskaia et al. 2016, Dusinska et al. 2017). So, an evaluation of the immune system function exposed to $Cu_2CO_3(OH)_2$ NPs may be warranted.

In conclusion, we observed a marked difference in the severity of the pathological lesions in various organs (e.g. GI-tract, kidney, spleen, and thymus) between CuO NPs and $Cu_2CO_3(OH)_2$ NPs after oral exposure comparing dose effects in our rat study. For $Cu_2CO_3(OH)_2$ NPs body weight and severe organ weight loss was observed. In spleen and thymus the severe weight loss was accompanied by lymphoid depletion that warrants further immunotoxicological evaluation. However, for risk assessment the BMD with a 5% deviation of the vehicle control, is surprisingly similar for the serum liver enzyme AST as a first indication for liver toxicity, being 26.2 mg/kg for CuO NPs and 30.8 mg/kg for $Cu_2CO_3(OH)_2$ NPs, respectively. These data may be useful for deriving an acceptable daily intake for these toxic wood preservatives which may then be used for a risk assessment including exposure scenarios.

Acknowledgements: We would like to thank P.K. Beekhof, A.J.F Boere, L.J.J. De La Fonteyne , E. Gremmer, K.M.P. Van Den Hurk, A. De Klerk, F. Kolkman, D.L.A.C. Leseman, B. Nagarajah, J.Rigters, C.M.R. Soputan, and H.W. Verharen for valuable technical assistance, and E. Gremmer for help with the BMD analysis.. Kai Werle is acknowledged for performing the dissolution experiments

Declaration of interest

The authors report that they have no conflicts of interest. The authors alone are responsible for the content and writing of the paper. This work was supported by the SUN project, Grant agreement no. 604305, funded by the

EC Seventh Framework Program FP7-NMP.2013.1.3-1 and by the RIVM Strategic Research Program (SPR, E/121504).

References

Adeleye, A.S., J.R. Conway, T. Perez, P. Rutten, and A.A. Keller,2014. 'Influence of Extracellular Polymeric Substances on the Long-Term Fate, Dissolution, and Speciation of Copper-Based Nanoparticles', *Environmental Science & Technology*, 48: 12561-12568.

Akhtari, M., H.R. Taghiyari, and M.G. Kokandeh. 2013. Effect of some metal nanoparticles on the spectroscopy analysis of Paulownia wood exposed to white-rot fungus. *Eur J Wood Prod* 71: 283–285.

Agency for Toxic Substances and Disease Registry (ATSDR) 2013. Toxicological Profile for Copper. 201307/01/2013r, http://www.atsdr.cdc.gov/toxprofiles/tp.asp?id=206&tid=37

Bove, P., M.A. Malvindi, S.S. Kote, R. Bertorelli, M. Summa, S. Sabella. 2017. Dissolution test for risk assessment of nanoparticles: a pilot study. *Nanoscale* 19:6315-6326.

Chen, Z., H. Meng, G. Xing, C. Chen, Y. Zhao, G. Jia, T. Wang, H. Yuan, C. Ye, F. Zhao, Z. Chai, C. Zhu, X. Fang, B. Ma, and L. Wan. 2006. Acute toxicological effects of copper nanoparticles in vivo. *Toxicol Lett* 163:109-120.

Cho, W-S, R. Duffin, M. Bradley, I.L. Megson, W. MacNee, J.K. Lee, J. Jeong, and K. Donaldson. 2013. Predictive value .of in vitro assays depends on the mechanism of toxicity of metal oxide Nanoparticles. *Part Fibre Toxicol* 10:55.

Civardi, C,, L. Schlagenhauf, J.P. Kaiser, C. Hirsch, C. Mucchino, A. Wichser, P. Wick, and F.W. Schwarze. 2016. Release of copper-amended particles from micronized copper-pressure-treated wood during mechanical abrasion. *J Nanobiotechnol* 14:77.

Clausen, C.A. 2007. Nanotechnology: Implications for the wood preservation industry. Report IRG/WP 07-30415.

Cookson, L.J., J.W. Creffield, K.J. McCarthy, and D.K. Scown. 2010. Trials on the Efficacy of Micronized Copper in Australia. *For Prod J* 60: 6–12.

Cronholm, P., H.L. Karlsson, J. Hedberg, T.A. Lowe, L. Winnberg, K. Elihn, I.O. Wallinder, and L. Möller. 2013.
Intracellular uptake and toxicity of Ag and CuO nanoparticles: a comparison between nanoparticles and their corresponding metal ions. *Small* 9: 970-982.

De Jong, W.H., L.T. Van Der Ven, A. Sleijffers, M.V.D.Z. Park, E.H.Jansen, H. Van Loveren, and R.J. Vandebriel. 2013. Systemic and immunotoxicity of silver nanoparticles in an intravenous 28 days repeated dose toxicity study in rats. *Biomaterials* 34: 8333-8343.

DeLoid, G.M., Y. Wang, K. Kapronezai, L.R. Lorente, R. Zhang, G. Pyrgiotakis, N.V. Konduru, M. Ericsson, J.C. White, R. De La Torre-Roche, H. Xiao, D.J. McClements, and P. Demokritou. 2017. An integrated methodology for assessing the impact of food matrix and gastrointestinal effects on the biokinetics and cellular toxicity of ingested engineered nanomaterials, *Part Fibre Toxicol* 14: 40.

Dobrovolskaia, M.A., M. Shurin, and A.A. Shvedova. 2016. Current understanding of interactions between nanoparticles and the immune system. *Toxicol Appl Pharmacol* 299:78-89.

Dusinska, M., J. Tulinska, N. El Yamani, M. Kuricova, A. Liskova, E. Rollerova, E. Rundén-Pran, and B. Smolkova. 2017. Immunotoxicity, genotoxicity and epigenetic toxicity of nanomaterials: New strategies for toxicity testing? *Food Chem Toxicol* 109:797-811.

EFSA. 2009. Guidance of the Scientific Committee on a request from EFSA on the use of the benchmark dose approach in risk assessment. *EFSA J* 1150:1–72.

ECHA. European Risk Assessment Report. COPPER, COPPER II SULPHATE PENTAHYDRATE, COPPER(I)OXIDE, COPPER(II)OXIDE, DICOPPER CHLORIDE TRIHYDROXIDE. European Copper Institute. 2008. Published at the website of the European Chemicals Agency (http://echa.europa.eu/nl/home).

Evans, P. H., Matsunaga and M. Kiguchi. 2008. Large-scale application of nanotechnology for wood protection. *Nat Nano* 3: 577-577.

Freeman, B. M. H., and C.R. McIntyre, 2008. A Comprehensive Review of Copper-Based Wood Preservatives with a focus on new micronized or dispersed copper systems. *For Prod J* 58: 6-27.

Gosens, I., A. Kermanizadeh, N.R. Jacobsen, A.G. Lenz, B. Bokkers, W.H. De Jong, P. Krystek, L. Tran, V. Stone, H. Wallin, T. Stoeger, and F.R. Cassee. 2015. Comparative hazard identification by a single dose lung exposure of zinc oxide and silver nanomaterials in mice. *PLoS One* 10: e0126934.

Gosens, I., F.R. Cassee, M. Zanella, L. Manodori, A. Brunelli, A.L. Costa, B.G. Bokkers, W.H. De Jong, D. Brown, D. Hristozov, and V. Stone.2016. Organ burden and pulmonary toxicity of nano-sized copper (II) oxide particles after short-term inhalation exposure. *Nanotoxicology* 10:1084-1095.

Hébert, C.D., 1993. NTP Technical Report on toxicity studies of cupric sulphate (CAS N°7758-99-8) administered in drinking water and feed to F344/N rats and B6C3F1 mice. National Toxicology Program, Toxicity Report Series N° 29, United States Department of Health and Human Services (NIH Publication 93-3352); Not GLP; Published.

Jantratid, E., N. Janssen, C. Reppas, and J.B. Dressman. 2008. Dissolution media simulating conditions in the proximal human gastrointestinal tract: an update. *Pharm Res* 25:1663-1676.

Jing, X, J.H., Park, T.M. Peters, and P.S. Thorne. 2015. Toxicity of copper oxide nanoparticles in lung epithelial cells exposed at the air–liquid interface compared with in vivo assessment. *Toxicol in Vitro* 29, 502-511.

Kartal, S. N., F. Green, and C.A. Clausen. 2009. Do the unique properties of nanometals affect leachability or efficacy against fungi and termites? *Int Biodeter Biodegrad* 63: 490-495.

Keller, A.A., A.S. Adeleye, J.R. Conway, K.L. Garner, L. Zhao, G.N. Cherr, J. Hong, J.L. Gardea-Torresdey, H.A. Godwin, S. Hanna, Z. Ji, C. Kaweeteerawat, S. Lin, H.S. Lenihan, R.J. Miller, A.E. Nel, J.R. Peralta-Videa, S.L. Walker, A.A. Taylor, C. Torres-Duarte, J.I. Zink, and N. Zuverza-Mena. 2017. Comparative environmental fate and toxicity of copper nanomaterials. *NanoImpact* 7: 28-40.

Kent, R.D., and P.J. Vikesland. 2016. Dissolution and Persistence of Copper-Based Nanomaterials in Undersaturated Solutions with Respect to Cupric Solid Phases. *Environ Sci Technol* 50:6772-6781.

Liao, M., and H. Liu. 2011. Gene expression profiling of nephrotoxicity from copper nanoparticles in rats after repeated oral administration. *Environ Toxicol Pharmacol* 34:67-80.

Lebow, S., and D. Foster, 2005. Environmental concentrations of copper, chromium, and arsenic released from a chromated-copper-arsenate- (CCA-C-) treated wetland boardwalk. *For Prod J* 55; 62-70.

Lei, R., C. Wu, B. Yang, H. Ma, C. Shi, Q. Wang, Q. Wang, Y. Yuan, and M. Liao. 2008. Integrated metabolomic analysis of the nano-sized copper particle-induced hepatotoxicity and nephrotoxicity in rats: a rapid in vivo screening method for nanotoxicity. *Toxicol Appl Pharmacol* 232:292-301.

Marques, M., R. Loebenberg, and M. Almukainzi. 2011. Simulated Biological Fluids with Possible Application in Dissolution Testing, *Dissolution Technologies* 18:15-28..

OECD. 2008. OECD Guidelines for the testing of chemicals: Acute Oral Toxicity: Up-and-Down Procedure. Test Guideline 425. Organisation for Economic Co-operation and Development. Paris, France. 27 pp.

Pantano, D., N. Neubauer, J. Navratilova, L. Scifo, C. Civardi, V. Stone, F. Von Der Kammer, P. Müller, M.S. Sobrido, B. Angeletti, J. Rose, and W. Wohlleben. 2018. Transformations of Nanoenabled Copper Formulations Govern Release, Antifungal Effectiveness, and Sustainability throughout the Wood Protection Lifecycle. *Environ Sci Technol* 52:1128-1138.

Platten, W., T. Luxton, S. Gerke, N. Harmon, K. Sylvest, B. Rogers, and K. Rogers. 2014. Release of Micronized Copper Particles from Pressure Treated Wood Products; US Environmental Protection Agency.

Privalova, L.I., B.A. Katsnelson, N.V. Loginova, V.B. Gurvich, V.Y. Shur, I.E. Valamina, O.H. Makeyev, MP. Sutunkova, I.A. Minigalieva, E.P. Kireyeva, V.O. Rusakov, A.E. Tyurnina, R.V. Kozin, E.Y. Meshtcheryakova, A.V. Korotkov, E.A. Shuman, A.E. Zvereva, and S.V. Kostykova. 2014. Subchronic toxicity of copper oxide nanoparticles and its attenuation with the help of a combination of bioprotectors. *Int J Mol Sci* 15: 12379-12406.

Qualls-Creekmore, E., M. Tong, and G.M. Holmes. 2010. Time-course of recovery of gastric emptying and motility in rats with experimental spinal cord injury. *Neurogastroenterol Motil* 22:62-69.

Santiago-Rodríguez, L., J.L. Griggs, K.D. Bradham, C.Nelson, T. Luxton, W.E. Platten Iii, and K.R. Rogers. 2015. Assessment of the bioaccessibility of micronized copper wood in synthetic stomach fluid. *Environmental Nanotechnology, Monitoring & Management* 4: 85-92.

Sarkar, A., J. Das, P. Manna, and P.c. Sil. 2011. Nano-copper induces oxidative stress and apoptosis in kidney via both extrinsic and intrinsic pathways. *Toxicology* 290:208-217.

Strauch, B.M., R.K. Niemand, N.L. Winkelbeiner, and A. Hartwig. 2017. Comparison between micro- and nanosized copper oxide and water soluble copper chloride: interrelationship between intracellular copper concentrations, oxidative stress and DNA damage response in human lung cells. *Part Fibre Toxicol* 14:28.

Ude, V.C., D.M. Brown, L. Viale, N. Kanase, V. Stone, and H.J. Johnston. 2017. Impact of copper oxide nanomaterials on differentiated and undifferentiated Caco-2 intestinal epithelial cells; assessment of cytotoxicity, barrier integrity, cytokine production and nanomaterial penetration. *Part Fibre Toxicol* 14:31.

Vandebriel, R.J., E.C. Tonk, L.J.J. De La Fonteyne-Blankestijn, E.R. Gremmer, H.W. Verharen, L.T. Van Der Ven, H. Van Loveren, and W.H. de Jong. 2014. Immunotoxicity of silver nanoparticles in an intravenous 28-day repeated-dose toxicity study in rats. *Part Fibre Toxicol* 11:21.

Vencalek, B.E., S.N. Laughton, E. Spielman-Sun, S.M. Rodrigues, J.M. Unrine, G.V. Lowry, and K.B. Gregory. 2016. In Situ Measurement of CuO and Cu(OH)2 Nanoparticle Dissolution Rates in Quiescent Freshwater Mesocosms. *Environmental Science & Technology Letters* 3: 375-80.

Wang, Z., A. Von Dem Bussche, P.K. Kabadi, A.B. Kane, and R.H. Hurt. 2013. Biological and environmental transformations of copper-based nanomaterials. *ACS Nano* 7; 8715–8727.

Wohlleben, W., H. Waindok, B. Daumann, K.Werle, M. Drum, and H.Egenolf. 2017. Composition, Respirable Fraction and Dissolution Rate of 24 Stone Wool MMVF with their Binder. *Part Fibre Toxicol* 14: 29.

Table 1A. Cu in organs of male rats after 5 days consecutive oral administration of CuO NPs.

Day 6					Day 26	
Dose (mg/kg)	0	32	64	512	0	32
Organ						
Liver	13±0.4[a]	42±16[*]	75±4 (2)[*]	914±541	14±3	12±1.5
Lung	6±1	6±1	5 (1)	70±69	7±0.2	6±1.3
Kidney	41±6	62±14	64 (1)	76±42	62±9	52±4 (3)
Spleen	6±0.4	6±0.3	6±1 (2)	10±5	6±0.6	5±1
Thymus	4±0.3	5±1 (3)	8±4 (2)	10±7	5±1	5±2
MLN[b]	5±1	8±2	10±0.3 (2)[***]	26±11	4±2	5±2
Testis	11±0.3	11±0.1	11±0.3 (2)	12±1	12±1	11±1
Brain cortex	9±0.1	9±0.5	ND	10±1	10±3	9±0.4

a)Cu content in organs (µg/g tissue) at day 6 and day 26 after oral administration on 5 consecutive days (days 1-5) with CuO NPs. Results are presented as mean ± SD, n=4 unless otherwise indicated within brackets.
ND, not done. .Significant differences compared to vehicle treated animals. *<0.05, ***<0.001 students t-test, one sided.
b)MLM, mesenteric lymph node.

Table 1B. Cu in organs of male rats after 5 days consecutive oral administration of $Cu_2CO_3(OH)_2$ NPs.

Day 6				Day 26	
Dose (mg/kg)	0	64	128[a]	0	64
Organ					
Liver	13±0.5[b]	451±58***	1399±307***	13±1	29±9*
Lung	8±0.4	9±3	259±335 (8)*	7±0.3	7±06
Kidney	29±6	55±13 (3)*	810±369 (8)***	36±17	28±4
Spleen	5±0.2	6±0.6	35±26 (7)*	5±0.2	5±0.3
Thymus	4±0.5	6±0.6***	29±20 (8)***	3±0.3	3±0.4
MLN[c]	6±1	7±1	48±23 (8)**	6±3	6±2
Testis	11±0.3	12±0.2*	15±0.3 (8)**	11±0.2	13±1**
Brain cortex	9±0.2	10±0.4*	11±1 (8)***	9±0.5	10±7

a)Dose of 128 mg/kg b.w. $Cu_2CO_3(OH)_2$ NP determination at days 6 and day 7 after start of experiment. Animals received $Cu_2CO_3(OH)_2$ NP by oral administration at days 1 –5. Recovery animals were taken out of the study in view of poor condition (day 7 being day 2 after last $Cu_2CO_3(OH)_2$ NP administration).

b)Cu content in organs (µg/g tissue) at day 6 and day 26 after oral administration on 5 consecutive days (days 1-5) with $Cu_2CO_3(OH)_2$ NPs. Results are presented as mean ± SD, n=4 unless otherwise indicated within brackets. Significant differences compared to vehicle treated animals. *<0.05, **<0.01, ***<0.001 students t-test, one sided.

c)MLN, mesenteric lymph node.

Table 2 Bench mark dose calculations for toxic effects after oral CuO NPs exposure for 5 consecutive days.

Parameter	BMD[a]	BMDlow	BMDhigh	Ratio
RBC	35.7	23.8	115.7	4.9
Hgb	32.9	24	81.5	3.4
Hct	33.2	28.8	132	4.6
AST	26.2	16.1	27	1.7

a)BMD (bench mark dose) is presented in mg/kg of orally administered CuO NPs for 5 consecutive days. BMD using the PROAST program for calculations of the BMD. BMDlow and BMDhigh indicate the lower and upper end of the 90% confidence interval. The ratio calculated between the BMDlow and BMDhigh gives an indication of the size range of the confidence interval and the reliability of the data. BMD was set at 5% deviation of control vehicle treated animals.

Table 3 Bench mark dose calculations for toxic effects after oral $Cu_2CO_3(OH)_2$ NPs exposure for 5 consecutive days.

Day 6-7 Parameter	BMD[a]	BMDlow	BMDhigh	Ratio
Body weight	92.7	43.7	153.9	3.5
Liver weight	32.2	9.5	75.5	7.9
Thymus weight	69.1	43.1	97.2	2.3
Spleen weight	89.7	50.2	99.9	2.0
AST	30.8	18.8	42.9	2.3
ALP05[b]	91.5	65.6	95.6	1.5
ALP10	98.4	75.2	102.8	1.4
Fe	101.5	34.9	122.7	3.5
Uric acid	90.5	36.1	93.7	2.6
SHP	95.1	77.6	100.8	1.3
RBC	108.6	70.8	112.5	1.6
Hgb	100.5	67.7	115.1	1.7
Hct	113.1	74.6	117.2	1.6
Lymph rel	94.4	65.2	97.9	1.5
Lymf Absol	99.7	45.4	106.1	2.3
LDP05	61.8	32.2	91.1	2.8
LDP10	70.3	41.2	97.9	2.4
Day 26				
AST	45.8	33.6	57.0	1.7

a)BMD is presented in mg/kg of orally administered $Cu_2CO_3(OH)_2$ NPs for 5 consecutive days.
b)ALP05. The figure 05 indicates a change due to treatment compared to control levels with more than 5%. ALP10. Similarly for a change of more than 10%.
BMD using the PROAST program for calculations of the BMD. BMDlow and BMDhigh indicate the lower and upper end of the 90% confidence interval. The ratio calculated between the BMDlow and BMDhigh gives an indication of the size range of the confidence interval and the reliability of the data. BMD was set at 5% deviation of control vehicle treated animals.

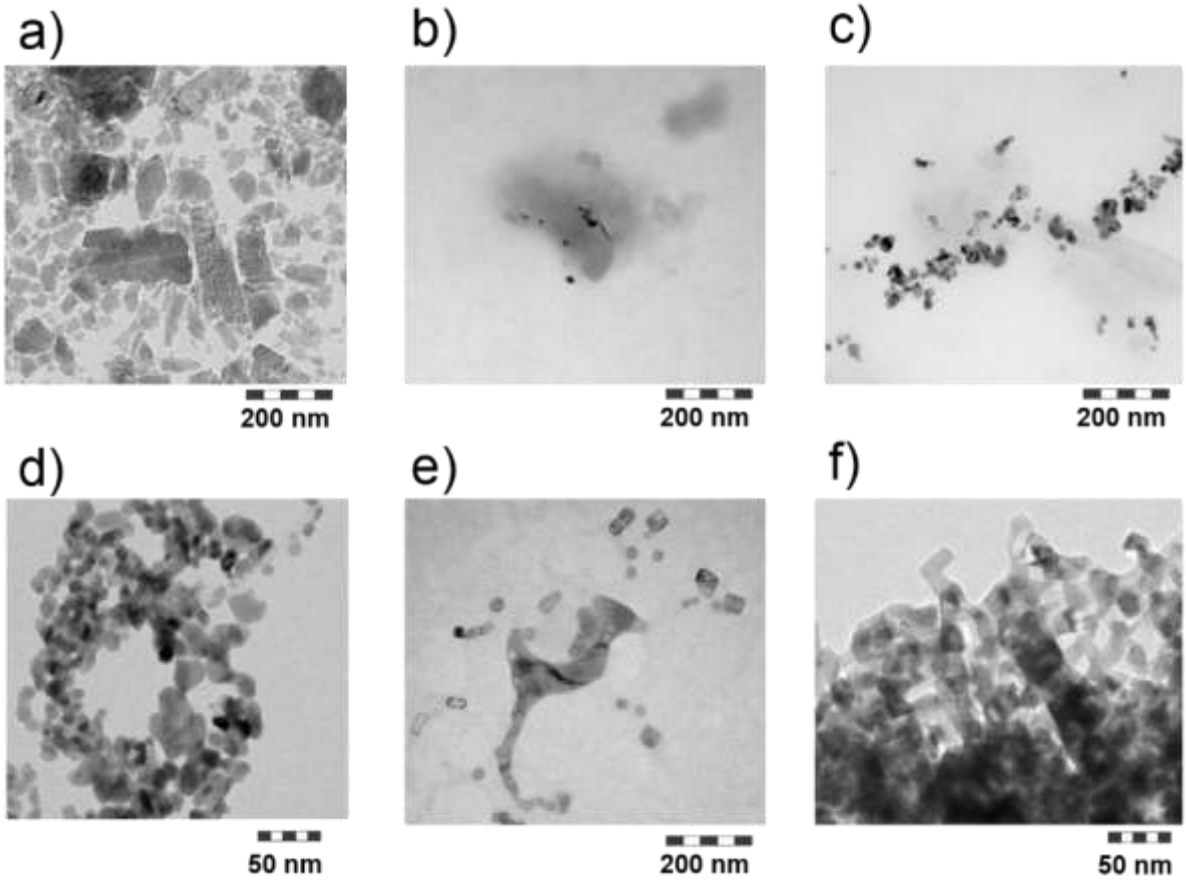

Figure 1. Morphology of pristine and transformed NPs by transmission electron microscopy (TEM): $Cu_2CO_3(OH)_2$ NPs (top row = a,b,c) and CuO NPs (bottom row = d, e, f) before (a,b) and after dissolution testing at 37°C in pH1.6 stomach simulant (b,e) and independently in pH5.8 FeSSIF-V2 middle intestine simulant (c,f.). EDXS finds no Cu content in the b,e structures.

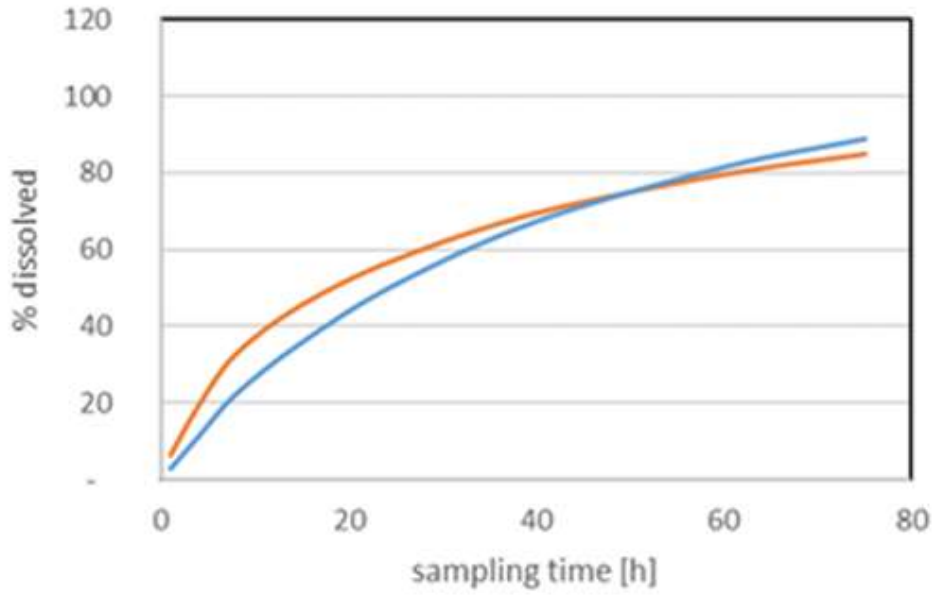

Figure 2: Dissolution of $Cu_2CO_3(OH)_2$ NPs (blue) and CuO NPs (orange) during flow-through testing at 37°C with pH1.6 stomach simulant. Quantification of ions by ICP-OES.

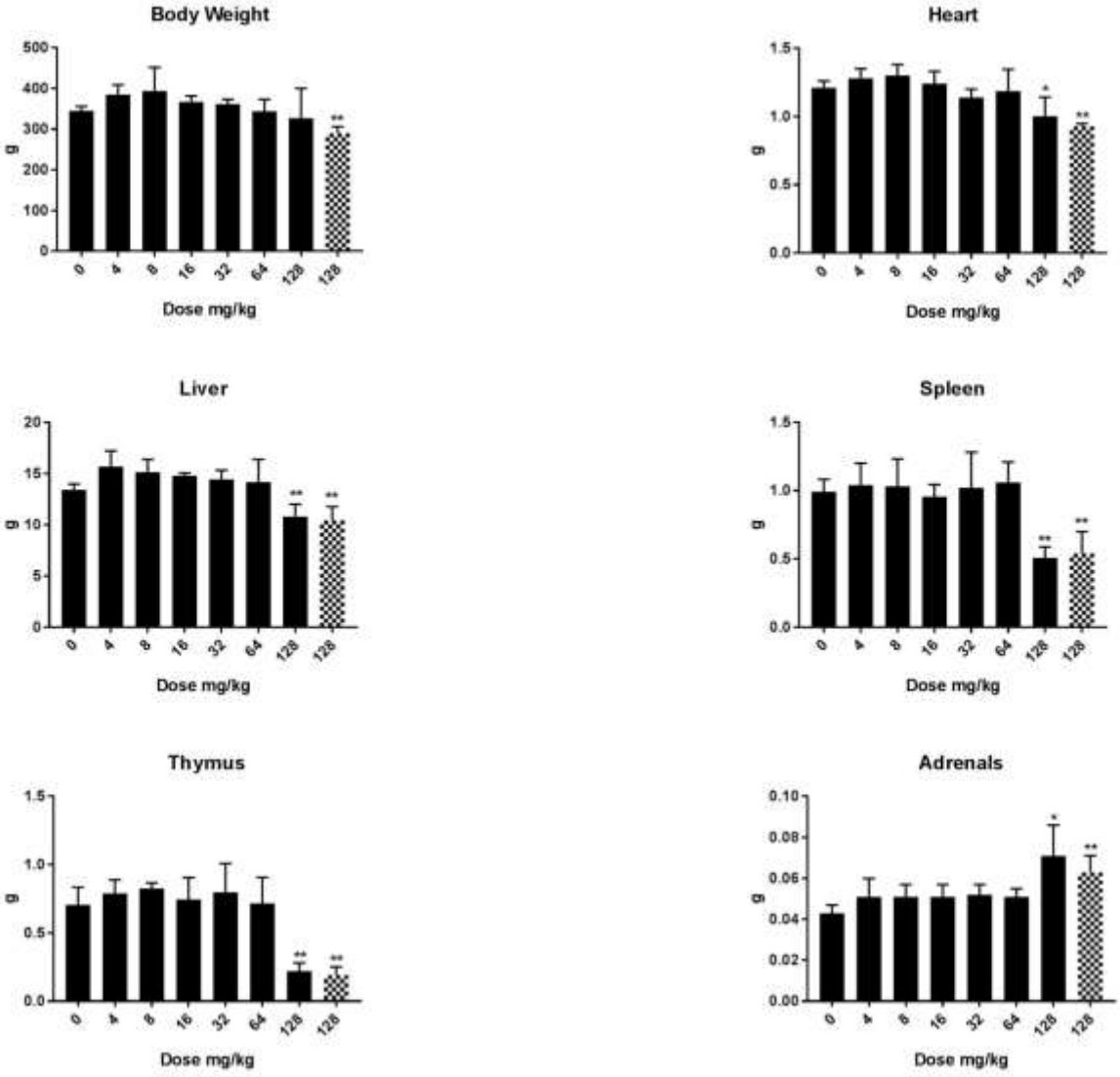

Figure 3. Body and organ weight (g) in male rats at after 5 days consecutive oral administration of $Cu_2CO_3(OH)_2$ NPs - At day 6/7 (24/48 hours after the last administration). The number of animals per group is 4 (n=4). Two groups of dose group of 128 mg/kg b.w. are presented for autopsy at days 6/7 after treatment. For one group (blocked column) an unscheduled autopsy was done of in view of poor condition of the animals intended for recovery. Significant differences compared to vehicle treated animals. *p<0.05, **P<0.01 (ANOVA).
An extended set of body weight data are presented in Supplementary Table 2C and 2D.

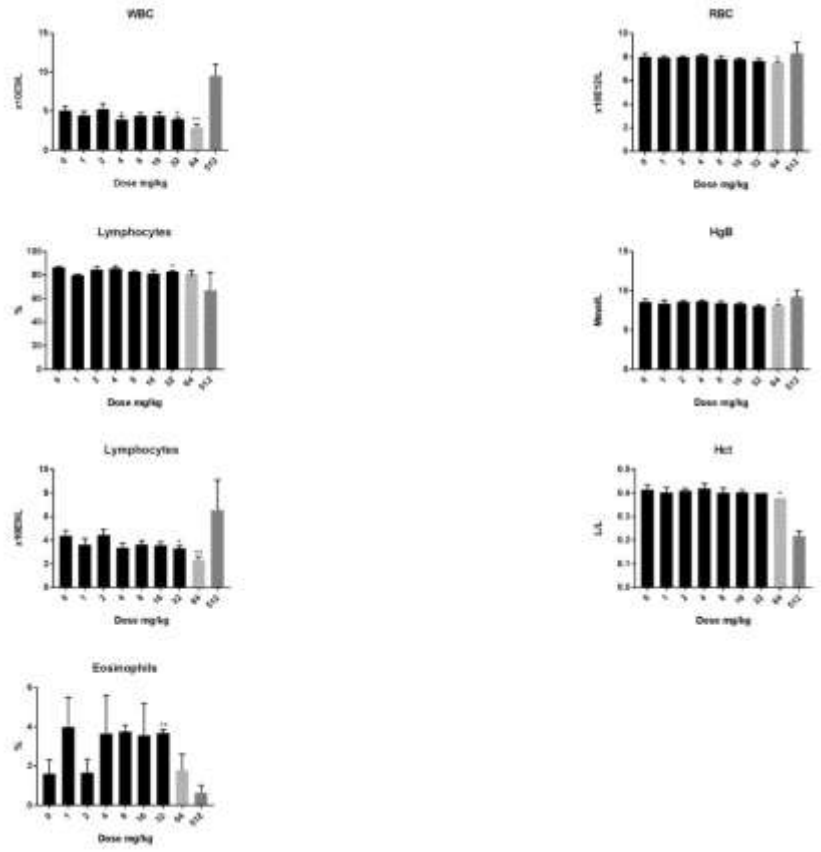

Figure 4 Haematology in male rats after 5 days consecutive oral administration of CuO NPs - At day 6 (24 hours after the last administration). Animals with dose 512 mg/kg as extra group were treated without concurrent contempary control. Significant differences with vehicle treated animals was determined by ANOVA for the dose response study followed by one sided students t-test between groups. * P<0.05, ** p<0.01, *** p<0.01. An extended set of haematology parameters are presented in Supplementary Tables 3A and 3B.

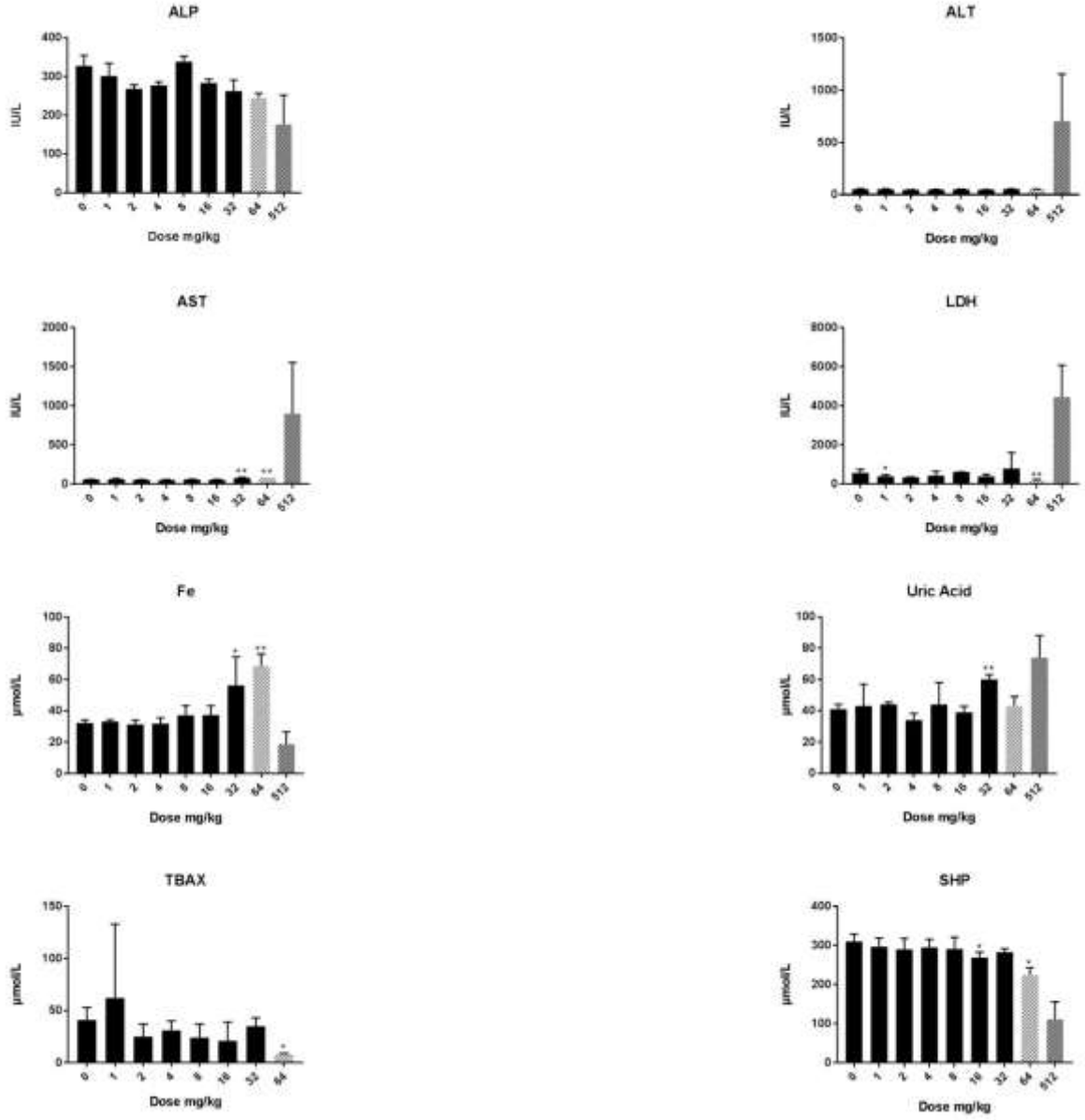

Figure 5 Clinical chemistry in male rats after 5 days consecutive oral administration of CuO NPs - At day 6 (24 hours after the last administration).

ALP, alkaline phosphatase, ALT, alanine aminotransferase; AST, aspartate aminotransferase; Fe, iron; GGT, gamma glutamyltransferase; GLU, glucose; LDH, lactate dehydrogenase; SHP, plasmatic thiol groups; TBAX, total bile acids.

Number of animals n=4. For the dose of 64 mg/kg in the pilot study two (n=2) animals were evaluated.

Significant differences compared to vehicle treated animals. *$p<0.05$ compared to vehicle control (ANOVA), **$p<001$ compared to vehicle control (ANOVA).

Animals with dose 512 mg/kg as extra group were treated without concurrent contempary control.

An extended set of clinical chemistry parameters are presented in Supplementary Tables 5A and 5B.

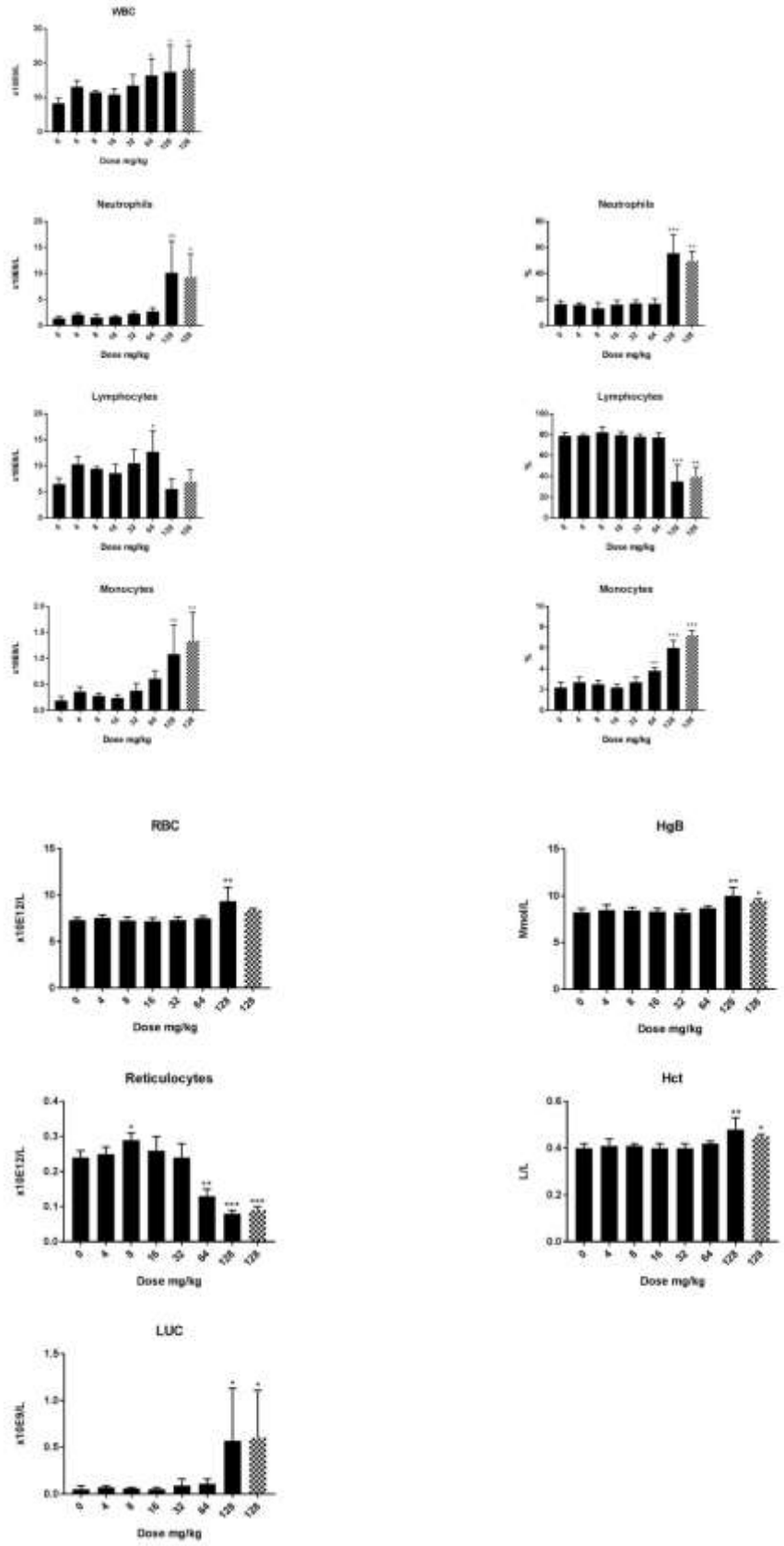

Figure 6 Haematology in male rats after 5 days consecutive oral administration of $Cu_2CO_3(OH)_2$ NPs - At day 6 (24 hours after the last administration).

The number of animals per group is 4 (n=4) For some animal blood was not available for evaluation.

Unscheduled autopsy of dose group of 128 mg/kg at days 6/7 after treatment in view of poor condition of the animals (n=3).
Significant differences compared to vehicle treated animals.One sided students t-test, * $P<0.05$, ** $p<0.01$, *** $p<0.01$.An extended set of haematology parameters are presented in Supplementary Tables 3C and 3D.

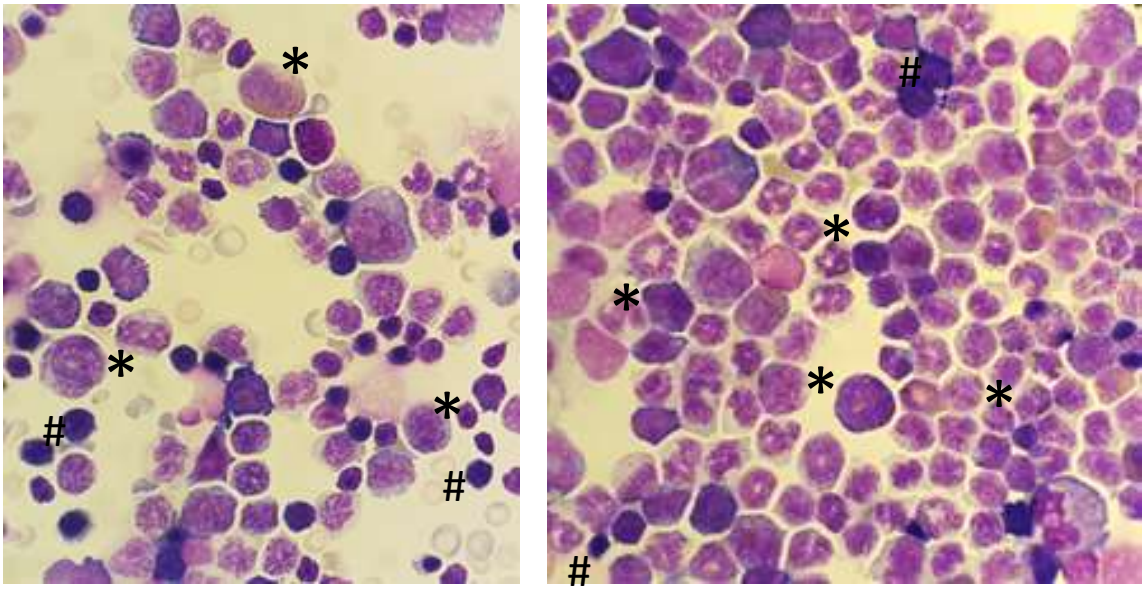

Figure 7. Abundant presence of myeloid cells in bone marrow cell population at day 6 (24 hours after last treatment). Left vehicle control (day 6), right animal treated with 128 mg/kg $Cu_2CO_3(OH)_2$ NPs for 5 consecutive days (day 1-5), day 7. * Myeloid progenitor cells, # erythroid progenitor cells. Magnification x400.

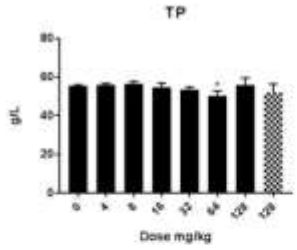
TP
g/L
Dose mg/kg

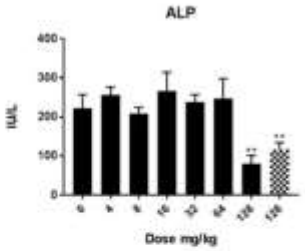
ALP
IU/L
Dose mg/kg

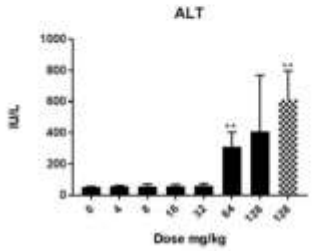
ALT
IU/L
Dose mg/kg

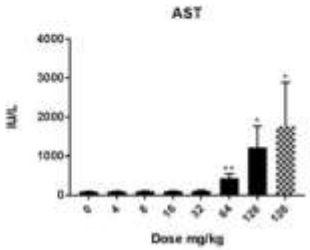
AST
IU/L
Dose mg/kg

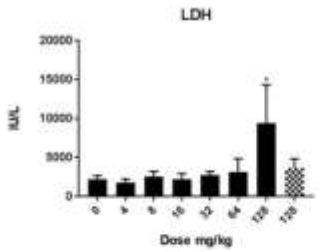
LDH
IU/L
Dose mg/kg

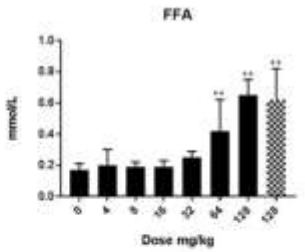
FFA
mmol/L
Dose mg/kg

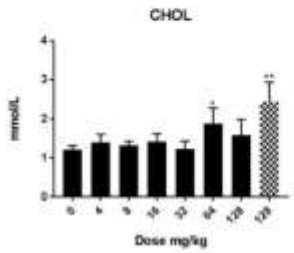
CHOL
mmol/L
Dose mg/kg

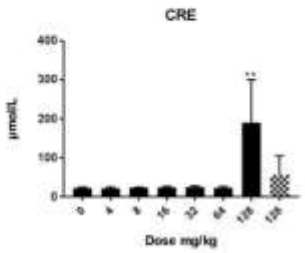
CRE
μmol/L
Dose mg/kg

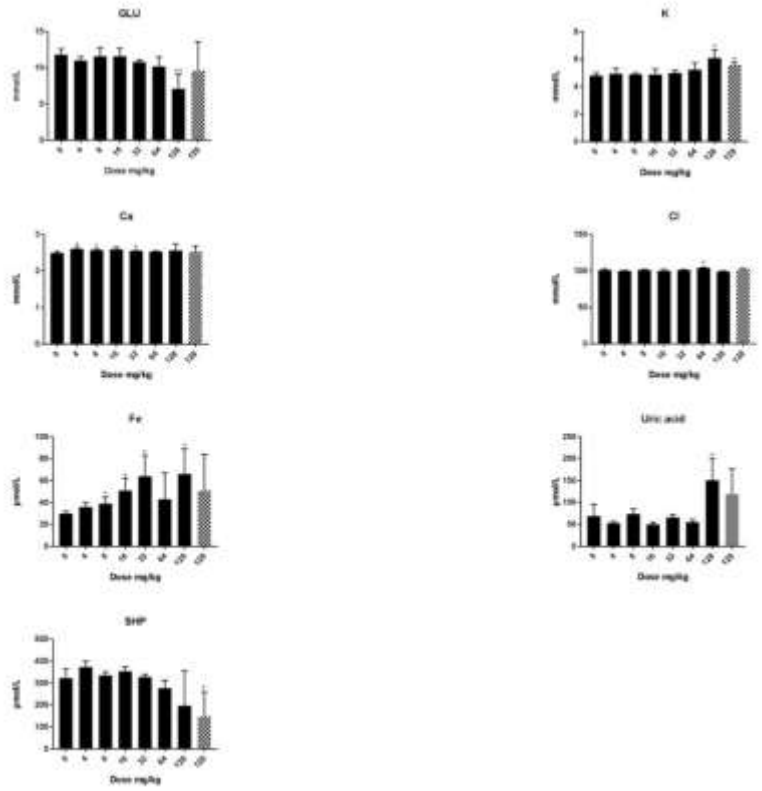

Figure 8. Clinical chemistry in male rats after 5 days consecutive oral administration of $Cu_2CO_3(OH)_2$ NPs - At day 6 (24 hours after the last administration).

ALB, albumin; ALP, alkaline phosphatase, ALT, alanine aminotransferase; AST, aspartate aminotransferase; BAP, biological anto-oxidant potential; Ca, calcium; Cl, chloride; ; CHOL, cholesterol; CRE, creatinine; Fe, iron; GGT, gamma glutamyltransferase; GLU, glucose; K, potassium; LDH, lactate dehydrogenase; Na, sodium; ROM, reactive oxygen metabolites; SHP, plasmatic thiol groups; TBAX, total bile acids; TBIL, total bilirubin; TG, triglycerides; TP, total protein; TTT, total thiols. DL, detection limit.

Number of animals n=4. .

Unscheduled autopsy of dose group of 128 mg/kg at days 6/7 after treatment in view of poor condition of the animals.

Significant differences compared to vehicle treated animals. *$p<0.05$ compared to vehicle control (ANOVA), **$p<.001$ compared to vehicle control (ANOVA).

An extended set of clinical chemistry parameters are presented in Supplementary Tables 5C and 5D.

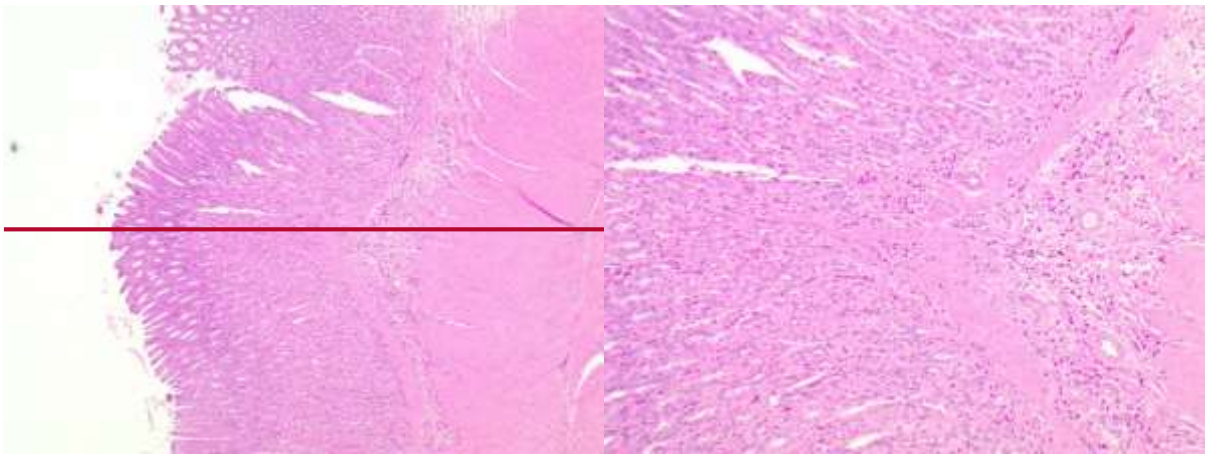

Figure 9 Presence of inflammation (arrows) in the submucosa of the stomach in a rat treated with a dose of 64 mg/kg b.w. of $Cu_2CO_3(OH)_2$ NP for 5 consecutive days. Autopsy at day 6, 1 day after the last $Cu_2CO_3(OH)_2$ NP administration. Left overview, right detail of inflammatory cells (arrows).

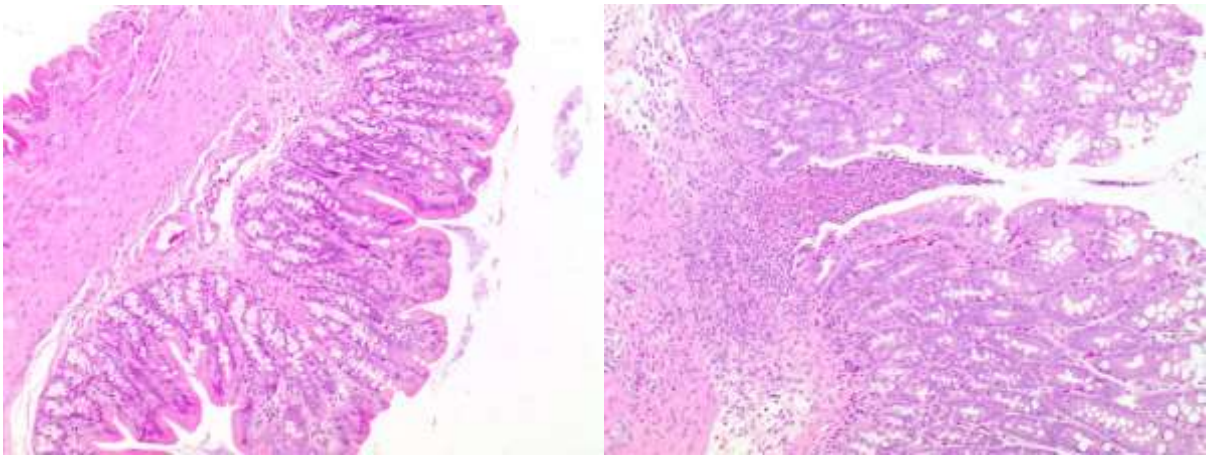

Figure 10 Presence of ulceration of colon mucosa (arrows, figure on the right) of rat treated with 128 mg/kg b.w. of $Cu_2CO_3(OH)_2$ NPs for 5 consecutive days. Note severe inflammation and loss of colon epithelium above inflammation. Autopsy at day 6, 1 day after the last $Cu_2CO_3(OH)_2$ NP administration. Left colon of vehicle treated control animal.

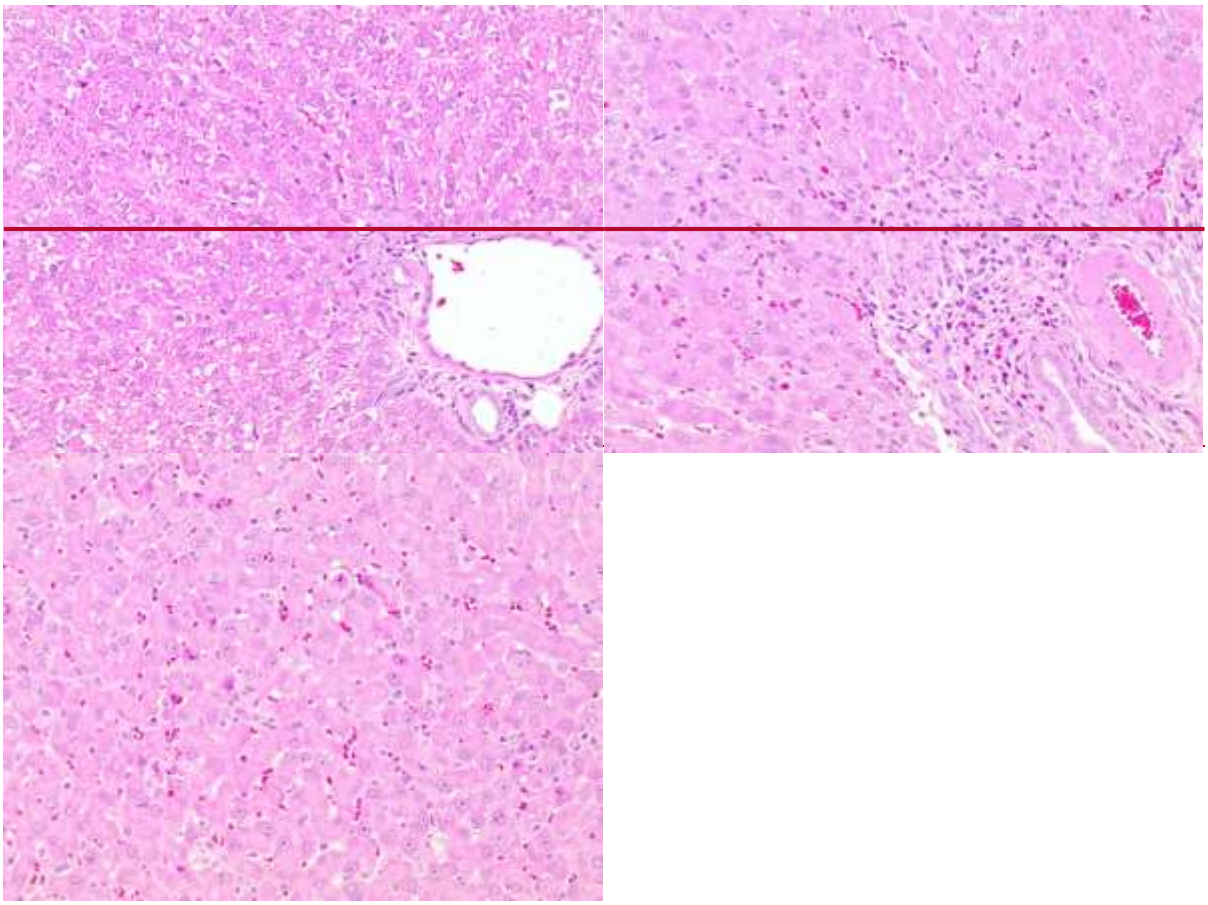

Figure 11 Presence of toxic effects in the liver. Top left, liver of vehicle control treated animal. Top right presence of inflammation(arrows) and vacuolisation (asterisks) of liver parenchyma cells. Bottom single cell necrosis of liver cells (arrows). Autopsy at day 7, 2 days after the last Cu2CO3(OH)2 NP administration. Animal treated with 128 mg/kg b.w. of $Cu_2CO_3(OH)_2$ NPs for 5 consecutive days (days 1-5).

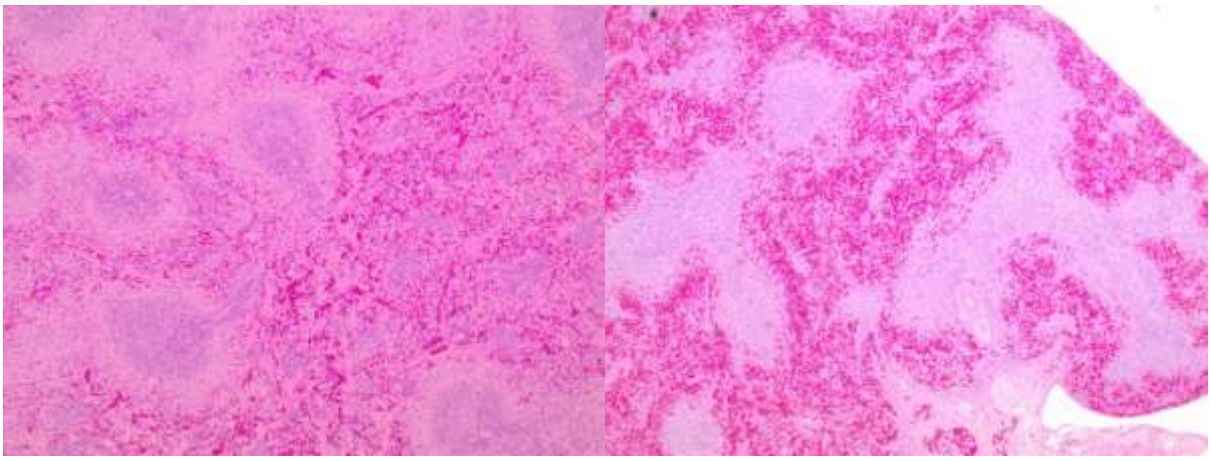

Figure 12 Presence of toxic effects in the spleen. Left histology of normal spleen of control animal. Note extensive presence of lymphocytes (white pulp) (asterisks). Right lymphoid atrophy as shown by the depletion of lymphocytes (white pulp) (asterisks). Day 6 rat treated with $Cu_2CO_3(OH)_2$ NPs 128 mg/kg b.w. for 5 consecutive days (days 1-5).

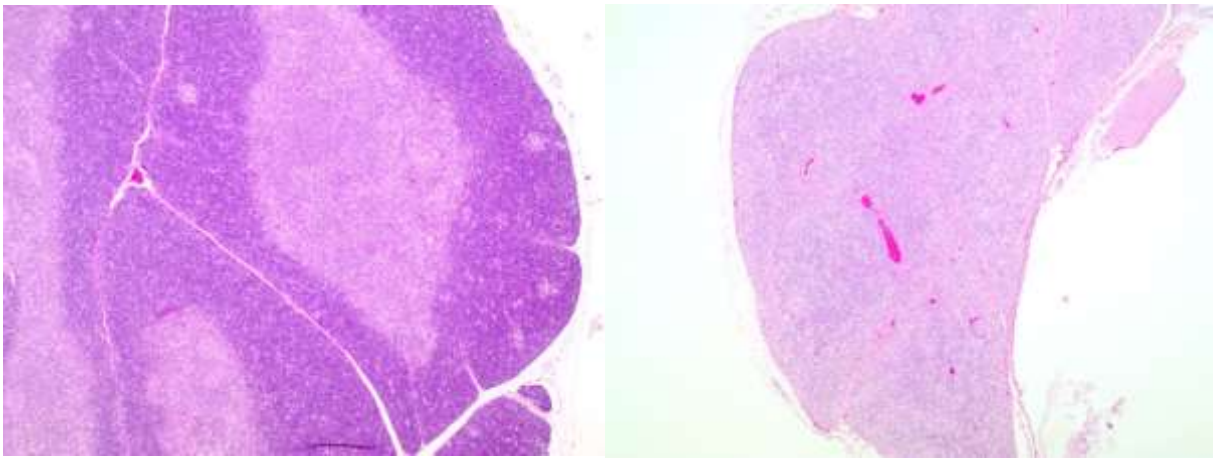

Figure 13 Effects on thymus. Left histology of normal thymus of control animal. Note extensive presence of lymphocytes in cortex (asterisks) and medulla (xxxx). Right lymphoid atrophy as shown by the low number of lymphocytes present resulting in a disappearance of demarkation between cortex and medulla. Day 6 rat treated with $Cu_2CO_3(OH)_2$ NPs 128 mg/kg for 5 consecutive days (days 1-5).